Voltammetric Comparisons of Structurally Homologous Nitrite Reducing Cytochromes from *Thioalkalivibrio nitratireducens* and *Escherichia coli*

Rose-Marie Doyle

PhD Thesis, September 2011

University of East Anglia

School of Chemical Sciences

Norwich

Abstract

The reduction of nitrite to ammonia by the pentaheme cytochrome *c* nitrite reductase, NrfA, has been well studied. The NrfAs are catalytically promiscuous enzymes that also reduce hydroxylamine and nitric oxide to ammonia and sulphite to sulphide [1-5]. There are structural differences between NrfA enzymes from different organisms and the evolutionary related group of catalytic multi-heme cytochromes, which appear to have different catalytic and functional specificities. It is of interest to determine which structural features are important for effective catalysis and if the differences in the structure of these enzymes are indicative of evolved specificity or function.

Here nitrite reduction by the octaheme cytochrome *c* nitrite reductase from the obligately haloalkaliphilic *Thioalkalivibrio nitratireducens*, TvNir, was compared to nitrite reduction by *Escherichia coli* NrfA using protein film electrochemistry. The kinetics of nitrite reduction by each enzyme were distinctive. The K_M of TvNir decreased by ca. 500 μM as the pH was increased from pH 5 to pH 10, whereas contrastingly the K_M of NrfA increased by less than 100 μM from pH 4 to pH 9. Below pH 7 nitrite reduction by TvNir was substrate inhibited and this has never been detected for NrfA. Approximately 30% of the TvNir sample required reductive activation, whereas samples of purified NrfA are already catalytically competent. The possible origins of these differences in the sequence and structure of NrfA and TvNir are discussed.

Spectropotentiometry and protein film voltammetry defined the reduction potentials of NrfB, part of the redox pathway to NrfA. The reduction potentials of NrfA and NrfB are very similar to those of TvNir and so the thermodynamic pathways allowing electron transfer to their active sites, enabling catalysis by these nitrite reductases are similar. The results of the protein film electrochemistry experiments to assess nitrite reduction by NrfAB were ambiguous and the further experiments required to address this are discussed.

Acknowledgements

First and foremost I would like to thank my supervisor, Prof. Julea Butt, for all her encouragement, guidance, support and understanding throughout my PhD. For all this I am extremely grateful. I would also like to thank the other members of my supervisory team, Dr. Myles Cheesman and Dr. Nicholas Watmough for many helpful discussions and their continued support and interest in my project. Thank you also to my sponsors, the BBSRC.

I am grateful to Dr. Thomas Clarke for preparation and purification of NrfB and for so many interesting discussions regarding the biochemistry of NrfAB. I would also like to thank Dr. Tamara Tikhonova (A. N. Bach Institute of Biochemistry, Russian Academy of Sciences) for purification and preparation of TvNir and for her continued interest in the project.

Many Thanks to Prof. Jeff Cole and Claire Vine at the University of Birmingham for allowing me to visit their laboratory and perform site directed mutagenesis of NrfA, for their assistance with this and for a wonderful visit.

I would like to thank Dr. James Gwyer and Dr. Gemma Kemp whose studies of the pH dependence of NrfA laid the foundations of the studies of TvNir and NrfAB in this thesis. I would like to additionally thank Dr. Gemma Kemp for her guidance and support when I began my PhD. Thank you to Dr. Sophie Marritt for the spectroscopy of TvNir. A special thanks to Paul Nicholas, a project student who helped with experiments investigating the NaCl dependence of TvNir.

Thank you to Dr. Andrew Gates for his helpful advice on PFV and to Colin Lockwood for his assistance whilst working in The School of Biological Sciences on the expression of nrfA F218C. Special thanks also to Dr. Jason Crack for advice, discussions and for retrieving my lost hard drive, without which this thesis may have been significantly shorter. Thank you to all of my colleagues over the past years who have generously given their support, advice and inspiration.

A very big thank you to my housemates over the past four years; Edwina Clarke, Yann-Eric Courcha, Dr. Heather Felgate and Edwina McNaughton, I simply do

not know what I would have done without you. Thank you to and to all my friends and family. I cannot express the gratitude that I owe to my parents for their constant support in all my endeavours.

Contents

Abbreviations

CcNiR	Cytochrome *c* nitrite reductase
CHES	N-Cyclohexyl-2-aminoethanesulfonic acid
CV	Cyclic voltammogram
CVA	Cylic voltabsorptogram
DTT	Dithiothreitol
E_m	Midpoint reduction potential
EPR	Electron paramagnetic resonance
FdnGHI	Formate dehydrogenase-N complex
GPES	General purpose electrochemical software
HAO	Hydroxylamine oxidoreductase
Hepes	4-(2-Hydroxyethyl)piperazine-1-ethanesulfonic acid
hhw	Half height width
HTMA	Hepes, Taps, Mes and acetic acid buffer
i_{max}	Maximum catalytic current magnitude
IET	Interfacial electron transfer
k_{cat}	Turnover number
K_M	Michaelis constant
MCD	Magnetic circular dichroism
MES	2-(N-morpholino)ethanesulfonic acid
MQ	Menaquinone
MQH_2	Menaquinol
MOTTLE	MCD- Compatible optically transparent thin-layer electrochemistry
N-cycle	Nitrogen cycle
Nap	Periplasmic nitrate reductase

Nar	Membrane bound nitrate reductase
NrfA	Pentaheme cytochrome *c* nitrite reductase
OTR	Octaheme tetrathionite reductase
PFV	Protein film voltammetry
PGE	Pyrolytic graphite edge
RDE	Rotating disc electrode
PDB	Protein data bank
PGE	Pyrolytic graphite edge
SHE	Standard hydrogen electrode
TAPS	N-[Tris(hydroxymethyl)methyl]-3-aminopropanesulfonic acid
TvNir	Cytochrome *c* nitrite reductase from *Thioalkalivibrio nitratireducens*
UV-vis	Ultra-violet visible
V_{max}	Maximum turnover rate

Chapter One

Introduction

Chapter 1. Introduction

1.1 The Nitrogen cycle

Nitrogen compounds are essential to life on Earth. The nitrogen atom is a component of amino acids, the building blocks for the enzymes that catalyse the reactions of life, and an important component of DNA and RNA, the blueprints for life. Nitric oxide is used as part of the biological defence mechanism by human cells; ammonia is used as fertilizer in agriculture and nitrites as preservatives in our food. The nitrogen cycle represents the inter-conversion of these nitrogen containing species in the environment (figure 1.1). Anthropogenic production and manipulation of nitrogen compounds has shifted the balance of the different nitrogen species within the nitrogen cycle [6]. A combination of agricultural practices, the Haber-Bosch process (ammonia production) and the burning of fossil fuels (releasing ammonia) have nearly doubled the natural rate of terrestrial N-fixation [6]. It has been postulated that understanding and managing the way bacteria interconvert the species of the nitrogen cycle can help to re-balance the cycle to protect Earth's atmosphere for the future [6].

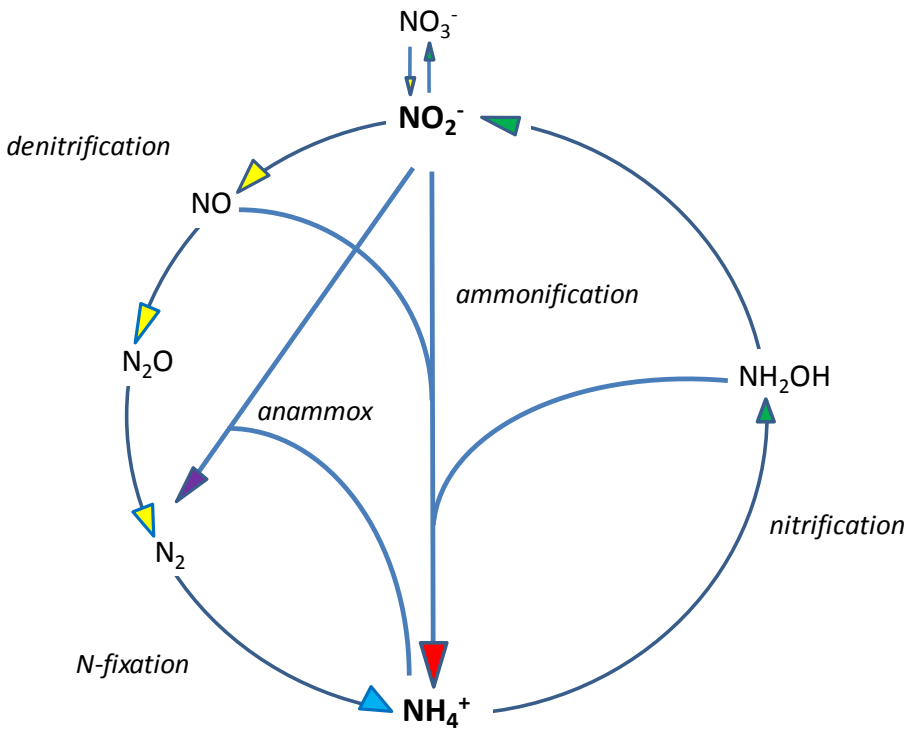

Figure 1.1 The biogeochemical nitrogen cycle. The steps indicated by different coloured arrowheads represent the inter-conversions involved in denitrification, nitrification, ammonification, anammox and the N-fixation as indicated.

The interconversions of nitrogen species depicted by the different paths in the N-cycle can each be catalysed by enzymes from many different bacteria [7-11]. The stepwise reduction of NO_3^- to N_2 via NO_2^-, NO and N_2O is known as denitrification. The denitrification pathway operates under anoxic conditions in the presence of N oxide compounds [11]. The first concerted step in the denitrification pathway is the one electron reduction of NO_2^- to NO and is catalysed primarily by two different enzymes; the cytochrome *c*d_1 nitrite reductase and the copper nitrite reductase [12]. The cytochrome *c*d_1 nitrite reductase is a homodimeric enzyme comprised of an α-helical N- terminal domain containing a covalently attached *c*-type heme and a β-propeller C-terminal domain that contains an unusual d_1 type catalytic heme [13]. The copper nitrite reductases are homotrimeric, each monomer has two domains, a type I and a type II copper centre. Whilst overall the cytochrome *c*d_1 nitrite reductases are more prevalent, both enzymes are widely dispersed amongst the α-, β- and γ- subgroups of bacteria [11].

The reduction of NO to N_2O is catalysed by nitric oxide reductase (NOR), this is a heterodimer made up of two subunits; a larger NorB subunit and the smaller NorC subunit [14]. NorB is a transmembrane α-helical subunit containing a low-spin and a high-spin heme *b* and a non-heme iron (Fe_B). The NorB subunit is thought to have evolved from the heme copper oxidases as it shows a high structural similarity to these enzymes. The small NorC subunit is also α-helical, with one transmembrane helix, the rest of the protein is membrane associated in the periplasm. The NorC subunit contains one *c*-type his-met co-ordinated heme.

The final step in the denitrification pathway is the two electron reduction of N_2O to N_2, this reaction is catalysed by NosZ, the nitrous oxide reductase [15]. NosZ is a heterodimer comprised of a CuA and CuZ subunit [12]. The CuA subunit contains a binuclear copper centre, co-ordinated by two cysteines, two histidines and the carbonyl oxygen atom from either methionine or glutamine. The CuA subunit is proposed to transfer electrons to the CuZ active site. The CuZ active site is a μ4-sulphide bridged tetranuclear copper centre within a β-propeller head-group [16].

The two electron reduction of nitrate to nitrite forms part of the denitrification pathway, but could also be a precursor to nitrite ammonication and therefore is not the first 'concerted' step in denitrification. Three main types of nitrate reductases have been characterised depending on their cellular location and assimilatory/respiratory role; Nap the periplasmic dissimilatory nitrate reductases, Nas the assimilatory cytoplasmic nitrate reductases and Nar, the membrane associated cytoplasmic nitrate reductase [17, 18]. Each of these groups of nitrate reductase contain a catalytic subunit (e.g NapA or NarG) with molydopterin active site cofactor comprised of molybdenum and two molybdopterin guanine dinucleotides, together with an iron-sulfur cluster proposed to transfer electrons to the active site [12]. The peptide structure and electron transfer complexes formed by these nitrate reductases are diverse, depending on their role and cellular location.

The denitrification enzymes allow the N oxides reduced in the denitrification pathway to act as terminal electron acceptors in place of oxygen in anaerobic respiration [11]. Bacteria also use the denitrifying enzymes to protect themselves from nitrosative stress, as some of the N oxide compounds such as NO are cytotoxic [9]. Bacteria in different communities have evolved to perform various steps in the denitrification pathway and not all bacteria are capable of performing complete denitrification. It has been found that approximately one third of all the sequenced denitrifying bacteria lack the gene that encodes for the nitrous oxide reductase, NosZ [19]. This is thought to be due to the fact that NosZ is a copper containing enzyme and it has been proposed that copper dependent enzymes evolved later than those with iron cofactors. Early in Earth's history, before photosynthesis evolved and atmospheric oxygen became dissolved in the oceans, copper was insoluble and therefore unavailable, whereas Fe^{2+} was abundant in the early Ocean and so many nitrogen cycle enzymes make use of Fe redox cofactors such as heme and iron-sulfur clusters [6]. For this reason when mapping the evolution of the nitrogen cycle enzymes the metal co-factors required for catalysis by different enzymes can be used to suggest when they were likely to have appeared, with copper containing enzymes such as NosZ and the copper nitrite reductases predicted to be more recent than enzymes such as cytochrome *c* nitrite reductases that will be discussed in more detail.

The oxidation of ammonia to nitrite via hydroxylamine is known as nitrification, this occurs without the release of intermediates such as N_2, NO and N_2O and is catalysed by ammonia mono-oxygenase (AMO) and hydroxylamine oxidoreductase (HAO). HAO is a multi-heme cytochrome and will be discussed in more detail later in this chapter. AMO is thought to be a copper containing enzyme and would not have evolved before the oxygenation of the oceans made copper bioavailable [20]. However it has been proposed some precursor of these enzymes was present in the earlier forms of the N cycle, when ammonia and nitrate dominated the early ocean chemistry [6].

Nitrite ammonifying enzymes complete the six electron reduction of nitrite to ammonia, without the formation of 'harmful' intermediates such as nitric oxide, or the potent greenhouse gas nitrous oxide [21, 22]. Enzymes that catalyse nitrite ammonification (figure 1.1) work under anaerobic conditions and are only dependent on the availability of heme iron, these enzymes were therefore likely to have evolved prior to the enzymes catalysing the complete denitrification pathway [20]. Nitrite ammonifying enzymes provide a short circuit to the nitrogen cycle and allow bacteria to respire anaerobically under conditions of low nitrate and high nitrite; they protect bacteria from nitrosative stress and allow for the formation of ammonia that can be assimilated by the cell to produce amino acids and nucleotides. There are two main types of nitrite ammonifying enzymes, the siroheme assimilatory nitrite reductases and the multi-heme cytochrome *c* nitrite reductases (CcNiRs). The siroheme nitrite reductases are found in the cytoplasm of bacteria and have a siroheme active site cofactor and a Fe_4S_4 cluster that is reduced by NADH and shuttles electrons to the active site via a cysteine thiolate bridge [23]. The siroheme nitrite reductases are produced anaerobically under conditions of excess nitrate and nitrite, where assimilation will not limit respiration [24]. The CcNiRs are found in the periplasm of gram negative bacteria and it is these CcNiRs that are the focus of the work presented in this thesis.

1.2 Escherichia coli NrfA

1.2.1 The Roles of NrfA in Anaerobic Respiration and Detoxification

The CcNiR in the periplasm of *Escherichia coli* is the pentaheme protein termed NrfA; NrfA catalyses the six electron reduction of nitrite to ammonia (equation 1.1).

$$NO_2 + 6e^- + 8H^+ \rightarrow NH_4^+ + 2H_2O \qquad \text{(Equation 1.1)}$$

In *E. coli* and other γ-proteobacteria nitrite reduction by NrfA is coupled to the oxidation of formate by the formate dehydrogenase complex (FdnGHI) via the menaquinol pool and the NrfDCB complex (figure 1.2 A) [25]. NrfD is an archetype of the NrfD/PsrC family of enzymes that are thought to have eight transmembrane spanning helices and behave as quinol oxidases [26]. Reduced NrfD is then proposed to transfer electrons to NrfC. Sequence analysis predicts that NrfC will contain an iron sulfur cluster and will be associated with the membrane, it is therefore thought to mediate electron transfer between NrfD and NrfB [26]. NrfB is a pentaheme cytochrome *c* type protein that under physiological conditions, where NrfA and NrfB are present in micromolar concentrations, forms a tightly bound complex to NrfA with a K_d of 50 nM [27]. Formation of this complex allows NrfB to transfer electrons received from NrfCD to NrfA, enabling the reduction of nitrite to ammonia at the NrfA active site.

Nitrite reduction by formate allows ATP synthesis in the absence of oxygen as a terminal electron acceptor. Nitrite reduction by NrfA does not directly generate a proton motive force since NrfA is not a proton pump. Nitrite reduction and formate oxidation both occur in the periplasm such that the electrons generated by the oxidation of formate are consumed by the reduction of nitrite on the same side of the membrane (figure 1.2 A) [28]. The mechanism by which NrfABCD drives ATP synthesis is by cycling of the quinol pool, where protons are taken up from the cytoplasm as FdnGHI reduces menaquinone to menaquinol and are released to the periplasm by NrfD as it oxidises menaquinol in order to transfer electrons to NrfA for catalysis. The re-oxidation of menaquinol by nitrite reduction provides fresh menaquinone to be reduced by FdnGHI, allowing more proton translocation across the periplasm and the cycle to continue. NrfA has also been purified and studied in the δ- and ε-

proteobacteria. The NrfA enzymes from these bacteria catalyse the same reaction as the *E. coli* enzyme but they have a different electron transfer pathway from the menaquinol pool (figure 1.2 B) [22]. Instead of electron transfer to NrfA via NrfDCB, the δ- and ε- enzymes receive the electrons directly from NrfH which acts as both electron donor to NrfA and quinol dehydrogenase (figure 1.3) [22].

In *E. coli* the genes encoding NrfA and the enzymes involved in the synthesis of, and electron transfer to, NrfA are found on the *nrf* operon [26]. Under anaerobic conditions FNR activates the expression of the genes for Nar and Nap nitrate reductases and Nrf nitrite reductase, whereas under aerobic conditions oxygen inhibits FNR binding to the promoter of the *nrf* and *nap* operons [29, 30]. Regulation of *nrf* expression is complex; *E. coli* will preferentially use NO_3^- as a respiratory terminal electron acceptor under anaerobic conditions and so in the presence of high NO_3^-, NarL and NarP will repress/ (induce only when NO_3^- runs out) *nrf* expression. The repressors Fis and IHF (Integrated Host Factor) will also bind to the FNR binding site and prevent FNR from inducing expression under certain conditions, however IHF can also stimulate the *nrf* promotor in the absence of NarL and NarP [30, 31]. Other proteins also linked to regulation of the *nrf* operon are NarX and NarP that sense nitrate and nitrite and CRP (cyclic AMP receptor protein) that interacts with a promotor of a gene upstream to the *nrf* operon. Expression of the *nrf* genes is therefore carefully and precisely controlled and this is indicative of their importance to the survival of *E. coli*.

In addition to its role in anaerobic respiration in *E. coli*, NrfA is also proposed to have a role in the detoxification of the cytotoxins nitric oxide and sulphite. This is because NrfA catalyses the reduction of nitric oxide and hydroxylamine to ammonia and of sulphite to sulphide (equations 1.2-4)[1, 5, 32].

$$NO + 6H^+ + 5e^- \rightarrow NH_4^+ + H_2O \qquad \text{(Equation 1.2)}$$

$$NH_2OH + 3H^+ + 2e^- \rightarrow NH_4^+ + H_2O \qquad \text{(Equation 1.3)}$$

$$SO_3^{2-} + 6e^- + 7H^+ \rightarrow HS^- + 3H_2O \qquad \text{(Equation 1.4)}$$

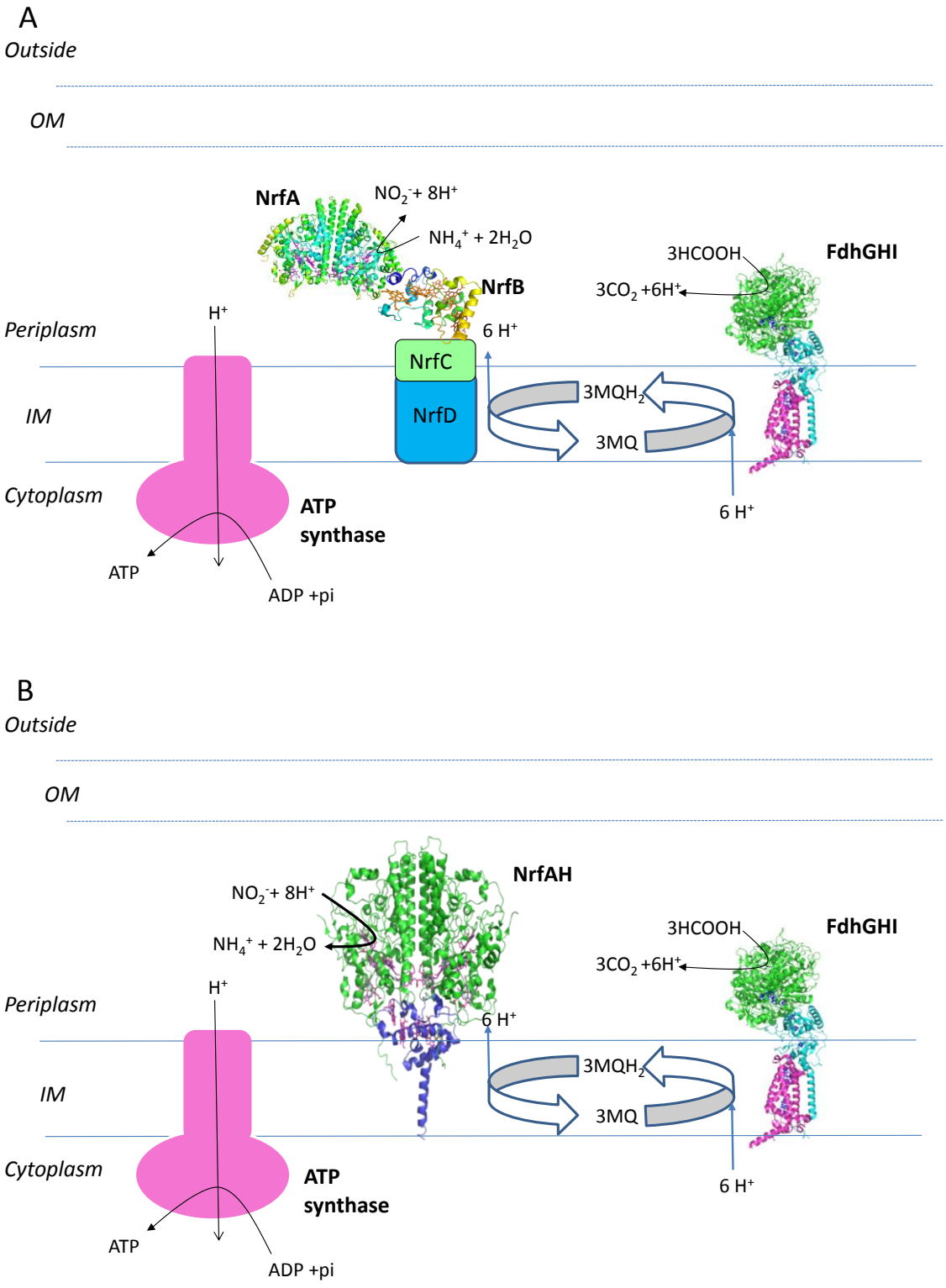

Figure 1.2 The coupling of nitrite reduction to formate oxidation A. in Escherichia coli and B. in δ- and ε- proteobacteria. IM is the inner membrane, OM is the outer membrane, MQ is menaquinone and MQH_2 is menaquinol. The crystal structures are taken from pdb files 2RDZ (*E. coli* NrfA), 2OZY (NrfB), 2J7A (*Desulfovibrio vulgaris* NrfA) and 1KQF (FdhN) and were rendered with PyMol.

The *nrf* genes are expressed when a high concentration of nitric oxide is present. NsrR binds to DNA, close to the position of the FNR binding site and modulates the expression of the *nrf* genes in the absence of NO, so that their expression will be decreased, but not completely inhibited [33]. When NO is present it binds to the 2Fe2S cluster of NsrR, disengaging it from the DNA, removing the repressive effect of NsrR on transcription [34]. NO is a tool that human macrophages utilise in fighting pathogenic infection, but it is also produced in varying quantities by the acidification of NO_3^- containing foods in the gut [35, 36]. The ability to cope with nitrosative stress may confer a selective advantage to *E. coli* in its host environment. NrfA has a high turnover rate for NO of 840 s^{-1} and a K_M of 300 μM [5]. As NrfA is found in the periplasm, it may reduce nitric oxide before it has the opportunity to enter the cytoplasm and damage the cell. Cytoplasmic NO reductases such as flavorubredoxin, NorVW, have a lower K_M but also a lower turnover number, indicative of the lower levels of NO that are predicted to reach the cytoplasm than the periplasm [37]. In *Campylobacter jejuni* and *Salmonella enterica nrf*A expression has been shown to confer resistance to high levels of nitric oxide and therefore its expression not only confers respiratory flexibility but a valuable protective mechanism to the bacteria [38, 39].

1.2.2 The Structure of NrfA

NrfA nitrite reductases have been purified and crystallised from *Wolinella succinogenes, Desulfovibrio desulfuricans, Sulfurospirillum deleyianum, Desulfovibrio vulgaris* and *E. coli* representing members of the γ-, δ- and ε- classes of proteobacteria in which NrfA are found [22, 40-44]. Inspection of these crystal structures reveals some common distinctive structural features as illustrated by the structure of *E. coli* NrfA in Figure 1.3. NrfA is predominantly an α-helical homodimer, where the NrfA-NrfA interface is comprised of parallel α-helices. This α-helical interface provides an axis of symmetry for the two monomers that dimerise mirroring one another.

Each NrfA monomer has five *c*-type hemes that are numbered according to the order of the occurrence of the corresponding CXXCH/K heme binding motif in the amino acid sequence (figure 1.3 B) [40]. Hemes 2 to 5 have bis-histidine co-ordination

and provide pathways for electron transfer to the active site heme 1. Heme 1 has a lysine proximal ligand and the distal ligand is water/hydroxyl. The bis-histidine hemes are characterised by the typical CXXCH heme binding motif, the active site heme is co-ordinated by an unusual CXXCK heme binding motif thus far only found in NrfAs and evolutionarily related nitrite reductases [2, 45]. The maximum distance between adjacent hemes is 12.6 Å between hemes 2 and 3, this is less than 14 Å that is proposed to be the maximum distance for physiologically relevant rates of electron transfer [46]. The hemes in the 5-5 pair at the NrfA-NrfA interface are only 11.9 Å apart and thus it may be possible for electrons to transfer between monomers within the NrfA dimer [40].

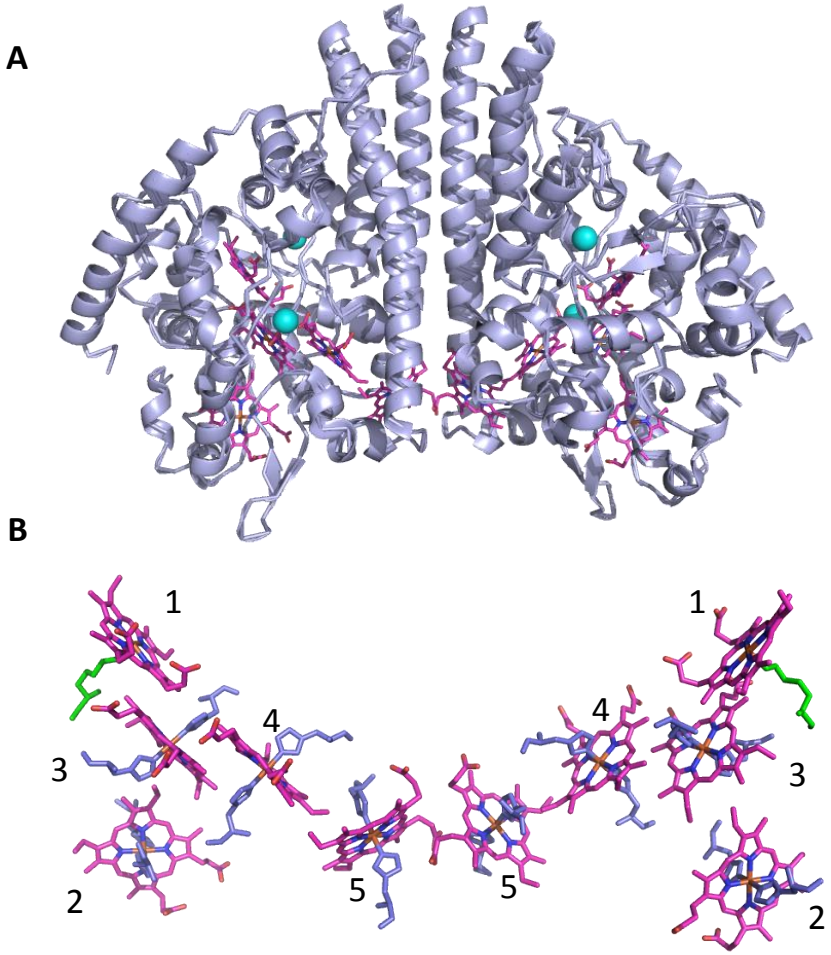

Figure 1.3 The crystal structure of E. coli NrfA. (A) Representation of the dimer shape and α helical composition, the hemes are shown in pink and purple and the calcium atoms are shown in blue. (B) The heme arrangement and axial ligands of NrfA, the histidines are shown in blue and the lysine residues in green, the heme iron is shown in orange. PDB file 2RDZ rendered with PyMol.

All NrfA structures so far identified have a positively charged substrate entry channel and a negatively charged product egress channel, aiding the entry of the negatively charged substrate and egress of the positively charged product from the active site [40-43, 47]. Whilst the net charges of the substrate and product channels are consistent amongst the different NrfAs there are some differences in the structure of these channels amongst the enzymes [2]. The product egress channel of *D. desulfuricans* NrfA has a loop blocking the 'normal' product egress route, this loop is maintained by co-ordination to a 'non-active site' calcium ion [41]. It has been proposed that in order for the product to leave the active site there must be something dynamic about the structure of this loop or that perhaps the product leaves through the substrate entry channel [2]. More divergently, in *S. deleyianum* NrfA the product egress channel splits into two paths, in contrast to the single channel found in the other NrfA structures [2, 42].

The active site of NrfA is centred on the lysine co-ordinated heme 1 (figure 1.4). The substrate binds to the active site heme iron atom as the distal ligand (shown as sulphite in figure 1.4). Tyr *216*, His *264* and Arg *106* are involved in hydrogen bonding the substrate and the histidine and arginine are thought to act as proton donors during catalysis [4, 48]. These residues form an electropositive environment for binding the negatively charged NO_2^- substrate. The active site also contains a highly conserved calcium ion that is octahedrally co-ordinated by Gln *263*, Glu *215*, Lys *261*, Tyr *216* and two water molecules; it is thought to prevent His *264* binding as a distal ligand to the catalytic heme ion [49]. These active site residues are highly conserved in all NrfA structures [40-44].

D. vulgaris NrfA has been crystallised in a complex with its redox partner NrfH (figure 1.2 B). In the NrfHA complex NrfA provides a lysine ligand to the NrfH heme iron that is closest to NrfA [47]. The region of *D. vulgaris* NrfA that interacts with NrfH is the area in proximity to heme 2 of NrfA and an electropositive patch has been observed in this region of all NrfA structures, indicating that it could be a consistent point of electron entry to *E. coli* NrfA. However the NrfHA complex is a poor model for the NrfBA complex. Unlike NrfH, NrfB has five bis-histidine co-ordinated hemes and there is no indication that NrfA binding displaces one of these ligands [50]. NrfB is still

proposed to bind NrfA in the electropositive region close to heme 2 and experimental data has shown that the interaction of NrfB with NrfA does not affect the formation of the NrfA dimer, eliminating the dimer interface as an area for NrfB binding [27]. *Shewanella oneidensis* is the only bacteria that has been identified that has a NrfA, but has neither NrfBCD nor NrfH [51]. NrfA in *S. oneidensis* is thought to receive electrons from the NrfH homolog CymA.

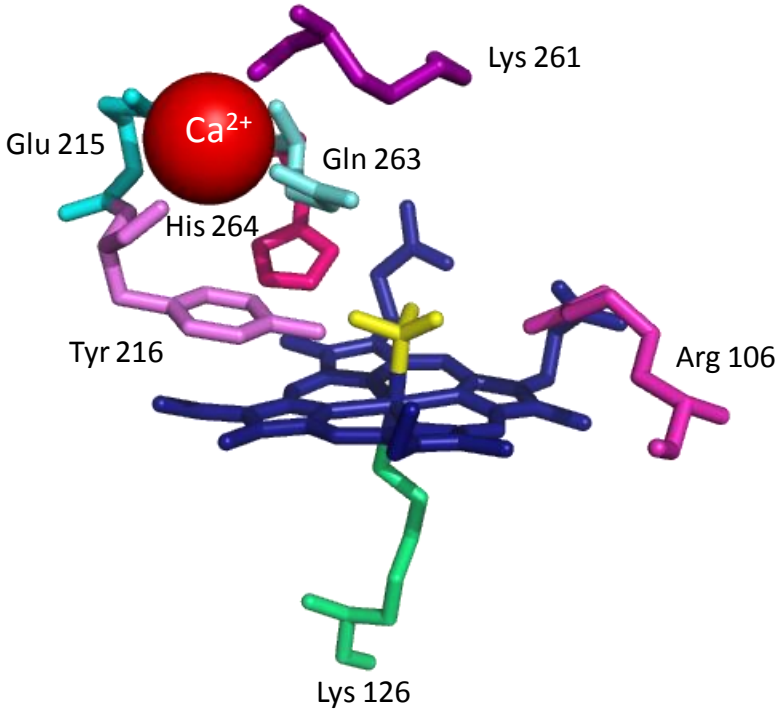

Figure 1.4 NrfA active site with sulphite bound. The residues thought to be involved in catalysis and co-ordinating the calcium ion are indicated, the dark blue is the porphyrin and the yellow sulphite.

1.2.3 NrfA reduction potentials and spectroscopy

The reduction potentials of redox centres within NrfA map an energy pathway through the enzyme and the necessary driving force for catalysis to occur. The Nernst equation (equation 1.5) describes to what extent a sample will be oxidised (Ox) or reduced (Red) based upon the sample potential (E) and the reduction potential (E_m) of the redox couple:

$$E = E_m + \frac{RT}{nF} \ln \frac{[Ox]}{[Red]} \qquad \text{(Equation 1.5)}$$

Here R is the gas constant, T is the temperature in Kelvin, n is the number of electrons involved in oxidation/reduction and F is the Faraday constant. The reduction potential of a sample defines the potential at which it is 50 % oxidised and consequently 50 % reduced. The reduction potentials of the NrfA hemes have been studied using various spectroscopic techniques, including electron paramagnetic resonance (EPR), magnetic circular dichroism (MCD) and electronic absorbance spectroscopy.

The reduction potentials of the NrfA hemes were initially investigated using EPR (figure 1.5). EPR spectroscopy is a useful tool for studying enzymes with transition metal cofactors as this technique is able to study centres with unpaired electrons. When such a centre is placed in a magnetic field it is restricted to one of two orientations or spin directions. Transitions between these two orientations occur at fields that are characteristic of the centre where the electron resides. For NrfA this allows paramagnetic Fe^{3+} hemes to be distinguished by EPR [40]. Thus to use EPR spectroscopy to investigate the reduction potentials of the NrfA hemes, a potentiometric titration was performed as described by Dutton [52]. A sample of NrfA was poised at a defined potential in a carbon pot electrode in order to avoid the use of chemical reductants such as dithionite that might alter the spectroscopic properties of NrfA. A mediator cocktail was used to facilitate electron exchange between the NrfA solution and the carbon pot electrode and once the sample had equilibrated with the applied potential it was frozen and the EPR spectra recorded (figure 1.5). Spectra were recorded for positive potentials where the NrfA sample is fully oxidised and increasingly negative potentials until no more change in the spectra were detected and the sample could be deemed ‘fully reduced.’

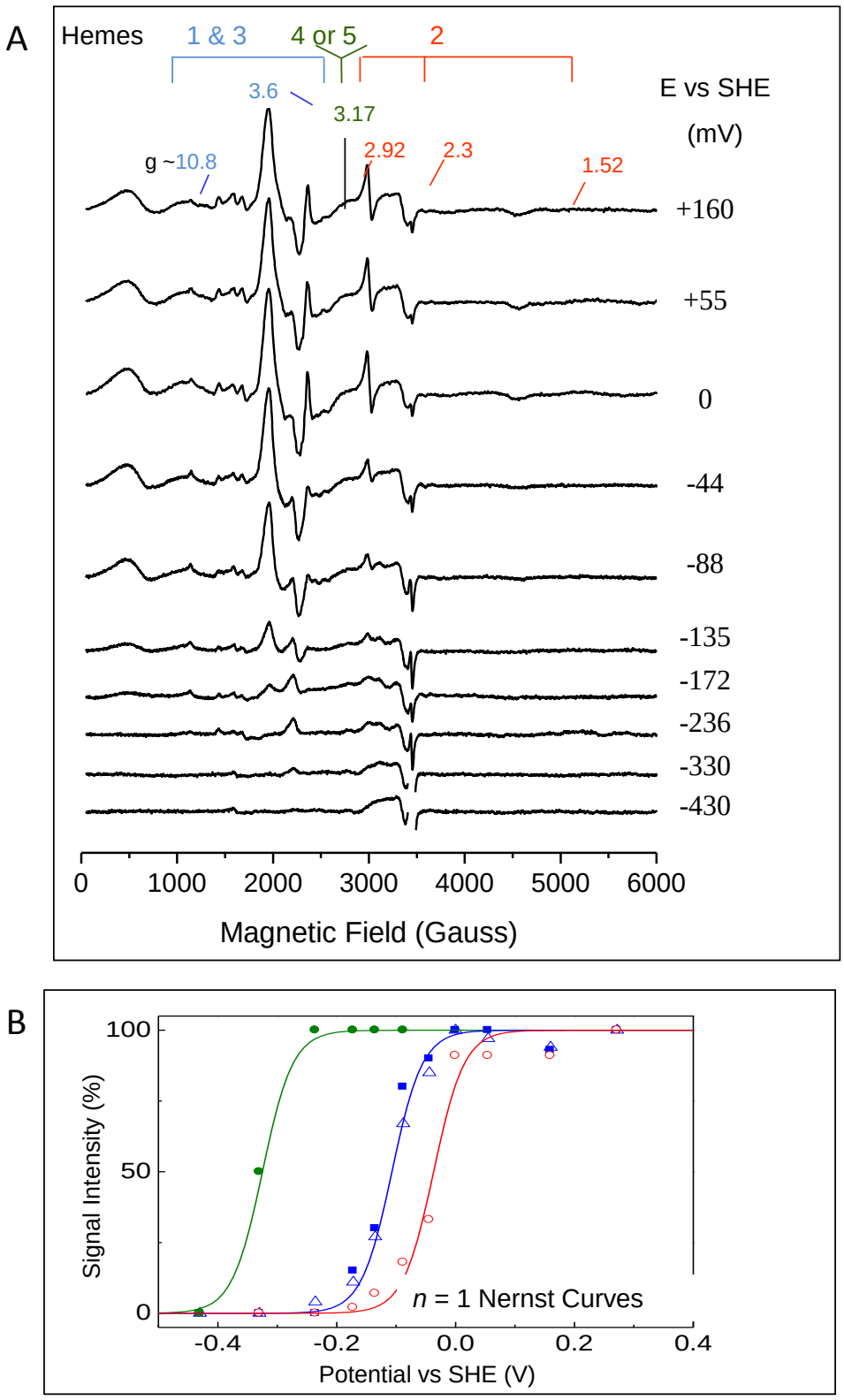

Figure 1.5 EPR monitored potentiometric titration of E. coli NrfA. (A) X-band perpendicular mode EPR spectra of NrfA poised at indicated potentials. The *g* values for the features attributed to hemes 1 and 3 are shown in blue, those attributed to heme 4 or 5 are shown in black and those attributed to heme 2 are shown in red. B. The fit of the reduction of these features to three n = 1 centres with E_m = -37 (red), -107 (blue) and -323 mV (green). Reprinted with permission from [40]. Copyright 2002 American Chemical Society.

The EPR spectra of oxidised NrfA were comprised of a rhombic trio at *g*= 2.92, 2.3 and 1.5 assigned to heme 2, magnetically coupled signals at *g*= 10.8 and 3.5 assigned to hemes 1 and 3 and a 'large g max' feature at g= 3.17 assigned to heme 4 and/or heme 5. A heme pair similar to hemes 1 and 3 in *Nitrosomas europaea* cytochrome *c*554 had a similar EPR signal, indicating conservation of electromagnetic features of these heme pairs [40, 53]. On reduction all hemes are invisible to EPR. Monitoring the change in these three signal sets with changes in the solution potential gave Nernst curves from which reduction potentials were determined as -107 mV for the heme 1 and 3 pair (although this was only a n= 1 electron curve), -37 mV for heme 2 and -323 mV for heme 4 and/or 5 [40]. Therefore the reduction potentials of these hemes were still largely ambiguous.

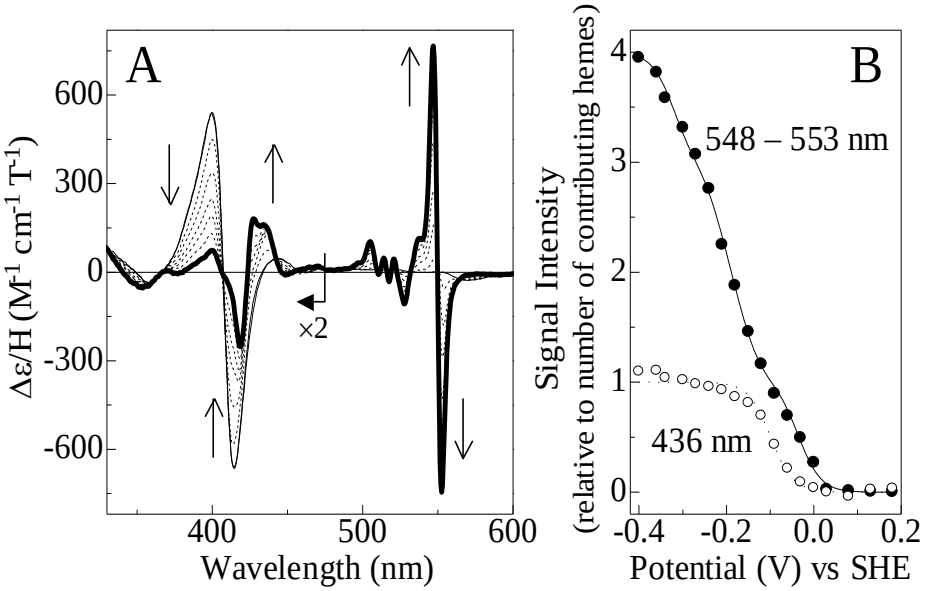

Figure 1.6 MCD monitored potentiometric titration of E. coli NrfA. (A) The ambient temperature MCD spectra of NrfA over a range of potentials where the open headed arrows indicate changes upon sample reduction. (B) The variation of MCD signal intensity with potential at the wavelengths indicated. The solid line indicates the fit to four n=1 Nernstian components with E_ms = -35, -164,- 217 and -326 mV. The broken line indicates the fit to one n=1 Nernstian component with an E_m = -99 mV. Buffer electrolyte was 50 mM Hepes, 100 mM NaCl, pH 7. Reprinted with permission from [54]. Copyright 2008 American Chemical Society.

Recently, mesoporous tin oxide electrodes and electrodically controlled MCD have been utilised to provide a more finite definition of the reduction potentials of *E. coli* NrfA [54]. The ambient temperature MCD monitored potentiometric titration allowed an 'in solution' perspective of the redox properties of NrfA, in contrast to the

frozen solutions used for EPR spectroscopy (figure 1.6). A solution of NrfA containing a mediator cocktail was placed into the MCD cuvette under the potential control of a gold mesh electrode. The low-spin bis-histidine co-ordinated ferrous hemes gave rise to a sharp bisignate feature centred at 550 nm that was fitted to give reduction potentials of -35, -164, -217 and -326 mV. A separate signal contribution at 436 nm originating from the reduced active site high-spin heme, was seen to titrate as an n= 1 centre with a reduction potential of -99 mV [54].

Mesorporous nanocrystalline tin oxide electrodes provide a large semi-transparent surface onto which a large amount of protein can be adsorbed [55]. The transparent nature of the tin oxide electrode allows for the electronic absorption spectrum to be recorded as the sample is oxidised and reduced under the electrodic control of the potentiostat (figure 1.7) [55]. The tin oxide electrodes therefore provide a two-fold tool for determining reduction potentials, by monitoring the change in the electronic absorption spectrum with the changes in potential (dAbs/dE, figure 1.7 red and blue plots) and by fitting the current-voltage profile from cyclic voltammograms arising from the oxidation and reduction of adsorbed proteins (figure 1.7 black plots). For NrfA the low-spin heme reduction potentials could be defined by recording changes in the electronic absorption spectrum at 552 nm, these fit to four n = 1 Nernstian components with reduction potentials of +22, -117, -189 and -275 mV. These reduction potentials can be assigned to the four low-spin hemes within NrfA. The change in absorbance at 442 nm is indicative of the change in the oxidation state of the high-spin active site heme and gave a fit to n =1 Nernstian component with an E_m of -56 mV [54]. Although there is a difference of about 50 mV with respect to the data collected by MCD, the reduction potentials defined by both types of spectroscopy indicate the same relative reduction potentials for high-spin and low-spin hemes thus the same energetic landscape for moving electrons to the active site from heme 2. The reduction of heme 2 occurs most readily from a thermodynamic perspective as it has the most positive potential (this can be assigned by correlation to the EPR spectra). The active site has the next most positive potential and so there is an uphill thermodynamic pathway via heme 3, from the proposed electron entry site at heme 2, to the active site.

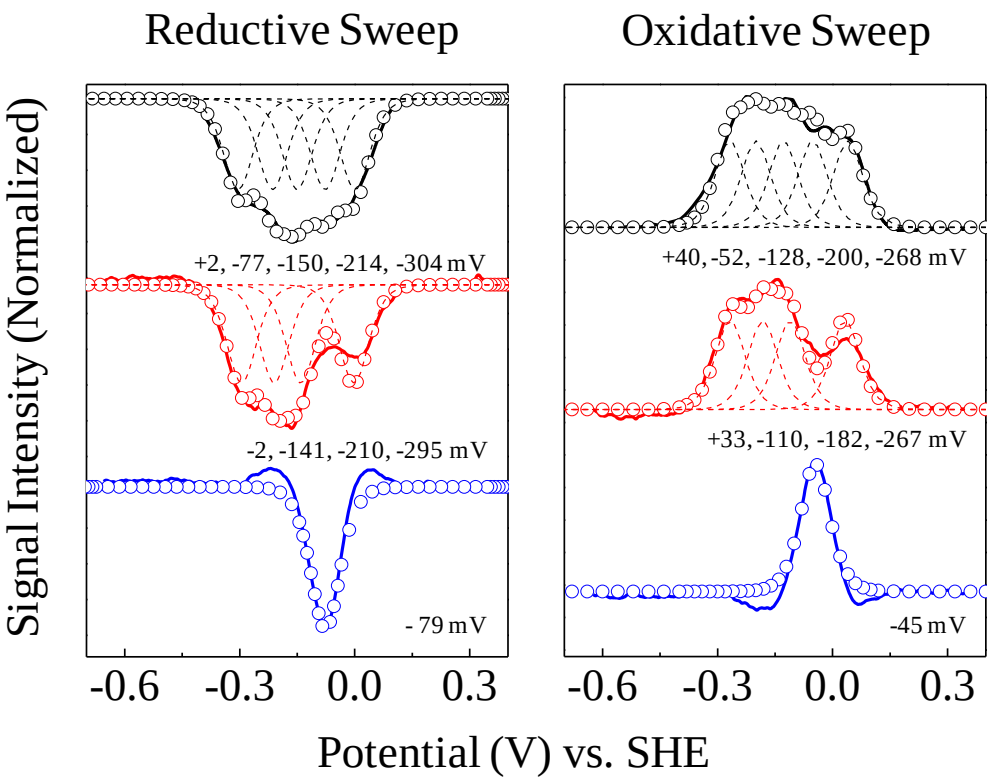

Figure 1.7 Spectroelectrochemical characterisation of NrfA adsorbed on SnO_2. The faradaic current (black), $dA_{552\ nm}$/ dE (red) and $dA_{442\ nm}$/dE (blue)for experimental data (solid lines), fits (circles) and n= 1 Nernstian contributions (broken lines). The reduction potentials for each fitted component are as indicated. Buffer electrolyte 50 mM Hepes, 2 mM $CaCl_2$, pH 7, 24 °C. Scan rate 5 mV s^{-1}. Reprinted with permission from [54]. Copyright 2008 American Chemical Society.

1.2.4 NrfA Nitrite Reductase Activity

1.2.4.1 The mechanism of nitrite reduction

The finding that NrfA reduced nitrite, nitric oxide and hydroxylamine to ammonia suggested that the latter two substrates were intermediates of nitrite reduction. Studies of the oxidised crystal structure of *W.succinogenes* NrfA with nitrite, hydroxylamine and nitric oxide, combined with functional density calculations allowed a mechanism for the reduction of NO_2^- to NH_4^+ to be proposed (figure 1.8)[56]. The first step in the catalytic cycle is the dissociation of the H_2O/OH^- exogenous ligand to

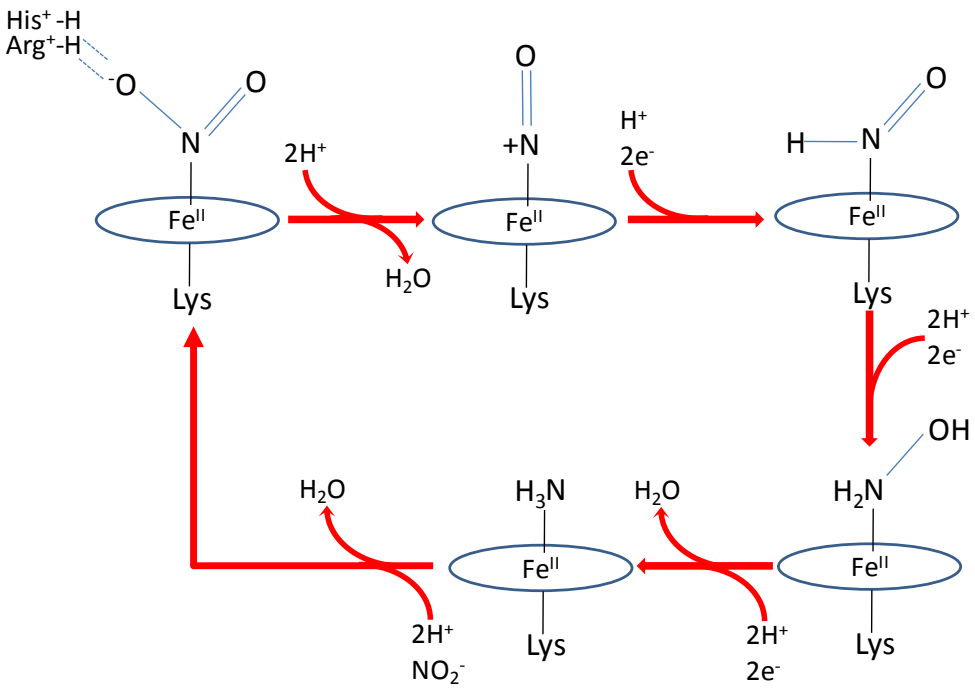

Figure 1.8 The proposed mechanism of nitrite reduction by NrfA [56, 57].

the active site heme iron coupled to reduction of the active site Fe (III). Reduction is thought to occur before water dissociation as the Fe(II)-OH_2 bond is weaker [56]. Nitrite then binds to the active site heme iron by the N atom. The nitrite O atoms are asymmetrically H-bonded to His *264* and Arg *106* (*E. coli* numbering). This asymmetry plus a back-bonding effect between the iron and the nitrogen, causes one N-O bond to become double bonded and the other to be weakened, facilitating its heterolytic cleavage to give rise to a $\{FeNO\}^6$ adduct [48]. A recent computational study has highlighted the importance of this back-bonding effect in the activation of the substrate to the $\{FeNO\}^6$ adduct [48]. This review also highlights the importance of the role of His *264* and Arg *106* as proton donors in the sequential steps where this $\{FeNO\}^6$ adduct then undergoes a rapid two electron reduction, coupled to a proton transfer to become the Fe-HNO species depicted in figure 1.8. The next step involves the alternate addition of two protons and two electrons to give rise to the hydroxylamine-Fe intermediate. Another two electron reduction, coupled to the transfer of two protons is required to convert the hydroxylamine intermediate to ammonia. Ammonia has a weak interaction with the active site heme iron and is

proposed to freely dissociate, allowing the next substrate molecule to bind, continuing the catalytic cycle [56].

1.2.4.2 The activity of NrfA

The rate at which NrfA catalyses the reduction of nitrite, nitric oxide and hydroxylamine to ammonia has been characterised for NrfA from many different bacteria (table 1). The rate of catalysis varies from species to species, despite the highly conserved active site. The rate of catalysis by NrfA has been studied using two principle methods; solution based spectrophotometric activity assays (figure 1.9 A) and protein film voltammetry (PFV) (figure 1.9 B and C). The advantage of solution based assays is that they can be readily performed and require no 'special' equipment not found in most laboratories. Solution based assays usually follow the oxidation of chemically reduced methyl viologen, as methyl viologen transfers electrons to NrfA for catalysis (figure 1.9 A). The rate of the oxidation of methyl viologen directly reflects the rate of catalysis and can be followed by monitoring the decrease in absorbance at 600 nm, since reduced methyl viologen has a blue colour and oxidised methyl viologen is colourless [58]. As the concentration of NrfA used in these assays is known the rate of methyl viologen oxidation can be converted into a turnover number, the substrate concentration present can be varied in order to provide information about the dependence of the rate on substrate concentration and therefore kinetic parameters such as K_M and k_{cat} can be defined. K_M is the Michaelis constant and is equal to the substrate concentration at half the maximum rate and k_{cat} is the rate of catalysis per enzyme. The disadvantage of this technique is that frequently dithionite has been used as a chemical reductant and this has been shown to inhibit NrfA and can cause interference in the experimental data [3]. In addition to this these assays can be technically challenging as cuvettes must remain anaerobic and large amounts of enzyme may be consumed if the enzyme has low activity or by repetition of the assay to achieve greater accuracy.

Enzyme	NO_2^- Reduction			NH_2OH Reduction			NO Reduction		
	k_{cat} (s^{-1})	K_M (μM)	k_{cat}/K_M ($s^{-1}\mu M^{-1}$)	k_{cat} (s^{-1})	K_M (μM)	k_{cat}/K_M ($s^{-1}\mu M^{-1}$)	k_{cat} (s^{-1})	K_M (μM)	k_{cat}/K_M ($s^{-1}\mu M^{-1}$)
NrfA									
-E. coli	770	28	27.50	2380	30000	0.079	840	300	2.80
-W. succinogenes	779	-	-	-	-	-	-	-	-
-S. deleyianum	1102	-	-	514	-	-	3.6	-	-
-D. vulgaris	641	-	-	-	-	-	-	-	-
-D. desulfuricans	490	1140	0.429	-	1135	-	-	-	-
TvNir									
-T. nitratireducens	4082	16700	0.244	45	16400	0.002	-	-	-
OTR									
-S. oneidensis	2.8	5.2	0.530	849	2200	0.385	-	-	-

Table 1.1 CcNiR k_{cat} and K_M values for N-cycle substrates. These values have been determined from PFV and solution assay data [5, 40, 44, 59-64].

In the PFV experiment, NrfA is adsorbed to the surface of a freshly polished graphite electrode and if the NrfA film is electrocatalytically active, the enzyme is directly reduced by the electrode when sufficient potential is applied and NrfA can then reduce nitrite (figure 1.9B)[65]. The flow of electrons to the enzyme in the presence of substrate is measured as the catalytic current and is a measure of the rate of catalysis [66]. The most common PFV experiment is cyclic voltammetry (figure 1.9 C), where the current is measured as the applied potential is swept from positive to negative and back at a set speed, the scan rate. PFV therefore allows the voltage dependence of the rate of enzyme catalysis to be measured. Kinetic parameters such as K_M and i_{max} can be obtained much more rapidly using PFV than solution based assays, where the i_{max} is the maximum catalytic current i.e. the maximum activity of the adsorbed enzyme. Once NrfA is adsorbed to the electrode increasing amounts of substrate can be added to the experimental solution and so the effect of substrate concentration on the rate of catalysis by one sample can be measured rapidly. Films of absorbed enzyme can also be transferred to solutions of different pH and buffer composition to determine their effects on the enzyme activity. The equipment required for these experiments is not available in all laboratories, but it is becoming more widespread.

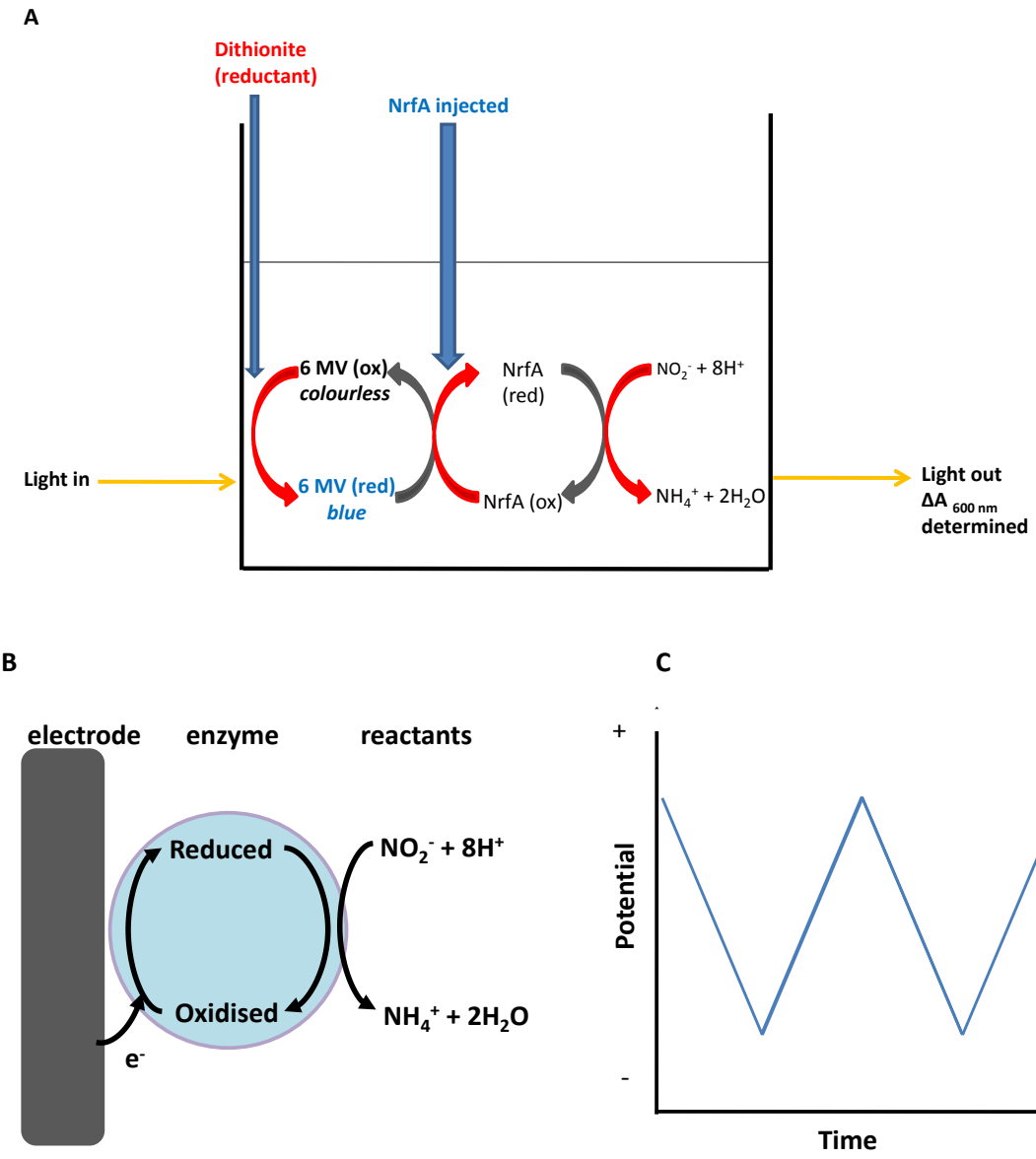

Figure 1.9. Methods used to obtain kinetic information about catalysis by NrfA. (A) Schematic of solution activity assay of NrfA. (B) The PFV experiment. (C) Cyclic voltammetry.

Results of a typical experiment to resolve the Michaelis Menten parameters of NrfA by PFV are shown in figure 1.10. In the absence of substrate cyclic voltammetry PFV of NrfA (figure 1.10 dotted line) gives rise to a featureless response. When nitrite is added (figure 1.10 solid lines), as the potential is swept below 0 mV there is a negative current indicating the onset of catalysis. The negative current arises from the flow of electrons to the active site being used in reductive catalysis. The onset of nitrite reduction occurs at a potential that is significantly more negative than the reduction potential of NO_2^-/NH_4^+ couple (+340 mV at pH 7) and is indicative of the driving force

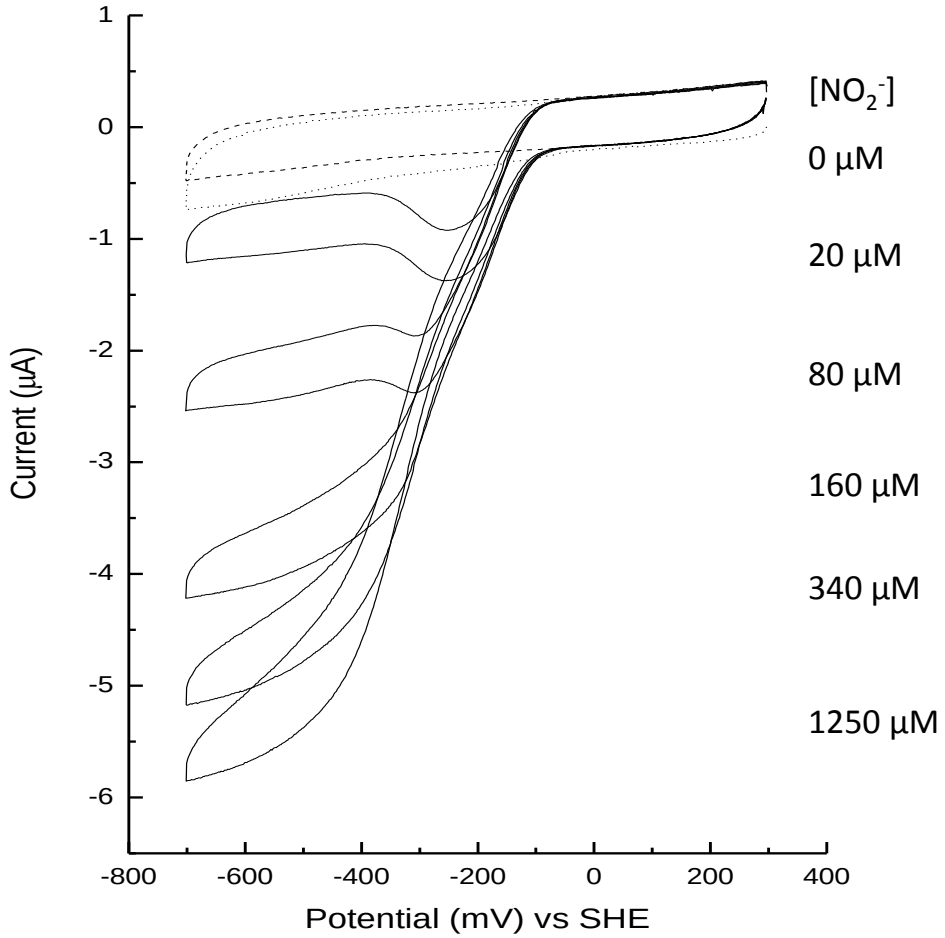

Figure 1.10 .Cyclic protein film voltammetry of E. coli NrfA. The dashed line represents the electrode prior to adsorption of the enzyme; the dotted line represents the NrfA adsorbed to the electrode in the absence of substrate. The consecutive solid voltammograms represent NrfA catalysis at increasing substrate concentrations as indicated. 50 mM Hepes, 2 mM $CaCl_2$, 18 °C, 20 mV s^{-1}, 3000 rpm.

necessary to reduce the redox centres within the enzyme [1]. At low nitrite concentration the potential where there is most increase in current with decrease in potential (i.e. where the cyclic voltammogram has the steepest gradient) is ca. -100 mV, this is in the same region as the reduction potential for the active site heme 1 [1, 54]. At ca. -300 mV in 20 μM NO_2^- (figure 1.10) the catalytic current is attenuated and decreases after a maximum current has been reached ca. -220 mV. Decreasing the potential further beyond this attenuation leads to rates of catalysis that are independent of further decreases in potential (i.e. the current no longer changes as the potential is decreased) [1]. At higher nitrite concentrations the attenuation feature

becomes less apparent and a second sigmoidal increase in the catalytic current is seen at ca. -380 mV. As the nitrite concentration is increased the features of the catalytic wave move to increasingly more negative potentials as the nitrite concentration is increased. It is clear that the rate defining events of catalysis are altered by variation of potential, this is likely to relate to altered oxidation states of redox centres in NrfA [67]. Due to low protein film coverage, non-catalytic signals arising from oxidation and reduction of the NrfA hemes (as described for cyclic voltammetry on tin oxide electrodes) have not been detected on graphite and so the amount of electrocatalytically active enzyme in each experiment cannot be quantified. The solution based assays (figure 1.9) are complementary to PFV experiments and the similarities between the values obtained in solution based experiments help to confirm that NrfA does not become perturbed when adsorbed to the electrode.

1.2.4.3 The role of the active site residues in nitrite reduction

Although there is little sequence similarity between the NrfAs they all share a highly conserved active site (figure 1.4) centred on a lysine co-ordinated heme where the key conserved residues are Y216, H264, R106 and Q263 (*E. coli* numbering). Studies of the mechanism of nitrite reduction have suggested that H264 and R106 have an important role as proton donors to the substrate during catalysis [48, 56]. It has been suggested that this is not the role of Y216, as this is proposed to make an ineffective proton donor [48]. The role of the active site tyrosine in catalysis has been probed using site directed mutagenesis to produce the mutant Y218F in *W. succinogenes* [4]. This mutation resulted in nearly complete loss of nitrite reductase activity. However this was assayed by measuring the formation of ammonia and it is possible that this mutation allows nitrite reduction to an alternate substrate. Y218 does not directly co-ordinate NO_2^- in structures of the wild type NrfA co-crystallised with that substrate, but clearly has an important role in nitrite reduction. Possibilities are that it may stabilize radical intermediates during catalysis or assist in proton coupled electron transfer, but the specific function of this key amino acid in the catalytic machinery remains to be established [48].

The role of glutamine 263 was also investigated using site directed mutagenesis, this time in *E. coli*, where Q263 was converted to E [49]. This mutation resulted in a ten-fold higher K_M for nitrite reduction and lower potentials required for catalysis. The crystal structure shows that Q263 co-ordinates the highly conserved calcium ion found in the active site of all structurally characterised NrfAs, but this is unusual and E is a more common calcium ligand in other enzymes [2]. It was proposed that the glutamine and calcium ion play a role in hydrogen bonding to conserved water molecules in the NrfA active site, increasing the affinity for the substrate and lowering the K_M [49]. The presence of a Q instead of E as a calcium ligand will also make a more positively charged active site, that might be more attractive to the NO_2^- anions.

1.3 The octaheme nitrite reductase, TvNir

1.3.1 Anaerobic respiration in *Thioalkalivibrio nitratireducens*

Another CcNiR is the octaheme nitrite reductase, TvNir, isolated from the periplasm of the extremophile *Thioalkalivibrio nitratireducens*. *T. nitratireducens* is a bacterium from the sediments of Lake Fazda in the Wadi Natrun in Egypt, this lake is a nearly constant pH 10 and has a salt concentration of 4.3 M [68, 69]. *T. nitratireducens* has adapted to these conditions and is a faculatively anaerobic, obligately alkaliphilic and moderately halophilic bacterium [68]. In order to survive its highly alkaline conditions *T. nitratireducens* must make use of specific enzymes and ion exchange channels to ensure that it has an ambient cytoplasmic pH and to generate a proton motive force (pmf) for driving ATP synthesis and anaerobic respiration. It has been frequently noted that the generation of a pmf under alkaline conditions is a great challenge to the survival of alkaliphiles [70]. Several mechanisms to overcome this difficulty have been proposed; an increased number of c subunits in the ATP synthase, use of a Na^+ motive force, optimising the transmembrane difference in electrical potential ($\Delta\psi$) part of the pmf and localisation of proton gradients and ATP synthases [70]. A comprehensive description of alkaliphilic ATP synthesis is yet to be put forward, but it is clear that alkaliphilic bacteria must optimise the use and capture of protons in a highly controlled manner.

T. nitratireducens respires using a NarG like nitrate reductase under anaerobic conditions, coupling the reduction of nitrate to the oxidation of sulphide, thiosulphate, tetrathionate or polysulphide to sulphate (figure 1.11) [68, 71]. The conversion of nitrate to nitrite consumes two electrons and two protons (equation 1.6):

$$2e^- + NO_3^- + 2H^+ \rightarrow NO_2^- + H_2O \qquad \text{(Equation 1.6)}$$

T. nitratireducens cannot survive using nitrite as its terminal electron acceptor during anaerobic respiration and so TvNir cannot have a respiratory role [68]. *T. nitratireducens* is thought to lack the functional genes for an appropriate quinol dehydrogenase/ electron shuttle protein (like NrfH or NrfDCB) to couple nitrite reduction by TvNir to respiration. The reduction of nitrite to ammonia by TvNir is a process that consumes eight protons, which could be considered as an extravagant process in the soda lake environment where protons are limited. Nitrite ammonification may then be important to the survival of *T. nitratireducens*, or it may be that TvNir has an alternate physiologically relevant function. In *E. coli* and many other bacteria that survive under anaerobic conditions, nitrate is used preferentially to nitrite as the terminal electron acceptor during respiration [72]. Nitrate reduction occurs in the cytoplasm and so contributes directly to the generation of a pmf when coupled to the oxidation of formate via the quinol pool [28]. Substrate is oxidised in the periplasm, leading to the reduction of menaquinone (MQ) to menaquinol (MQH_2), the nitrate reductase then oxidises menaquionol on the periplasmic side of the membrane leading to the release of protons coupled to the reduction of nitrate in the cytoplasm and recycling of the quinol pool. The coupling of these two processes produces a proton motive force of $4H^+/2e^-$ [28]. Nitrate reduction by *T. nitratireducens* leads to the accumulation of nitrite [68]. Nitrite is potentially cytotoxic and so TvNir may play a role in the survival of *T. nitratireducens* by nitrite detoxification. Certainly TvNir was expressed when *T. nitratireducens* was grown using thiosulphate as an energy source and nitrate as a terminal electron acceptor. This is converse to the system in *E. coli*, where under conditions of nitrate respiration the expression of the *nrf* genes is repressed [24].

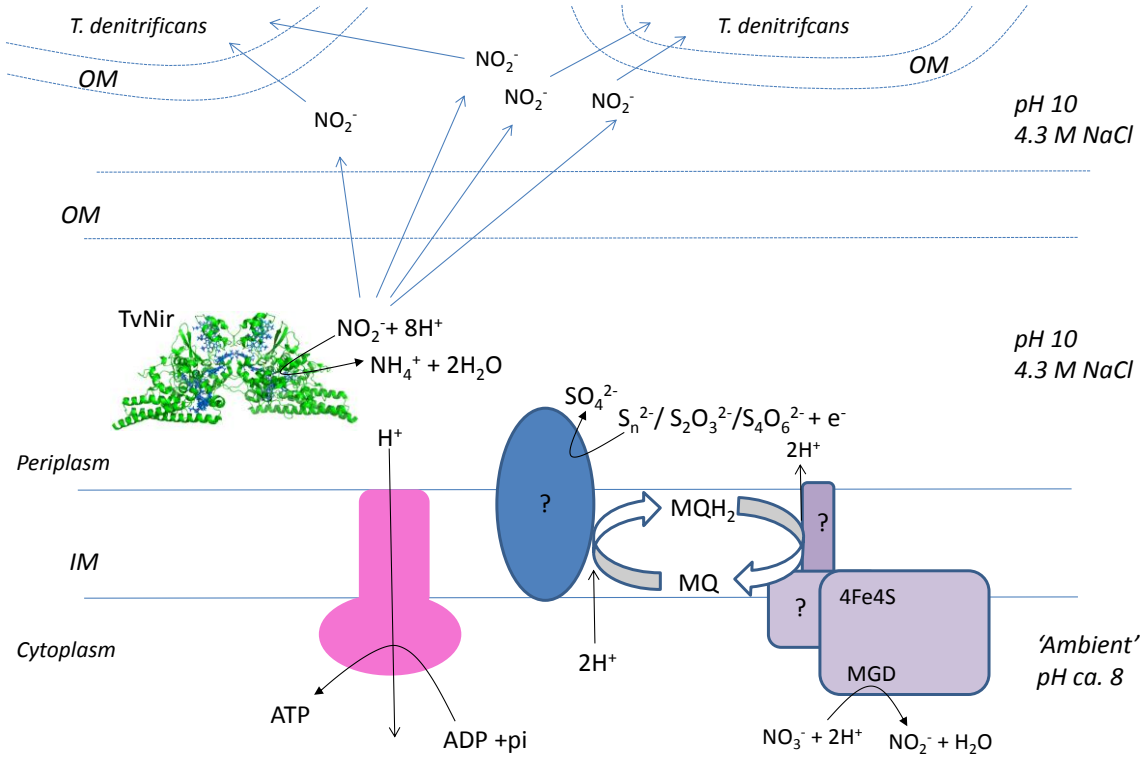

Figure 1.11 A schematic of anaerobic respiration by T. nitratireducens. IM is the inner membrane and OM is the outer membrane. TvNir is shown here as dimer, although it has a hexameric structure, due to the format of the pdb file.

In Lake Fazda *T. nitratireducens* is part of a bacterial consortium [68]. Each bacterium within the consortium grows using different inorganic compounds as terminal electron acceptors. *T. nitratireducens* has shown the capacity to survive independently and to tolerate high concentrations of nitrite, although it survives alongside *T. denitrificans* that is dependent on *T. nitratireducens* to supply NO_2^- for its respiration [68]. It is possible that *T. nitratireducens* expresses TvNir to control the growth of *T. denitrificans* by withholding this substrate by nitrite reduction. Deletion TvNir strains have not yet been produced in order to test this hypothesis.

1.3.2 The structure of TvNir

The structure of TvNir shares all of the key highly conserved traits of the NrfAs described in section 1.2. but there are also some structural features that clearly distinguish TvNir from NrfA (figure 1.12) [73]. TvNir is an octaheme enzyme that consists of two domains; the catalytic domain containing four bis-histidine co-

ordinated *c*-type hemes and a lysine co-ordinated active site *c*-heme, together with the N- terminal domain containing three additional bis-histidine co-ordinated *c*-hemes. The five catalytic domain hemes (number 4-8 figure 1.12 B) align with those within NrfA with an r.m.s.d of 0.5 Å. Hemes 2 and 3 of the N terminal domain show homology to the arrangement in NrfB. NrfB is the protein that serves as the redox partner to NrfA in γ- proteobacteria and it has been proposed that this N-terminal region is the result of fusion with a NrfB like redox partner (figure 1.12) [73].

The active site of TvNir also has marked similarities to that of NrfA. The catalytic triad of His, Arg and Tyr are present in close proximity to the active site heme iron and their arrangement superimposes the NrfA active site (figure 1.13) [73]. The active site calcium ion is also present in TvNir. The only prominent difference in the active site of TvNir compared to the active site of NrfA is that the tyrosine residue is covalently bound to a cysteine residue. This modification causes the pK_a for this tyrosine to drop by ca. 1 unit and also for the position of the tyrosine to shift; shortening H-bond distances of His *361* and Tyr *303* to the nitrite oxygen and compacting the active site [73]. Lowering the pK_a of the side chain of tyrosine means that this will ionise more readily and may be an adaptation for the role of the enzyme in an alkaliphilic bacterium. Cys-tyr covalent linkages have been found in a series of other enzymes such as galactose oxidase, cysteine dioxygenase and the siroheme sulphite reductase NirA [74-76]. When the cys-tyr bond was found in close proximity to the siroheme active site of NirA it was though to be a marker of sulphite reductase activity over nitrite reductase activity [74]. At pH 7 TvNir catalyses the reduction of sulphite at rates that are comparable to the SiR from *D. desulfuricans* [77, 78]. However TvNir lacks sulphite reductase activity at pH > 9 [78].

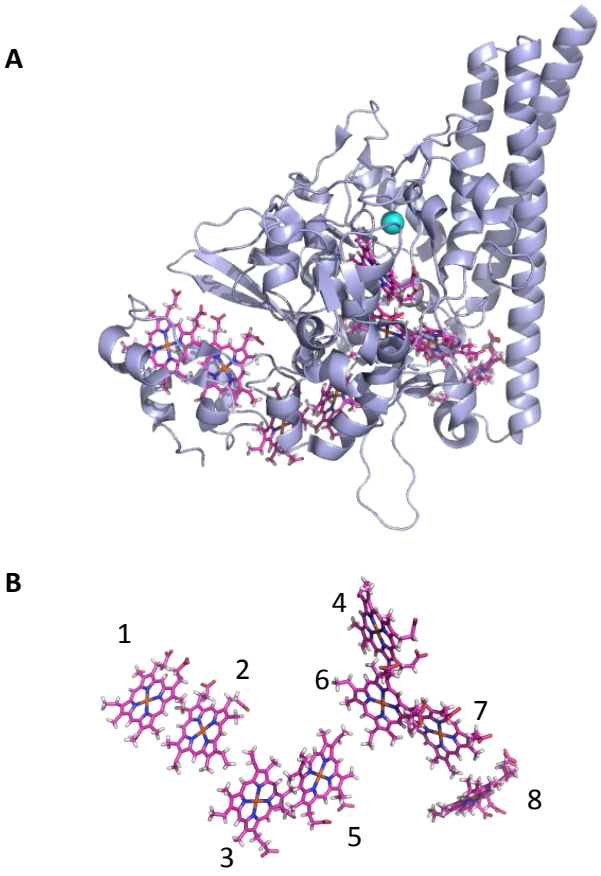

Figure 1.12.The structure of TvNir. (A) Representation of the α helical composition and heme arrangement of a TvNir monomer, where the peptide is shown in light grey, the hemes are shown in magenta and the calcium atom is a light blue sphere. (B). The arrangement and numbering of TvNir hemes within the monomer. This image was produced in PyMol using the pdb file 2OT4.

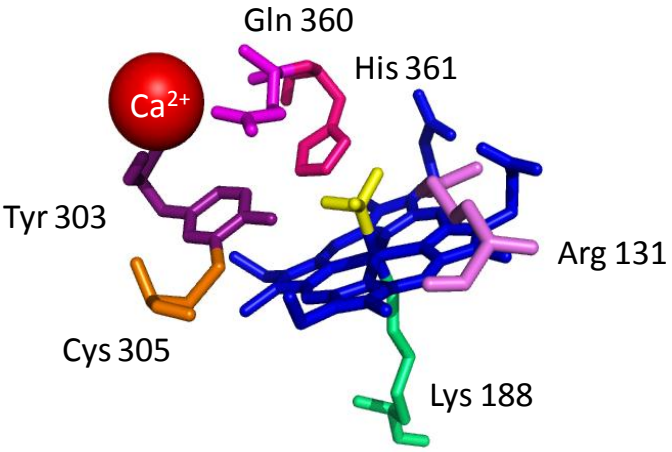

Figure 1.13. The active site of TvNir, sulphite is shown as the exogenous ligand. This image was produced in PyMol from the pdb file (2OT4).

The TvNir catalytic domain has only 18% sequence identity to *W. succinogenes* NrfA and only 6% to *E. coli* NrfA, this is surprising as *E.coli* and *T. nitratireducens* are both γ- proteobacteria. These differences are most apparent in the structure of the product egress channel. The substrate entry channel of TvNir, like that of NrfA, has a positively charged entrance and then further along there is a conserved negatively charged Arg centred within a patch of neutral charge. This Arg is thought to help drive the substrate towards the active site [73]. Like NrfA the product egress channel in TvNir is negatively charged, but unlike within NrfA this channel does not direct the product to the surface of the enzyme but into the central cavity formed by the interaction of TvNir monomers within the TvNir hexamer. The opening of the product egress channel is comprised of a series of positively charged residues (Asp and Glu) and these residues are conserved in similar octaheme enzymes found through Blast searching TvNir [73]. It is possible that these residues provide a marker for differentiation of the preferred product, or more challenging environments. The second calcium ion (non active site) found in TvNir superimposes with the position of the second calcium site in NrfA [73]. In most NrfAs this calcium atom has an incomplete co-ordination sphere, the exception to this is *D. desulfuricans* NrfA, as discussed in section 1.2 [41]. In TvNir this second calcium ion has a complete octahedral co-ordination sphere comprised of propionates from hemes six and seven (figure 1.12) and a proline residue, the rest of its co-ordination sphere is comprised of water molecules. What is interesting about this calcium residue is that it appears to block the path of product egress, not unlike role of this second calcium atom in *D. desulfuricans* [41, 73]. It was suggested for *D. desulfuricans* NrfA that this implied nitrite was not the preferred substrate of enzyme and that instead *D. desulfuricans* NrfA was optimised for sulphite reduction [2]. That is not the case for TvNir as was explained above, but the natural substrate for TvNir remains to be established.

1.3.3 TvNir activity

The nitrite reductase activity of TvNir has been assayed by monitoring the oxidation of dithionite reduced methyl viologen as described in section 1.2.4.3 and also by stopping the reaction at a time point and quantifying the amount of nitrite that has not been reduced. It was found that TvNir had a K_M for nitrite reduction of 16.7 ± 4

mM and a k_{cat} of 4082 s^{-1} at pH 7 (table 1) [63]. Considering the homology of this enzyme to NrfA these values are surprising, the K_M is extremely high and the turnover number is also high compared to NrfA. Interestingly this provides a k_{cat}/K_M around the same order of magnitude as *D. desulfuricans* NrfA [61].

TvNir also catalyses the reduction of hydroxylamine to ammonia and has a K_M for hydroxylamine of 16.4 mM, slightly less than that for nitrite reduction, but with a turnover number of 45 s^{-1} which is extremely low considering that hydroxylamine may be an intermediate in the reduction of nitrite to ammonia and the turnover number for nitrite reduction by TvNir is so high [63]. TvNir has also been shown to catalyse the reduction of sulphite to sulphide, however this process did not occur at pH ≥ 9 and whilst sulphite reduction was detected at 6 mM sulphite, increasing the concentration of sulphite inhibited catalysis [78].

1.4 CcNiRs: From Five Hemes to Eight

Analysis of the structurally characterised NrfA enzymes (section 1.2.) and TvNir (section 1.3) revealed many highly conserved structural features; the active site, substrate entry channel, product egress channel and heme arrangement. Discovery of genes predicted to encode for homologous proteins in a number of microbes, in addition to the purification of proteins that share some of the structural features of NrfA has led to much comparative analysis and speculation of an evolutionary link between them. The purified enzymes that have been discussed in this context are the *S. oneidensis* octaheme tetrathionite reductase (OTR), *N. europaea* hydroxylamine oxidoreductase (HAO) and *T. nitratireducens* TvNir (figure 1.14). The structures of these enzymes, their amino acid sequences and their kinetic properties have all been rigorously compared [2, 22, 45, 79].

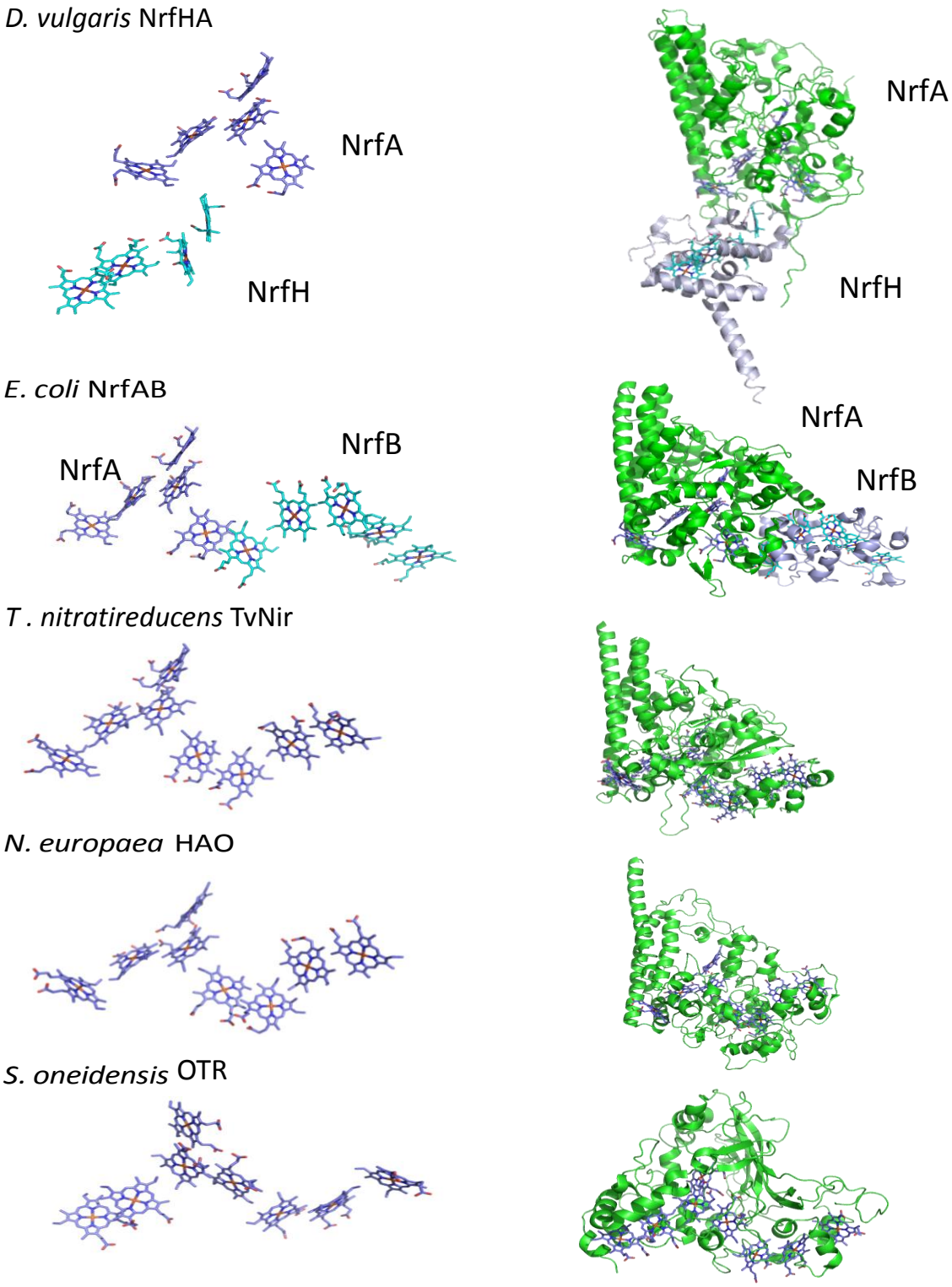

Figure 1.14. The heme arrangement and structures of multi-heme cytochromes proposed to be evolutionary related. Pictures were rendered in Pymol from Pdb files 2J7A (NrfHA), 2RDZ (NrfA), 2OZY (NrfB), 2OT4 (TvNir), 1FGJ (HAO) and 1SP3 (OTR).

The arrangement of hemes amongst these enzymes is very similar. The hemes of *S. oneidensis* OTR align with the NrfA hemes with an r.m.s.d of 0.4 Å, whereas the r.m.s.d between the hemes of OTR with TvNir and HAO are 2.4 Å and 2.3 Å respectively. This could reflect the fact that OTR is proposed to have evolved divergently to the other octaheme enzymes [45]. For all the enzymes the three hemes in proximity to the active site (labelled number 1, 3 and 4 in the NrfA, figure 1.3) are arranged with parallel heme planes [80]. Divergence between the heme arrangements of the enzymes occurs in the remaining two (for NrfA) and five hemes (HAO, OTR and TvNir). All these enzymes contain classical parallel stacking and diheme elbow motifs, where the heme pairs are arranged either parallel or perpendicular to one another [80]. Interestingly the heme arrangements of HAO and TvNir closely align with those of NrfA and the proposed arrangement of the first two hemes of NrfB too (figure 1.14) [73]. For both the NrfA and TvNir active site hemes are co-ordinated by a lysine ligand that is given by a CXXCK motif in the amino acid sequence. A crystal structure has shown that the proximal ligand to the active site heme in OTR is a lysine residue, but it is given by CXXCH in the amino acid sequence that usually denotes histidine ligation and so the lysine is drawn from elsewhere in the protein sequence [64, 81].

There are also differences in the reactions catalysed by NrfA, TvNir, OTR and HAO and also the rates at which catalysis occurs. OTR reduces tetrathionite, not sulphite as its sulphur oxide containing substrate [64]. The physiological role of HAO is to catalyse the oxidation of hydroxylamine to nitrite, whilst the other enzymes have only been shown to perform reductive catalysis [1, 61, 63, 64, 82, 83]. However when reduced by methyl viologen (E_m= -450 mV) HAO has also been shown to catalyse the reduction of nitrite to ammonia [84].

Alignment of the available protein sequences with homology to NrfA namely, HAO, OTR, TvNir and predicted gene products from other microbes produced a phylogenetic tree providing further insight into how closely related these different proteins may be [45]. The enzymes formed two distinct evolutionary groups; the pentaheme nitrite reductases and the octaheme cytochromes. The octaheme nitrite reductase, TvNir, is proposed to provide the evolutionary link between the two groups of enzymes. Sequence comparison found that HAO was the most evolutionary distant

of these enzymes from NrfA [45]. Enzymes from different subgroups of bacteria were interspersed amongst the phylogenetic tree, indicating that evolution of these multiheme cytochromes did not progress in a solitary bacterial subgroup [45]. On the basis of the phylogenetic analysis, it was postulated that NrfA was the evolutionary precursor for the octaheme enzymes that evolved to differentiate and become gradually more distinct. The tertiary structures of these related enzymes were then compared in order to test this hypothesis.

It was also proposed that *S. oneidensis* OTR evolved as an octaheme enzyme from the pentaheme NrfA, divergently to the evolution of TvNir and HAO [45]. This correlates to some notable differences in the sequence and the tertiary structure of OTR compared to the other enzymes (figure 1.14)[45]. Although OTR is a largely α-helical enzyme, it has some β-sheet structure and the arrangement of peptide around the heme core is different to the other enzymes [64].

The tertiary structure of HAO appears to be very similar to NrfA and TvNir, with respect to the heme arrangement and α- helical arrangement of peptide around the hemes (figure 1.11). The greatest distinction between HAO and the other enzymes is in their active sites. The active site of HAO has a P_{460} heme that is cross-linked to a tyrosine within another subunit of the HAO homotrimer [85, 86]. P_{460} hemes were once only identified in *Nitrosomonas europaea* (from which HAO was isolated) and *Methylococcus capsulatus,* isolated from sewage treatment works, but more nitrifying bacteria are being discovered that also share P_{460} hemes [85, 87, 88]. The inter-subunit cross-link to the P_{460} heme is thought to confer the ability of this heme to oxidise its substrate [85]. It has been shown that although HAO has evolved this different active site capable of oxidising hydroxylamine to nitrite, HAO can catalyse the reduction of nitrite and hydroxylamine to ammonia and so nitrite reductase activity is retained even though HAO is no longer optimised for this role [84]. It has been postulated by some that the selective pressure for the evolution of HAO was applied by 'leaky' early nitrite ammonifying enzymes, perhaps the remnant nitrite reductase activity of HAO can be considered as evidence of this evolution [20].

Recently this research has been extended analysing the evolutionary relationship of all multi-heme cytochromes. Structure, function and sequence were all compared to give rise to distinct clusters of enzymes [79]. Despite the extended N terminal domain, TvNir was fitted into the NrfA cluster of enzymes and OTR and HAO were located in their own unique clusters. It was discussed that the enzyme clusters that were more widespread amongst different groups of bacteria were likely to be the earliest evolved, particularly those that were present in both bacteria and archaea. HAO and OTR were both found to be present across a wider variety of bacterial subgroups (OTR was the most widespread) than NrfA and these clusters were both found in archaea, whereas the NrfAs were not [79]. This is highly suggestive that perhaps NrfA was not the earliest ancestor, but the product of evolution that has evolved a smaller and less energetically costly enzyme to perform nitrite ammonification and to efficiently catalyse a number of other reactions. The earlier research argues that HAO, OTR and TvNir lose their specificity for nitrite reduction as they evolved, but perhaps it makes more sense if it is considered that the most efficient nitrite ammonifiers are the most highly evolved enzymes.

1.5 Aims of thesis

The aim of this thesis is to investigate the electron transfer pathways and the kinetics of nitrite ammonification in selected CcNiRs. A route to better understanding of nitrite ammonification is studying and establishing the kinetics of nitrite reduction by the novel octaheme nitrite reductase TvNir and comparing these to those of the well characterised pentaheme nitrite reductase, NrfA (*E.coli* representative). It is hoped that this will provide insight into the importance of the conserved structural features between the NrfA nitrite reductase and TvNir and also perhaps to highlight specific roles of the structural differences between these two enzymes. A comparative study of these two enzymes aimed to increase the understanding of precisely what is required for catalysis of nitrite ammonification and help to determine more of the mechanistic features of these enzymes and perhaps work towards an understanding of how different enzymes might be optimised to catalyse the same reaction under different conditions.

NrfA forms a tight complex with its redox partner, NrfB and the heme arrangement of the decaheme NrfAB complex is proposed to be homologous to seven of the eight hemes within TvNir (figure 1.14) [27, 73]. It has been proposed that the extended N terminal domain of TvNir could have occurred due to the merging of the gene for a 'NrfB-like' redox partner [73]. This thesis also aimed to study the redox properties of NrfB using PFV, in order to deduce more information about how it is poised for its role in electron transfer to NrfA. Once PFV of NrfB was established the aim was then to use PFV to study electron transfer through the NrfAB complex, to determine whether the formation of the NrfAB complex caused a change in the reduction potentials of these enzymes and to compare the catalysis of nitrite reduction by the decaheme NrfAB complex to both the pentaheme NrfA and the octaheme TvNir using PFV. PFV was selected as a tool for these studies as it had already been used successfully to characterise the kinetics and thermodynamics of NrfA, making results obtained in this thesis directly comparable to PFV of NrfA. PFV can also be used to investigate the reduction potentials, catalytic capabilities and electron transfer kinetics of adsorbed redox proteins, making it the ideal technique for this study.

Chapter Two

Methods

Chapter 2. Methods

2.1 Reagent preparation

For the preparation of all buffer solutions Milli Q water was used that had a resistivity of > 18 MΩ cm and the chemicals used were of Analar quality. The pH of buffer solutions were adjusted (when required) using additions of 5 M NaOH or 5M HCl. The pH of the solution was measured using a Radiometer Copenhagen PHM 82 pH meter, with a Russell pH electrode and was calibrated using standards of pH 4.0, 7.0 or 9.2 as appropriate prior to measurements.

The buffer electrolyte used depended upon the type of experiment performed and the enzyme being studied. Experiments studying *E. coli* NrfA and NrfB were primarily performed using 50 mM Hepes, 2 mM $CaCl_2$, pH 7.0. For experiments over a range of pH a multi-component buffer (HTMA) containing 20 mM each of Hepes, Tap, Mes and Acetic Acid, and 2 mM $CaCl_2$ was used. For experiments with TvNir the standard buffer was 50 mM Hepes, 0.1 M NaCl, pH 7.0. For experiments studying TvNir over a range of pH, a buffer of 20 mM HTMA, 0.1 M NaCl was used (pH 4.0 to 9.0), for experiments above pH 9.0 this buffer became 20 mM HCMA, 0.1 M NaCl, where CHES replaced Taps in the HTMA buffer mixture. For studies of TvNir, experiments were also performed in 20 mM HTMA, 4.3 M NaCl.

A fresh stock of $NaNO_2$ or KNO_2 as required was prepared each day (typically 500 mM) and diluted as appropriate using the experimental buffer electrolyte where one pH solution was being used or Milli Q water when the nitrite was being used for experiments at a range of different pH. $NaNO_2$ was used unless otherwise stated. The pH of experimental solutions after the addition of nitrite was checked using a Radiometer Copenhagen PHM 82 pH meter, with a Russell pH electrode, calibrated using standards of pH 4.0, 7.0 or 9.2 as appropriate, prior to measurement.

2.2 Protein Samples

Samples of *E. coli* NrfA and NrfB stored in 50 mM Hepes, 2 mM $CaCl_2$, pH 7.0 (NrfA) or 50 mM Hepes, 100 mM NaCl, pH 7.0 (NrfB) and were kindly provided by Dr. Tom Clarke and Dr. Gemma Kemp (the School of Biological Sciences and School of

Chemistry, UEA). The samples were stored frozen as aliquots in liquid nitrogen. The concentration of NrfA and NrfB were determined from electronic absorbance spectra recorded using a Jasco V500 Spectrophotometer, using a baseline of buffer vs. air. The Beer-Lambert Law was used to determine the concentration of protein using an ε_{409nm} for NrfA of 497 650 M^{-1} cm^{-1}, for NrfB an ε_{408nm} of 613 686 $M^{-1}cm^{-1}$ (see below) [40].

TvNir samples were kindly provided by Dr. Tamara Tikhonova (A. N. Bach Institute of Biochemistry, Russian Academy of Sciences). Stock samples were stored in 0.1 M potassium phosphate buffer, pH 7.0. Samples used for electrochemistry were stored in 50 mM Hepes, 0.1 M NaCl at pH 7.0. The concentration of TvNir was determined from the electronic absorption spectra and using the Beer-Lambert law and an $\varepsilon_{408\ nm}$ of 884,000 $M^{-1}cm^{-1}$ (determined by Dr. Sophie Marritt, School of Chemistry, UEA).

Cytochrome *c* (horse heart) and Myoglobin were purchased from Sigma Aldrich and used without further purification. Cytochrome *c'* samples were kindly provided by Dr. Simon George (University of California Berkeley).

2.3 Electrophoresis

Sodium dodecyl sulphate polyacrylamide gel electrophoresis (SDS PAGE) analysis was used to check the purity of NrfA and NrfB samples (figure 2.1). SDS PAGE gels were prepared according the method described by Laemmlli for a discontinuous buffer system comprised of a stacking (Tris-HCl, pH 6.8) and resolution gel (Tris-HCl pH 8.8) that were 5% and 15% (v/v) acrylamide respectively [89]. Approximately 10 µg of protein was added to each lane in a loading solution of 100 mM Tris-HCl, pH 6.8, 200 mM dithiothreitol (DTT), 4% SDS (w/v), 1 grain bromophenol blue and 15% glycerol (v/v). The running buffer was 25 mM Tris, 200 mM glycine, pH 8.3. Electrophoresis was performed at room temperature using Hoefer vertical slab gel apparatus (Hoefer Scientific Instruments, USA) where a potential of 200 V was applied for approximately 1 hour. Gels were stained to identify protein bands by submersion over night with rocking in a solution of 0.1 % Coomassie Brilliant Blue (w/v), 40 % methanol (v/v) and 10 % acetic acid (v/v). A de-staining solution was then applied to wash away non

bound Coomassie Blue and the gel rocked for another 2 hours. All Blue Precision Protein Standard (BioRad) was used as a molecular weight marker according to the manufacturer's instructions.

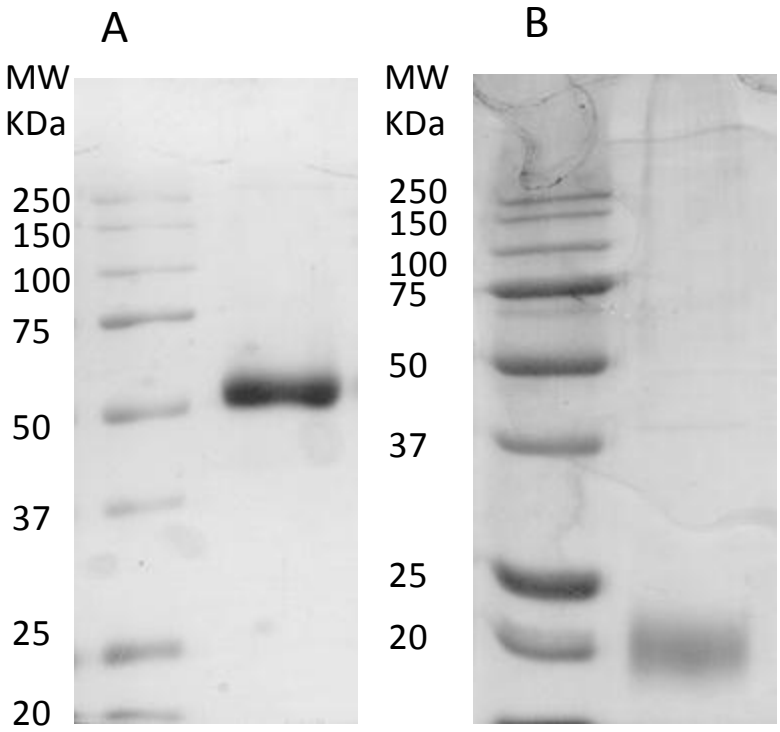

Figure 2.1 Electrophoretic analysis of protein purity. SDS PAGE gel of (A) NrfA and (B) NrfB where the left hand lane is the protein standard ladder as indicated and the right hand lane is the sample. Both gels were stained using Coomassie blue.

2.4 Pyridine Hemochrome Analysis to Define the Extinction Coefficient of NrfB

To determine the extinction coefficient of NrfB the heme content was defined by the pyridine hemochrome method, using cytochrome *c* as a standard [90]. The absorbance spectrum of ferricyanide oxidised cytochrome *c* (horse heart) was measured in 50 mM Hepes, 2 mM $CaCl_2$, pH 7.0 and the concentration of the sample determined using $\varepsilon_{410\ nm}$ = 106, 000 $M^{-1}cm^{-1}$ [91]. A 2.5 ml sample of 5 µM cytochrome *c* was prepared in 50 mM Hepes, 2 mM $CaCl_2$ to which 0.68 ml of pyridine (to make 0.5 M), 0.5 ml of 0.6 M NaOH (to make 75 mM) and 0.32 ml of MilliQ water were added. This solution was split between two cuvettes (1.7 ml volume each). The pyridine treated cytochrome *c* in one cuvette was oxidised by addition of 3.2 mM ferricyanide.

The pyridine treated cytochrome *c* in the other cuvette was reduced with 7.5 mM dithionite. The electronic absorption spectra of each of these solutions were measured and the oxidised spectrum was subtracted from the reduced spectrum and the difference in absorbance at 550 nm and the absorbance at 535 nm (ΔA) was extracted (figure 2.2). The concentration of the sample of cytochrome *c* has already been determined and so, using the Beer Lambert law (equation 2.1) with pathlength of the cuvette (l), an extinction coefficient (Δε) for the difference in absorbance between 535 and 550 nm for one pyridine treated *c*-type heme was defined (figure 2.2 A).

$$\Delta\varepsilon = \frac{\Delta A}{[\text{cyt}c]\times l} \qquad \text{(Equation 2.1)}$$

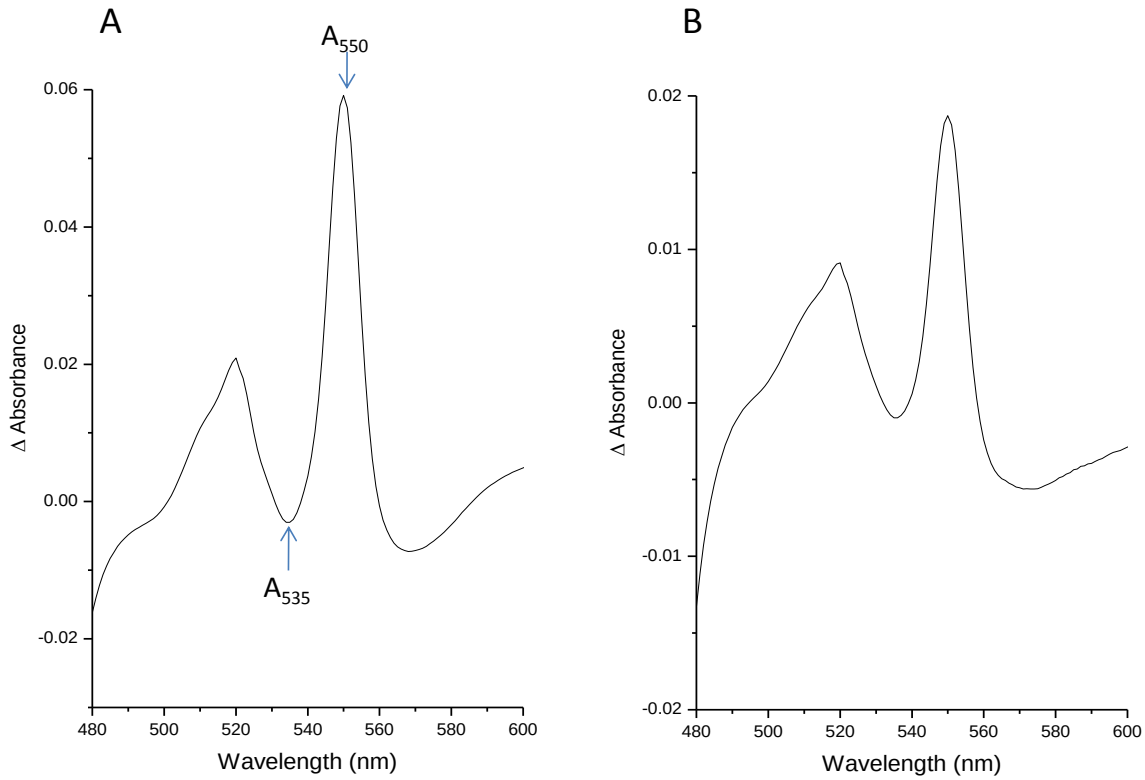

Figure 2.2 The reduced minus oxidised difference spectrum of pyridine bound (A). cytochrome c and (B) NrfB. See text for details.

To determine an extinction coefficient for NrfB the oxidised spectrum of the NrfB sample was first recorded. The sample of NrfB was then treated as described for cytochrome *c* above; 2.5 ml of the NrfB sample was treated with 2.6 mM pyridine and 75 mM NaOH and split between two cuvettes, where one cuvette was then oxidised with 3.2 mM ferricyanide, the other was reduced by 7.5 mM dithionite and the

electronic absorbance spectra of the solutions in each cuvette were recorded. The spectrum of the oxidised pyridine treated NrfB was subtracted from the spectrum of reduced pyridine treated NrfB and as with cytochrome *c*, the difference between the absorbance at 550 nm and the absorbance at 535 nm was calculated (figure 2.2 B). The extinction coefficient for the difference in absorbance between 550 and 535 nm was earlier defined from the experiment with cytochrome *c* for one *c*-type heme under these experimental conditions and this was used to determine the concentration of the NrfB sample in this experiment. Using equation 2.2, where the number 5 in the equation accounts for the presence of five *c*-type hemes in NrfB.

$$5[\text{NrfB}] = \frac{\Delta A}{\Delta \varepsilon \times l} \qquad \text{(Equation 2.2)}$$

$$\varepsilon_{408\ nm} = \frac{A_{408\ nm}}{[\text{NrfB}] \times l} \qquad \text{(Equation 2.3)}$$

From equation 2.3 and the absorbance of the oxidised NrfB at 408 nm, the extinction coefficient of the oxidised NrfB was calculated to be 613, 686 $M^{-1}cm^{-1}$.

2.5 Spectrophotometric Assays of NO_2^- Reductase Activity

Nitrite reductase activities were measured spectrophotometrically by following the oxidation of reduced methyl viologen (figure 1.9). Reduced methyl viologen has a blue colour and an extinction coefficient at 600 nm of 13,700 $M^{-1}cm^{-1}$, oxidised methyl viologen is colourless. The rate that methyl viologen is oxidised in order to supply electrons to the nitrite reductase for catalysis of nitrite can be monitored spectrophotometrically by the decrease in absorbance of methyl viologen at 600 nm (figure 1.9) [92].

Separate stock solutions of 100 mM methyl viologen, 10 mM sodium dithionite and 50 mM sodium nitrite in anaerobic 50 mM Hepes, 2 mM $CaCl_2$, pH 7 were prepared in an anaerobic glovebox. In the anaerobic glovebox cuvettes were then prepared containing 3 mL of 0.1 mM methyl viologen and 225 µM NO_2^- in 50 mM Hepes, 2mM $CaCl_2$, pH 7. Methyl viologen was reduced to give an absorbance at 600 nm of ca. 1.4 by the addition of 75 µM sodium dithionite. Cuvettes were stoppered

with suba-seals to maintain anaerobic conditions and allow injection of the nitrite reductase when appropriate. The absorbance at 600 nm was measured vs. time until no change in absorbance was detectable (figure 2.3). The cuvette was taken out and the chemicals re-mixed by inversion and the absorbance measured again to ensure that the reagents were properly mixed and that any un-dissolved oxygen was mixed into the solution before the enzyme was added and so would not affect the results. Once a steady reading for absorbance was obtained the reaction was initiated by addition of 2 µl of 3 µM nitrite reductase and mixed by inversion.

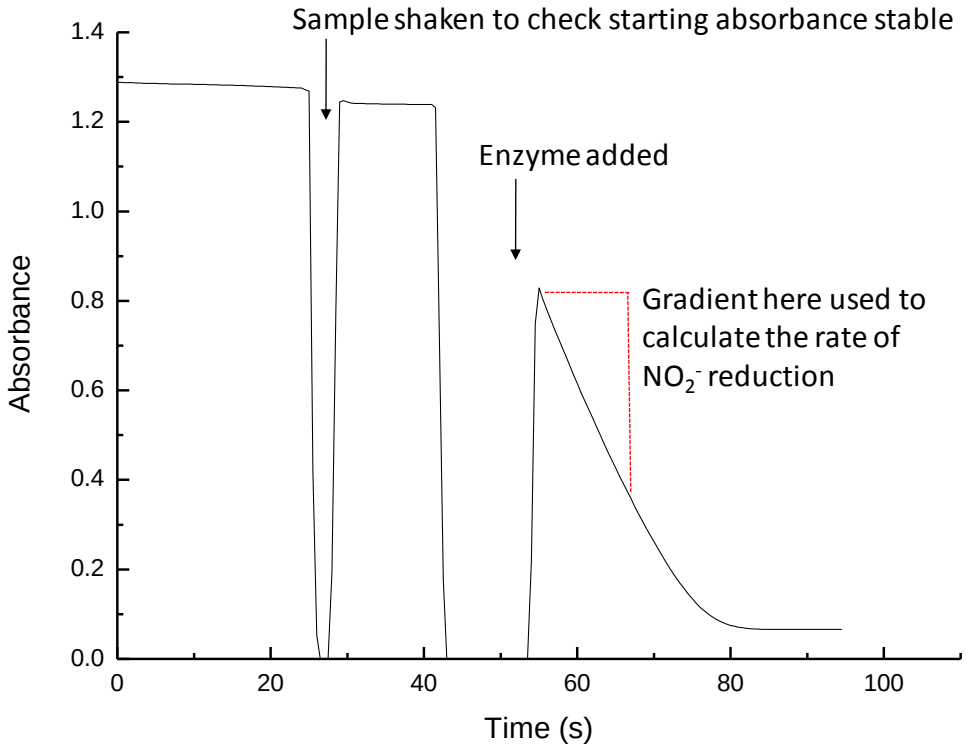

Figure 2.3 Representative result of a methyl viologen assay showing the change in absorbance at 600 nm with time.

The rate of nitrite reductase activity can be calculated from the gradient of the slope that is indicative of the initial reaction rate, before the concentration of substrate electrons becomes limiting. Using the extinction coefficient of methyl viologen at 600 nm and the Beer Lambert law, the change in absorbance per second can be converted to the change in the concentration of methyl viologen per second and as the volume of the solution is known this can be converted to the change in the

number of moles of methyl viologen per second. Six methyl viologens will be oxidised for each reduction of nitrite to ammonia, therefore the number of nitrites reduced per second will be one sixth of the methyl viologen oxidised per second. This gives the turnover number of NO_2^- reduced s^{-1}.

2.6 Spectropotentiometry

As discussed in chapter 1 spectroscopy of redox proteins is frequently used to determine whether a sample is oxidised or reduced as the spectroscopic properties of redox centres change with changes to their oxidation state. Depending on the redox centre, different types of spectroscopy will be appropriate such as electronic absorbance (UV-vis), EPR or MCD. Spectropotentiometry is where the potential of the sample being studied is poised and the spectra recorded, allowing for the extent of oxidation/reduction of the sample at that set potential to be determined. This allows thermodynamic information about the redox protein to be defined.

2.6.1 Theory of spectropotentiometry

For the redox reaction (Ox + ne- $\leftrightarrow$ Red) the Nernst equation (equation 1.5) relates the concentrations of oxidised (Ox) and reduced (Red) species to their reduction potential and the sample potential. The Nernst equation can be rearranged such that:

$$\frac{[Ox]}{[Red]} = \exp\left(\frac{nF}{RT}(E - E_m)\right) = \theta \qquad \text{(Equation 2.5)}$$

The sum of the oxidised and reduced forms is 1 and so this can be related to the [Red]:

$$[Red] = \frac{1}{(\theta + 1)} \qquad \text{(Equation 2.6)}$$

And consequently:

$$[\mathrm{Ox}] = \left(\frac{\theta}{(\theta + 1)} \right) \qquad \text{(Equation 2.7)}$$

The variation of [Ox] and [Red] as predicted by equation 2.5 for E_m = 0 V and n =1 is illustrated by the darker lines in figure 2.4. At potentials well above E_m, essentially all of the molecules are oxidised. As the potential is lowered toward E_m, conversion of Ox to Red is observed and at potentials well below E_m, essentially all of the molecules are reduced. At the reduction potential [Ox] = [Red] as expected. When E_m = -100 mV the potential dependence of [Ox] and [Red] changes in the predicted manner (figure 2.4, light lines). The electron stoichiometry of a redox couple is reflected in the steepness of plots of concentration versus potential. The higher the electron stoichiometry the steeper the transition from oxidised to reduced (or vice versa) since the transition occurs over a narrower potential range, Figure 2.5.

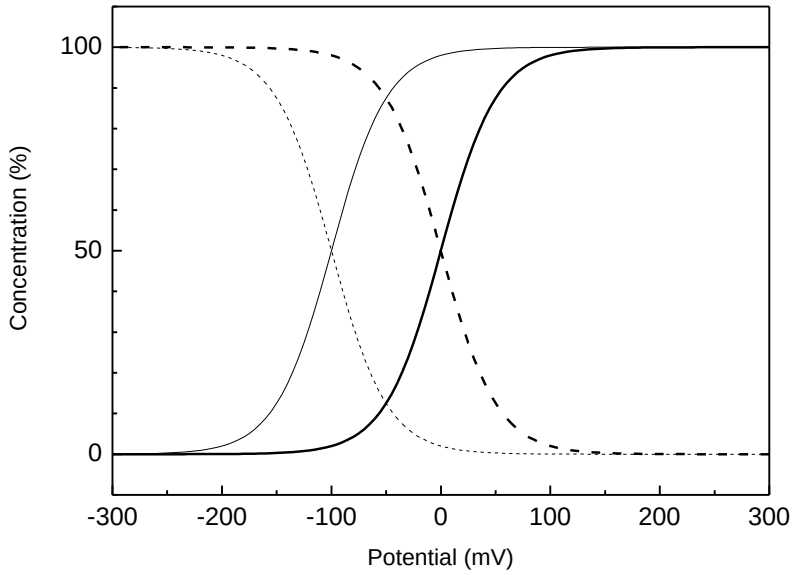

Figure 2.4 Potential dependence (Variation of) of the concentrations of oxidised (solid lines) and reduced (broken lines) species (with potential) as predicted by the Nernst Equation for an n =1 process. The bolder lines illustrate the case for E_m = 0 mV and the lighter lines for E_m = -100mV. In both cases T = 25 °C.

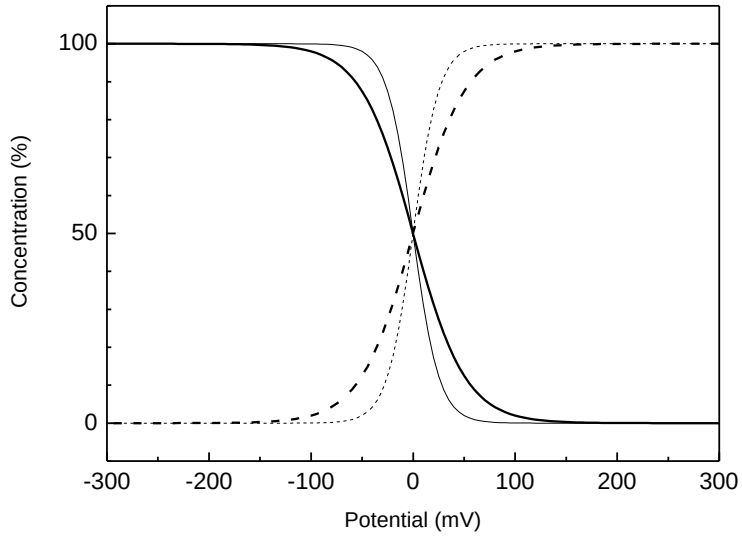

Figure 2.5 Potential dependence of the concentrations of oxidised (solid lines) and reduced (broken lines) species as predicted by the Nernst Equation for an n =1 and n =2 processes. The bolder lines illustrate the case for n =1 and the lighter lines for n =2. In both cases E_m = 0 mV and T = 25 °C.

2.6.2. The practicalities of spectropotentiometry

If the concentrations of the oxidised (ox) and reduced (red) protein can be measured as a function of potential then the experimental data can then be fitted to equation 1.5 to define reduction potentials. This experimental approach is called potentiometry or spectropotentiometric titration as the sample concentration is normally determined by a spectroscopic method.

The potential of samples can be adjusted *in situ* using chemical oxidants and reductants, such as ferricyanide and dithionite, in the presence of redox mediators that allow the sample to equilibrate with the potential imposed by the oxidants/ reductants [52]. This is usually performed in a two electrode cell, where the potential of the sample is monitored using a voltmeter and the bulk solution is stirred to make sure a steady potential is reached. Once a stable potential is obtained the sample can be transferred into EPR tubes and frozen to allow the potentiometric titration to be followed via EPR [40, 93]. Alternatively the sample can be measured using electronic absorption spectroscopy and the potentiometric titration can be carried out in a

cuvette, although this can create problems because mediators commonly have a spectrum of their own that can interfere with the results of the titration. Other instrumentation can be used to follow the potentiometric titration as long as it allows for changes in the sample signal to be obtained with changes in oxidation state [52].

Another approach to vary the sample potential is using electrodes, where the potential of the sample is under the control of a potentiostat [94]. Electrodic potentiometric titrations can be carried out in graphite pot electrodes, and if there is direct electron exchange between the electrode and the protein then the electrode will effectively oxidise and reduce the protein without mediators (although they are frequently required to improve the efficiency of this process) so that it can then be transferred to the appropriate tube or cuvette for spectroscopy such as MCD or EPR [52]. Electrodic potentiometric titrations can also be carried out in situ using gold mesh electrodes, or tin oxide electrodes that are optically transparent and so allow for electronic absorption spectroscopy, MCD or Fourier transform infrared (FTIR) spectroscopy to be carried out as the sample is being oxidised or reduced [54, 55]. Sample equilibration times can be rapid if a very thin cell is used or the sample is effectively stirred. The advantages of these methods are that they do not necessarily require the use of mediators that can interfere with the spectroscopy of the sample, and it is possible to determine where the electron goes at each potential, as the spectroscopy of the characteristic change of signal for the cofactor being observed is recorded.

The spectropotentiometry in this thesis was electrodic potentiometry using a nanocrystalline mesoporous tin oxide electrode (figure 2.6) [55]. Tin oxide electrodes adsorbed onto conducting glass supports were kindly provided by Professor James Durrant (Imperial College, London). They were first cut to a width < 8 mm to fit into the cuvette-electrochemical cell. Electrodes were then baked at 450 °C in a furnace for 30 minutes in order to remove any impurities that may have adsorbed to the surface.

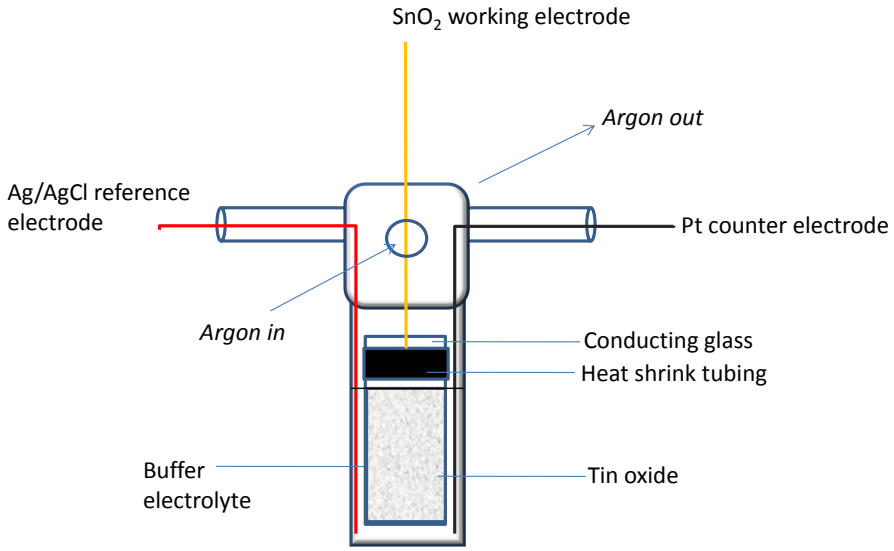

Figure 2.6 The set up of a tin oxide working electrode in a cuvette-electrochemical cell.

A platinum wire was connected to the tin oxide electrode to the conducting glass above the tin oxide layer using Heat Shrink tubing (figure 2.6). The electrode was soaked overnight at 4 °C in ca. 3 µM enzyme, 50 mM Hepes, 2 mM $CaCl_2$ in order for the enzyme to adsorb to the surface of the electrode. PFV and UV-vis spectroscopy were performed with the tin oxide working electrode as part of a three electrode cell configuration. The cuvette-electrochemical cell was sparged with argon so that experiments were anaerobic and the experimental solution contained anaerobic buffer; 50 mM Hepes, 2 mM $CaCl_2$, pH 7. The counter electrode was a platinum wire and the reference electrode a AgCl coated Ag wire. The reference wire was prepared by electrolysis of a silver wire in 5 M HCl for 30 minutes at 1.5 V. The reference electrode was calibrated at the end of each set of experiments by performing PFV of 3 mM ferricyanide dissolved in 50 mM Hepes, 2 mM $CaCl_2$, pH 7. The electrode potential was controlled by an Autolab PGSTAT 30 instrument, interfaced by General Purpose Electrochemical System (GPES) software. The electronic absorption spectra were measured at various potentials using a Jasco V-550 spectrophotometer. Control experiments using tin oxide electrodes without adsorbed enzyme were performed prior to each experiment.

2.6.3 Data Analysis

Spectropotentiometric data of NrfB adsorbed on tin oxide (chapter 5) was analysed using Microcal Origin to extract the absorbance values at 552 nm and to plot the change in this absorbance with the change in potential. This data was fitted to the Nernst equation (equation 1.5) using Tablecurve 2D. The error in the reduction potentials calculated by spectropotentiometry was calculated by Tablecurve and reflects how well the calculated values fitted to the data.

2.7. Cyclic Voltammetry of Adsorbed Proteins

In addition to the potentiometry described above the three electrode cell configuration also allows for dynamic electrochemistry where the changes in current flow through the adsorbed protein with changes in potential and/ or time can be investigated providing multi-dimensional information about the redox protein adsorbed. When a sample is electro-actively adsorbed to an electrode it is possible to use cyclic PFV, this is one of the most informative and prevalent uses of PFV.

2.7.1 Theory of Cyclic Voltammetry for Nernstian (non-catalytic) Systems

In the cyclic voltammetry experiment the current is measured as the potential is swept linearly, in a saw tooth fashion, between two values at a defined scan rate (V s^{-1}) (figure 1.9 C). A redox molecule adsorbed on the surface of an electrode can change oxidation state in response to the change in potential when there is direct electron exchange between the electrode and the protein (figure 1.9 B) [94]. The adsorbed molecules will be oxidised and reduced depending on their reduction potential and the sample potential as described by equation 1.5. Changing the oxidation state of the adsorbed molecule gives a flow of current, negative current for reduction and positive for oxidation, due to electron exchange from the electrode to the enzyme and to the electrode from the enzyme respectively. From figure 2.4 and 2.5 it is clear that at potentials much higher and much lower than the reduction potential there will be negligible current flow with change in potential since there is little change in the concentration of oxidised or reduced protein. At potentials close to the reduction potential there are large changes in the concentrations of oxidised and reduced molecules for small changes in potential and so current flow is detected. The

result is a negative peak for reduction and a positive peak for re-oxidation in the current vs. potential plot (figure 2.7) [95].

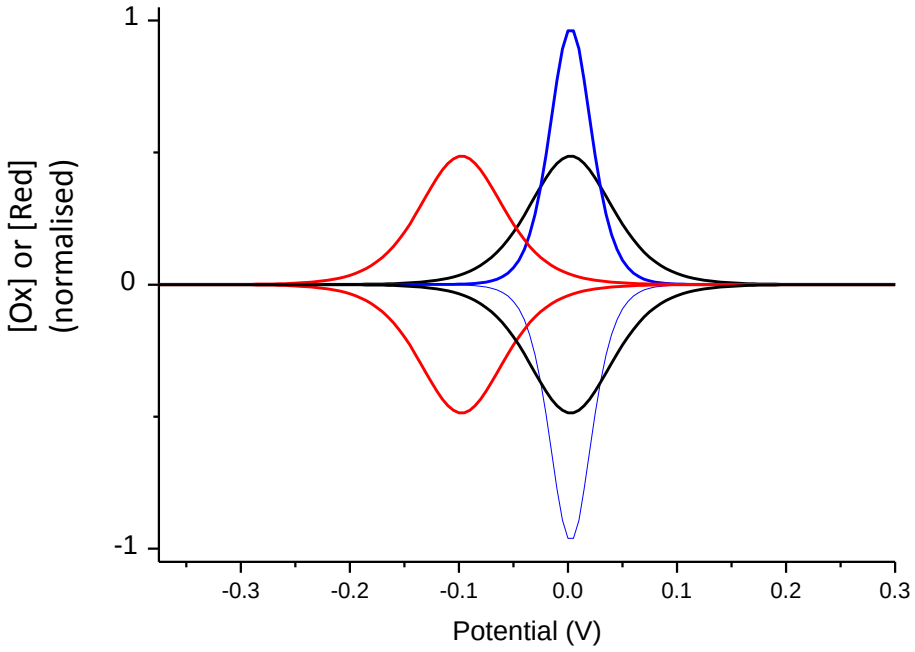

Figure 2.7.The ideal redox profiles for three 'species' with distinct redox properties. The blue shows E_m = 0 and n=1, black shows E_m = 0 and n=2, E_m = 1 and n=1 is shown in red. For each species only one parameter has changed with respect to another, any other variables (e.g. temperature) are constant.

The current flow can be considered as the derivative of the change in the concentration of oxidised and reduced molecules with potential**.** The peak of the derivative plot and the current vs. potential plot appears at E_m where [Ox]=[Red]. Fractional surface concentrations per cm^2 of oxidised (Γ_{Ox}) and reduced (Γ_{Red}) adsorbed species can be calculated at a given potential, as Γ_{total} is independent of potential and so then the negative change in the surface concentration of oxidised species, Γ_{Ox} (t) with time is equal to the positive change in the surface concentration of reduced species:

$$-\frac{d\Gamma_{Ox}(t)}{dt}=\frac{d\Gamma_{Red}(t)}{dt}=\frac{i}{nFA} \qquad \text{(Equation 2.5)}$$

Where i is the current and A is the area of the electrode. Equation 2.5 can be related to the scan rate (ν), the change of potential with time, which during cyclic voltammetry PFV affects the rate of change of Γ_O to Γ_R, and therefore the current at any time:

$$\frac{i}{nFA} = -\frac{d\Gamma_{Ox}(t)}{dt} = \left[\frac{d\Gamma_{Ox}(t)}{dE}\right]\nu \qquad \text{(Equation 2.6)}$$

Using the relationship $E = E_{initial} - \nu t$ allows current at each time and therefore potential to be calculated and so the current magnitude as a function of potential is described by:

$$i(E) = \frac{n^2F^2}{RT}\nu A\Gamma\left(\frac{\theta}{(\theta+1)^2}\right) \qquad \text{(Equation 2.7)}$$

Where θ is defined by equation 2.5 and the peak current amplitude (ip) is given by:

$$ip = \left(\frac{n^2F^2}{RT}\right)Av\Gamma_{total} \qquad \text{(Equation 2.8)}$$

From these equations key analytical parameters of the voltammetric response of the adsorbed species are defined. For example the peak area defines the number of moles of electrons exchanged between the protein and the electrode and if the number of redox cofactors within the protein are known, then the moles of electroactive protein at the electrode surface can also be derived from the peak area [94]. Under ideal conditions the peak potentials for oxidative and reductive processes are equal and equal to the reduction potential. The peak width at half height (δ) is also directly related to the electron stoichiometry of oxidation/reduction by equation 2.9 (all the symbols are as previously stated):

$$\delta = \frac{3.53RT}{nF} = \frac{0.089}{n}\text{ V at 20 °C} \qquad \text{(Equation 2.9)}$$

Cyclic PFV can also be used to derive information about the kinetics of catalysis by adsorbed redox enzymes [65, 96]. As described for NrfA in chapter one, in the presence of substrate, when the potential is swept to sufficiently negative potentials to allow reduction of the necessary redox centres within the enzyme a negative catalytic current is seen. The catalytic current arises from the flow of electrons from

the electrode, through the enzyme to allow reduction of the substrate under interrogation and reflects the rate of catalysis by the enzyme. Due to the nature of the cyclic voltammetry experiment, substrate can be added to the electrochemical cell to obtain information such as K_M and i_{max} and the dependence of the rate of catalysis on applied potential is also investigated. Catalytic PFV will be discussed in more detail in chapter 3.

2.7.2. Experimental Approaches

The working electrode used for PFV can be made of different materials, depending on the species being studied. In the PFV experiment the protein is adsorbed directly onto the surface of the electrode. The direct adsorption of the protein means that only small amounts of precious samples are required (typically ca. 1 µl of a 3 µM sample) [96]. Another advantage of PFV is that mediators are not required for electrochemistry as the sample 'talks' directly to the electrode [96]. Gold working electrodes are often used to study proteins via specific interactions, making use of the chemistry of gold [97-100]. However graphite electrodes are most frequently used in PFV and for the experiments in this thesis. There are two main types of graphite electrode; the basal electrode and the edge electrode (figure 2.8). The pyrolytic graphite edge (PGE) electrode has the planes of the carbon rings vertical to the surface of the electrode i.e. the edge of the graphite ring is exposed. Once polished the PGE surface provides a mixture of hydrophobic, hydrophilic and charged surfaces for the many varied surfaces of a protein to interact with [101]. Basal electrodes provide a hydrophobic surface for protein interaction and film formation. Different electrochemistry with different surface types may also give structure function information about the behaviour of the protein. Due to the set up of the PFV experiment the protein film can readily be transferred between solutions of different pH, salt concentration, buffer electrolyte etc. to check the effect that these conditions have on the redox properties of the adsorbed protein.

A disadvantage of using PFV on graphite or gold electrodes, is that unlike experiments using tin oxide electrons, you cannot 'see' where the electrons are going.

This could raise questions as to whether all cofactors or metal centres in the protein are being oxidised and reduced on the electrode surface, or if they are unaffected and are inaccessible to electron transfer on the electrode. This is why PFV experiments are frequently coupled to other types of spectroscopy; the experiments using tin oxide electrodes described above optimise the advantages of using both techniques simultaneously. However experiments using tin oxide electrodes are slow to set up and prepare when compared to experiments with graphite electrodes that can be repeated many times during a day. Whilst tin oxide experiments can be performed in stirred solutions this is ineffective in transporting substrate to the enzyme for studies of catalysis when compared to the rapid electrode rotation achieved with graphite electrodes. The importance of electrode rotation in eliminating mass transport limitations to catalysis will be discussed in more detail in chapter 3.

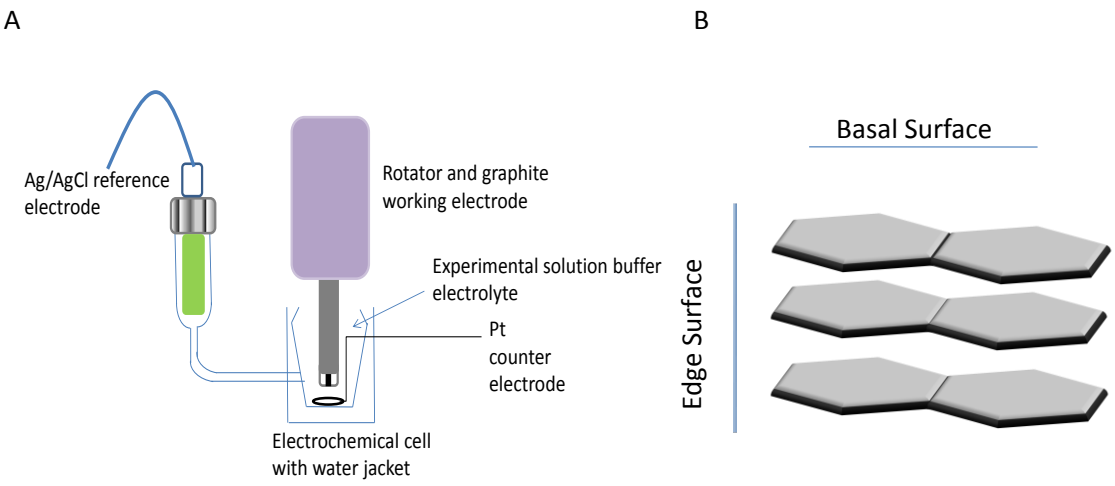

Figure 2.8 The experimental set up for protein film electrochemistry using a PGE electrode. A. The three electrode electrochemical cell with a rotatable graphite electrode. B. The planes of the carbon rings in edge and basal electrodes.

PFV at graphite electrodes was performed with a three electrode cell configuration. The reference electrodes used for all experiments were either Ag/AgCl or Hg/Hg_2Cl_2, saturated KCl (Russell) electrodes. Both electrodes were calibrated regularly by performing PFV of a 3 mM potassium ferricyanide solution diluted in 50 mM Hepes, 2 mM $CaCl_2$, pH 7 (E_m= +0.42 V vs. SHE) to check that the electrode potential did not drift and potentials could still be converted to vs. the standard hydrogen electrode (SHE) using the standard values (+0.197 V for Ag/AgCl electrodes

and +0.241 V for Hg/Hg_2Cl_2). The reference electrode was housed in a side arm filled with buffer electrolyte, adjoined to the main chamber of the electrochemical cell by a luggin capillary tip. The counter electrode in all experiments was a platinum wire placed in the experimental solution.

Oxygen has an electrochemical response therefore experiments were performed inside a nitrogen atmosphere glovebox (Belle Technology), with oxygen levels maintained < 10 ppm. The electrochemical cell was housed in a Faraday cage to minimise electrochemical noise and experiments were thermostated as appropriate by the water jacket surrounding the electrochemical cell (figure 2.8 A).

Directly before each experiment the PGE electrode was polished with an aqueous slurry of 0.3 µm aluminium oxide, sonicated to remove excess slurry, rinsed with Milli Q water and dried with a tissue. For experiments with TvNir the electrode was lightly abraded with fine grain sandpaper to increase the surface area of the electrode upon which the protein can adsorb. The electrode was then rinsed with Milli Q water, sonicated and polished with the aluminium oxide slurry as described above.

Control experiments were performed using a freshly polished electrode in buffer to confirm that there was no Faradaic current in the absence of a protein film and/or substrate. Protein films were made by taking 1-2 µl of ice cold enzyme into the anaerobic glovebox (< 1 µM NrfA, ca. 3 µM NrfB and ca. 30 µM TvNir) in an ice cold Hamilton syringe and injecting this solution onto the surface of the freshly polished electrode. After approximately 10 seconds the excess protein was removed with the Hamilton syringe and stored on ice, the electrode was then rapidly placed in buffer electrolyte in the electrochemical cell, to prevent the enzyme film 'drying out.' For catalytic experiments the electrode was rotated using an EG&G model 636 rotator to minimise/ eliminate problems of mass transport in the bulk solution.

2.7.3 'Fast' Protein Film Voltammetry

Protein film cyclic voltammetry can also be used to explore the rates of electron transfer within an absorbed protein, between the adsorbed protein and the electrode and potentially between proteins within a complex [102]. In order to

investigate these electron transfer rates the scan rate of cyclic voltammetry is varied and the peak potentials are recorded for non catalytic PFV and the catalytic current magnitude recorded for catalytic PFV experiments [103]. The analysis described above is for scan rates where the Nernst equation describes the [Ox] and [Red] at all times in the experiment. To study electron transfer kinetics it is necessary to increase the scan to the point where electron transfer between the electrode and the adsorbed protein is too slow for the adsorbed protein to be reduced in the time frame where sufficiently reducing potentials are applied and will discussed in more detail in chapter 5. The normal electrochemical cell set up is sufficient for exploring scan rates up to ca. 500 mV s^{-1}, however this is inadequate for probing the scan rates up to 150 V s^{-1} that might be required in order to see shifting of non-turnover waves and decreases in catalytic current magnitude that reveal details about electron transfer rates, for such experiments a 'fast' electrochemical cell set up is required (figure 2.11) [102]. The primary difference in the set up of this electrochemical cell is that the electrode is held very close to the luggin capillary tip separating the reference electrode to the main chamber of the electrochemical cell. In conjunction with the fast electrochemical cell, a pin point electrode is used that has a much smaller diameter than the electrode used in the standard cell, focusing the reactions at the working electrode directly at the luggin tip to the reference electrode. This means that there will be faster equilibration between the working electrode and the reference electrode. Use of the fast electrochemical cell means that the electrode is required to be held directly above the luggin capillary tip and so cannot be rotated as this would cause turbulence in the solution and so for catalytic PFV substrate concentrations must be determined where catalysis is not limited by mass transport as described in chapter 5.

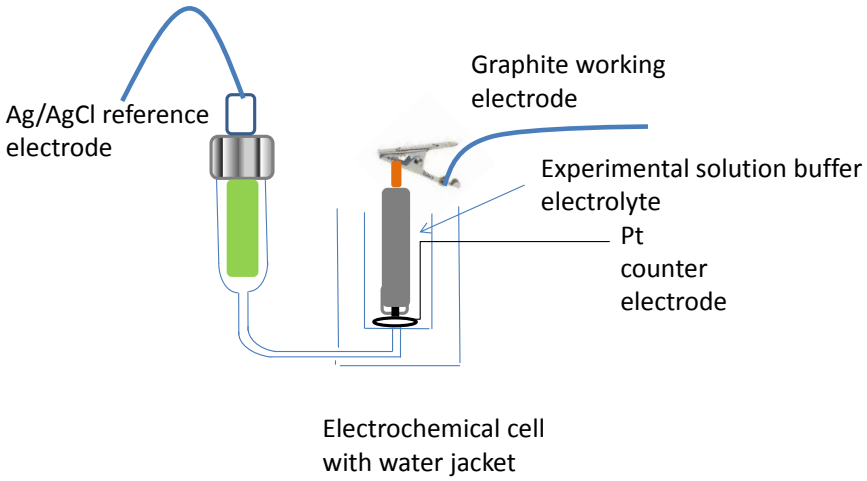

Figure 2.11 The set up of the 'fast' electrochemical cell. A three electrode configuration cell designed for high scan rate experiments, the main components of which are as indicated.

2.7.4. Data Analysis

The interface for the electrochemical experiments was Autolab General Purpose Electrochemical Software (GPES). Data analyses were predominantly performed in Microcal Origin. Baselines of non-turnover cyclic voltammograms were subtracted to give rise to the Faradaic current using the Utilities for Data Analysis 010716 Program kindly provided by Dr. Dirk Heering. Faradaic currents were fitted to equation 2.7 using Tablecurve 2D.

Analysis of catalytic cyclic voltammetry was also predominantly performed using Microcal Origin. For these experiments the current of the 'baselines' recorded at the same scan rate as the enzyme adsorbed electrochemistry, were directly subtracted from the cyclic voltammograms of the adsorbed enzyme. For titration experiments, in order to determine the kinetic parameters K_M and i_{max}, the baseline subtracted catalytic current from the reductive sweep was selected at one potential (either -143 or -600 mV, see chapter 3 for more details) for each nitrite concentration, from the second cyclic voltammogram recorded at that nitrite concentration. The catalytic current for each nitrite concentration was then corrected for the loss of signal magnitude with time, as will be described in chapter 3. The corrected current vs. nitrite concentration can then be plotted and fitted to the Michaelis Menten equation

(equation 3.2) to extract the parameters K_M and i_{max}. Catalytic nitrite titrations monitored by chronoamperometry were analysed in a similar way to the cyclic voltammetry data.

The statistical error in the data points extracted from analysis of experiments where the enzyme was adsorbed to a graphite edge or basal electrode was predominantly calculated in Microsoft Excel as the standard deviation of at least three experiments (where more experiments were performed for a data set these were all used to calculate the standard deviation). The exceptions to this were the catalytic current magnitudes determined at high scan rates for NrfA and NrfB in the 'fast' electrochemical cell, shown in chapter 5. The error for these values was assessed as these catalytic current magnitudes were collected and were noted as the maximum deviation from the collected data point that could be reasonably accepted as the catalytic current.

Chapter 3

Protein Film Voltammetry of The Octaheme Nitrite Reductase from *Thioalkalivibrio nitratireducens,* TvNir

Chapter 3. Protein Film Voltammetry of the Octaheme Nitrite Reductase from *Thioalkalivibrio nitratireducens* (TvNir)

3.1 Introduction

Protein film voltammetry has provided a detailed description of the catalysis of nitrite reduction by NrfA (chapter 1). This technique has also been exploited to show how rates of nitrite reduction by NrfA are dependent on many different parameters such as pH and the presence of inhibitors [1, 65, 104, 105]. This chapter describes the use of PFV to characterise the nitrite reductase activity of TvNir and the variation of the catalytic response with changes in nitrite concentration, pH and NaCl. These results will be compared in the discussion of factors defining the activity of cytochrome *c* nitrite reductases.

3.2 Establishing the Conditions for PFV of TvNir

To establish conditions for PFV of TvNir a graphite edge electrode was first prepared by light abrasion with sandpaper in order to increase the surface area for protein adsorption and then the electrode was polished with an aluminium oxide slurry (as described in chapter 2), providing a clean 'fresh' surface for protein adsorption. The freshly polished electrode was placed in a three electrode cell set up in an anaerobic glovebox, as described in chapter 2, where the buffer electrolyte was 20 mM HTMA, 0.1 M NaCl, 100 µM NO_2^- at pH 7.0. Cyclic voltammetry was performed to determine the response of the 'bare' electrode between +197 and -603 mV (all potentials are quoted vs. SHE) predominantly using a scan rate of 30 mV s^{-1}. Cyclic voltammetry showed a featureless response (figure 3.1 A dashed line) indicating that there were no redox active molecules adsorbed to the electrode surface when the electrode was prepared in this way. Baseline responses were recorded in this way at the start of each day's experiments, for each set of conditions under investigation.

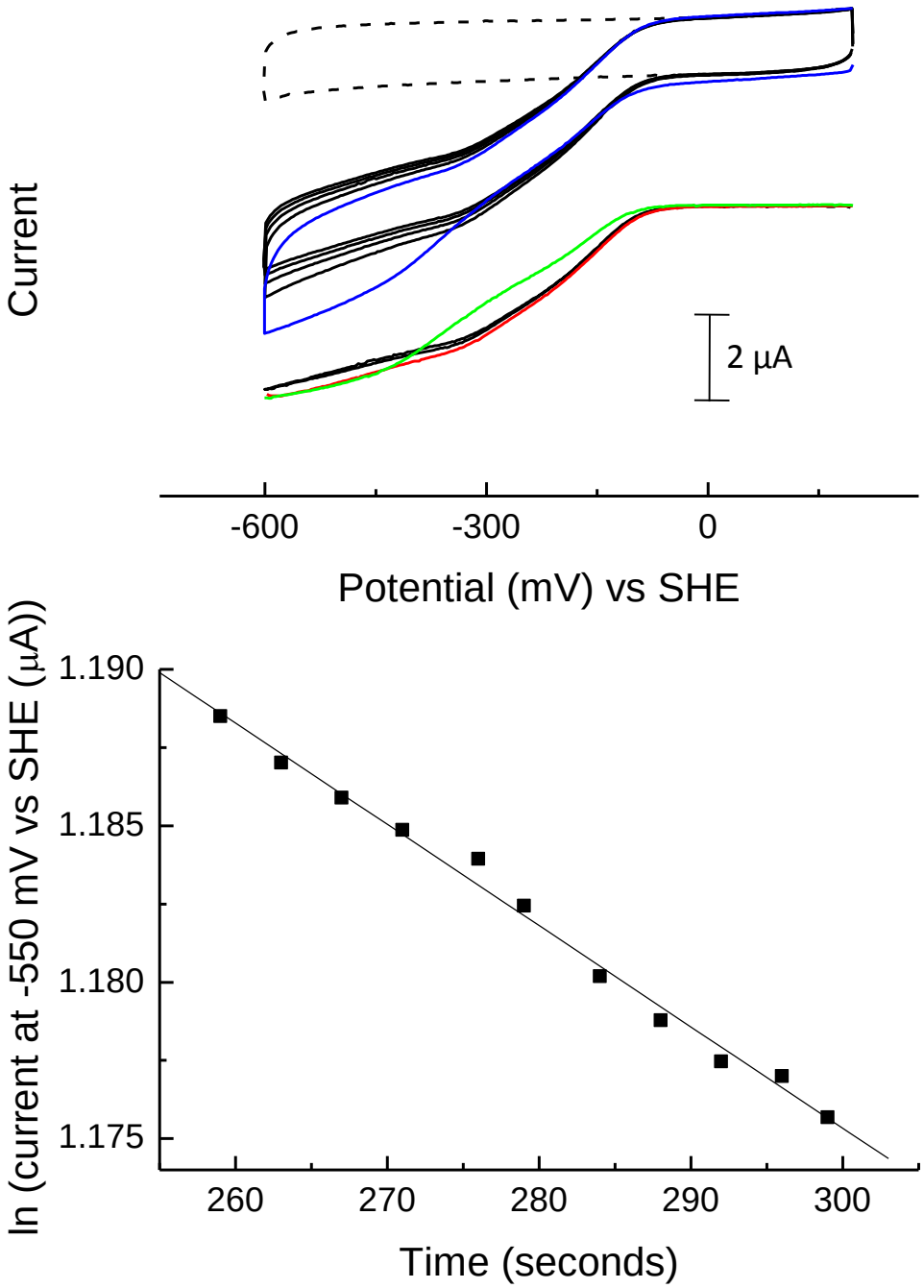

Figure 3.1 PFV of TvNir in 100 µM NO_2^- at pH 7.0. (A) The first cyclic voltammogram (blue) and the consecutively recorded cyclic voltammograms of TvNir recorded in the presence of 100 µM NO_2^- are offset to the first (reductive sweep green, oxidative sweep red) and second scan baseline subtracted (black), which have been displaced on the y-axis for clarity. The dashed line is a cyclic voltammogram in the absence of TvNir. (B) The semi-log plot for the decay in the catalytic current magnitude recorded at -550 mV, as a function of time from chronoamperometry 80 µM NO_2^-. Experiments were performed in 20 mM HTMA buffer, 0.1 M NaCl, pH 7, at 20 °C, where the electrode rotation speed was 3000 rpm and the scan rate was 30 mV s^{-1}.

Once a baseline had been measured the electrode was re-polished and taken into an anaerobic glovebox where 1 µl of ice cold 57 µM TvNir in 0.1 M phosphate buffer, pH 7.0, was then placed on the surface of the electrode for approximately 10 seconds, the excess solution was then removed. The electrode was then replaced in the electrochemical cell. The electrode was rotated at 3000 rpm and cyclic voltammetry performed between +197 and -603 mV at 30 mV s^{-1} (figure 3.1.A). At potentials more positive than -100 mV the response was featureless and nearly identical to that observed for the 'bare' electrode. For the first scan, as the potential was swept below ca. -100 mV a negative catalytic current was observed that increased steadily as the potential was decreased, until ca. -300 mV. Between ca. -300 and -450 mV there was a much sharper increase in the catalytic current with change in potential. Between -450 and -603 mV the increase in the catalytic current as the potential was lowered became smaller. The return sweep from -603 to +193 mV gave rise to a sigmoidal decrease in the catalytic current as the potential was increased to ca. -100 mV, where the response was again the same as at the 'bare' electrode and reflected the charging current of the electrode. The return sweep of the first scan showed no region of greater change in current with change in potential between -300 and -450 mV. Successive cyclic voltammograms showed a response that was featureless at potentials above -100 mV, at potentials below -100 mV the catalytic current showed a sigmoidal increase as the potential was swept towards -603 mV and the oxidative sweep had the same shape to the reductive sweep between -603 and +193 mV, indicating steady-state catalysis. From the second cycle the difference in the current magnitude between the oxidative and reductive sweeps arose from the charging current of the electrode. The increase in activity on the first sweep to low potential reflects reductive activation that will be discussed in more detail in chapter 4. The rest of the experimental data within this chapter should be considered as from the second scan onwards i.e. once the enzyme has been activated.

The contribution of the charging current of the electrode to the cyclic voltammetry of TvNir can be eliminated by directly subtracting the baseline cyclic voltammogram (recorded between the same potentials, at the same scan rate as the cyclic voltammogram with the adsorbed enzyme) using Microcal Origin. The resulting

current is the Faradaic current or the catalytic current and is directly attributed to the response of TvNir adsorbed on the electrode (figure 3.1 A). Inspection of the baseline subtracted cyclic voltammograms confirms the observations made from the raw data; the first reductive sweep has a smaller catalytic current between -100 and -450 mV compared to the return oxidative sweep, indicating that reductive activation occurred between these potentials and that once the potential has swept to -450 mV the sample of TvNir adsorbed to the electrode has reached full activity. The baseline subtracted cyclic voltammograms also confirm that the differences between the oxidative and reductive sweeps of the consecutive cyclic voltammograms are attributed to the charging current of the electrode and that catalysis from the second scan onwards is steady-state.

A catalytic response for TvNir was detectable by PFV for more than 40 scans, which typically take 40 minutes to perform. However, it was observed that over time the catalytic current magnitude decreased as is typical for studies of enzymes using PFV [96]. A semi-log plot of the catalytic current magnitude at -550 mV vs. time is linear indicating that signal loss is a first order process (figure 3.1 B). The first order rate constant for film decay (k) is the gradient of this plot and for this experiment was $3x10^{-4}$ s^{-1} (figure 3.1B). Using the integrated rate equation the catalytic current can be adjusted to correct for this decay, such that:

$$i=i_o exp^{-kt} \qquad \text{(Equation 3.1)}$$

Where i is the corrected catalytic current, i_o is the Faradaic current measured at -550 mV and t is time. This method of correcting the catalytic current for the loss of signal magnitude with time was applied to all catalytic currents measured and in subsequent work used to determine the kinetic parameters K_M and i_{max}.

During these catalytic PFV experiments the electrode was rotated at 3000 rpm, with the aim of minimising the problem of substrate delivery to the enzyme on the surface of electrode [94, 106]. This is more of an experimental problem when the rate of catalysis is high and the substrate concentration is low; substrate is depleted by enzyme at the electrode surface and the rate determining step becomes transport of substrate from the bulk solution to the adsorbed enzyme and not processes intrinsic to

enzyme catalysis that we are interested in. For enzymes such as NrfA electrode rotation does not completely eliminate the problem of mass transport and Levich analysis must be performed to determine the catalytic current unhindered by mass transport limitations [94].

To determine whether or not electrode rotation is sufficient to eliminate mass transport limitations for catalysis by TvNir, chronoamperometry was performed at -550 mV at 50, 100 and 200 µM NO_2^-, and the electrode rotation speed was changed between 0, 500, 1000, 2000 and 3000 rpm (figure 3.2). For all nitrite concentrations the catalytic current significantly increased when the electrode rotation speed was increased from 0 to 500 rpm. The increase in catalytic current was considerably smaller when the electrode rotation speed was increased again from 500 to 1000 rpm and less again when the electrode rotation speed was increased from 1000 to 2000 rpm. Even at 50 µM NO_2^- there was no detectable difference between the catalytic current magnitudes when the electrode was rotated at 2000 or 3000 rpm. Thus, for electrode rotation speeds greater than 2000 rpm the transport of nitrite to the electrode surface does not limit the magnitude of the catalytic current from TvNir films. Consequently 3000 rpm was used in all subsequent experiments.

During the cyclic voltammetry PFV experiment, the rate at which the potential is swept from positive to negative and negative to positive, i.e., the scan rate, is important. A scan rate must be selected that is lower than the rate of electron transfer between the enzyme and the electrode (the interfacial electron transfer rate (IET)). If the scan rate is more rapid than the rate of IET then electrons will not move from the electrode to the enzyme to allow catalysis before more positive potentials are applied again. Thus the catalytic current will reflect the rate of IET between the enzyme and the electrode and not processes intrinsic to enzyme catalysis (i.e., maximum turnover number at the given substrate concentration). To confirm that 30 mV s^{-1} was an appropriate scan rate at which to study catalysis by TvNir, cyclic voltammetry of TvNir was performed in 250 µM NO_2^- in the earlier described pH 7 buffer conditions, where the scan rate was changed every three scans (figure 3.3). Cyclic voltammograms of TvNir were recorded at different scan rates between 30 mV s^{-1} and 1 V s^{-1}.

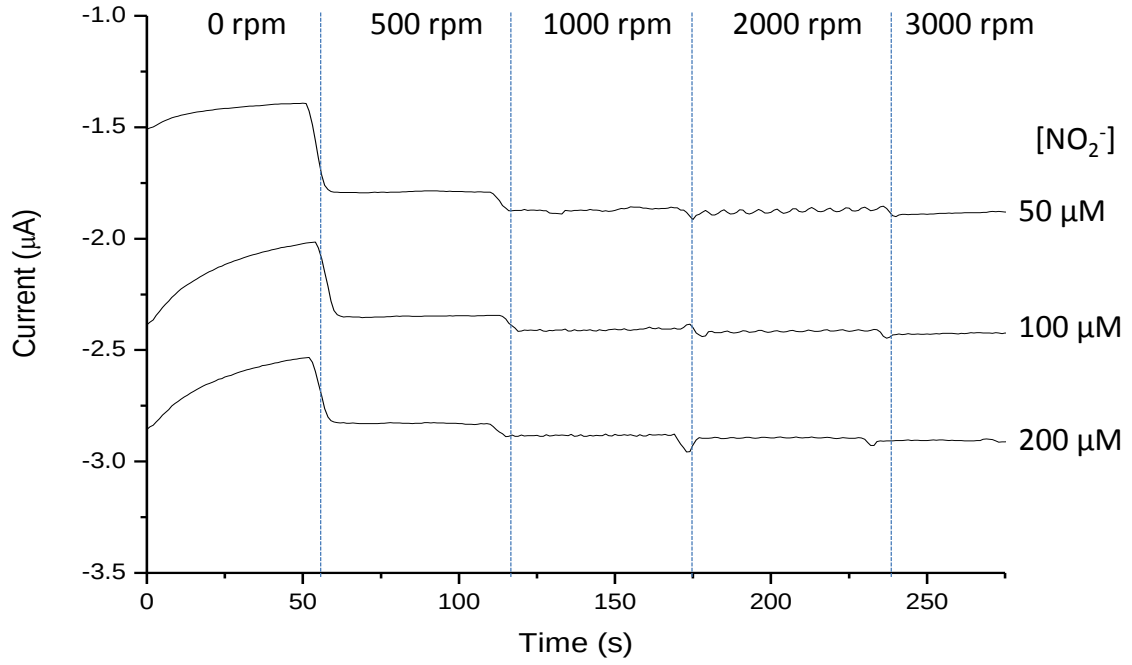

Figure 3.2 The influence of electrode rotation rate on the catalytic response of TvNir adsorbed on a PGE electrode. Chronoamperometry PFV of TvNir at -550 mV where the variations in electrode rotation speeds and [NO_2^-] are as indicated, the current has been smoothed using adjacent averaging in order to minimise the effect of signal noise. The experiment was performed in 20 mM HTMA, 0.1 M NaCl, pH 7.0 at 20 °C.

It would be expected that if the scan rate became too high to allow facile electron exchange between the adsorbed enzyme and the substrate that the catalytic current would decrease. The oxidative and reductive sweep of the TvNir cyclic voltammogram had the same shape indicating that catalysis was steady-state between 30 mV s^{-1} and 1000 mV s^{-1}(figure 3.3 A). At -550 mV the rate of catalysis was close to the fastest measured during cyclic voltammetry and so it would be expected that if IET slowed catalysis, the effect would be most obvious at this potential. The catalytic current -550 mV was compared for each scan rate, small changes in catalytic current magnitude were observed but these corresponded to the loss of signal magnitude with time and were not induced by changes in scan rate (figure 3.3 B and C). These experiments confirm that 30 mV s^{-1} is an appropriate scan rate to use to study nitrite reduction by TvNir.

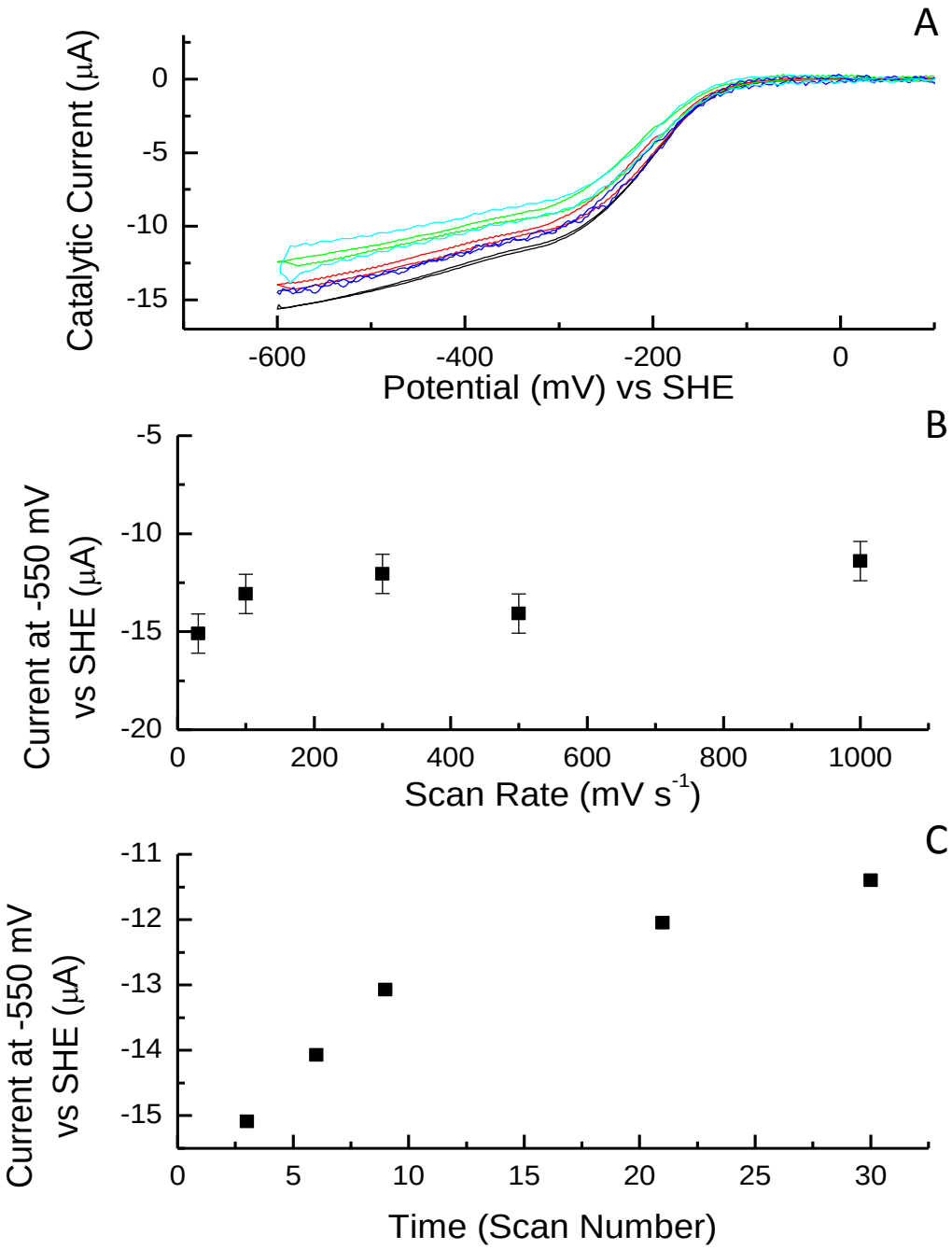

*Figure 3.3 The scan rate dependence of TvNir adsorbed on a PGE electrode. (*A) Baseline subtracted cyclic voltammograms of TvNir recorded at 30 mV s^{-1} (black), 100 mV s^{-1} (red), 300 mV s^{-1} (green), 500 mV s^{-1} (blue) and 1000 mV s^{-1} (cyan). (B) The dependence of the catalytic current at -550 mV vs. the scan rate and (C) the change in the catalytic current at -550 mV with the scan number. All experiments were performed in 20 mM HTMA, 100 mM NaCl, pH 7.0 with 250 μM NO_2^-, where the electrode rotation speed was 3000 rpm.

3.3 Catalytic PFV of TvNir at pH 7 in 0.1 M NaCl

Having established conditions appropriate for studying nitrite reduction by TvNir using PFV an investigation of the Michaelis-Menten enzyme kinetics was performed. For a normal enzymatic reaction proceeding in one direction the reaction can be written as [107, 108]:

$$E + S \underset{k_{off}}{\overset{k_{on}}{\rightleftharpoons}} ES \xrightarrow{k_{cat}} E + P \qquad \text{(Scheme 3.1)}$$

Where S is the substrate, E is the enzyme, ES is the enzyme-substrate complex (also known as the Michaelis complex) and P is the product. The rate at which this reaction proceeds is described by the Michaelis-Menten equation:

$$V = \frac{V_{max}[S]}{K_M + [S]} \qquad \text{(Equation 3.2)}$$

Where V is the reaction velocity, characterised in the PFV experiments by the catalytic current (i), V_{max} is the maximum rate of catalysis intrinsic to the enzyme (defined as the maximum catalytic current during PFV, i_{max}) and K_M is the substrate concentration at half the V_{max}. In order to investigate the Michaelis-Menten kinetics of TvNir two methods were employed; cyclic voltammetry and chronoamperometry (figure 3.4). Both methods allowed the steady-state analysis of the effect of substrate concentration on the rate of nitrite reduction by TvNir.

For both cyclic voltammetry and chronoamperometry experiments baselines of the bare electrode under the experimental conditions were recorded and TvNir was then adsorbed to a freshly polished electrode as described earlier. The electrode was then placed in an electrochemical cell containing 20 mM HTMA, 0.1 M NaCl at pH 7, 20 °C and the electrode was rotated at 3000 rpm in the absence of nitrite. Nitrite was added to the electrochemical cell at regular intervals, doubling the concentration sequentially from 10 µM to 10.24 mM, the method of measuring the catalytic current is the key difference between these two experimental methods as described below (figure 3.4).

During cyclic voltammetry two complete scans (between +197 and -603 mV) were recorded for each nitrite concentration. The second scan at each nitrite concentration was baseline subtracted giving the catalytic current. The catalytic current was corrected for film loss as described in section 3.2 (figure 3.4 A). Cyclic voltammetry provides a multi-dimensional view of the dependence of catalytic current on both substrate concentration and applied potential. In order to inspect the Michaelis-Menten parameters the catalytic currents at -550 mV were plotted for each nitrite concentration and fit to the Michaelis-Menten equation giving a K_M of 250 ± 30 µM and an i_{max} 7.5 µA (figure 3.4 C). The i_{max} for PFV experiments will vary between experiments depending on the amount of enzyme adsorbed to the electrode and so is not a definite indicator of the maximal activity of TvNir under these experimental conditions. This K_M is much lower than that determined by solution assays, described in chapter 1 and is in closer to the K_M described by PFV and solution assays for NrfA, this shall be discussed in more detail at the end of this chapter.

During chronoamperometry PFV the current was measured over a time course while the electrode potential was held at -550 mV (figure 3.4 B). Nitrite was added to the electrochemical cell every sixty seconds, and so the change in the current with nitrite was only measured at -550 mV. The total time for the chronoamperometry experiment was 650 seconds, this was less than half the average 1706 seconds required for the cyclic voltammetry experiment and so this method rapidly allowed the change in the rate of nitrite reduction with nitrite concentration to be determined. The catalytic current can be obtained from the recorded chronoamperometry in the same way as for cyclic voltammetry (direct baseline subtraction, followed by film loss correction). As with the cyclic voltammetry data, the current at -550 mV for each nitrite concentration can then be plotted and fit to the Michaelis-Menten equation. This gave a K_M = 275 ± 25 µM and i_{max} = 14 µA, thus the chronoamperometry and cyclic voltammetry results are in good agreement (figure 3.4 C white squares). The average of seven cyclic voltammetry and chronoamperometry experiments gave an average K_M for TvNir at pH 7 of 250 ±30 µM. The i_{max} value is less informatively averaged because it depends on the time of each experiment (figure 3.4 C) but it does provide a useful guide as to the influence of pH as described below.

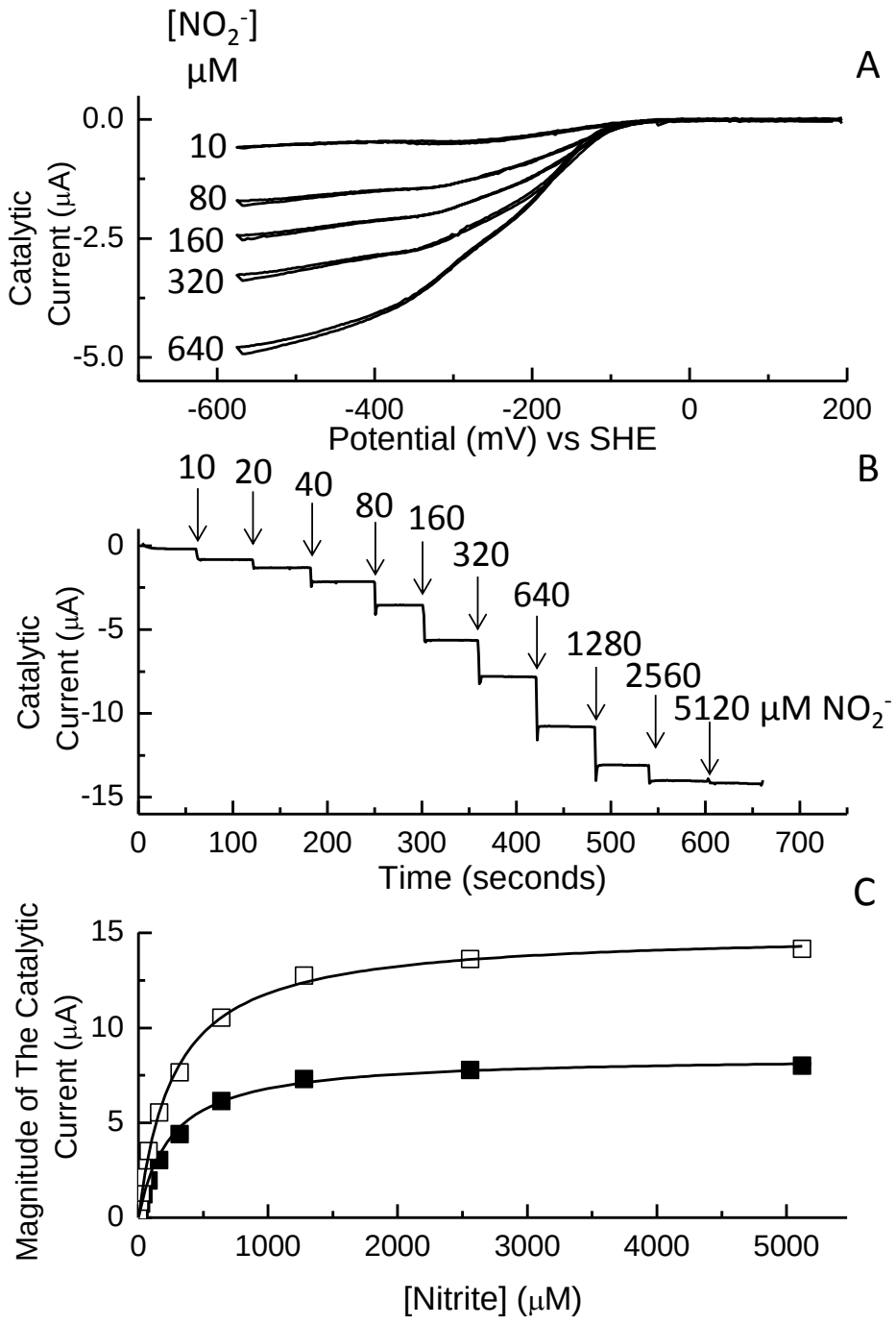

Figure 3.4 Defining the K_M and i_{max} for NO_2^- reduction by TvNir at pH 7.0. (A) Selected catalytic waveshapes from NO_2^- titration monitored by cyclic voltammetry where the scan rate was 30 mV s^{-1}. (B) NO_2^- titration monitored by chronoamperometry at -550 mV. For A and B the NO_2^- concentrations are as indicated. (C) The Michaelis-Menten plots of the catalytic current magnitude at -550 mV vs SHE for the chronoamperometry data (white squares) and the cyclic voltammetry data (black squares). The K_M for the chronoamperometry data is 275 µM and 250 µM by cyclic voltammetry. 20 mM HTMA, 100 mM NaCl, 20 °C with an electrode rotation speed of 3000 rpm.

3.4 The Dependence of The Steady- State Kinetics of TvNir Nitrite Reduction on pH and NaCl Concentration

3.4.1 pH dependence of V_{max} and K_M in 0.1 M NaCl at -550 mV

Having established the kinetic parameters describing steady-state catalysis at pH 7 the next step was to investigate how these parameters varied with pH. For this a multicomponent experimental buffer of 20 mM HTMA and 0.1 M NaCl was used. This was set to the desired pH between pH 5 and pH 9 and with 20 mM HCMA, 0.1M NaCl used at pH 9.5 and 10. Thus, the pH dependence of nitrite reduction by TvNir could be explored without changes of buffer composition.

Nitrite titrations were performed between pH 5 and pH 10 at every half pH unit, using both cyclic voltammetry and chronoamperometry PFV (figure 3.5). Chronoamperometry provided rapid insight into the kinetics at -550 mV for each experiment and cyclic voltammetry experiments provided information between +197 and -603 mV, showing catalytic waveshapes that varied with pH that will be discussed in more detail later in this chapter. For experiments at pH 7.5 and above the variation of rate with nitrite concentration was well described by the Michaelis Menten equation, i.e. increasing the concentration of nitrite increased the rate of catalysis to approach the maximum rate of catalysis (figure 3.5). Fits to the Michaelis-Menten equation showed that the K_M and i_{max} values from chronoamperometry and cyclic voltammetry experiments were in good agreement with one another (table 3.1).

At pH 5 and 6 a different variation of current magnitude with nitrite concentration was observed (figure 3.5). Initially the rate of catalysis increased as the nitrite concentration increased, but further increases in the nitrite concentration led to a decrease in the catalytic current. When additional nitrite was added to the electrochemical cell the catalytic current decreased in magnitude with each addition, indicating that at these concentrations nitrite was likely to be inhibiting.

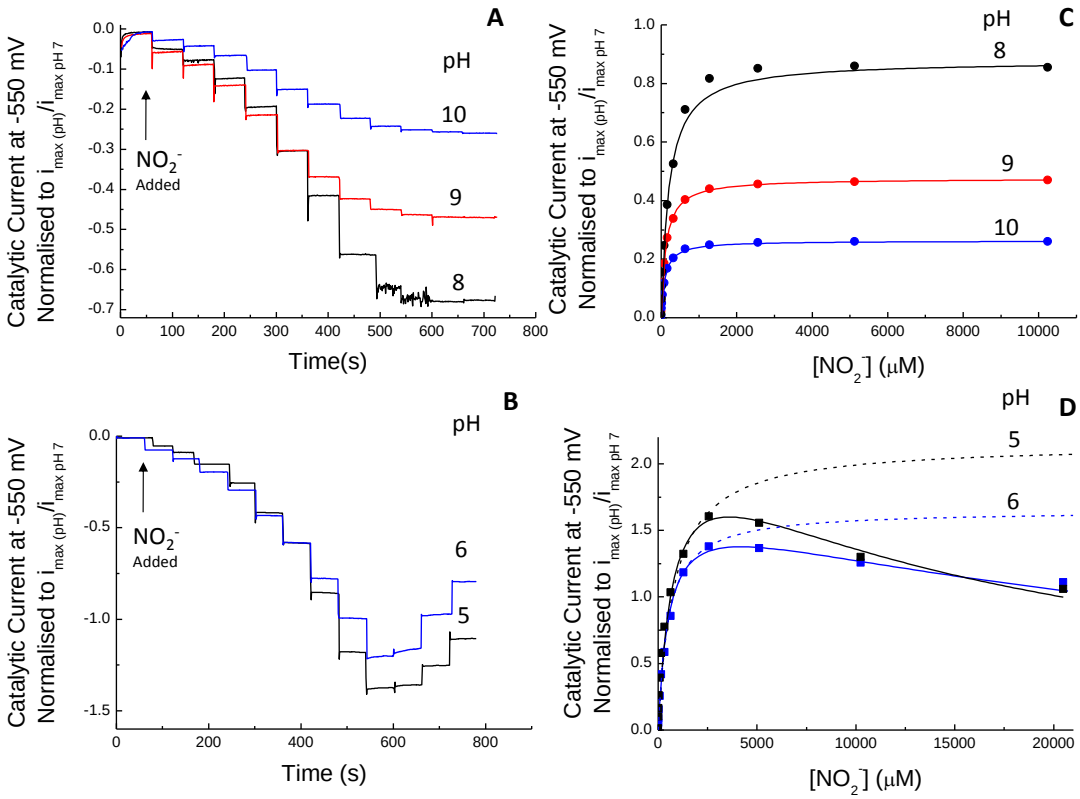

Figure 3.5 The pH dependence of steady-state nitrite reduction by TvNiR at -550 mV. (A) Chronoamperometry of TvNir at pH 8 (black), pH 9 (red) and pH 10 (blue) and the $[NO_2^-]$ was as indicated in figure 3.4 B: the first addition is indicated by an arrow (B) The fit of the data from A to the Michaelis-Menten equation. (C) Chronoamperometry of TvNir at pH 6 (blue) and pH 5 (black) where nitrite was titrated as indicated in figure 3.4 B. (D) The fit of the data from C to equation 3.3 (solid lines) and simulated inhibition free Michaelis-Menten plots (dashed lines). The catalytic current magnitudes are normalised with respect to the calculated i_{max} at pH 7. All experiments were performed in 20 mM HTMA or HCMA buffer, 0.1 M NaCl at 20 °C and the electrode rotation speed was 3000 rpm.

Under conditions where there is substrate inhibition leading to inactive enzyme the reaction scheme for catalysis changes from scheme 3.1 to:

$$\begin{array}{c} ESS \\ \downarrow\uparrow k_i \\ E + S \rightleftharpoons ES \longrightarrow E + P \end{array}$$

(Scheme 3.2)

ES is the enzyme substrate complex and ESS is the enzyme: substrate: substrate complex. The rate for catalysis under these conditions is described by the substrate inhibition equation:

$$i_{cat} = \frac{i_{max}}{\left(1+\left(\frac{K_M}{[S]}\right)+\left(\frac{[S]}{K_i}\right)\right)} \qquad \text{(Equation 3.3)}$$

pH	K_M by CV 0.1 M NaCl	K_M by CA 0.1 M NaCl	K_M by CV 4.3 M NaCl	K_M by CA 4.3 M NaCl	Average K_M all conditions
5	600 ± 50	604 ± 32	-	589 ± 91	595 ± 53
6	387 ± 163	425 ± 106	558 ± 56	-	422 ± 138
7	203 ± 20	274 ± 35	-	325 ± 9	238 ± 57
8	186 ± 70	232 ± 36	-	249 ± 30	208 ± 65
9	102 ± 14	118 ± 20	-	108 ± 18	106 ± 14
10	62 ± 22	93 ± 20	101 ± 20	90 ± 5	88 ± 13
pH	i_{max} by CV 0.1 M NaCl	i_{max} by CA 0.1 M NaCl	i_{max} by CV 4.3 M NaCl	i_{max} by CA 4.3 M NaCl	Average
5	42 ± 15	80 ± 30	-	40 ± 10	48 ± 20
6	27 ± 5	52 ± 5	20 ± 10	-	35 ± 15
7	13 ± 5	15 ± 5	-	30 ± 8	18 ± 9
8	12 ± 2	10 ± 4	-	24 ± 5	12 ± 6
9	9 ± 6	6 ± 2	-	10 ± 1	9 ± 4
10	2 ± 0.5	3 ± 1	3 ± 2	6 ± 1	4 ± 2

Table 3.1. The kinetic parameters describing steady-state nitrite reduction by TvNir at -550 mV between pH 5 and 10. The K_M and i_{max} values are determined from the fits to either equation 3.2 (pH 7-10) or equation 3.3 (pH 5 and 6). The stated values are averages of a minimum of three independent determinations carried out in 20 mM HTMA (pH 5-9) or 20 mM HCMA (pH 9.5 and 10), 0.1 M or 4.3 M NaCl, at 20 °C. The error was calculated as the standard deviation of the data points. Typical data sets are displayed in Figures 3.5, 3.8 and 3.11.

Where K_i is the equilibrium constant for inhibitor binding i.e. formation of the enzyme: substrate: substrate complex and the other symbols are as in equation 2. At pH 5 and 6 the dependence of the catalytic current on the nitrite concentration shows a good agreement to equation 3.3 and from this fit a K_M and K_i can be determined (table 3.1). The i_{max} and K_M determined from the fit to equation 3.3 can be put into the Michaelis-Menten equation to show a theoretical inhibition-free plot to help visualise the effects of inhibition on the current magnitudes of TvNir under these conditions (figure 3.5D dashed lines). The K_i for TvNir at pH 5 and 6 were 17.5 ± 5 and 45 ± 13 mM respectively, this is significantly higher than the K_M. The K_i increases with increasing pH and at ≥ pH 7 is undetectable within the parameters of the experiment. These studies show that the K_M for nitrite reduction by TvNir at -550 mV decreases by an order of magnitude as the pH is increased from 5 to 10, i_{max} also decreases by ca. 25 times as

the pH is increased, although these experiments cannot accurately quantify i_{max} due to variations between experiments that will be discussed below (table 3.1).

The cyclic voltammetry and chronoamperometry nitrite titrations suggest that the i_{max} decreased as the pH increased (table 3.1). This general trend is evident from the multiple measurements that were carried out at each pH; however the amount of enzyme varies each time a protein film is made. In order to precisely quantify the effect of changes in pH on the i_{max} of TvNir a new experimental approach was adopted. Cyclic voltammograms were recorded using one protein film that was transferred between solutions of different pH (figure 3.6 A). A TvNir film was adsorbed onto a freshly polished graphite edge electrode and placed into the electrochemical cell in a solution at one pH, where the nitrite concentration was the K_M for that pH and three cyclic voltammograms were recorded; the electrode was then transferred into a solution of pH 7, 250 µM NO_2^- (ca. the K_M of TvNir at pH 7) and three cyclic voltammograms were recorded; the electrode was then finally transferred back into the solution of the original pH and nitrite concentration and a further three cyclic voltammograms were recorded. The effect of substrate inhibition was ignored at low pH, as the K_M nitrite concentrations used are much lower than the K_i. The catalytic current magnitude at -550 mV for the measured pH was then calculated with respect to the catalytic current magnitude at pH 7 using equation 3.4:

$$\frac{1}{i_{max\,pHx\,vs.\,pH7}} = \left(\frac{\left(\frac{i_{pH7}}{i_{pHx(1^{st})}} + \frac{i_{pH7}}{i_{pHx(2^{nd})}} \right)}{2} \right) \qquad \text{(Equation 3.4)}$$

For this calculation the third scan at each pH was analysed. The i_{max} normalised with respect to that at pH 7 obtained from these experiments was plotted as a function of pH (figure 3.6 B). This confirmed that i_{max} decreased as the pH was increased and quantified the relationship. Across the pH range explored in these experiments nitrite reductase activity increases linearly as the pH is decreased, no plateau or inflection is seen that would indicate that the change with pH is due to the protonation of one or more amino acids and their pK_a.

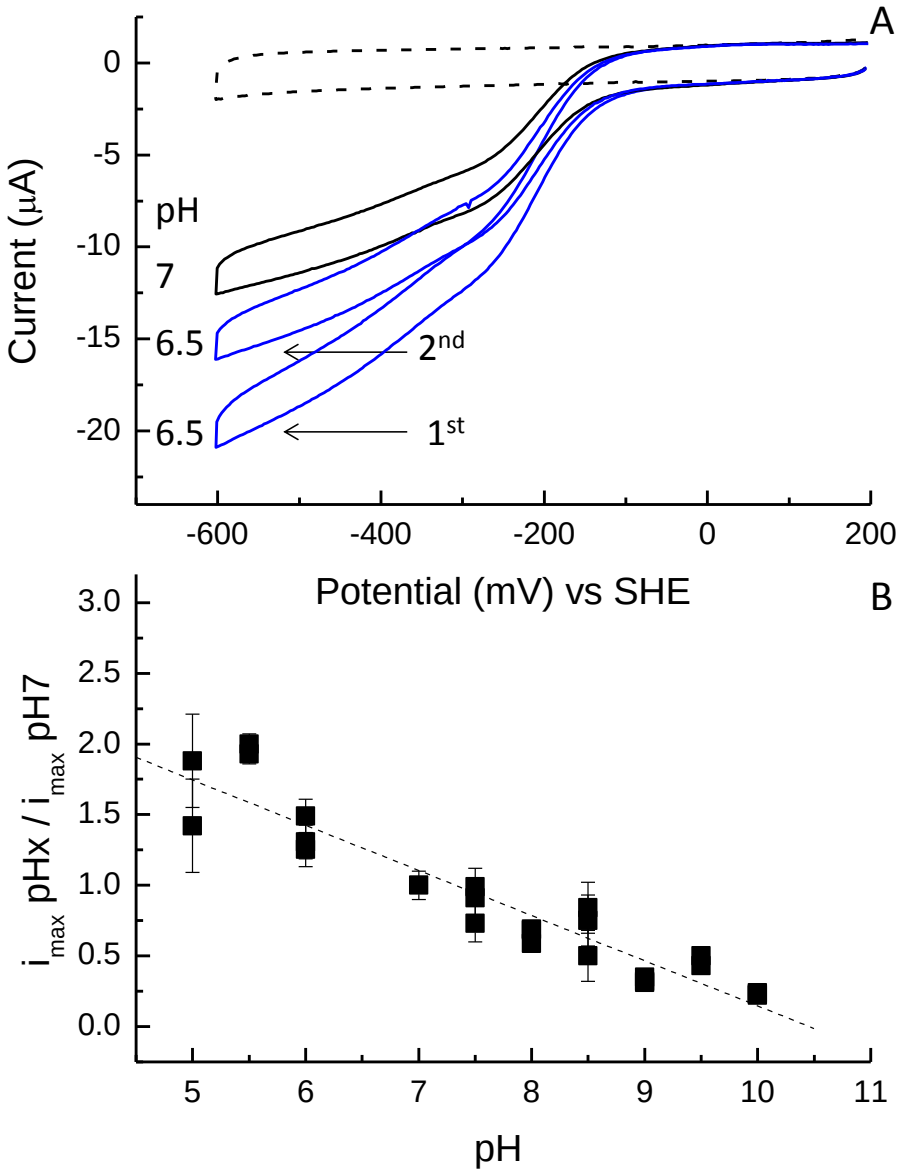

Figure 3.6 Defining the pH dependence of i_{max} in 0.1 M NaCl. (A) The cyclic voltammogram of one film of TvNir, where the electrode is transferred to 20 mM HTMA, 0.1 M NaCl, 525 μM NO_2^- pH 6.5, then to pH 7, 250 μM NO_2^- then back to pH 6.5, 525 μM NO_2^- (top). The voltammogram of the electrode prior to TvNir adsorption is shown (dashed line). (B) The i_{max} compared to the i_{max} at pH 7 is shown for TvNir in 0.1 M and 4.3 NaCl, determined by film transfer experiments (black). Other conditions are as in figure 3.5.

The specificity constant (k_{cat}/K_M) is used as an indication of how specific an enzyme is for catalysis of a particular substrate and is a useful way to compare different enzymes that catalyse the same reaction. Here the specificity constant provides insight into how the specificity of TvNir for nitrite reduction changes between

pH 5 and pH 10 (figure 3.7). The experiments in figure 3.6 A allowed an i_{max} at -550 mV to be determined that was normalised to the amount of enzyme present in the experiment, this normalised i_{max} can be then be used to calculate a specificity constant at -550 mV as it is proportional to the k_{cat}. The specificity constant is essentially unchanged between pH 5 and pH 10.

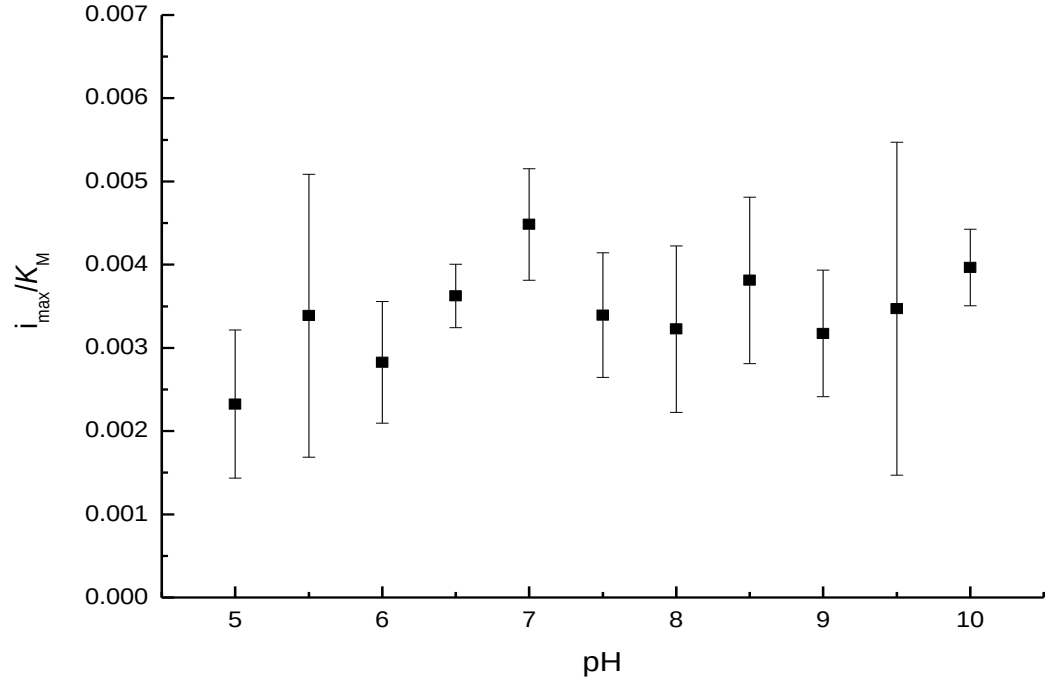

Figure 3.7 The pH dependence of the specificity constant of TvNir in 0.1 M NaCl. The i_{max} at each pH was determined from the experiments in section 3.4.1 where the i_{max} was normalised for protein film coverage, the average K_M was calculated from experiments in section 3.4.1.

3.4.2 The kinetics of nitrite reduction by TvNir in 4.3 M NaCl

To investigate the impact of 4.3 M NaCl on nitrite reduction by TvNir chronoamperometry PFV was performed between pH 5 and 10 in 20 mM HTMA, 4.3 M NaCl (figure 3.8). All the other experimental conditions were identical to those used for experiments in 0.1 M NaCl. In contrast to data from all pH values from 5 to 10 in 0.1 M NaCl, no substrate inhibition was detected in 4.3 M NaCl and the dependence of the catalytic current at -550 mV on the nitrite concentration gave a good fit to the Michaelis Menten equation. Thus 4.3 M NaCl appears to have alleviated the substrate inhibition effect that was detected below pH 7 in 0.1 M NaCl. This indicates that

whatever contributes to substrate inhibition it is dependent on both salt concentration and pH.

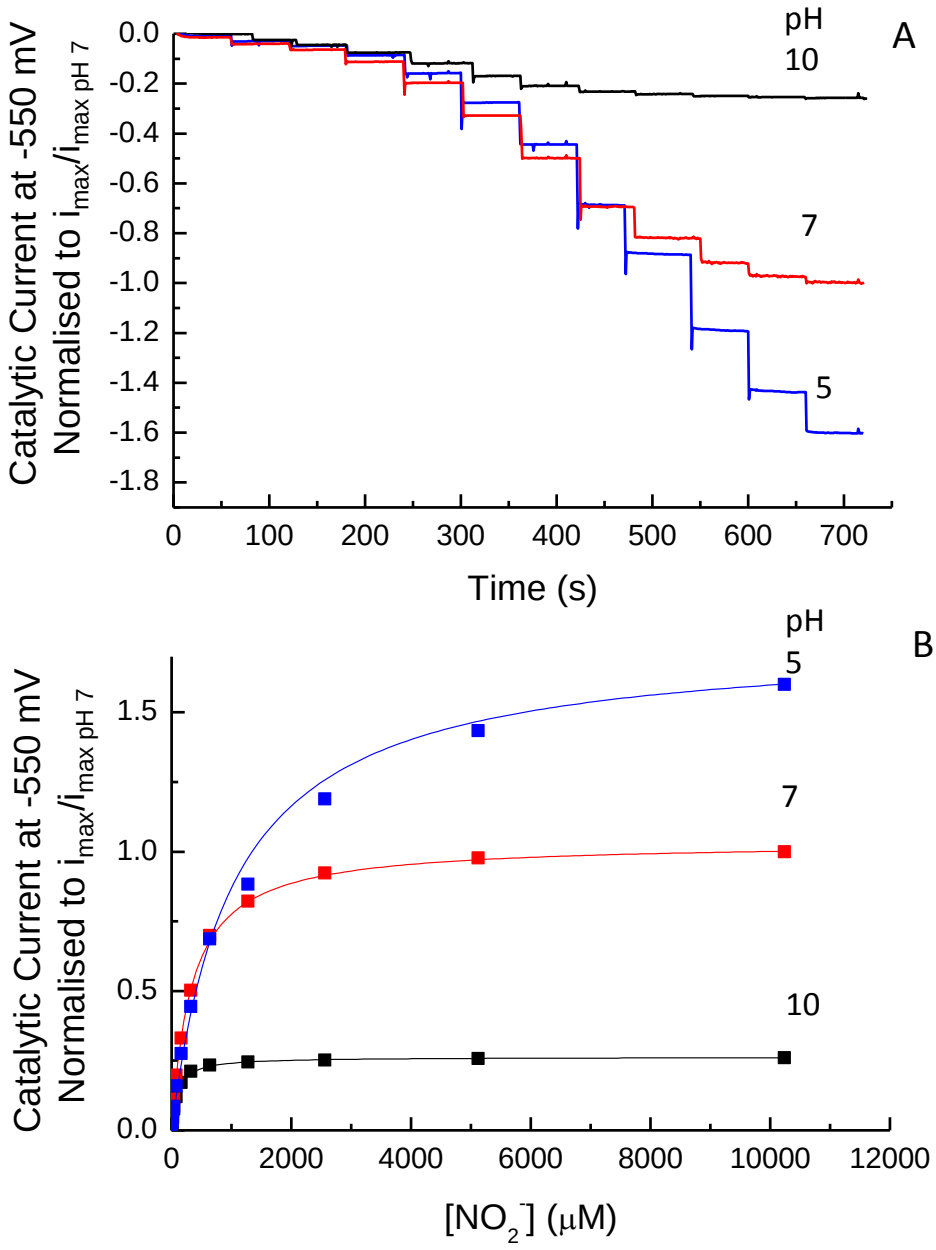

Figure 3.8 PFV analysis of the enzyme kinetics of TvNir in 4.3 M NaCl. (A) Nitrite titration to a TvNir film adsorbed on a PGE electrode monitored by chronoamperometry at -550 mV, where the $[NO_2^-]$ was as indicated in figure 3.4. The current magnitude has been calculated with respect to the i_{max}. (B) The catalytic current at -550 mV vs. $[NO_2^-]$ at pH 5 (blue), pH 7 (red) and pH 10 (black). The fit of these data to equation 2 (black lines) gives a K_M of 654 ± 78, 319 ± 50 and 95 ± 20 μM for pH 5, 7 and 10 respectively. All catalytic currents are normalised with respect to the calculated i_{max} at pH 7. Experiments were performed at 20 °C, with an electrode rotation speed of 3000 rpm in 20 mM HTMA (pH 5 and 7) or 20 mM HCMA (pH 10), 4.3 M NaCl.

The K_M for nitrite reduction was unaffected by the high salt concentration, when compared to data recorded at 0.1 M NaCl (table 3.1). Although the average values for K_M in 4.3 M NaCl appear to be slightly higher compared to those in 0.1 M NaCl, graphical analysis shows they are within reasonable error of one another and the K_M still appears to change linearly with the change in pH, with a gradient of ca. 100 µM/ pH unit (figure 3.9).

In 4.3 M NaCl similar i_{max} values were observed as those determined by nitrite titrations in 0.1 M NaCl (table 3.1). To more accurately assess the impact of 4.3 M NaCl on the i_{max} of TvNir a series of film transfer experiments were performed at pH 5 and pH 6 in 4.3 M NaCl, as described in section 3.4.1. For these experiments pH 5 and 6 were selected as the rate of nitrite reduction most substantially differed at these pH in 4.3 M NaCl compared to 0.1 M NaCl. From an average of three experiments the relative $i_{max}/i_{max\ pH7}$ of TvNir in 4.3 M NaCl at pH 5 and 6 were 1.33 and 1.5 respectively. Inspection of figure 3.6 B indicates that these relative i_{max} values agree with those determined for TvNir in 0.1 M NaCl.

To further investigate the effect of salt binding and alleviating possible substrate inhibition at low pH, chronoamperometry PFV nitrite titrations were performed at pH 6 using KNO_2, KCl and KBr at 0.1 M and 4.3 M concentrations. The aim of these experiments was to systematically substitute sodium in the substrate by swapping $NaNO_2$ for KNO_2, and sodium and chloride in the buffer electrolyte by swapping NaCl for KCl and then KBr. At 0.1 M salt concentration for all experiments substrate inhibition was detected and this effect was alleviated in 4.3 M in each salt buffer assayed. The only significant change apparent on substituting these buffer salts was that the K_M for nitrite reduction was increased to 780 ± 44 µM in 4.3 M KBr, compared ca. 550 µM in all the other experimental buffers used. This is suggestive that chloride might have some role in the specific binding of nitrite in the active site of TvNir, but this requires further investigation and could possibly be attributed to an ionic strength effect as opposed to an ion specific effect.

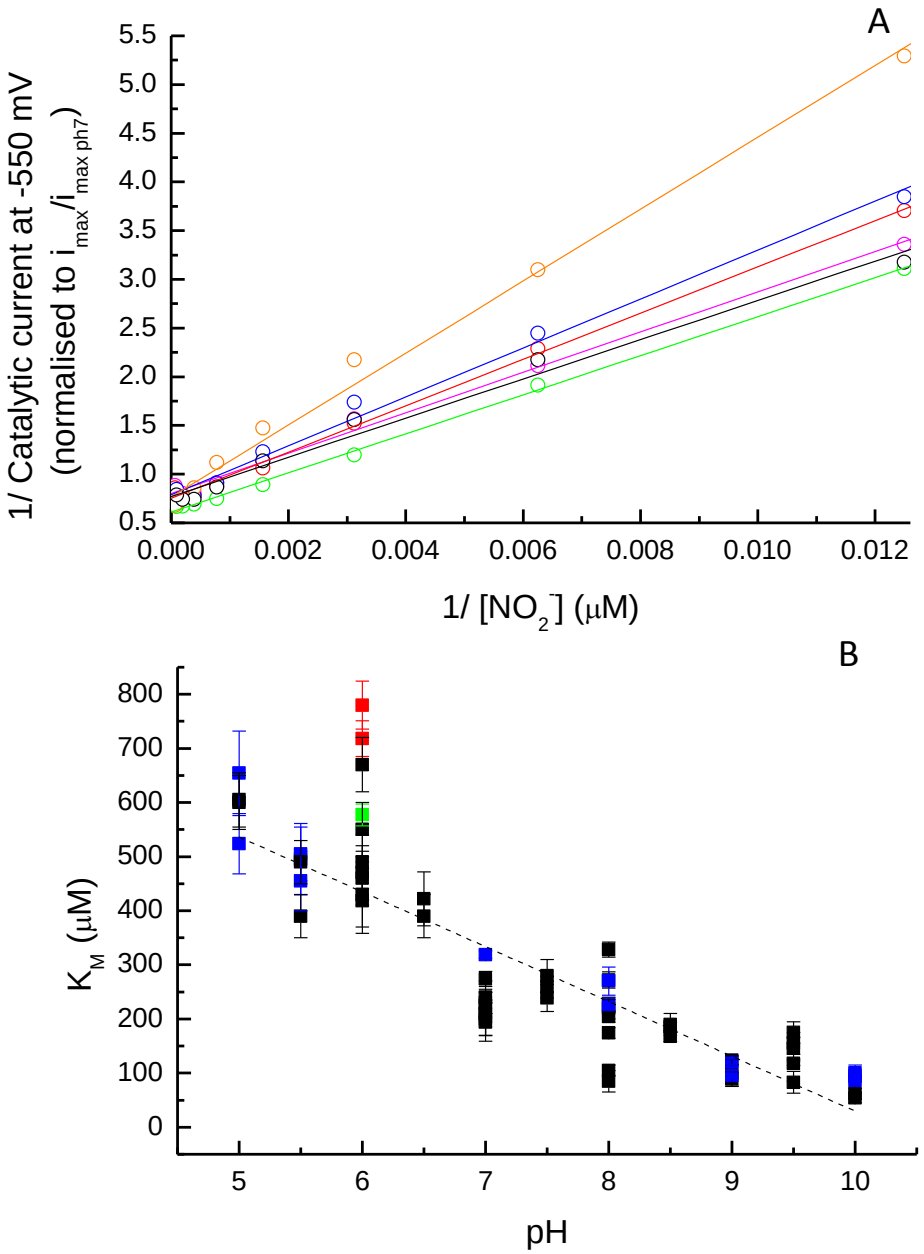

Figure 3.9 The effect of variations in salt concentration and composition on the K_M of TvNir. A. Lineweaver-Burke plots of nitrite reduction by TvNir measured by PFV chronoamperometry at -550 mV, where the catalytic current has been normalised to $i_{max}/i_{max\ pH7}$. Experiments were performed in 0.1 M KBr (magenta), 0.1 M KCl (red), 4.3 M KCl (green), 4.3 M KBr (orange) and 0.1 M NaCl (blue) where the nitrite stock used was KNO_2 and 0.1 M NaCl (black) where $NaNO_2$ was the substrate, these experiments were all performed at pH6. B. The K_M for nitrite reduction vs. pH in 0.1 M NaCl (black), 4.3 M NaCl (blue) where $NaNO_2$ was the substrate and 4.3 M KCl (green) and 4.3 M KBr, where KNO_2 was the substrate. A linear fit to the change in K_M with change in pH is shown (dashed line). All experiments were performed at 30 mV s^{-1}, 20 °C, where the electrode rotation speed was 3000 rpm and the principle buffer component was 20 mM HTMA.

3.4.3 Steady-state nitrite reduction at -143 mV in 0.1 M NaCl

The preceding part of this chapter has focused on the changes in the kinetic parameters describing steady-state nitrite reduction by TvNir at -550 mV. Around -550 mV the maximal catalytic current is seen for nitrite reduction by TvNir and there is the least potential dependent change in catalytic current magnitude. Electrochemical studies of *E. coli* NrfA have also been predominantly performed close to this potential and so it is useful to have profiled kinetics of TvNir in this region in order to compare nitrite reductase activity. However it is very unlikely that under physiological conditions TvNir will be exposed to such reducing potentials, and so it is also of interest to assess catalysis of nitrite reduction at more positive potentials [28].

In order to asses the effect of nitrite concentration at more positive potentials, where the hemes of TvNir are not 100 % reduced (see chapter 5), the catalytic current at -143 mV was inspected. This data could be extracted from the cyclic voltammetry experiments described in section 3.4. Substrate inhibition was evident from pH 5 to 9 and the data at these pH showed a good agreement with equation 3.3 (figure 3.10). Although inspection of the cyclic voltammograms, as described earlier at pH 7, shows that this is not because nitrite is binding and producing inactive enzyme, but that the waveshape of the cyclic voltammograms shifts to more negative potentials. This will be discussed in more detail in the next section.

The K_Ms determined at -143 mV are approximately an order of magnitude lower than those determined at -550 mV, although the K_M still followed the same pH dependence trend as at -550 mV and decreased as the pH increased. The i_{max} values also showed the same trend as the values collected at -550 mV and decreased as the pH was increased and were also lower at -143 mV than those determined at -550 mV such that at pH 9 there was very little change in catalytic current as the nitrite concentration was increased and at pH 10 the catalytic current was too small measure accurately.

The K_M and i_{max} were also determined at -143 mV in 4.3 M NaCl for pH 6 and pH 10. The values obtained from the fits to this data gave an average K_M for nitrite reduction at pH 10 of 6 ± 2 μM, an i_{max} of 0.25 ± 0.09 μA and a K_i of 55 ± 10 mM and at

pH 6 an average K_M of 60 ± 9 µM, an i_{max} of 1.8 ± 0.5 µA and a K_i of 50 ± 10 mM. The K_M and i_{max} values calculated at -143 mV for pH 6 were very similar to those calculated in 0.1 M NaCl, but in 4.3 M NaCl the K_i is much higher, indicating that 4.3 M NaCl effects the shift in the cyclic voltammetry waveshape with increasing nitrite concentration, this will be discussed in more detail below.

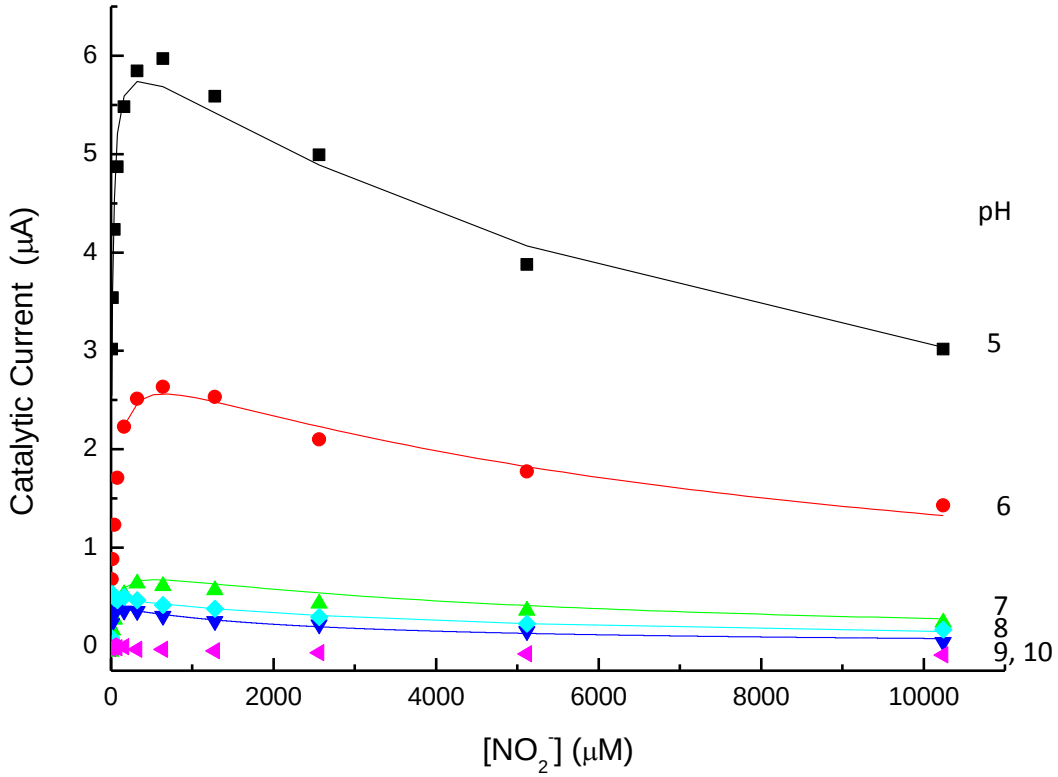

Figure 3.11 The rate of nitrite reduction by TvNir at -143 mV 0.1 M NaCl. The baseline subtracted, film loss corrected catalytic current for nitrite reduction by TvNir at pH 5 (black), pH 6 (red), pH 7 (green), pH 8 (blue), pH 9 (cyan) and pH 10 (magenta) and the corresponding fits to equation 3.3. These fits produced which gave respective K_Ms (pH 5, 6, 7, 8 and 9) of 30, 50, 12, 6 and 5 µM, K_is of 9059, 8363, 5556, 2097and 2676 µM and i_{max} of 6.4, 2.7, 0.77, 0.4 and 0.57 µA; the data at pH 10 could not be fit to this equation. B. All experimental conditions were as described figure 3.9.

3.5 The Catalytic Waveshape of Nitrite Reduction

3.5.1 The waveshape of nitrite reduction in 0.1 M NaCl

The cyclic voltammetry PFV of TvNir has so far been exploited to extract the kinetic parameters, K_M and i_{max} for TvNir at fixed potentials and to probe the effects of salt concentration and pH on these kinetic parameters. In order to better understand why these parameters at -550 mV differ so much from those at -143 mV, cyclic voltammetry experiments also provide information about the necessary driving force (i.e. applied potential) required for nitrite reduction as the substrate concentration is varied. This can provide information on the optimum operating potentials of enzymes and perhaps insight into the redox cofactors that may be affected by changes in pH, NaCl concentration and the presence of inhibitors [65, 103].

Cyclic voltammetry PFV of TvNir was performed as described in sections 3.3 in mixed buffers of 20 mM HTMA, 0.1 M NaCl (pH 5-9) and 20 mM HCMA, 0.1 M NaCl (pH 9.5 and 10), where the potential was swept between +197 to -603 mV at 30 mV s^{-1} and nitrite was titrated into the electrochemical cell every second scan to double the nitrite concentration going from 10 µM to 10240 µM. This produced cyclic voltammograms for TvNir for a range of pH conditions and nitrite concentrations (figure 3.11). Figure 3.11 shows the cyclic voltammograms for each pH at 10 and 10240 µM NO_2^- and the voltammograms in between those nitrite concentrations are those closest to the K_M at that pH. It is immediately clear that changing the pH from 5 to 10 changes the dependence of the catalytic current magnitude on both applied potential and nitrite concentration (figure 3.11). At pH 5 and 6 the cyclic voltammograms are largely sigmoidal across the full nitrite concentration range shown. At pH 7 and above catalysis is attenuated slightly at lower nitrite concentration and ca. -350 mV. The substrate inhibition that was found at -550 mV at pH 5 and 6 is apparent in the cyclic voltammograms at 10240 and 1280 µM. Inspection of cyclic voltammograms at all pH at 10240 µM NO_2^- shows the entire waveshape is shifted towards more negative potentials and this is most apparent at low pH. To summarise, increasing pH gives rise to a more attenuated, less sigmoidal cyclic voltammogram and increasing nitrite

concentration increases the potential required to obtain the highest rates of catalysis i.e. the catalytic waveshape is shifted to more negative potentials.

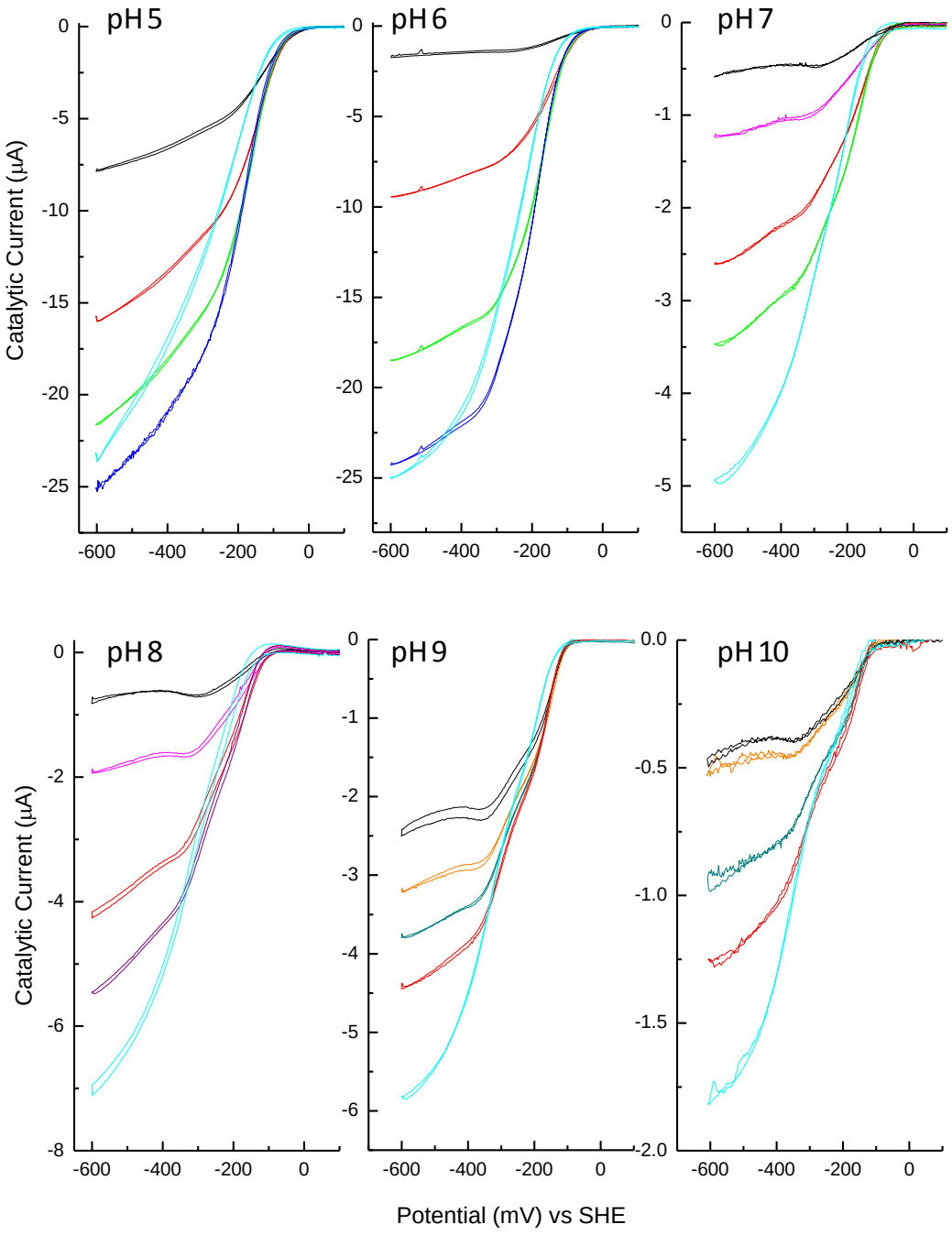

Figure 3.11 Baseline subtracted cyclic voltammograms of TvNir. The pH for each experiment is as indicated, the nitrite concentrations shown are 10 µM (black), 20 µM (orange), 40 µM (magenta), 80 µM (dark cyan), 160 µM (red), 320 µM (purple), 640 µM (green), 1280 µM (blue) and 10240 µM (cyan). Experiments at pH 5-9 were performed in 20 mM HTMA, 100 mM NaCl, at pH 10 the buffer was 20 mM HCMA, 100 mM NaCl, all experiments were carried out at 20 °C where the electrode rotation speed was 3000 rpm and the scan rate was 30 mV s^{-1}.

In order to gain better insight into the variation of the potential dependence of the catalytic current of TvNir with changes of nitrite concentration the first derivative of the cyclic voltammograms were examined (figure 3.12). At pH 5 at all nitrite concentrations only one feature is apparent in the derivative cyclic voltammograms. This feature appears at ca. -125 mV at 10 µM NO_2^- and shifted to ca. -210 mV as the nitrite concentration was increased to 10.24 mM NO_2^- (figure 3.12). The maximum of this feature occurs at a potential that shall be defined as E_{cat}.

As the pH is increased the onset of catalysis moves to more negative potentials, whereas the E_{cat} feature shifts very little. However the width of the corresponding peak in the derivative broadened as the pH was increased. At pH 6, at higher nitrite concentrations a shoulder is seen at negative potential on the E_{cat} feature. At pH 7 this shoulder feature appears at lower nitrite concentration and as a more distinct separate peak, E_{boost} (figure 3.12), where another increase in catalysis is seen on reducing the potential. As the pH is further increased E_{boost} appears at lower nitrite concentrations and moves to more negative potentials, becoming more distinct from E_{cat}. The half-height width of the peak in the derivative corresponding to E_{cat} at 10 µM NO_2^-, where substrate concentration is limiting for every pH, systematically decreased as the pH increased reflecting the increasing prominence of the E_{boost} feature (figure 3.13).

As mentioned previously, at low nitrite concentration, at pH 7 and 8, an attenuation of the catalytic current is seen at ca. -330 mV; this appears as a negative feature in the di/dE plot of TvNir at these pH values. Attenuation can also be detected in the 10 µM NO_2^- cyclic voltammograms at pH 6 and 9 although it is less easily distinguished.

At potentials sufficiently negative for catalysis a point of zero change in current with change in potential was not observed in the y-axis of the di/dE plots, for any pH or nitrite concentration. This would represent a point where the catalytic current was independent of further applied potential, but this is not observed for TvNir even at the most negative applied potentials.

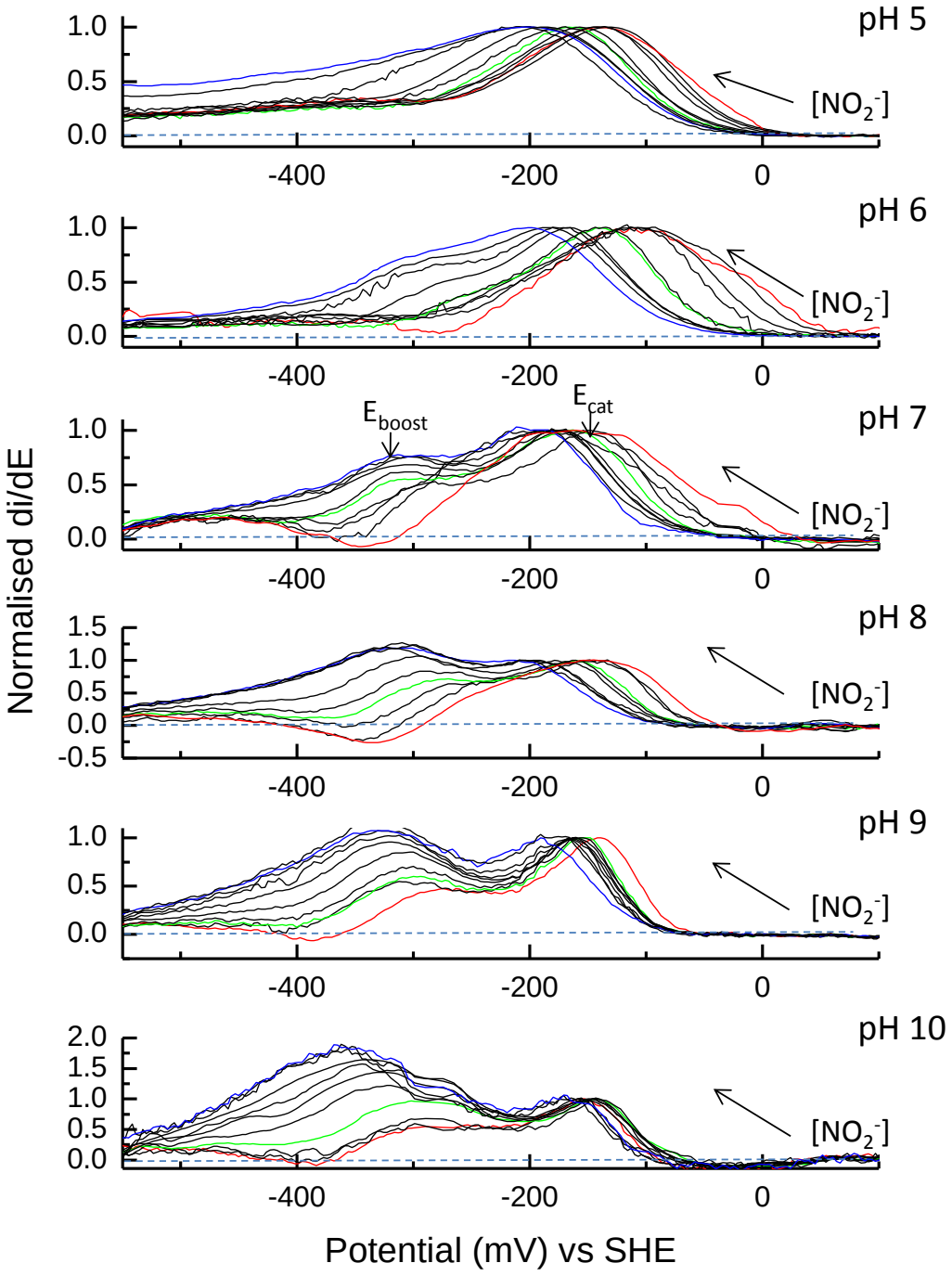

Figure 3.12. Derivative cyclic voltammograms of TvNir in 0.1 M NaCl. The arrow indicates the shift of the derivative voltammograms as the concentration of nitrite is increased, plots show derivative voltammograms shown range from at 10 (red) and 10240 (blue) μM nitrite. The nitrite concentration closest to the K_M is shown in green. The dashed line represents zero change in the current with the change potential. The di/dE is normalised to the peak height of E_{cat}. The experiments were performed as described in section 4.3.

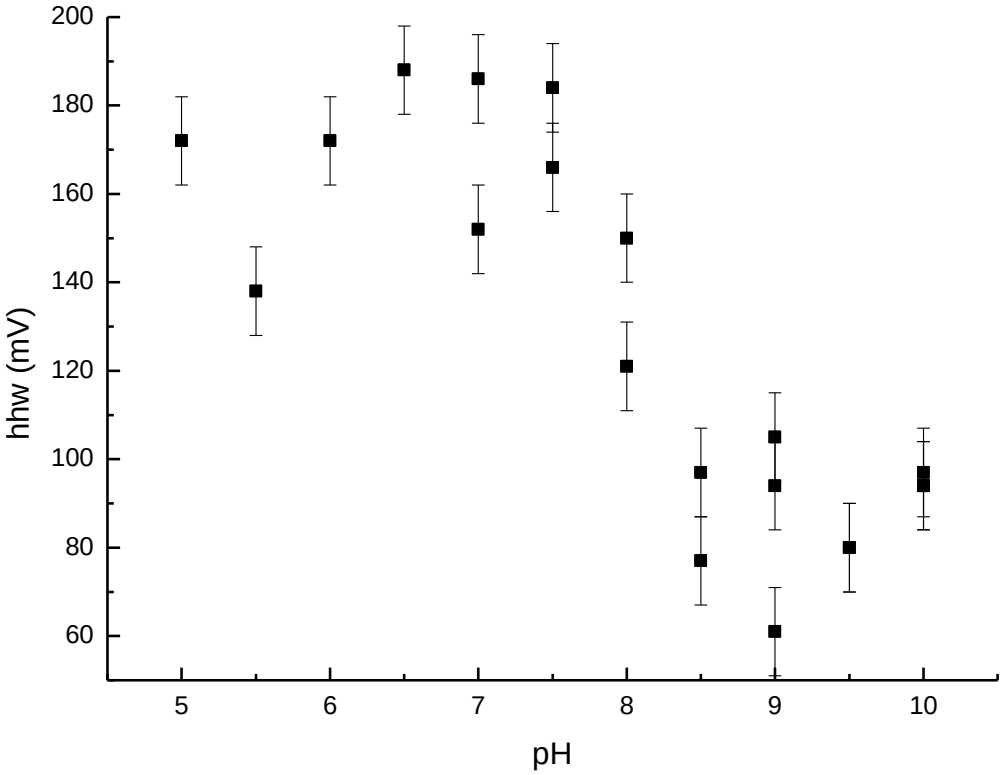

Figure 3.13 Half height width of the peak at E_{cat} in 10 µM NO_2^- for each pH. The cyclic voltammograms were recorded as described in section 4.3 in 20 mM HTMA (pH 5-9) and 20 mM HCMA (pH 9.5 and 10), 100 mM NaCl at 20 °C, where the electrode rotation speed was 3000 rpm.

In order to further assess the impact of nitrite concentration and pH on the position and incidence of the features E_{boost} and E_{cat} the potentials of these features were plotted against the log of the nitrite concentration (figure 3.14). It is clear that the position of E_{cat} shifts to more negative potentials as the nitrite concentration is increased and that this effect is more evident at low pH. Similarly where E_{boost} is detected, increasing the nitrite concentration causes this feature in the di/dE plot to shift to more negative potentials. This is consistent with the analysis from examination of the baseline subtracted and derivative cyclic voltammograms (figure 3.11 and 3.12).

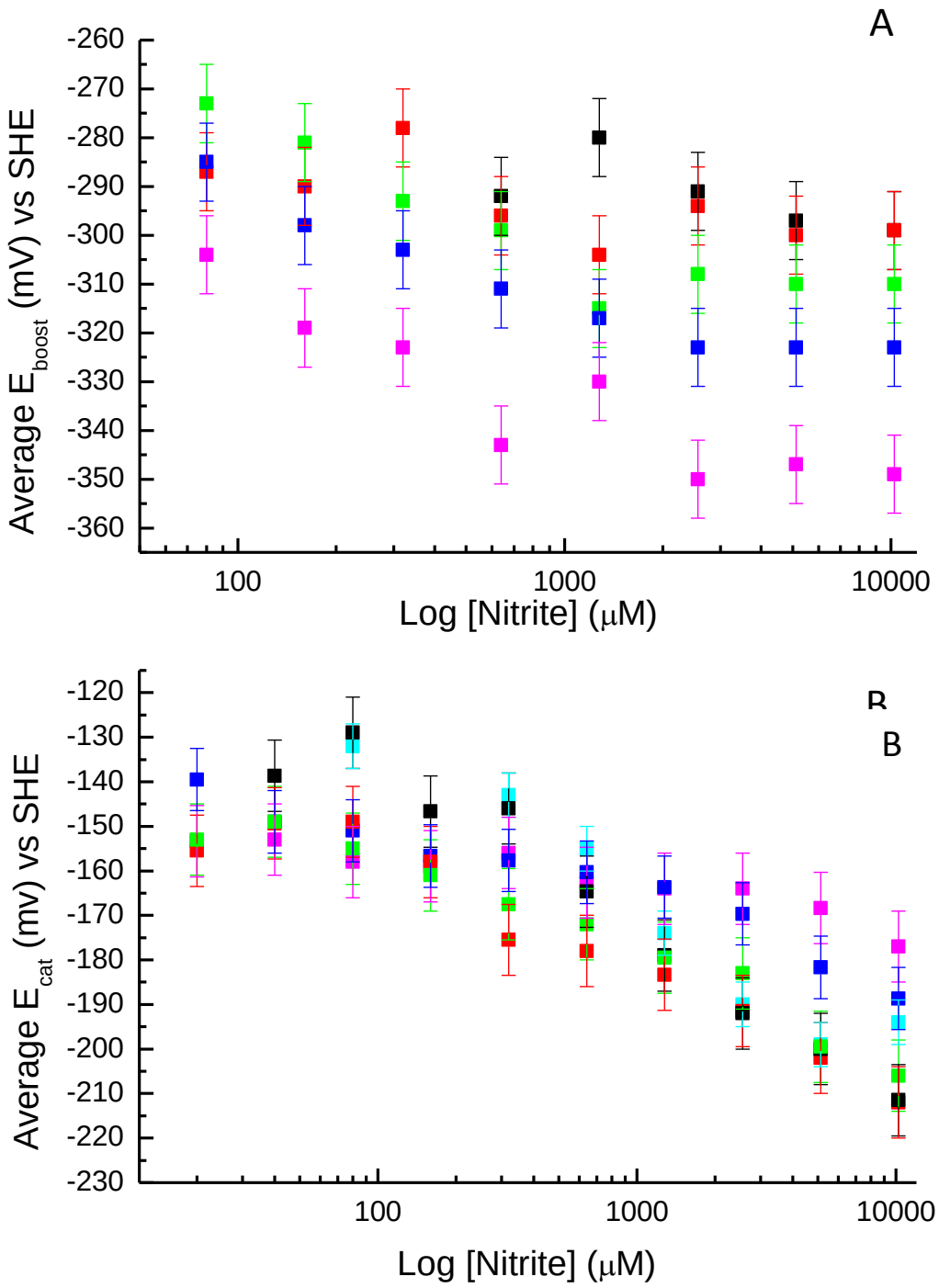

Figure 3.14 The features of the derivative cyclic voltammograms of TvNir at different pH and [NO_2^-].(A, B) The average position of E_{cat} and E_{boost} respectively, from the derivatives of three experiments at pH 5 (cyan), pH 6 (black), pH 7 (red), pH 8 (green), pH 9 (blue) and pH 10 (magenta). All experiments were performed as previously described in figure 4.5

The variation of the K_M for nitrite reduction by TvNir has been defined across the pH range at -550mV and it has been shown to decrease by an order of magnitude as the pH is increased. However, comparison of the features E_{cat} and E_{boost} from the di/dE plot at the nitrite concentration closest to the K_M for each pH showed very little variation in the position of these features with pH (figure 3.15).

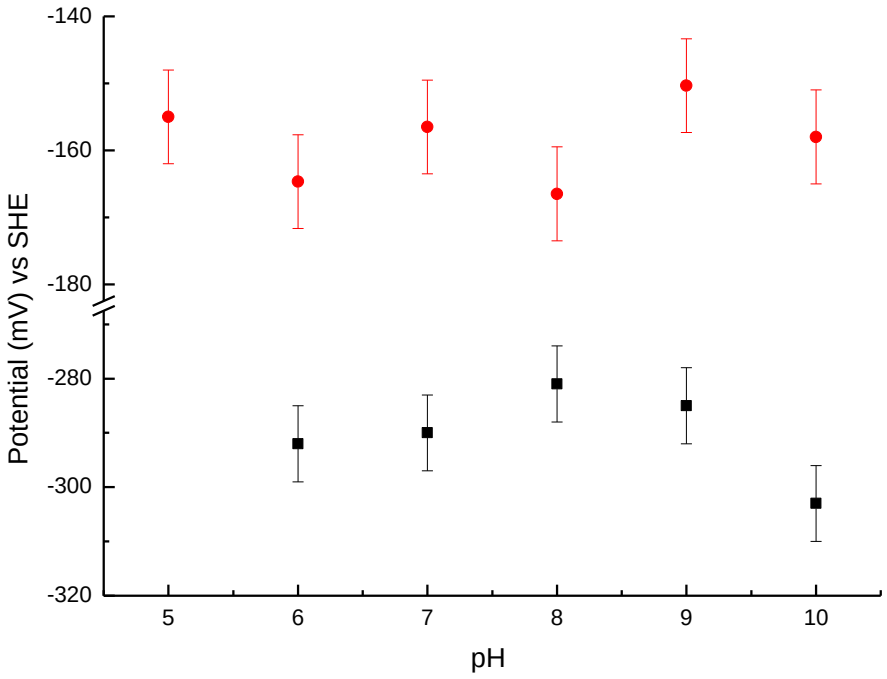

Figure 3.15 The features of the derivative cyclic voltammograms for TvNir at the K_M. Showing the potential of E_{cat} (red) and E_{boost} (black). The nitrite concentration is that closest to the K_M for each pH. All experiments were performed as previously described in figure 3.11.

3.5.2 The waveshape of nitrite reduction in 4.3 M NaCl

Cyclic voltammetry nitrite titration experiments were performed as described in section 3.4 in 4.3 M NaCl at pH 6 and pH 10 (figure 3.16). Cyclic voltammograms in 10 µM, 10.24 mM nitrite and at the nitrite concentrations around the K_M calculated at -550 mV are shown in figure 3.16. The key features of the cyclic voltammograms in 4.3 M NaCl are the same as those in 0.1 M NaCl; the onset of catalysis is ca. -100 mV, nitrite reduction is attenuated around -300 mV at low nitrite concentrations and increasing nitrite concentration gives rise to a more sigmoidal dependence of current magnitude on applied potential. Whilst in 4.3M NaCl the current magnitudes of TvNir

at pH 10 are still significantly lower than those at pH 6, the potential dependence of nitrite reduction at 4.3 M is much more like that at pH 6. Cyclic voltammograms of TvNir at pH 10, 4.3 M NaCl are less featured than those in 0.1 M NaCl and the catalytic current shows a more sigmoidal dependence on applied potential than the cyclic voltammograms in 0.1 M NaCl. Whilst no significant change in the kinetic parameters of nitrite reduction at -550 mV were detected, the apparent changes in the cyclic voltammogram indicated there might be some difference in the kinetics of nitrite reduction at -143 mV.

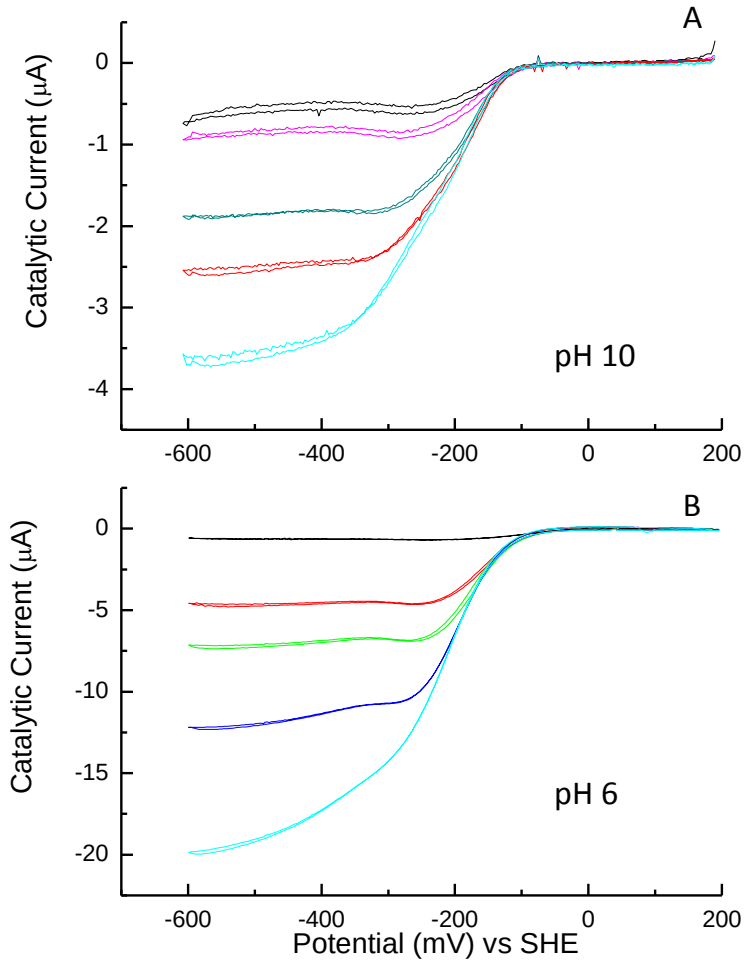

Figure 3.16 Nitrite reduction by TvNir in 4.3 M NaCl. A. Baseline subtracted cyclic voltammograms of TvNir in 20 mM HCMA, 4.3 M NaCl, pH 10 at 10 µM (black), 20 µM (magenta), 80 µM (dark cyan), 160 µM (red) and 10.24 mM (cyan) NO_2^-. B. Baseline subtracted cyclic voltammograms of TvNir in 20 mM HTMA, 4.3 M NaCl, pH 6 where the nitrite concentrations are represented the same as in (A) and 640 µM (green) and 1280 µM (blue) NO_2^-.

To better appreciate the effect of increased salt concentration on the applied potential required for catalysis derivatives were taken of the cyclic voltammograms in 4.3 M NaCl at pH 6 and pH 10, at all nitrite concentrations from 10 µM to 10.24 mM and compared to those in 0.1 M NaCl (figure 3.16). For pH 6 in 4.3 M NaCl at high nitrite concentration there is no shoulder on the feature E_{cat}. Attenuation in nitrite reduction ca. -300 mV is apparent in the low nitrite concentration derivatives of TvNir at pH 6, although this was not readily detected in 0.1 M NaCl. At pH 10 in 0.1 M NaCl the E_{boost} feature is seen at low nitrite concentrations and increasing the nitrite concentration increases the contribution of this centre to catalysis until it dominates the derivative plot. In 4.3 M NaCl there is no E_{boost} feature at low nitrite concentrations and this only becomes apparent, to a much lesser extent as the concentration of nitrite is increased. The redox centre/s that usually requires increasingly negative applied potentials to reduce as the nitrite concentration and pH are increased in 0.1 M NaCl, appear to be reduced at more positive potentials even at high nitrite concentrations and pH in 4.3 M NaCl.

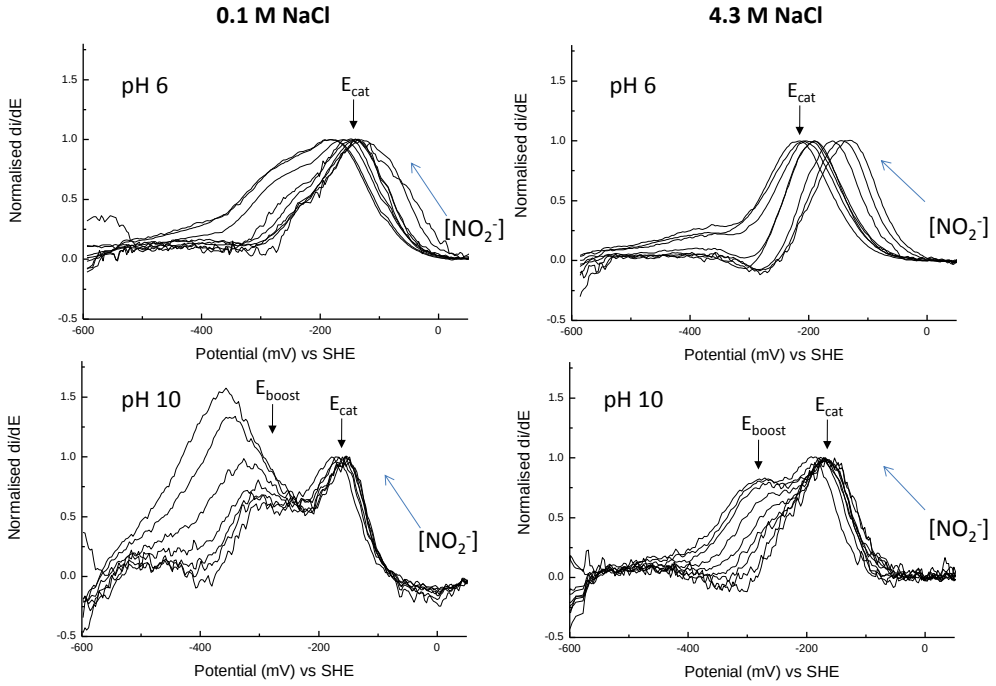

*Figure 3.16.The derivatives of TvNir at varying [NO_2^-], pH and [NaCl].*The arrow indicates the direction increasing [NO_2^-]. All [NO_2^-] shown are between 10 µM and 10.24 mM. The salt concentration and pH are as indicated. The pH 6 experiments were performed in 20 mM HTMA buffer and the pH 10 were performed in 20 mM HCMA. All experiments were performed at 20 °C, where the electrode rotation speed was 3000 rpm. The derivative is normalised to the height of the feature at E_{cat}.

To attempt to quantify the effect of NaCl concentration on nitrite reduction by TvNir, film transfer experiments were performed in 20 mM HCMA, with 60 µM NO_2^- at pH 10. In these experiments a fresh TvNir film was prepared and three cyclic voltammograms were initially performed in 0.1 M NaCl, the film was transferred to an identical solution of a different NaCl concentration and three cyclic voltammograms recorded, the TvNir film was then transferred back to a solution of 0.1 M NaCl and three further cyclic voltammograms were recorded.

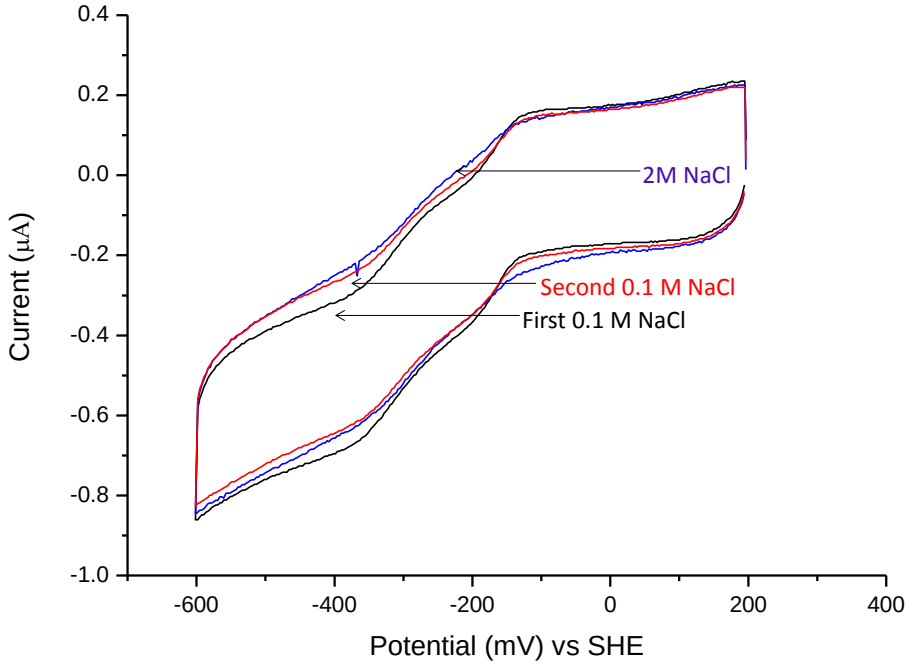

Figure 3.17 Film transfer experiments to explore the salt dependence of i_{cat} for TvNir. The third cyclic voltammogram for the first series of cyclic voltammetry in 0.1 M NaCl (black), cyclic voltammetry in 2 M NaCl (blue) and the second series of cyclic voltammetry in 0.1 M NaCl (red). All experiments were performed in 20 mM HCMA at pH 10 with 60 µM NO_2^-, where the temperature was 20°C, the electrode was rotated at 3000 rpm and the scan rate was 30 mV s^{-1}.

The current of the third cyclic voltammogram for each data set i.e 0.1 M NaCl (1^{st}), the NaCl concentration being investigated and 0.1 M NaCl (2^{nd}), were extracted and compared at -200 and -350 mV as inspection of the cyclic voltammograms suggested these were the potential regions where catalysis was most affected by NaCl

concentration. The effect of salt concentration on catalysis at these potentials was quantified using equation 3.5:

$$i_{(x\text{mM NaCl})} = \left(\frac{\frac{i_{(x\text{mM NaCl})}}{i_{(100\text{ mM NaCl 1st})}} + \frac{i_{(x\text{mM NaCl})}}{i_{(100\text{ mM NaCl 2nd})}}}{2} \right) \qquad \text{(Equation 3.5)}$$

Normalising the values to a first and second data set recorded in 0.1 M NaCl eliminated the effect of film loss that would be expected during these film transfer experiments, so that changes in the catalytic current detected on changing the NaCl concentration could directly be attributed to the change in NaCl concentration. Between 0.1 and 2 M NaCl a slight increase in catalysis was detected at -200 and -350 mV as the NaCl concentration increased (figure 3.18). However further increasing the NaCl concentration to 4 M decreased the catalytic current at -200 and -350 mV. These experiments indicated that 4 M NaCl appeared to inhibit catalysis.

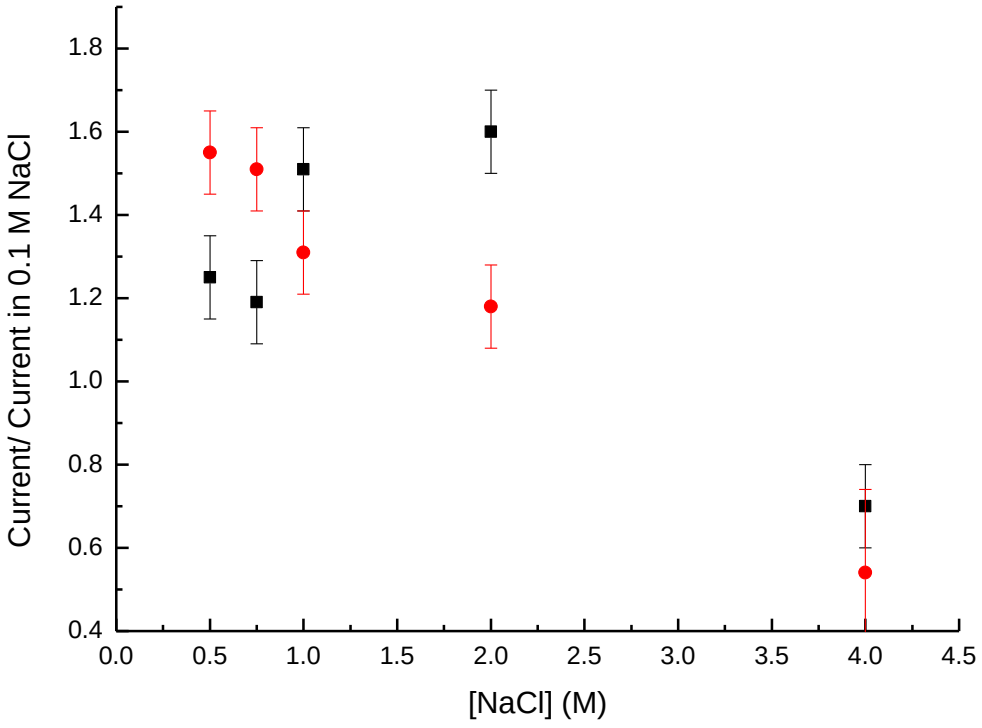

Figure 3.18 The dependence of the catalytic current for nitrite reduction by TvNir on the concentration of NaCl. The catalytic current, normalised with respect to the current in 0.1 M NaCl is shown at -200 mV (black) and -350 mV (red) and these values represent the average of at least three experiments. Experimental conditions were as described in figure 3.17.

To investigate whether the inhibition of catalysis seen at 4 M NaCl was a NaCl specific effect the film transfer experiments were repeated under exactly the same conditions, but with KBr instead of NaCl in the buffer (figure 3.19). Control experiments at 0 mV where there is no catalysis showed no change in the current between the salt concentrations. However, as the electrolyte concentration was increased from 0.5 to 4 M KBr the catalytic current at both -200 and -350 mV increased. This suggests that an inhibitory effect at 4 M is NaCl specific and that general increased ionic strength improves the rate of catalysis by TvNir.

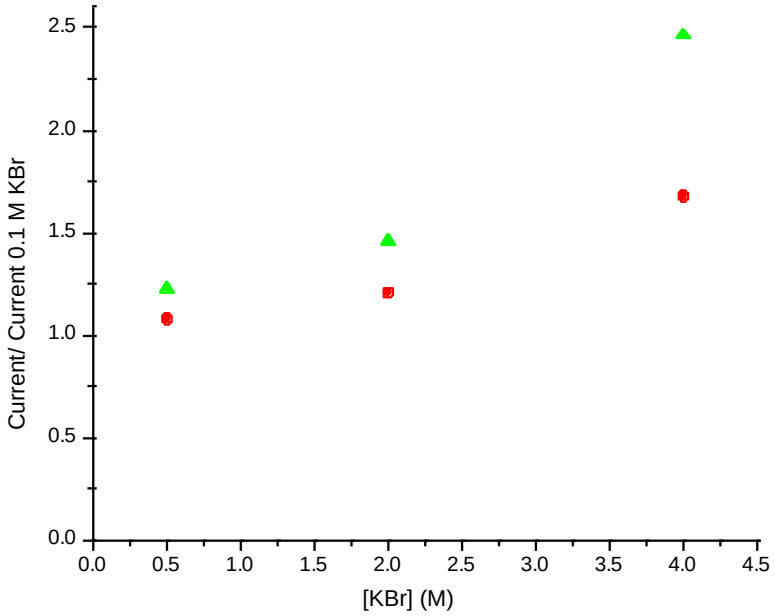

Figure 3.19 The effect of KBr concentration on the catalytic current of TvNir for nitrite reduction. The current normalised to the current in 0.1 M KBr at -200 mV (red) and -350 mV (green). Experimental conditions are identical to those in figure 3.17, excepting KBr is used instead of NaCl.

3.6 Inhibition of Nitrite Reduction by TvNir

The inhibition of NrfA has been well characterised [3, 105]. In light of the novel substrate inhibition detected for nitrite reduction by TvNir, some inhibitors of NrfA were screened to see whether they had an effect on catalysis by TvNir and to discern whether there were differences in the anions that bind to the active sites of TvNir and NrfA [105]. Chronoamperometry at -550 mV was used to assess whether sulphite and dithionite were inhibitors of nitrite reduction (figure 3.20). A TvNir protein film was

adsorbed to a freshly polished electrode and placed in an electrochemical cell containing 20 mM HTMA, 0.1 M NaCl at pH 7 and the sample was poised at -550 mV for 700 s. After 30 s 250 µM NO_2^- was added to the electrochemical cell and an increase in the catalytic current, corresponding to this addition was observed. At 300 s 100 µM of either dithionite or sulphite was added to the electrochemical cell and the catalytic current decreased indicating that both these compounds were inhibitors of TvNir (figure 3.20). Further additions of sulphite or dithionite further decreased the catalytic current corresponding to each increase in inhibitor concentration, confirming the inhibitory effect.

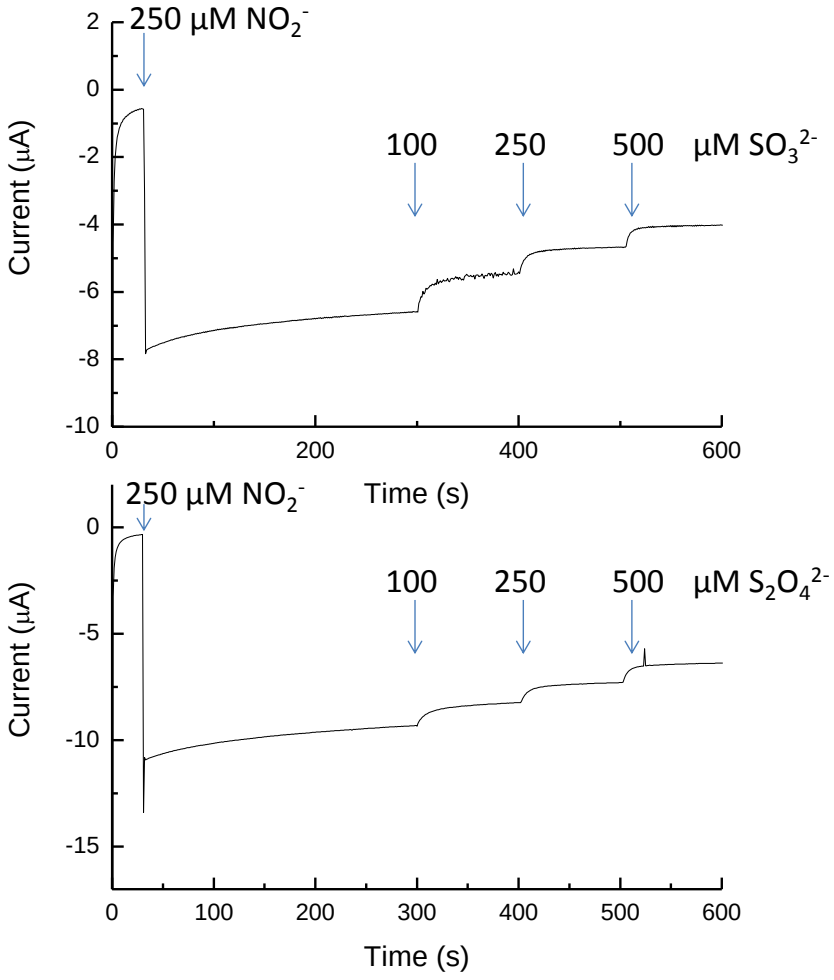

Figure 3.20. Inhibition of nitrite reduction by sulphite and dithionite. The arrows show the addition of either nitrite, sulphite or dithionite as indicated. Both experiments were performed in 20 mM HTMA, 0.1 M NaCl, pH 7 at 20 °C where the electrode rotation speed was 3000 rpm.

Cyclic voltammetry was also used to investigate the effect of the NrfA inhibitor cyanide on nitrite reduction by TvNir. Cyclic voltammetry was performed of a TvNir film adsorbed on a freshly polished graphite electrode between +197 and -603 mV at 30 mV s^{-1} in 20 mM HTMA, 0.1 M NaCl at pH 7 where the nitrite concentration was 200 µM (figure 3.21). Cyclic voltammetry in nitrite gave the catalytic response expected from earlier studies. After three cyclic voltammograms, when the potential was > 0 mV, 0.5 mM NaCN was added to the electrochemical cell. The addition of cyanide to the electrochemical cell caused no change in cyclic voltammetry at potentials > -100 mV, the onset of catalysis occurred at this point as it did in the absence of cyanide. However scanning to more negative potentials quickly decreased the catalytic current and once the potential was swept to -300 mV catalysis was no longer detected. Catalysis did not return with further cyclic voltammograms, indicating that cyanide binds to the active site of TvNir upon reduction and that once it has it is slow to reverse (if it does at all).

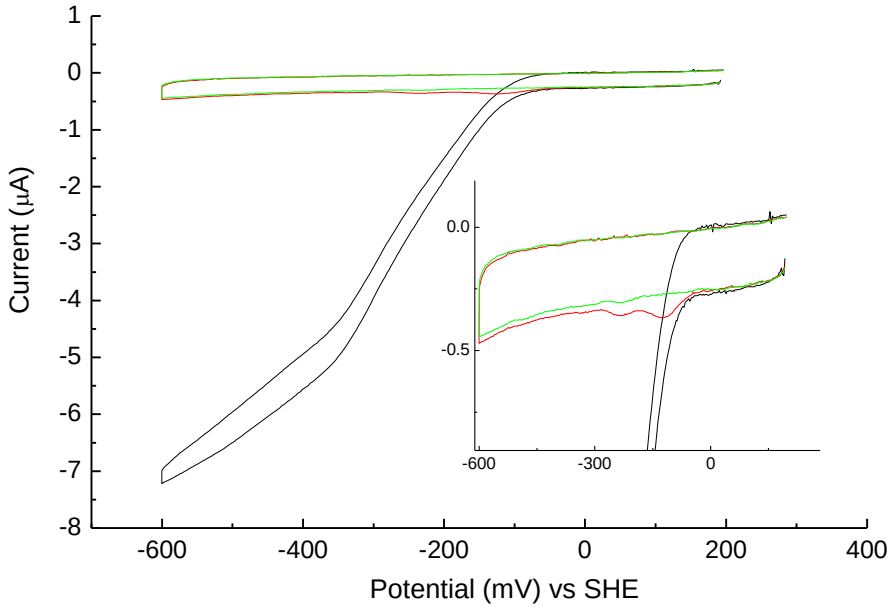

Figure 3.21 Cyanide inhibition of nitrite reduction by TvNir. Cyclic voltammetry of TvNir in 200 µM NO_2^- (black), when 525 µM cyanide initially is added to the electrochemical cell at positive potential (red) and the second cyclic voltammogram after the addition of cyanide (green). Inset shows a larger image of the main figure to clarify the effects of cyanide addition. Experiments were performed in 20 mM HTMA, 0.1 M NaCl at pH 7 at 20 °C, where the scan rate was 30 mV s^{-1} and the electrode was rotated at 3000 rpm.

3.7 Discussion

The experiments in this chapter have found that the K_M of TvNir is much lower than that which has been previously published (16.7 mM NO_2^- at pH 7) [63]. This is likely to be because the activity was previously measured using methyl viologen assays (described in chapter 2) where the electron donor to TvNir, methyl viologen, was reduced using 15-20 mM sodium dithionite [63]. Here sodium dithionite has been shown to inhibit nitrite reduction by TvNir at concentrations as low as 100 µM (figure 3.20) and so this large excess of inhibitor in solution was likely to affect the results of the activity assays. The K_M determined by PFV of TvNir in this chapter is more similar to the K_M of NrfA (28 µM at pH 7), which is what would be expected due to the similarities between the active sites of these enzymes (chapter 1) [40, 73]. PFV of TvNir has also found that the enzyme is inhibited by sodium sulphite and sodium cyanide which are also inhibitors of NrfA [3, 105]. At more positive potentials cyanide did not inhibit catalysis, but as the potential was decreased the catalytic current disappeared suggesting that cyanide more favourably binds to reduced TvNir. This is also in agreement with findings for NrfA that have shown cyanide binds more favourably to the reduced enzyme [105]. Cyanide inhibition of TvNir shown by PFV agrees with previous solution based assays of this inhibition and in addition to this the similarities of PFV of TvNir to the structurally homologous NrfA suggest that TvNir retains its intrinsic properties and is not perturbed by electrode adsorption for PFV [78].

Cyclic voltammetry has shown that, like *E. coli* and *D. desulfuricans* NrfA, TvNir is redox active at potentials below ca. -100 mV and that this activity increases as the potential is swept to -600 mV [1, 82]. The onset of catalysis therefore occurs at potentials well below the reduction potential of the NO_2^-/NH_4^+ redox couple and for NrfA has been shown to reflect the reduction of the active site heme (E_m = -107 mV), due to their structural similarities this is also likely to be the case for TvNir (figure 3.22) [54, 65]. The siroheme nitrite reductases that also catalyse the reduction of nitrite to ammonium, also have low reduction potentials compared to the NO_2^-/NH_4^+ redox couple, where the siroheme active site reduction potential is -340 mV and the iron-sulphur cluster that transfers electrons to the active site reduction potential is -405 mV [109]. This suggests that low potentials are required for the reduction of nitrite to

ammonium regardless of the enzyme type that catalyses the reaction. Contrastingly PFV of the copper nitrite reductase, that catalyses the one electron reduction of nitrite to nitric oxide, has shown that catalysis is initiated when potentials below +300 mV are applied [110]. Quantification of the reduction potential of the type-2 copper active site in this enzyme has been challenging, as substrate binding is proposed to increase the reduction potential by ca. 100 mV, such that it is thermodynamically favourable for electrons to move from the type-1 copper site (E_m = +247 mV) [111]. The enzyme cytochrome *cd*$_1$ nitrite reductase that also catalyses the reduction of NO_2^- to NO has a positive active site reduction potential of +175 mV [112]. It is clear that the reduction of nitrite to nitric oxide does not require such a large thermodynamic driving force for catalysis as nitrite ammonification. The steps that are intrinsic to nitrite ammonification and not nitrite reduction are the reduction of the intermediates of NO to NH_2OH and NH_2OH to NH_4^+. The reduction of NH_2OH to NH_4^+ has a very positive reduction potential (E_m = +840 mV), but the reduction potential of the NO/NH_2OH redox couple is more negative (E_m= -70 mV). It is possible that nitrite ammonifying enzymes have lower operating potentials in order to efficiently catalyse the reduction of this intermediate step.

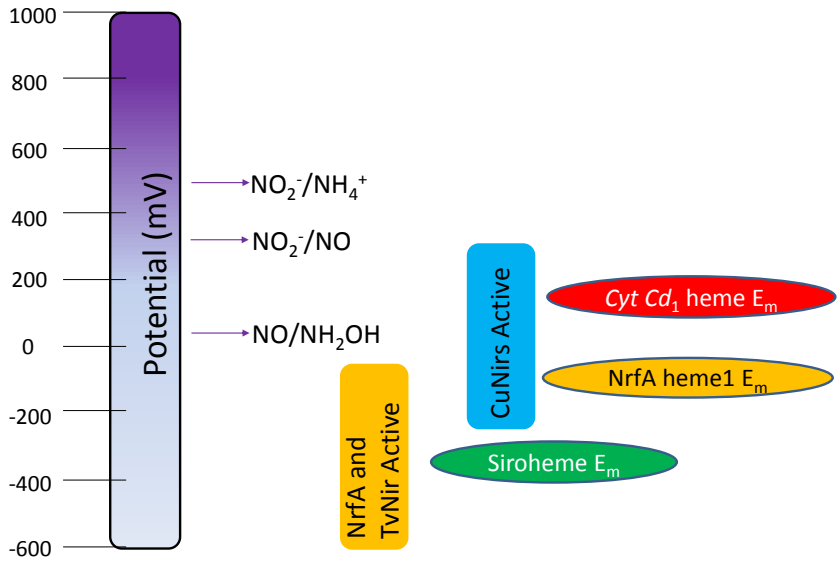

Figure 3.22. The relationship between the activity window for nitrite reduction and potential for TvNir, NrfA and the Copper nitrite reductases. The reduction potential of the NrfA and the siroheme nitrite ammonifying active sites and the cytochrome *cd*$_1$ active site are shown, along with the standard reduction potentials determined for the intermediates of nitrite ammonification.

As the potential is swept from positive to negative during cyclic voltammetry the catalytic current is expected to reach a limiting value [103]. However, analysis of the derivative cyclic voltammograms found that once the applied potential was more negative than that required for the onset of catalysis, a potential was not obtained where catalytic current was independent of potential, at any pH or nitrite concentration. PFV studies of the [NiFe]-hydrogenase from *Allochromatium vinosum* found that this effect was due to the enzyme being adsorbed to the electrode in multiple different conformations [113]. Using high temperatures where the rate of catalysis by the [NiFe]-hydrogenase was very fast, different rates of IET were revealed due to the slightly different conformations of the enzyme adsorbed to the electrode.

The key features in the waveshapes of the cyclic voltammograms of TvNir and NrfA have many similarities. Both NrfA and TvNir have cyclic voltammograms that are attenuated at low nitrite concentration and become more sigmoidal at high nitrite concentration, at pH 7.0 (figure 1.10 and 3.11). Comparison of the first derivatives of the cyclic voltammograms of TvNir and NrfA at pH 7.0 confirms that both enzymes are attenuated ca.-300 mV at 'low' nitrite concentration and both have the E_{cat} and E_{boost} features (figure 3.20). For both TvNir and NrfA E_{cat} broadens as the nitrite concentration is increased and E_{boost} becomes more prominent at higher nitrite concentration. However in the derivative cyclic voltammogram of TvNir at pH 7.0 E_{boost} does not become as clearly defined as a separate feature at high nitrite concentration, as it does for NrfA and the E_{cat} feature does not broaden as much in the TvNir derivative as it does in that of NrfA. The derivative cyclic voltammogram of NrfA at pH 7.0 is very similar to that of TvNir at pH 10 and this suggests that the pH dependence of the catalytic waveshape for NrfA is different to that of TvNir, whilst the key mechanistic steps that define the catalytic current potential profile features are the same for these enzymes.

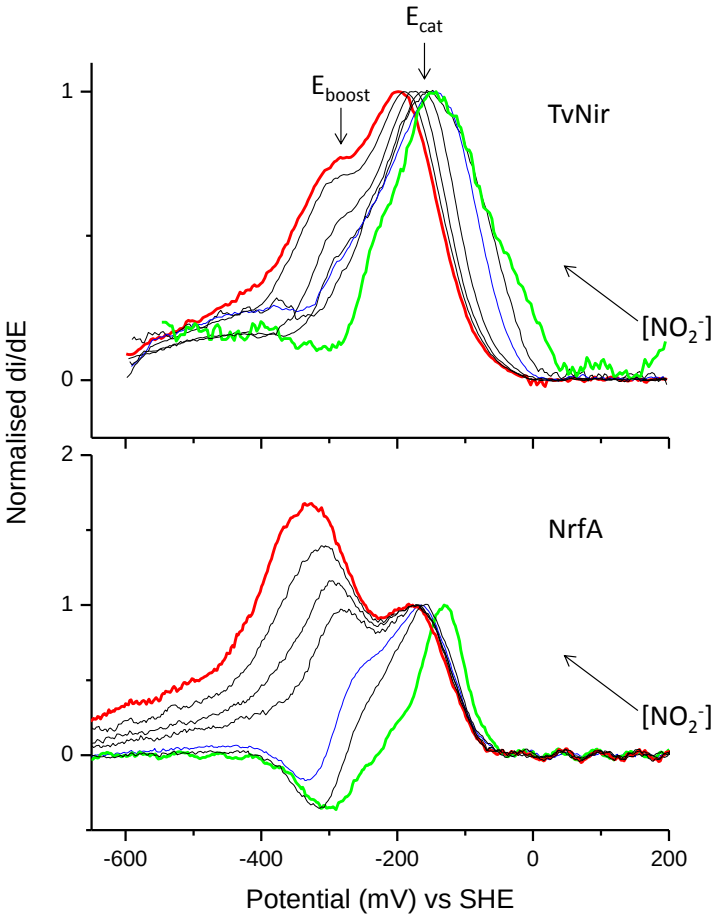

Figure 3.23 Derivative cyclic voltammograms of NrfA (E. coli) and TvNir at pH 7.0. Derivative cyclic voltammograms from nitrite titrations to TvNir and NrfA where the green line show the lowest nitrite concentration used (10 µM TvNir, 1 µM NrfA), the blue line shows the derivative at the nitrite concentration closest to the K_M at low potential (160 µM TvNir and 16 µM NrfA) and red shows the highest nitrite concentration (5000 µM TvNir and 320 µM NrfA). These are the derivatives of the oxidative sweeps of cyclic voltammograms recorded at 30 mV s^{-1}, at 20 °C in buffer containing 20 mM HTMA, 0.1 M NaCl (TvNir) or 50 mM Hepes, 2 mM $CaCl_2$.

To further elucidate the differences in the pH dependence of the catalytic waveshapes of TvNir and NrfA the features of the derivative cyclic voltammgrams can be compared for TvNir and NrfA at low nitrite concentration (figure 3.23). At nitrite concentrations << K_M not all the enzyme will have substrate bound and so changes in the catalytic current with changes in potential can be seen to reflect the oxidation or reduction of redox centres within the enzyme that effect catalysis.

The E_{cat} feature of the derivative cyclic voltammogram at low nitrite concentration shows a much greater change with pH in NrfA compared to TvNir (figure

3.21). Studies of NrfA between pH 4-9 found that at low pH the peak in the derivative at E_{cat} had a hhw of 52 ± 5 mV, reflecting a two electron reduction and that at high pH the hhw increased to ca. 90 mV indicating a one electron reduction [104]. The position of the feature E_{cat} in the NrfA derivative plot at 1.7 μM NO_2^- had a pH dependence of ca. -38 mV per pH unit and this was proposed to reflect a two electron reduction coupled to a protonation step. However, more recent resolution of the reduction potentials of the NrfA hemes showed that there was no evidence for a two electron transition and it is thought that this must be a consequence of interactions between the substrate with the enzyme and that the two electron reduction occurs when nitrite is bound to the enzyme [54, 82]. The position of E_{cat} is centred on the reduction potential of the NrfA active site heme and the pH dependence of E_{cat} together with the $pK_{a\ ox}$ of 5.4 and $pK_{a\ red}$ of 8.4 for this heme suggest that reduction of the active site heme is coupled to the protonation of a heme propionate group [104, 114]. Comparatively the position of E_{cat} shows little pH dependence in TvNir and the hhw has the opposite pH dependence in TvNir to that of NrfA and at pH 5 is ca. 170 mV and this decreases as the pH is increased to ca. 90 mV, reflecting a one electron reduction (figure 3.12, 3.13). There are clearly some distinct differences in the oxidative/reductive parameters that give rise to this feature in both of these enzymes. The reduction potential of the active site heme is unknown in TvNir, but it is likely that this is also centred upon E_{cat}, the lack of pH dependence of this feature for TvNir suggests that the reduction of the TvNir active site is not coupled to protonation of a heme propionate group. The differences in the half height width of E_{cat} for these enzymes could reflect differences in the substrate interactions with the enzyme and therefore the presence of the cys-tyr bond in the active site of TvNir.

At low nitrite concentration the attenuation feature shows similar pH dependence in both enzymes (figure 3.24). It has been previously suggested that the attenuation feature for NrfA reflects the reduction potential of the lowest potential heme at -320 mV, this reduction has been assigned to either heme 4 or heme 5 that is distant to the active site [40, 54]. As TvNir has a very similar heme arrangement to NrfA it is likely that this attenuation reflects the reduction of corresponding heme in TvNir (figure 1.3 and 1.12).

The boost feature was not detected for NrfA at low nitrite concentration at pH 4-9, but was detected at pH 9 and above for TvNir. This could be because the lowest nitrite concentrations used for TvNir and NrfA are different, but as the K_M for these enzymes is different that should not be too important, the nitrite concentration is still << K_M. Analysis of the waveshape of TvNir found that some of the redox centres contributing to catalysis in the E_{cat} feature become reduced at lower potentials as the nitrite concentration and pH are increased, giving rise to the feature at E_{boost}. Earlier inspection of the derivatives of TvNir and NrfA at all nitrite concentrations showed that the E_{boost} feature is more prominent in NrfA at pH 7 than TvNir, in TvNir the derivative cyclic voltammogram at pH 10 most closely resembles that of NrfA at pH 7.0 (figure 3.12). This could suggest that the redox centres in NrfA contributing to E_{cat} and E_{boost} are more susceptible to changes in pH than those in TvNir, but it is not possible to confirm this at this stage.

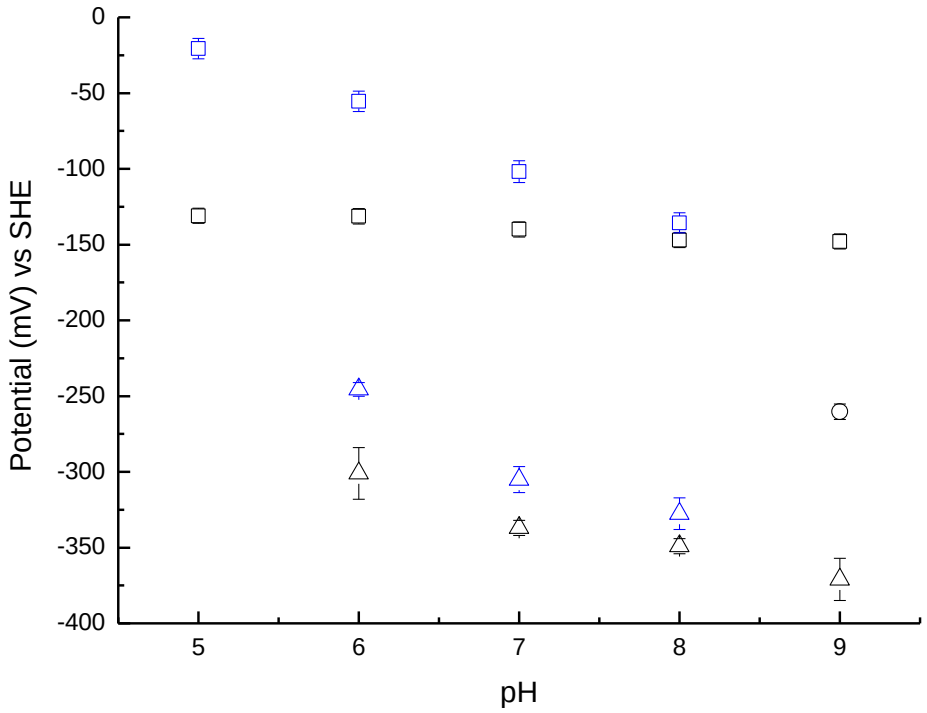

Figure 3.24 The features of the derivative cyclic voltammograms for TvNir and NrfA at low nitrite concentration. The attenuation feature (triangles), the boost feature (circles) and E_{cat} (squares) for NrfA (blue) and TvNir (black). The TvNir data points are extracted from the average of at least three experiments in 10 µM nitrite and the NrfA data points were collected at 1 .7 µM nitrite. the buffer and experimental conditions were as described for each enzyme in figure 3.20 [115].

For TvNir it has been established that the largest catalytic currents are obtained at low pH (figure 3.6). Comparison of the i_{max} of NrfA normalised to the i_{max} at pH 7 shows that both of these enzymes follow the same trend of i_{max} decreasing as the pH is increased (figure 3.25)[115]. For TvNir the pH dependence of i_{max} does not reflect the pK_a of an amino acid within the enzyme i.e. a key proton binding step in the catalytic mechanism. The reduction of nitrite to ammonia is a process that requires eight protons and it is likely that this is the reason that both NrfA and TvNir have the same pH dependence; the i_{max} for each enzyme at that pH reflects the maximum rate that can be obtained in a solution of that proton concentration by these enzymes. If this is the case then at i_{max} it can be considered that the proton concentration is limiting the rate of catalysis.

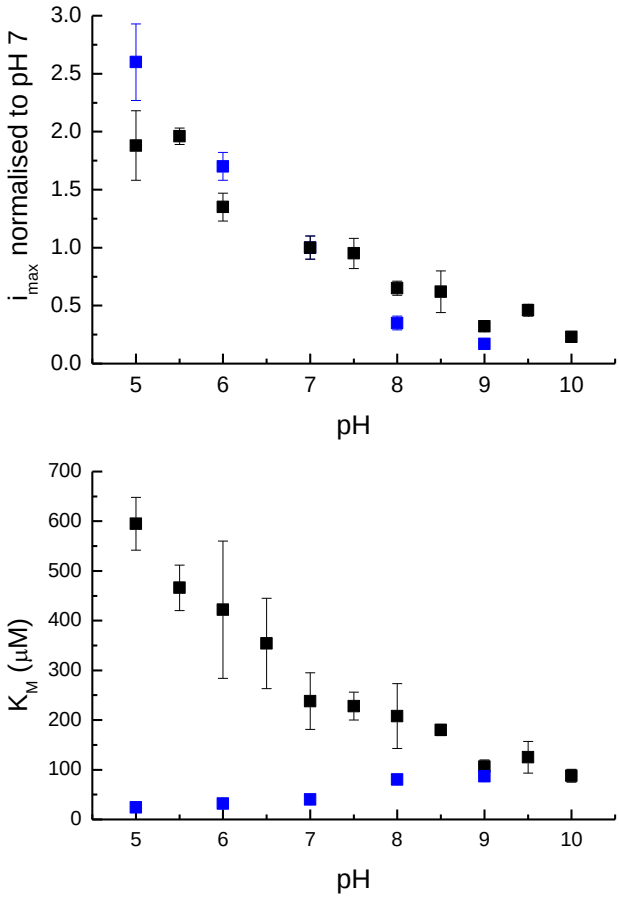

Figure 3.25 The pH dependence of i_{max} and K_M for TvNir and E. coli NrfA. The K_M for TvNir (black) was determined at -550 mV and is the average of the experimental data collected via cyclic voltammetry and chronoamperometry in 20 mM HTMA, 0.1 or 4.3 M NaCl. The K_M for NrfA (blue) at -600 mV was determined by cyclic voltammetry in 25 mM HTMA, 2 mM $CaCl_2$ [115].

It has been shown that the K_M for TvNir is pH dependent and decreases by an order of magnitude as the pH increases (figure 3.22). The pH dependence of NrfA is very different to that of TvNir and shows a comparatively small increase as the pH is increased [115]. The pH dependent increase in the K_M of NrfA had a pK_a of 7.8 and most likely reflected the protonation of the active site His 264 (figure 1.4) [40, 115]. Whilst a corresponding active site histidine is present in the structure of TvNir (figure 1.13), there is no indication that the pH dependence of the K_M of TvNir reflects such a pK_a [73]. It is clear that despite the similarities in the structures of the active sites of TvNir and NrfA another parameter is defining the K_M for TvNir. The K_M is comprised of the rate constants k_{on}, k_{off} and k_{cat} shown in scheme 3.1. Under conditions of steady-state catalysis the concentration of the enzyme-substrate complex is constant and so equation 3.6 can be derived:

$$\frac{d[E:S]}{dt} = k_{on}[E][S] - [E:S](k_{off}+k_{cat}) = 0 \qquad \text{(Equation 3.6)}$$

From this steady-state assumption it can be derived that:

$$\frac{[E][S]}{[E:S]} = \frac{k_{off}+k_{cat}}{k_{on}} = K_M \qquad \text{(Equation 3.7)}$$

The K_M of TvNir has similar pH dependence to the k_{cat} (the i_{max} normalised to enzyme amount), the decrease in the K_M of TvNir at high pH could directly reflect the decrease in the k_{cat}. It could be argued that the K_M of NrfA would then likely have the same pH dependence as TvNir, as the pH dependence of their k_{cat} is similar. The pH dependence of the K_M of NrfA is thought to reflect the pK_a of His 264, which is proposed to have a role as a proton donor during catalysis [48, 56]. There is only a small change in the active sites of TvNir and NrfA and that is that the Tyr 303 (or 216 NrfA) is covalently bound to a cysteine [73]. In the mechanism of nitrite reduction by NrfA Tyr 216 is thought to have a more structural H-bonding role and is not thought to directly interact with the substrate during catalysis [48, 56]. In TvNir the cys-tyr bond lowers the pK_a of the Tyr 303 to ca. 9.5, and the active site is also compacted by this bond formation [73]. At pH 9 the K_M of TvNir and NrfA are very similar, perhaps in TvNir the K_M might also reflect the protonation of the active site tyrosine, although there is little

evidence to suggest that a pK_a is being approached from inspection of the pH dependence. A different role for the active site histidine in catalysis by TvNir would explain why, in contrast to NrfA, the K_M for TvNir appears to directly reflect the proton limitation of k_{cat} and not the pK_a of this amino acid.

It is possible that there are other factors that define the pH dependence of the K_M for TvNir. The opposite pH dependence of the K_M for TvNir with respect to NrfA is similar to the opposite pH dependence of the hhw of the E_{cat} feature in the derivative cyclic voltammograms of these enzymes. Perhaps the structural difference contributing to these two phenomena are linked. Varying the concentration of salt and using different salts in the buffer electrolyte had little impact on the K_M of TvNir, with the exception of experiments performed in 4.3 M KBr (figure 3.9). At pH 6 use of 4.3 M KBr increased the K_M from 550 µM to 780 µM and interestingly further studies of the magnitude of the catalytic current showed that this was increased in 4 M KBr (figure 3.19). This further supports the idea that the K_M directly reflects the k_{cat} of TvNir.

At low pH and 0.1 M NaCl when monitoring the change in the catalytic current with increasing nitrite concentration, a point was reached where further increases in nitrite concentration decreased the catalytic current, indicating that under these conditions TvNir was substrate inhibited (figure 3.5). Substrate inhibition observed at low pH and 0.1 M NaCl for nitrite reduction by TvNir has not been detected for NrfA [82, 105]. The model used to determine the K_M and i_{max} when there was substrate inhibition, has a second nitrite binding to the enzyme substrate complex to form a dead-end enzyme-substrate-substrate complex (Scheme 3.2). With this method of substrate inhibition the second substrate molecule would have to bind either in the active site or at another location on their enzyme where binding will diminish the enzyme activity. It seems unlikely due to the similarity in the active sites of TvNir and NrfA, that another NO_2^- molecule would be able to bind in the active site of TvNir; there has been no evidence for substrate inhibition occurring in NrfA and the active site of TvNir is compacted compared to that of NrfA and therefore less likely to accommodate a second substrate molecule [73]. Inspection of the crystal structure suggests that the only patch where an extra nitrite binding and inhibiting seems sensible would be the positively charged patch at the opening of the product egress

channel [73]. The noted positively charged residues in this region, Lys 431, Arg 404, Arg 96, His 85 and Arg 81 predominantly have pK_a values such that if substrate inhibition reflected binding to this patch, it would likely not be restricted to pH < 7, excepting the histidine residue.

Whilst substrate inhibition has not been detected in other nitrite ammonifying enzymes, it has been found in the copper nitrite reductase from *Alcaligenes faecalis.* The copper nitrite reductase has two copper centres per monomer; the type 1 copper centre that receives electrons from the redox partner and transfers them to the active site type 2 copper centre that catalyses the reduction of NO_2^- to NO [110, 116]. Substrate inhibition of the copper nitrite reductase is also pH dependent occurring only at pH < 6.5. Another substrate molecule binding was proposed to be an unlikely mechanism for inhibition of this enzyme based upon the crystal structure [116]. They found that their kinetic data fit to a random sequential mechanism involving two different pathways to catalysis, one at low nitrite concentration where the type 2 site was reduced and then the substrate bound and another at high nitrite concentration where the substrate binds the type 2 site first and is then reduced [116]. They proposed that substrate inhibition occurred at low pH because electron transfer to the nitrite bound copper 2 site was slower than electron transfer to the H_2O bound copper 2 site, whereas at high pH electron transfer was faster to the nitrite bound copper 2 site than to the OH bound copper 2 site. These ideas can be applied to propose an alternative mechanism for the substrate inhibition of TvNir:

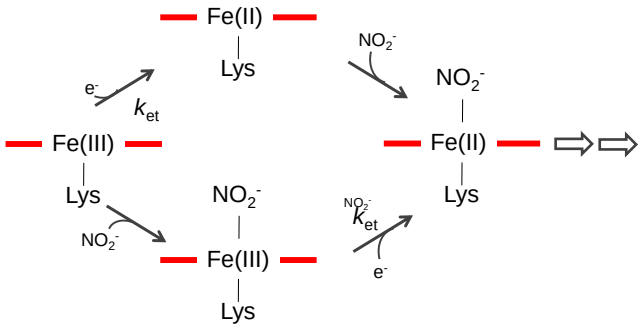

(Scheme 3.3)

For substrate inhibition according to scheme 3.3, at high NO_2^- concentrations the active site will first bind NO_2^- to form Fe(III)-NO_2^- and this would be followed by

reduction of the active site. In scheme 3.3 substrate inhibition would be caused by a slower electron transfer to the nitrite bound active site than to the free enzyme. The pH dependence of substrate inhibition by scheme 3.3 is not likely to be caused by water as opposed to a hydroxyl being the starting exogenous axial ligand to the active site heme, as is proposed for the copper nitrite reductase, as there is no evidence for a water bound active site in TvNir; MCD spectroscopy at pH 7.0 has found OH to be the 'resting' exogenous ligand to the active site heme (Chapter 4). In Scheme 3.3 the electron required to reduce the active site heme is represented as a second substrate and the inhibited form of the active site is electron limited by the high substrate concentration. Figure 3.11 shows the catalytic current at increasing nitrite concentrations at -143 mV, where the lower thermodynamic driving force means that electron addition will be slower and so you would predict that a smaller increase in nitrite concentration would be required to observe an inhibitory effect. At -143 mV nitrite reduction is substrate inhibited from pH 5 to pH 9, providing more evidence that this could be the more likely mechanism for substrate inhibition.

It is interesting that 4.3 M NaCl alleviates the substrate inhibition effect at low pH, appears to have an inhibitory effect at high pH, but does not affect the K_M value and so it is unlikely that it directly interacts with the active site. The effects of ions in solution have been well studied and have been found to activate enzymes, inhibit enzymes, destabilize or stabilize protein structure, change the pH of the protein or the pH dependence of catalysis, depending upon the interaction [117-120]. For the chloride dependent α-amylase enzymes, a chloride molecule binds specifically in close proximity to the active site and activates and stabilizes the enzyme [118, 120]. What is interesting about this interaction is that the conserved residues that are involved in the specific interaction with Cl^- are Arg 195, Asn 298, His 299 and Arg 337 (human salivary amylase) and these residues are very similar to those found at the positively charged patch at the exit of the product egress channel in TvNir [73, 120]. This suggests that these residues in TvNir could be involved in a Cl^- interaction. Although experiments where systematic substitution of Na^+ and Cl^- for K^+ and Br^- suggest that this effect might not be chloride specific and might be more to do with the ionic strength or a combination of both. Film transfer experiments in KBr suggested that

increased ionic strength produced higher catalytic currents and this effect was also seen in NaCl at concentrations below 4M (figures 3.17 to 3.19). This could be because larger ions are thought to bind more to hydrophobic patches than to interact specifically with charged groups and so KBr lacks specific inhibitory potency but still induced the same ionic strength response as high NaCl concentrations [120]. A specific chloride interaction in this region might prevent binding of a second nitrite molecule and prevent substrate inhibition of catalysis. It could be easily understood that this would be less effective at lower pH and Cl^- concentration, as the high proton concentration would 'mop up' the free Cl^- ions, thus allowing substrate inhibition.

Alternatively if the random sequential mechanism of substrate inhibition is correct then it could be concluded that the effect of increased ionic strength on TvNir is most likely to be why 4.3 M alleviates substrate inhibition. At low pH the overall solution has a large positive charge this could have a number of effects on the overall enzyme structure or the rates of electron transfer within the enzyme, the addition of 4.3 M NaCl increases the ionic strength of the solution and could redress the imbalance caused by low pH.

It is clear from analysis of the cyclic voltammetry nitrite titrations at pH 6 and pH 10 in 4.3 M NaCl that the presence of a high salt concentration has a greater effect on the catalytic properties of TvNir than could simply be attributed to a specific binding site at the product egress channel. These studies show that the redox centres within TvNir that require more negative potentials to be reduced as nitrite concentration and pH are increased in 0.1 M NaCl, are stabilised by the addition of 4.3 M NaCl.

In conclusion it is clear that while TvNir displays many features that are like *E. coli* NrfA with respect to nitrite reduction, there are also clear differences. The similarities are expected from the structural similarities between the enzymes are such that NrfA could be considered as a compact TvNir. In this context it is the differences that are striking and must arise from secondary co-ordination sphere effects relating to their differences in these enzymes.

Chapter 4

The Reductive Activation of TvNir

Chapter 4. The Reductive Activation of TvNir

4.1 Introduction

In chapter three PFV studies of TvNir indicated that the film underwent a reductive activation process, after which point steady-state catalysis was observed. Reductive activation has been previously shown in some bacterial nitrate reductases, NarGH, NarB and NapAB respectively from *Paracoccus pantotrophus, Synechoccocus elongatus* and *Rhodobacter sphaeroides* [121, 122]. These enzymes all contain molydopterin cofactors and EPR studies of *R. sphaeroides* NapAB have shown that changes at the Mo centre occur on reductive activation [122]. The iron-sulphur cluster containing enzyme fumarate reductase is also activated by reduction when it is purified in the presence of oxaloacetate [123]. Oxaloacetate is an inhibitor of fumarate reductase that has a much higher affinity for the oxidised enzyme than the reduced enzyme and so reduction releases oxaloacetate, activating fumarate reductase [123]. Whilst many NrfA cytochrome *c* nitrite reductases have been isolated from different bacteria, none have yet been shown to require reductive activation and so far this process seems to be unique to the *T. nitratireducens* TvNir.

The reduction potentials of TvNir have been investigated using spectroelectrochemistry and tin oxide electrodes (Dr Sophie Marritt, UEA, unpublished). TvNir was adsorbed to an optically transparent tin oxide electrode and the absorbance spectra of TvNir were collected as the electrode was poised at various potentials (figure 4.1). The spectra were typical of low-spin *c*-type hemes with oxidised absorbance maxima at 410 nm and broad α and β band absorbance between 500 and 600 nm. The reduced minus oxidised difference spectra of closely spaced sample potentials revealed changes reflecting the reduction of low-spin *c*-type hemes. The absorbance at 553 nm was recorded at each potential and could be modelled to the oxidation and reduction of 7 n=1 reductions (as described in more detail in chapters 2 and 5) this gave reduction potentials for the low-spin hemes of -50, -70, -180, -180, -250, -350 and -400 mV at pH 7.0 (figure 4.1).

Similar spectropotentiometric experiments for NrfA revealed a signal around 440 nm indicating the reduction of the high-spin active site heme, but no such signal

was detected for TvNir [54]. This is most likely to be due to the much greater intensity of the signals arising from seven low-spin bis-histidine co-ordinated hemes in TvNir compared to the four in NrfA [40, 73].

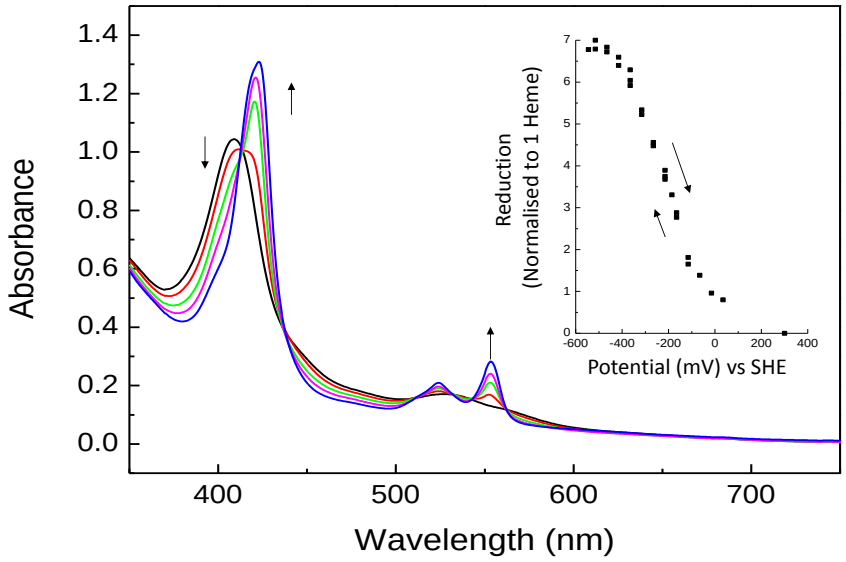

Figure 4.1 Spectroelectrochemistry of TvNir on tin oxide. The electronic absorbance spectra of TvNir adsorbed on a tin oxide electrode, where the arrows indicate the changes as the potential is decreased. The inset figure shows the absorbance at 553 nm at each potential, normalised to the reduction of one heme. Spectroelectrochemistry was performed in 50 mM Hepes, 0.1 M NaCl at pH 7.0 at ambient temperature. (Dr Sophie Marritt, UEA, unpublished).

To attempt to detect a spectroscopic signal from the high-spin active site heme that is present in the crystal structure of TvNir, ambient temperature MCD- compatible optically transparent thin-layer electrochemistry (MOTTLE) was employed (Dr. Sophie Marritt, UEA, unpublished). This is a spectroelectrochemical technique using a gold mesh electrode, a mediated enzyme solution and MCD spectroscopy. For oxidised TvNir MCD showed a broad negative feature with a maximum at 620 nm (figure 4.2). This is indicative of high-spin ferric heme co-ordinated by a nitrogenous ligand and a hydroxide. Low-spin hemes do not contribute to MCD at 600-650 nm. This signal decreased upon sample reduction, with a midpoint potential centred on -230 mV, but after poising at +180 mV for 30 minutes the high-spin ferric signal did not return. After poising the sample at +180 mV for 17 hours the high-spin ferric heme signal returned to 60 % of its original intensity. By comparison the signals between 500 and 560 nm arising from the low-spin ferrous hemes were oxidised and reduced reversibly within

20 minutes sample equilibration time. The hysteresis in the MCD spectroscopy of the high-spin heme band at 630 nm suggests a possible origin for reductive activation of the enzyme detected by PFV.

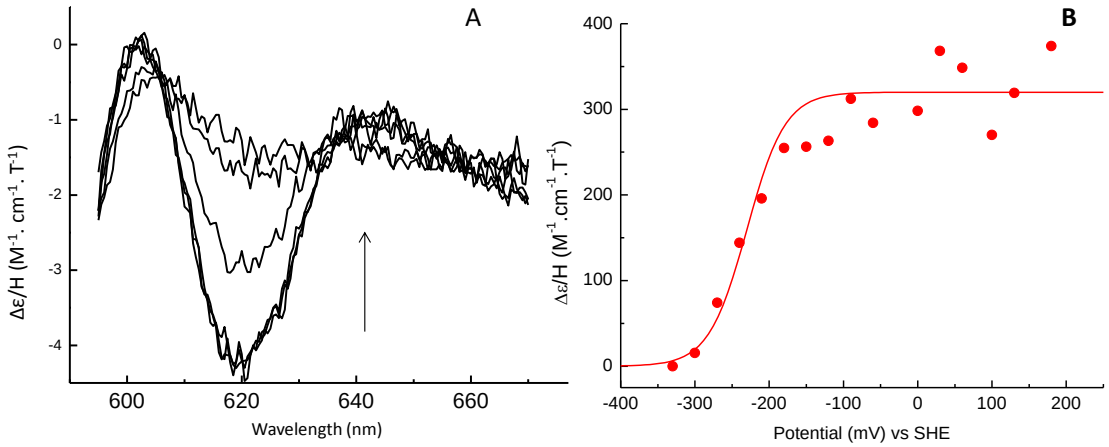

Figure 4.2 MOTTLE of TvNir between 600 and 660 nm. A. The ambient temperature MCD spectra of TvNir where the arrow indicates the changes upon lowering the potential. B. The change in the MCD at 620 nm as the potential is lowered. Spectra were recorded in 50 mM Hepes, 0.1 M NaCl at pH 7.0 in the presence of a mediator cocktail (Dr. Sophie Marritt, unpublished).

The aim of the work presented in this chapter was to characterise the reductive activation process for TvNir. To do this PFV was performed in a range of pH, salt and substrate conditions in order to provide insight into the activation process and the importance of the solution environment.

4.2 The Influence of Potential, pH and Nitrite Concentration on Reductive Activation

In chapter three cyclic voltammetry was described where the first scan of a TvNir film at pH 7.0 showed that an initial cycle was required for the maximum activity to be detected from the enzyme film (figure 3.1). Once the sample had undergone this first reduction and re-oxidation the oxidative and reductive sweeps of subsequent cyclic voltammograms overlaid which indicated steady-state catalysis.

To assess whether reductive activation of TvNir was detected across the pH range and not just at pH 7 cyclic voltammograms were recorded between pH 5 and pH

10 in 20 mM HTMA (pH 5-9) or 20 mM HCMA (pH 10), 0.1 M NaCl and 0.1 mM NO_2^-. For each set of experiments baseline cyclic voltammograms of the freshly polished bare electrode were recorded between +197 and -603 mV at 30 mV s^{-1}. The electrode was then freshly polished and a TvNir film adsorbed to the electrode and cyclic voltammetry was performed under the same conditions (figure 4.3). In order to clearly identify whether reductive activation occurred at each pH, the baseline corresponding to each scan number was directly subtracted from the corresponding cyclic voltammogram of TvNir adsorbed (i.e. the first scan baseline was subtracted from the first scan with TvNir adsorbed) using Microcal Origin.

Between pH 7 and pH 10 there was clearly a much larger catalytic current on the return oxidative sweep (-603 to +193 mV) than on the first reductive sweep (+193 to -603 mV) indicating that at pH 7 and above TvNir undergoes reductive activation (figure 4.3). As the pH is increased the region of the most difference between the oxidative and reductive sweep currents shifts to more negative potentials.

At pH 5 and 6 it is not immediately clear that reductive activation is occurring during the first cyclic voltammogram, although the reductive and oxidative sweeps of the first cyclic voltammograms at these pH are different from one another (figure 4.3). At pH 5 at the most positive potentials after the onset of catalysis the return oxidative sweep has a larger catalytic current than the first reductive sweep. However at lower potentials the return oxidative sweep has a lower catalytic current magnitude than the first reductive sweep. This suggests that at pH 5 TvNir is rapidly activated at high potential and that the difference between the potentials of the oxidative and reductive sweep at potentials below -100 mV, where the current profiles of the these sweeps intersect, is likely to be due to the high level of film loss on the first scan of the cyclic voltammogram. When TvNir is first adsorbed to the electrode the loss of film quickly becomes the first order process described in figure 3.1, but at the start of the experiment more loosely bound enzyme falls away more quickly and film loss is more rapid. This is likely to be more obvious at pH 5 due to the larger catalytic current magnitude. The baseline subtracted first cyclic voltammogram of TvNir at pH 6 was very similar to that at pH 5, but the region where the oxidative sweep has a larger catalytic current than the first reductive sweep, indicating that activation had

occurred, was at a slightly more negative potential than for the cyclic voltammograms at pH 5. For all pH values the reductive activation was complete after the first cyclic voltammogram and steady-state catalysis was observed in all the consecutive scans.

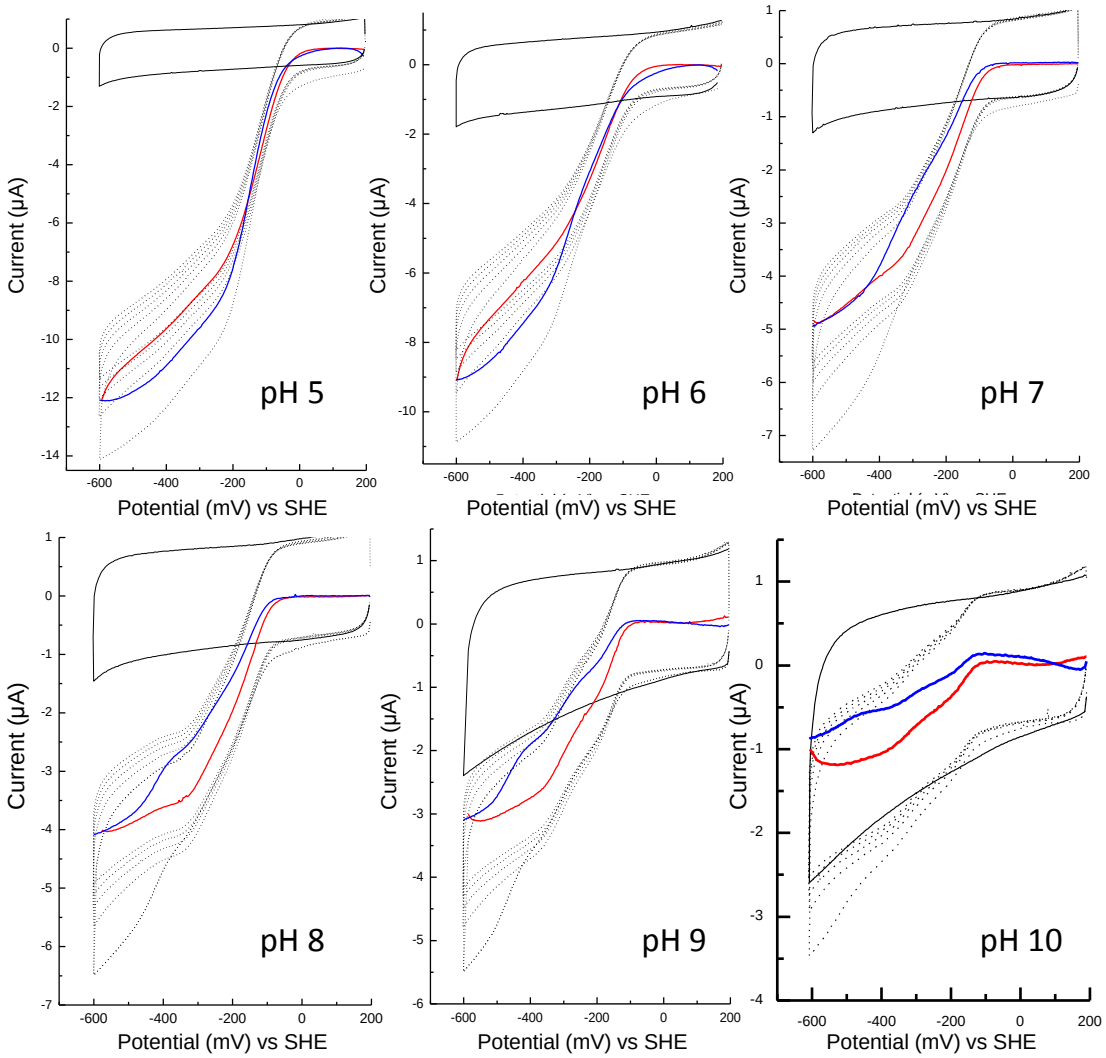

Figure 4.3. Cyclic voltammetry PFV of TvNir at pH 5-10 in 0.1 mM NO_2^-. The baseline subtracted oxidative (red) and reductive (blue) sweep of the first cyclic voltammogram of TvNir adsorbed on a PGE electrode at the indicated pH. The measured 1st to 5th cyclic voltammograms are shown (dotted lines) and the baseline of the first cyclic voltammogram (black line). All experiments were performed in 20 mM HTMA (pH 5-9) or 20 mM HCMA (pH 9.5 and pH 10), 0.1 M NaCl where the electrode rotation speed was 3000 rpm, the scan rate was 30 mV s^{-1} and the temperature was 20 °C.

It is clear from comparison of the baseline subtracted cyclic voltammograms that reductive activation occurs at more positive potentials at low pH (figure 4.3). This implies that reductive activation is a proton dependent process and that it occurs more

readily when there are more protons available. In order to better understand the pH dependence of reductive activation the derivative first and fifth cyclic voltammograms were compared for TvNir in 0.1 mM NO_2^- between pH 5 and pH 10 (figure 4.4). There was a difference in the derivative of the first (black line) and fifth (blue dashed line) cyclic voltammograms and that feature in the derivative of the first scan can be attributed to activation and is indicated by red arrows in figure 4.4. The difference in first and fifth derivative was most pronounced at pH 10 and the least noticeable at pH 5. It is clear on that increasing the pH the reduction of the species involved in activation occurs at more negative potentials. Thus reductive activation is a process that is dependent on both proton concentration and applied potential.

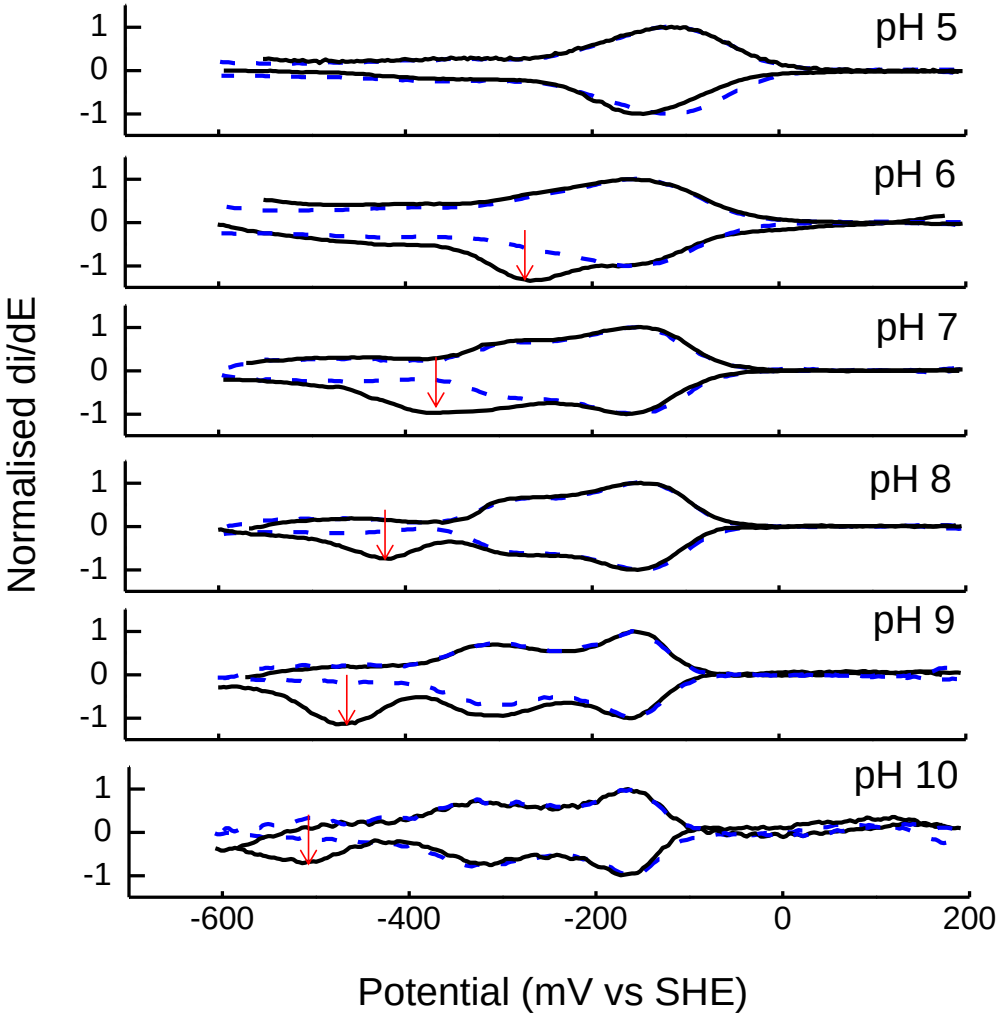

Figure 4.4 The derivative of the first baseline subtracted TvNir cyclic voltammogram (black) and the fifth subsequent cyclic voltammogram (blue dashed line) at the indicated pH. The experimental conditions are as in figure 4.1. The derivatives have been normalised to the height of the peak at the most positive potential. The feature corresponding to reductive activation is indicated by an arrow for each pH.

In order to investigate the effect of pH and applied potential on reductive activation in more detail chronoamperometry PFV was employed to study TvNir in 20 mM HTMA, 0.1 M NaCl at pH 7 in 0.1 mM NO_2^-. Here the current was measured as the potential was stepped through six potentials at 120 second intervals. The first selected potential (E_1) +143 mV was such that from the cyclic voltammetry (figure 4.3) you would not expect catalysis to be detected. The second potential step (E_2) -159 mV is where catalysis should be detected, but is at a potential suspected from the cyclic voltammetry to be too positive for reductive activation to occur. The third potential step (E_3) was selected as the region in the derivative cyclic voltammogram corresponding to reductive activation and so it would be expected that reductive activation would occur (figure 4.5 A). If the applied potential at E_3 is low enough that activation occurs then a steady increase in catalytic current will occur as the inactive enzyme adsorbed to the electrode is activated. The potential selected as E_4 is equal to E_2 and so will allow a comparison of the catalytic current magnitude at this potential before and after activation has occurred. The potential selected for E_5 of -309 mV is much more negative than the potential selected for E_3 and so if any of the sample remains inactive, this much more reducing potential should completely activate the sample and then for E_6 the potential is poised again at -159 mV (as in E_2 and E_4) so that the catalytic current when the enzyme is 100 % active can be determined.

Prior to the experiments with TvNir a baseline current was measured of the freshly polished bare electrode, using the six potential steps that would be applied in the forthcoming experiment in 20 mM Hepes, 0.1 M NaCl, pH 7 with 0.1 mM NO_2^- (figure 4.5 A). The electrode was then freshly polished and a TvNir film was prepared and this process was repeated. To obtain the catalytic current (figure 4.5 B) baseline of the bare electrode was directly subtracted from the experimental data using Microcal Origin and this data was then adjusted for the decrease in signal magnitude with time as described in chapter 3.2.

As predicted from the cyclic voltammetry experiments there was no catalysis observed at E_1 and some catalysis but not activation was observed on stepping to E_2. As E_3 of -269 mV was applied the catalytic current increased steadily and then reached a maximum catalytic activity after ca. 120 s (figure 4.5 A,B). Therefore at pH 7.0

applying an activating potential of -269 mV for 120 s was enough to achieve the maximum catalytic activity for that sample. Comparing the catalytic currents measured at E_4 and E_6 confirmed that maximum activity was obtained after 120 s poised at -269 mV as application of -309 mV (E_5) did not increase the catalytic current further.

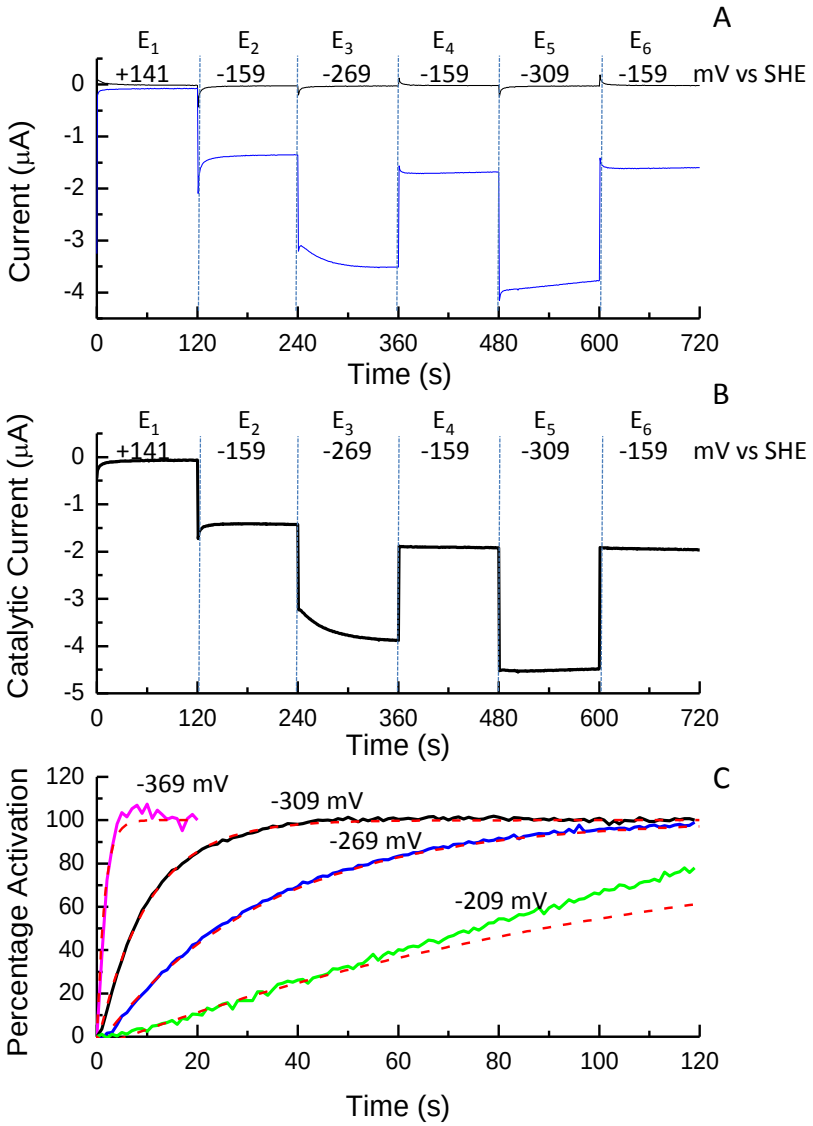

Figure 4.5. Chronoamperometry and the rate of reductive activation of TvNir at pH 7, 0.1 mM NO_2^-.(A) The chronoamperometry baseline (black line) and of TvNir absorbed (blue line). (B) Baseline subtracted, film loss corrected, chronoamperometry of TvNir at a series of potentials as indicated. (C) The percentage activation of TvNir at pH 7 when the activating potential (E_3) is -209 (green), -269 (blue), -309 (black) and -369 (magenta) mV vs. SHE and the fit of the percentage activation with time to the first order rate equation (dashed red lines) that gave rise to respective rates of activation of 0.008, 0.03, 0.098 and 0.66 s^{-1}. For all experiments the buffer electrolyte was 20 mM Hepes, 100 mM NaCl, 20 °C and the electrode rotation speed was 3000 rpm.

In order to determine a rate constant for the process of reductive activation at -269 mV the catalytic current when E_3 was applied was taken to have zero activation. After 120 s the current was taken to have 100 % activation (figure 4.5 C). The percentage activation can then be plotted as a function of time and this can be fitted to the first order rate equation:

$$PA=PA_te^{-kt} \qquad \text{(Equation 4.1)}$$

Where PA is the percentage activation, PA_t is the percentage activation at time (t), k is the first order rate constant and t is time. At -269 mV at pH 7.0 a rate constant for reductive activation was determined to be 0.03 s^{-1}.

The derivative cyclic voltammogram shows that -269 mV is just at the start of the region attributed to the reduction of the TvNir that leads to activation. To determine the dependence of the rate of activation on the applied potential, chronoamperometry was performed at different activating potentials (E_3), with the other experimental parameters unchanged. The percentage activation with time was determined at -209, -309 and -369 mV also and fitted to equation 4.1 (figure 4.5 C). When -209 mV is the activating potential TvNir adsorbed on the electrode is not 100 % activated after 120 seconds, however by comparison of E_4 and E_6 it was calculated that after 120 seconds TvNir is ca. 75% activated and therefore the percentage activation vs. time can still be plotted and fitted for this potential. The values for reductive activation at -209 mV however show a poor fit to equation 4.1 and therefore when the activating potential is this low activation might not be a first order process and there might be an alternative rate determining step (figure 4.5 C). As the applied potential for activation becomes more negative the rate of activation increases and good fits to the first order equation (equation 4.1) were obtained and showed that the first order rate constant increases (table 4.1).

The chronoamperometry experiments also allowed for quantification of the total amount of activity recruited by activation of TvNir. Comparing the catalytic current magnitude in E_2 to the catalytic current magnitude in E_6 (table 4.1) showed there was a small amount of variation in the percentage of TvNir that was activated in

each experiment but on average the sample became 27 % more active if reduced for sufficient time.

$[NO_2^-]$ (mM)	*Activating Potential (mV)*	*Rate constant activation (s^{-1})*	*Increase in Initial Activation (%)*
0.05	-209	0.007 ± 0.001	29
	-269	0.024 ± 0.006	29
	-309	0.093 ± 0.008	29
0.1	-209	0.008 ± 0.001	28
	-269	0.030 ± 0.005	25
	-309	0.096 ± 0.004	27
	-369	0.660 ± 0.005	25
1.0	-209	0.007 ± 0.001	33
	-269	0.019 ± 0.005	34
	-309	0.071 ± 0.021	32

Table 4.1 The first order rate constant for reductive activation in 0.05 and 1 mM NO_2^- and the amount of NO_2^- reductase activity recruited upon activation. Conditions were as described in figure 4.5. These are representative values from at least two experiments.

The chronoamperometry potential step experiments were also performed in 1 mM and 0.05 mM nitrite to determine whether or not nitrite concentration had an effect on the rate of reductive activation (table 4.1). Nitrite concentration was found to have no effect on the rate of reductive activation or the extent of activation.

The cyclic voltammetry experiments indicated that reductive activation was dependent on pH and that more negative potentials are required for reductive activation at higher pH. Chronoamperometry had established and quantified the potential dependence of reductive activation at pH 7 and this technique was then extended to quantify the pH dependence of the reductive activation of TvNir.

Prior to each experiment chronoamperometry baselines of the bare electrode were recorded with appropriate potential steps for the experimental pH chosen by inspection of data in figure 4.3. As with the experiments at pH 7.0, the change in the catalytic current as the activating potential (E_3) is applied can be plotted

as the percentage activation vs. time, where the current when E_3 is initially applied is 0% activated (figure 4.6). The percentage activation after 120 seconds poised at E_3 is calculated as the percentage of catalytic current gained at E_4 compared to E_6. The percentage activation with time was fitted to equation 4.1 in order to determine a rate constant for reductive activation at each pH and activating potential. Comparing the percentage activation profiles when -269 mV is the activating potential at pH 6, 7, 8 and 9 shows clearly that at low pH reductive activation occurs much faster than at high pH (figure 4.6 A). The corresponding rate constants determined for the reductive activation are in good agreement with this and confirm that as the pH is increased more negative potentials are required to rapidly activate TvNir.

pH	E_1 (mV)	$E_{2,4,6}$ (mV)	E_5 (mV)
6	+141	-73	-309
7	+141	-159	-309
8	+141	-159	-309
9	+141	-159	-453
10	+141	-159	-603

Table 4.2 The experimental poising potentials used to investigative the reductive activation of TvNir at each pH.

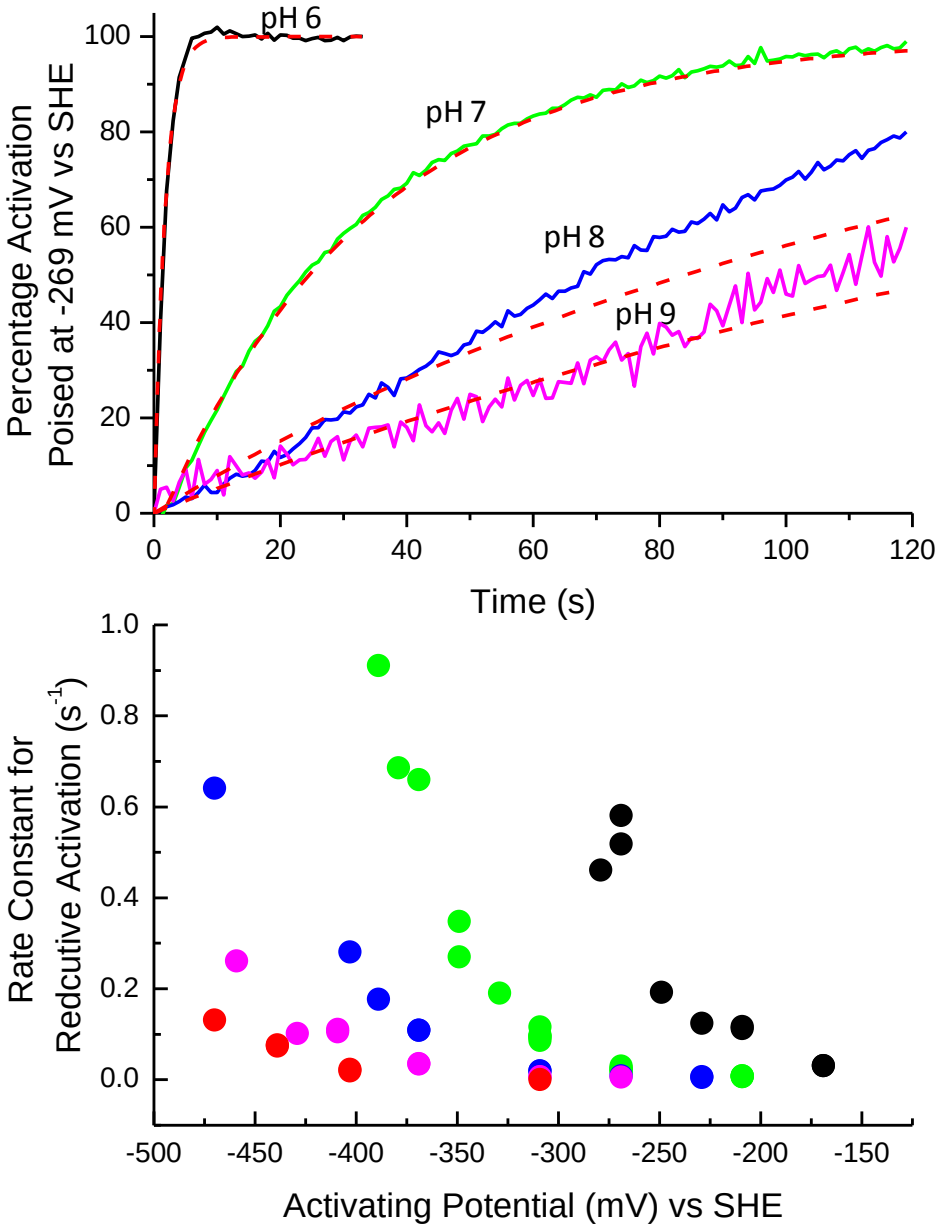

Figure 4.6 The rate of reductive activation at differing pH and applied potential. A. The percentage activation with time at -269 mV extracted from stepwise chronoamperometry of TvNir at pH 6 (black), pH 7 (green), pH 8 (blue) and pH 9 (magenta). The corresponding fit to equation 4.1 is shown (dashed red lines) where the rate constant for reductive activation at pH 6, 7, 8 and 9 were 0.58, 0.03, 0.008 and 0.005 s^{-1}. B. The rate constant for reductive activation derived from stepwise chronamperometry of TvNir and fits to equation 4.1 (as shown in A) at varying activation potentials and at pH 6 (black), pH 7 (green), pH 8 (blue), pH 9 (magenta) and pH 10 (red).

4.3 Discussion

The studies in this chapter clearly show that around 30 % of the TvNir sample is activated by reduction. MCD spectroscopy has shown that the signal arising from the high spin hydroxide bound active site heme irreversibly reduces with reduction centred on -230 mV. The irreversible change in the active site observed in the MCD upon reduction most likely reflects a change in the ligation of the active site heme, penta-coordinate heme has a very weak MCD signal and this might explain why there is no evidence for it in the MCD. PFV has shown that at low pH reductive activation occurs more readily, i.e. at more positive applied potential and so reductive activation is likely to be coupled to a protonation event. This cumulative evidence from the spectroscopy and the PFV experiments provide evidence for a mechanism for reductive activation (scheme 4.1):

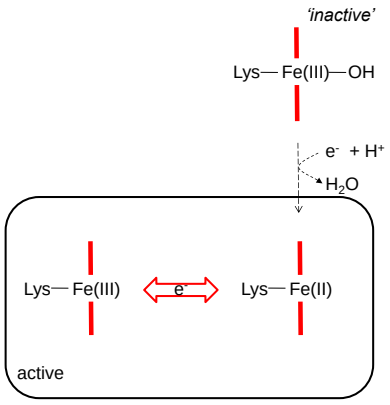

(Scheme 4.1)

In scheme 4.1 the oxidised hydroxide bound active site heme detected in the MCD spectroscopy is inactive and reduction of this, coupled to a protonation event, leads to the dissociation of water and formation of the active form of the enzyme. This is a similar mechanism to that proposed for fumarate reductase activation; that reduction releases an inhibitor that was previously bound to the active site [123]. This might also correspond to the observation in chapter 4 that TvNir is less active at high pH where more OH^- is present. Reductive activation by the mechanism proposed in scheme 4.1 is distinctly different to the mechanism of reductive activation proposed for the

molybdenum containing nitrate reductases, their reductive activation is related to the reduction of a dead-end Mo(V) active site, not to the release of an inhibitor [121, 122].

MCD spectroscopy and crystal structure analysis suggest that the structurally homologous NrfA enzyme has either a hydroxide or water bound in its active site. Computational and modelling studies of NrfA have suggested a similar mechanism to the scheme 4.1 for the dissociation of water or hydroxide from the active site of NrfA, that if hydroxide was bound in the active site it would first be protonated to give rise to a water molecule and that upon reduction the water molecule would readily dissociate from the Fe(II) active site heme [48]. They then propose that nitrite binds and the catalytic cycle begins, with nitrite binding again once the product dissociates (figure 1.8). If scheme 4.1 is an accurate model for reductive activation of TvNir it might be expected that NrfA would also require reductive activation, however extensive PFV of NrfA has shown that there is no evidence that this enzyme requires reductive activation [1, 40, 82, 115]. Alternatively it is possible that the transition from the resting to the active state is much faster in NrfA than for TvNir and so the change is not detected.

The hysteresis observed in the MCD spectroscopy of the active site heme clearly shows that the active site is directly affected by the reductive activation event (figure 4.2). At pH 7.0 the feature in the derivative cyclic voltammogram that is attributed to reductive activation is centred on -370 mV, at much lower potential than -230 mV that the reduction of the high spin hydroxyl bound heme is centred upon (figure 4.2 and 4.4). This indicates that whilst re-oxidation of the hydroxide bound active site heme might be linked to reductive activation there are two separate redox processes linked to this step.

A key difference in the active site of TvNir compared to that of NrfA is that the active site Tyr in TvNir is covalently bound to a cysteine residue. Whilst TvNir is the only CcNiR that has so far been found to have this cys-tyr bond, it has been found in the active sites three other enzymes: Galactose oxidase (*Pichia pastoris*), cysteine dioxygenase (rat liver cells) and the siroheme sulphite reductase NirA (*Mycobacterium tuberculosis*) [74, 76, 124]. The cys-tyr bond detected in these enzymes has frequently

been termed a protein derived cofactor and it is thought that it is formed by post-translational modification by an oxidative mechanism in cysteine dioxygenase and galactose oxidase [76, 125-127]. This suggests that cys-tyr bond formation is a final step in protein maturation for these enzymes. Site directed mutagenesis in the NirA sulphite reductase, that catalyses the six electron reduction of sulphite to sulphide, has shown that the cys-tyr cofactor is important for the catalytic efficiency of NirA [74]. Differences in the electronic absorbance spectroscopy of the NirA mutants indicated that the cys-tyr has some influence on the electronic properties of the active site siroheme [74]. It is possible that the reductive activation detected for TvNir might be linked to the formation of the cys-tyr bond that might be necessary for TvNir to be fully catalytically competent.

Chapter 5

An Electrochemical Investigation of Electron Transfer to NrfA

Chapter 5. An Electrochemical Investigation of Electron Transfer to NrfA

5.1 Introduction

NrfB is the redox partner to the NrfA pentaheme nitrite reductase in γ-proteobacteria such as *E. coli.* In chapter one the evidence that NrfB interacts with NrfA in the region of NrfA heme 2 was presented and it was also shown that the NrfAB complex is thought to position eight of its ten hemes in the same arrangement of those in TvNir and also HAO from *N. europaea* (figure 1.14) [2, 50, 128]. The NrfAH complex of *D. vulgaris* has been crystallised but the heme arrangement of this complex differs from the predicted arrangement for NrfAB and is likely to provide a poor model of NrfAB [47]. Although four of the NrfB hemes overlay the NrfH hemes with an r.m.s.d of 1.93 Å, the ligation of these hemes is different; all the NrfB hemes are bis-histidine co-ordinated, but one of the ligands to NrfH is a lysine supplied by NrfA [2, 47, 50]. There is no evidence from spectroscopic studies of NrfAB that there is any change in heme ligation of NrfA or NrfB when the NrfAB complex forms [50]. In addition to this there is very little protein sequence similarity between NrfH and NrfB, this reflects both the different functions of NrfH and NrfB (NrfH is also a quinol dehydrogenase, but NrfB acts an electron shuttle) and that the region of NrfB that interacts with NrfA is thought to be that around the fifth heme of NrfB, that is lacking in the structure of NrfH [129].

PFV has previously been used to study electron transfer complexes between yeast cytochrome *c* and cytochrome *c*d_1 nitrite reductase and nitric oxide reductase from *Paracoccus denitrificans* and between pseudoazurin and the copper nitrite reductase from *Alcaligenes faecalis* [98, 130]. These experiments used self assembled monolayers to specifically attach and orientate the redox shuttle protein (cytochrome or pseudoazurin) on a gold electrode; this was followed by interaction of that layer with the catalytic enzyme. Usually the catalytic enzyme will not directly interact with the electrode or preliminary formation of the self assembled monolayer will inhibit this interaction and so the enzyme must receive electrons for catalysis via the redox shuttle.

Given that NrfAB is reported to form a tight complex, with a K_d of 50 nM it was of interest to see if similar techniques could be used to study electron transfer through NrfAB and whether the electrochemistry of the NrfAB complex would show similarities to PFV of TvNir, perhaps identifying features to distinguish a five heme nitrite reductase (NrfA) from an octaheme nitrite reductase (TvNir) and again from a decaheme nitrite reductase (NrfAB) [27]. Given that NrfA is known to interact directly with graphite and gold electrodes, experiments to distinguish NrfAB would be a challenge. However, NrfA typically has a very low coverage on graphite such that non-catalytic signals are not detected, if NrfAB absorbs with monolayer coverage then non-catalytic signals may be detected and responses may be distinguished. PFV of NrfB has not previously been reported although NrfB has been studied by solution based potentiometry monitored by UV-visible spectroscopy, from which reduction potentials of the five hemes at pH 8.0 were found to be -63, -129, -129, -221 and -259 mV [93]. Consequently the initial stages of this work involved extensively characterising the PFV response of NrfB and NrfA alone, so that changes due to NrfAB may be identified.

5.2 Spectroelectrochemistry of NrfB on Tin Oxide

Tin oxide electrodes have proved to be useful tools in the characterisation of oxidation and reduction of redox proteins, and notably in the study of *E.coli* NrfA [54, 55]. The mesoporous surface of tin oxide electrodes provides a large surface area onto which enzymes can adsorb and when these electrodes are connected to a potentiostat (as described in chapter 2) current can be measured as the potential is swept in the cyclic voltammetry experiment and the current can also be measured as the potential is held at one 'poised' potential. Tin oxide is a semi-transparent material and so electronic absorbance spectra can also be recorded as the potential is poised and in favourable cases this can be used to determine the extent of reduction or oxidation of the material adsorbed to the electrode at that potential. Given that NrfB is a heme protein and the reduced and oxidised spectra have distinctive forms, it was decided to use this approach to define the PFV response of NrfB and allow comparison between the adsorbed and solution determined reduction potentials.

A tin oxide electrode was baked for 1 hour at 450 °C and then the electronic absorbance spectrum was recorded in 50 mM Hepes, 2 mM $CaCl_2$ at pH 7, at room temperature, in order to obtain a baseline for the absorbance spectra. This is important as tin oxide is semi-transparent and has a distinctive 'absorbance' due to scattering from its nanostructure and so the absorbance arising from adsorbed enzyme can clearly be quantified (figure 5.1). A fresh tin oxide electrode was then baked at 450 °C to ensure than there were no impurities on the surface of the electrode and a platinum wire was then attached to the conducting glass on top of the electrode as described in chapter 2 (figure 2.8). The clean electrode was then soaked overnight in 2.5 µM NrfB in 50 mM Hepes, 2 mM $CaCl_2$, pH 7.0 at 4 °C. The next day the electrode was removed from the solution of NrfB and rinsed with buffer to remove any loosely adsorbed NrfB and placed into the cuvette-electrochemical cell (chapter 2, figure 2.8) in 50 mM Hepes, 2 mM $CaCl_2$, pH 7.0. The UV-Vis spectra of the sample of NrfB that the electrode had been soaking in was measured and the absorbance at 408 nm (0.951) was used with the Beer Lambert equation to calculate that the concentration of the remaining solution was 1.55 µM, so this had dropped by 1 µM, indicating a significant amount of NrfB had adsorbed to the tin oxide electrode.

The cuvette-electrochemical cell containing the NrfB exposed tin oxide electrode was sparged with argon for thirty minutes. An initial spectrum was recorded to assess whether NrfB had in fact adsorbed to the tin oxide electrode (figure 5.1). A distinctive peak was seen at 408 nm and a broad shoulder at 525 nm that are characteristic of oxidised low-spin heme and have previously been described as features of the spectrum of oxidised NrfB [93].

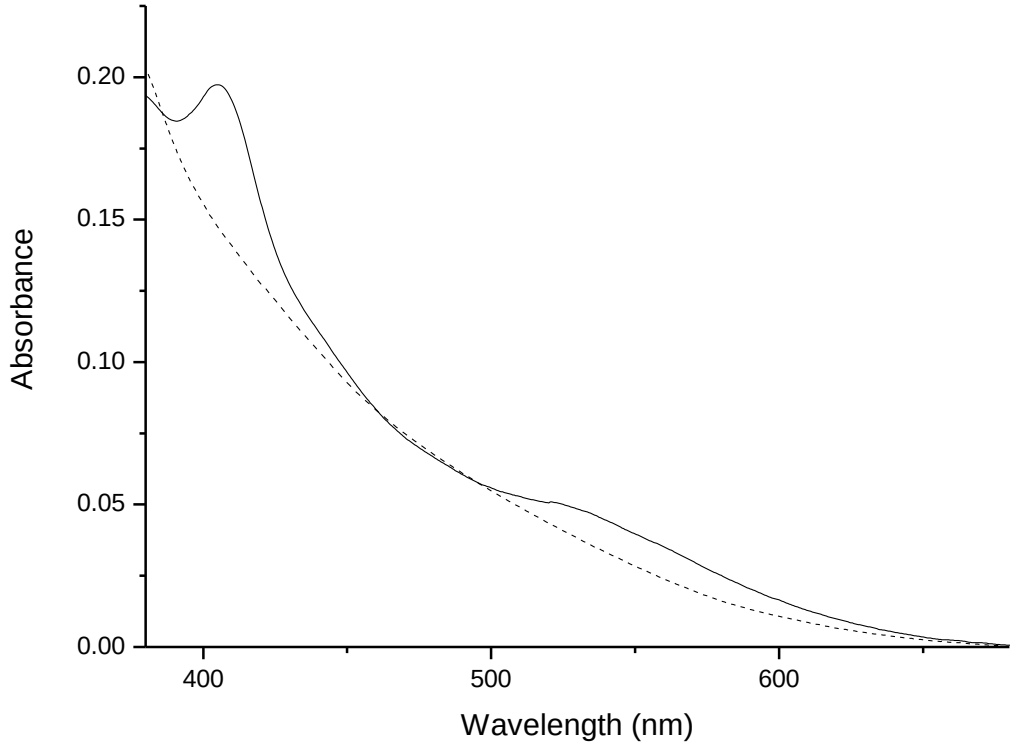

Figure 5.1. The electronic absorption spectrum of NrfB adsorbed on tin oxide. A tin oxide electrode (dashed line) and the spectrum with NrfB adsorbed (solid line). Both spectra were recorded in 50 mM Hepes, 2 mM $CaCl_2$ at pH7 and ambient temperature.

Once it was established that NrfB was adsorbed to the tin oxide electrode a potentiometric titration was performed. Using chronoamperometry the current was measured as the potential was poised initially at +380 mV for thirty seconds, then set to a potential of interest for 1000 seconds, while measuring the absorbance at 552 nm (figure 5.2 A). Once a steady absorbance was observed for the potential of interest, indicating equilibration of the protein film with the electrode potential, the electronic absorbance spectrum was recorded from 800 to 250 nm. The electronic absorbance spectrum was recorded at a series of potentials between +280 and -420 mV (figure 5.2 B). As more negative potentials were applied the absorbance at 552 nm increased until a maximum absorbance was reached, indicating that all the NrfB adsorbed was reduced (figure 5.2). In the soret region the absorbance at 408 nm decreases while the absorbance at 418 nm increases, giving rise to an isosbestic point at 412 nm. The changes in absorbance of NrfB adsorbed on tin oxide upon reduction are in good agreement with the absorbance maxima of 420 and 552 nm in the spectra of dithionite reduced NrfB in solution that are typical for reduced low-spin heme, this provides a further indication that NrfB retains its native structure upon adsorption [93].

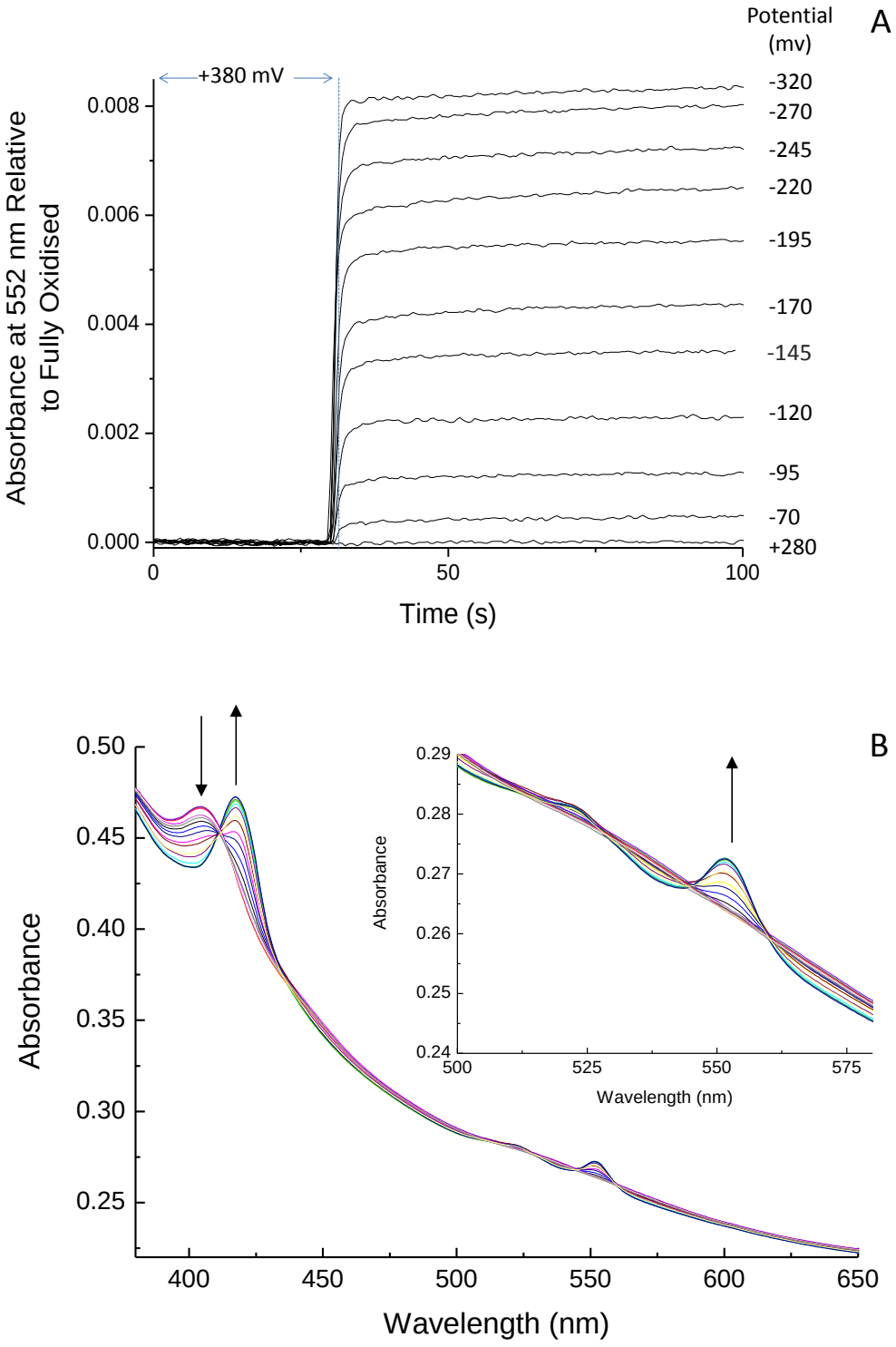

Figure 5.2 Spectropotentiometry of NrfB adsorbed on tin oxide. (A) The absorbance at 552 nm recorded whilst the electrode was poised at the indicated potentials using chronoamperometry. (B) Spectra of NrfB at each potential investigated between +280 and -420 mV. The arrows indicate the changes upon reduction and the inset shows an enlarged view of the change in absorbance ca. 500 nm. The experimental conditions were the same as in figure 5.1.

The absorbance at 552 nm for the NrfB film equilibrated at each potential was extracted from both the spectra and time course measurement (figure 5.2 A and B, figure 5.3). The maximum absorbance at 552 nm, at the most negative potentials, was normalised to 100 % reduced and the minimum absorbance at 552 nm, at the most positive potentials was set to 0 % reduced, converting the absorbance at 552 nm to the percentage reduced NrfB (figure 5.3). This was used to determine the reduction potentials for NrfB as:

$$\% \text{ Reduced} = \sum_{n=1}^{5} \frac{20\ \%}{1+ \theta_n} \qquad \text{(Equation 5.1)}$$

Where θ is defined by equation 2.5 and 100 % reduced is defined as the sum of 5 n=1 redox centres, representing the one electron reduction of each of the five hemes within NrfB. The crystal structure of NrfB shows that all five hemes are bis-histidine co-ordinated and so are low-spin [50]. The spectra showed the expected response of fully oxidised to fully reduced low-spin heme across the range of potentials investigated indicating that therefore all the five hemes are redox active. It was assumed that all the hemes contribute equally to the spectral changes observed on oxidation and reduction and that the change in absorbance at 552 nm arises from five n =1 redox centres. In support of this the best fit to equation 5.1 was for five n=1 redox centres (figure 5.3) and fits to three or four redox centres were not satisfactory.

The fits to equation 5.1 produced average reduction potentials of -139 ± 20, -139.5 ± 30, -167 ± 45, -236.5 ± 30 and -264 ± 30 mV for adsorbed NrfB at pH 7.0. The published reduction potentials were defined by spectropotentiometry performed by measuring the UV-Vis spectra of redox poised NrfB with the use of redox mediators at pH 8.0 [93]. Whilst the pH difference in the two experiments means that the values are not directly comparable, the reduction potentials defined by each method span a similar range further suggesting that NrfB was not significantly perturbed by adsorption.

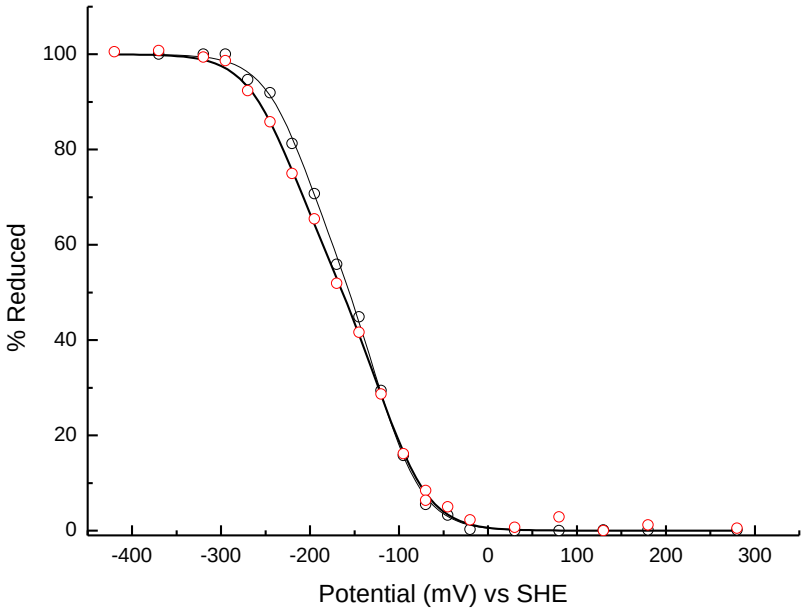

Figure 5.3 The percentage reduced NrfB as a function of tin oxide electrode potential derived from the absorbance change at 552 nm. The data points were derived from the time course absorbance monitored at 552 nm extracted at 75 seconds (black circles) and the full spectra recorded at each potential (red circles). The fit of the data to equation 5.1 (black line) giving reduction potentials for the time course at 552 nm of -170, -171, -175, -260 and -290 mV and for the full spectra extracted data -159, -108,-108, -213 and -238 mV.

Step-wise changes in the spectra as the potential is varied can be more readily detected by construction of reduced minus oxidised difference spectra for adjacently equilibrated potentials (figure 5.4). For potentials above +30 mV a flat line was observed for the reduced minus oxidised difference spectra, indicating no change in the electronic absorbance spectra as all the redox centres within NrfB were oxidised at these potentials. When the spectrum at -20 mV was subtracted from that at +30 mV, features appeared at 408 and 425 nm indicating some reduction. As the potential was further decreased the feature at 425 nm initially became more prominent and then broadened. When the spectrum recorded at -245 mV was subtracted from that -220 mV the broadened feature at 425 nm split and had two distinct peaks, one with a maximum ca. 425 nm and the other ca. 415 nm. This feature is commonly known as a split soret and has been detected in the difference spectra of several proteins with *c*-type hemes including NrfA [54]. Also upon reduction a clear positive feature becomes apparent in the difference spectra in the region of 552 nm as you would expect from the absorbance spectra of reduced NrfB. There is no more change in this feature at potentials below -295 mV, indicating that the sample is 100 % reduced here.

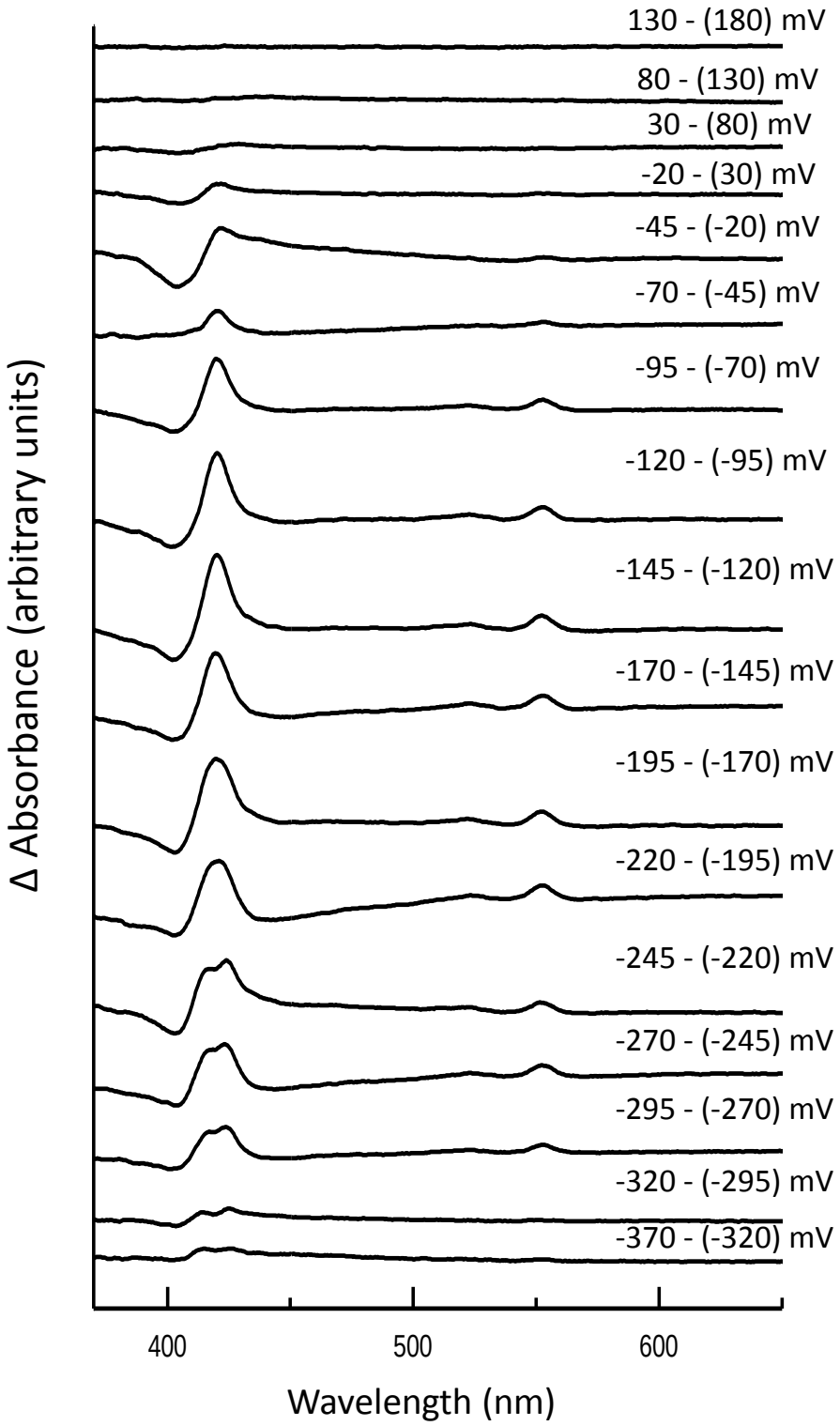

Figure 5.4 The reduced-oxidised difference spectra of NrfB adsorbed on tin oxide. The potential of the original spectra and that of the one subtracted from it are as indicated. Spectra have been displaced on the y-axis for clarity. Experimental conditions were as described in figure 5.1.

To gain insight into the origin of these spectroscopic features the oxidised and reduced absorbance spectra were recorded of two other cytochrome *c* containing proteins: the low-spin cytochrome *c* (horse heart), and the high-spin cytochrome *c*' (*Alcaligenes xylosoxidanes*). Two 30 µM solutions of each protein were prepared along with two 5 µM solutions of NrfB, one solution of each protein was oxidised with 3 mM ferricyanide and other was reduced with 7 mM dithionite. The reduced spectra of these proteins were subtracted from the oxidised spectra to produce difference spectra illustrating the changes upon reduction arising from high-spin and low-spin *c*-type heme (figure 5.5). The difference spectra of both NrfB and cytochrome *c* have the same key features; a large, sharp bis-signate feature with a minimum at 403 nm and a maximum at 425 nm (NrfB) and 421 nm (cytochrome *c*), a broad feature around 518 nm and a sharper feature with a larger contribution at 552 nm. The reduced minus oxidised spectrum of cytochrome *c*' is distinct from that of NrfB and cytochrome *c*, with a much broader bis-signate feature with a maximum around 435 nm and a minimum at 395 nm. The reduced minus oxidised spectrum of cytochrome *c*' also lacks the double feature between 500 and 560 nm and has a broad signal centred on 565 nm. The similarities between the reduced minus oxidised difference spectra of NrfB to cytochrome *c* and the differences compared to cytochrome *c*' show there was no evidence of any high-spin heme arising in NrfB as it was reduced.

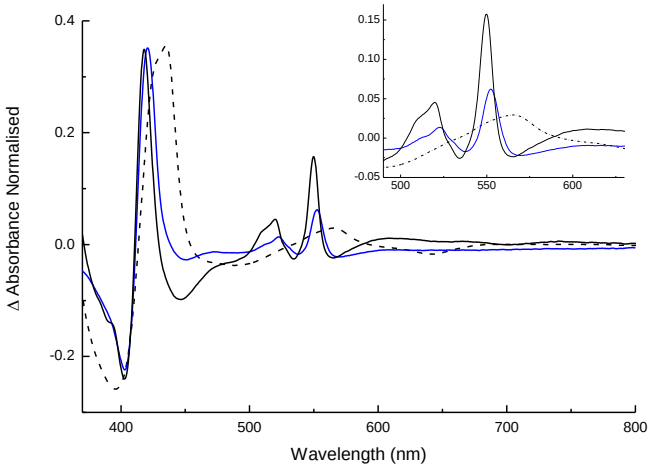

Figure 5.5 Comparison of the fully reduced minus the fully oxidised difference spectrum for NrfB, cytochrome c and cytochrome c'. The dithionite reduced spectra of NrfB (blue line), cytochrome c (black line) and cytochrome c' (dashed line) with the ferricyanide oxidised spectra subtracted. The inset shows an enlarged view of the region of these spectra between 490 and 640 nm. The difference spectra were normalised to the Δ absorbance maxima ca. 410 nm. All spectra were recorded at ambient temperature in 50 mM Hepes, 2 mM $CaCl_2$ at pH 7.

5.3 Cyclic voltammetry of NrfB on Tin Oxide

Tin oxide electrodes can also be used to study the absorbed protein using more 'normal' electrochemical methods such as cyclic PFV to complement and corroborate the findings of the spectroelectrochemical experiments. In order for a direct comparison between the cyclic voltammetry data and the spectroelectrochemical data, cyclic voltammetry was initially performed using the same NrfB tin oxide soaked electrode as prepared and used in the spectroelectrochemical experiments above. Cyclic voltammetry was performed where the current was measured as the potential was swept linearly between +380 and -602 mV at a scan rate of 15 mV s^{-1} in the standard experimental buffer of 50 mM Hepes, 2 mM $CaCl_2$ at pH 7 (figure 5.6 A). Cyclic voltammetry was also performed of the bare tin oxide electrode that had been baked, under the same experimental conditions but not exposed to NrfB and where a distinct 'triangular' baseline was observed that is thought to be due to the semi conducting nature of the tin oxide electrode [131]. Cyclic voltammetry of tin oxide with NrfB adsorbed showed this triangular shape onto which were superimposed clear peaks showing the oxidation and reduction of the NrfB hemes between ca. -100 and -350 mV (figure 5.6 A).

Due to the triangular shape of the tin oxide current-potential baseline, baseline subtraction of the NrfB cyclic voltammetry was performed using the Utilities for Data Analysis 010716 Program kindly provided by Dr. Dirk Heering. Baseline subtraction clearly showed that all oxidation and reduction occurred within one redox envelope (figure 5.6 B). The baseline subtracted peak given by the oxidation and reduction of NrfB adsorbed on tin oxide can be described by equation 5.2:

$$i = \sum_{n=1}^{5} Ip\left(\frac{\theta}{(1+\theta)^2}\right) \qquad \text{(Equation 5.2)}$$

Where θ is described by equation 2.5 and Ip is the peak height for an n= 1 response of the adsorbed protein described by equation 2.8. The reduction potentials determined from the fit of the cyclic voltammogram of NrfB to equation 5.2 were; -70 ±25, -160± 20, -178 ± 11, -222 ± 14 and -273 ± 11 mV. The more negative reduction potentials

show good agreement with those calculated by fits to the spectroscopic data, but there is some difference in two most positive potentials (figure 5.3).

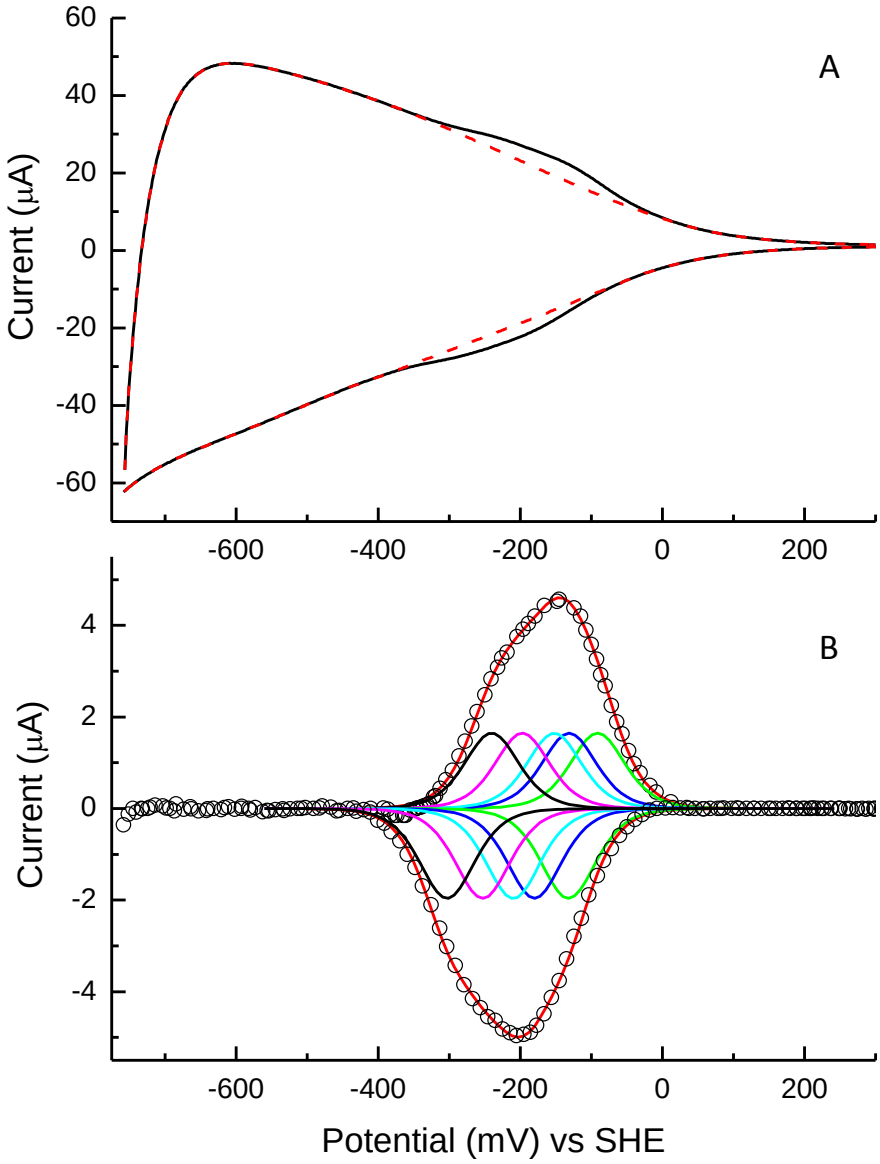

Figure 5.6 Cyclic voltammetry of NrfB adsorbed on tin oxide. (A) Cyclic voltammetry of NrfB adsorbed on tin oxide (black line) and of the tin oxide electrode prior to adsorption of NrfB (red dashed line). (B) The baseline subtracted cyclic voltammogram of NrfB (black circles) and the fit of this data to equation 5.2 (red line) and the individual redox profiles of each of the NrfB hemes using the reduction potentials determined from equation 5.2 (green, blue, cyan, magenta and black lines). The reduction potentials determined from the average of the fits of the oxidative and reductive peaks to equation 5.2 were; -70, -160, -178, -222 and -273 mV. Experiments were performed in 50 mM Hepes, 2 mM $CaCl_2$ at pH 7, at ambient temperature, where the scan rate was 30 mV s^{-1}.

The reduction potentials calculated by spectroscopy have a narrower range by ca. 70 mV, this could be linked to the errors in the simulated baseline subtraction method used to analyse the cyclic voltammetry data. At more negative potentials the tin oxide background changes linearly as the potential is swept from positive to negative, but at more positive potentials as the charging current of the tin oxide electrode decreases, the baseline shape becomes slightly curved and therefore more difficult to model (figure 5.6). This means that there is a greater error in the more positive reduction potential values determined by cyclic voltammetry.

Performing cyclic voltammetry of NrfB adsorbed on tin oxide also allowed for the absorbance at 552 nm to be recorded at the same time (figure 5.7). Cyclic voltammetry and measurement of the absorbance at 552 nm were started simultaneously to ensure that the time course of the absorbance at 552 nm could later be converted to potential by using the scan rate (30 mV s^{-1}). It is clear that as the potential is swept from positive to negative during cyclic voltammetry that the absorbance at 552 nm increases to a maximum and remains close to that maximum until sufficiently positive potentials are applied to re-oxidise the absorbed NrfB. There is a slight decrease in absorbance whilst the electrode is scanned across the most negative potentials, this modulation has been observed with experiments of NrfA absorbed on tin oxide and is thought to be due to the semiconducting properties of the tin oxide electrode [114]. At the most positive potentials where we would expect all the hemes within NrfB to be oxidised, the absorbance was expected to be equivalent to the tin oxide background. By direct baseline subtraction of the 'bare' tin oxide absorbance at 552 nm from the NrfB response this was found to be the case.

Using the scan rate of the cyclic voltammetry experiment the time course of the absorbance at 552 nm was converted to a plot of the absorbance vs. potential (figure 5.7 B). The absorbance upon reduction and re-oxidation almost overlay one another, a slightly higher maximum absorbance was obtained on re-oxidation than upon reduction and this was obtained at a slightly more negative potential than the maximum absorbance obtained on the reductive sweep. The differences in the NrfB absorbance at 552 nm upon oxidation and reduction are likely to be due to the

semiconducting nature of the tin oxide electrode and reflect the drop in absorbance as the electrode is scanned across 'fully reduced' potentials observed in figure 5.7 A.

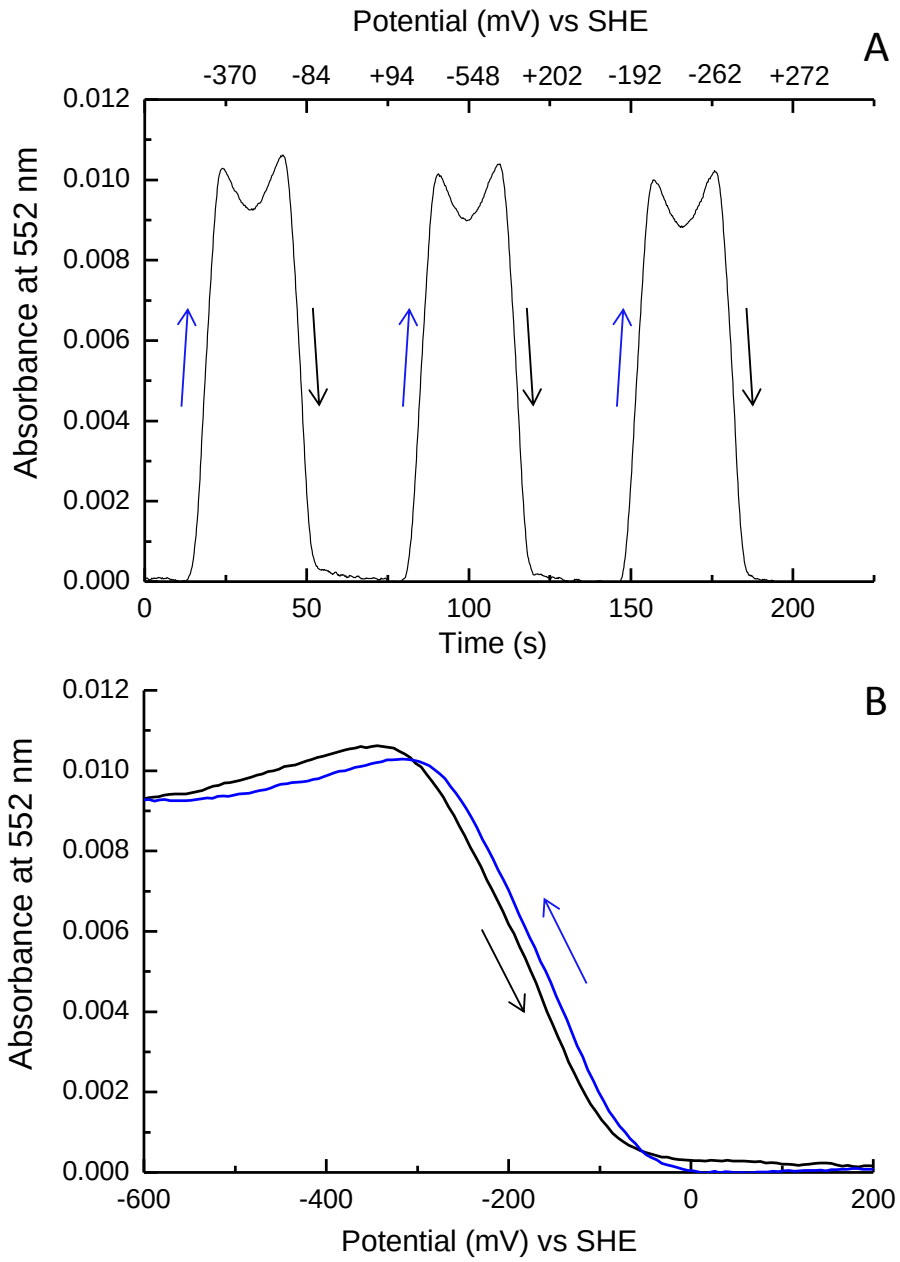

Figure 5.7 The change in absorbance at 552 nm during cyclic voltammetry of NrfB adsorbed on tin oxide. (A) The absorbance at 552 nm measured as a time course during cyclic voltammetry, blue arrows indicate reduction and black arrows indicate re-oxidation, the potential every 25 s is as indicated. (B) The data in (A) between 1 and 67 seconds plotted as absorbance vs. potential. Experiments were performed at 30 mV s^{-1} under experimental conditions described in figure 5.6.

A more in depth and useful analysis of the change in absorbance at 552 nm with the change in potential can be obtained by taking the derivative of this; plotting the $dA_{552\ nm}/dE$ to produce a cyclic voltabsorptogram (CVA) which is the spectroscopic equivalent of the cyclic voltammogram (CV) (figure 5.8). Comparison of the CVA (figure 5.8, black circles) to the CV (figure 5.8, dashed red line) of NrfB adsorbed on tin oxide that were normalised to the maximum intensity, shows they closely overlay one another. Thus they are in agreement with the redox description of the NrfB hemes. As described earlier with the CV data, the CVA can be fitted to equation 5.2 to determine reduction potentials for the five NrfB hemes. The oxidative and reductive peaks were fitted separately and the values were averaged to provide true reduction potentials. The reduction potentials defined from the fit were -108.5 ±5, -154 ±5, -177 ±6, -232 ±7 and -264.5 ±8 mV and are in good agreement with the values obtained from the fit of the cyclic voltammogram.

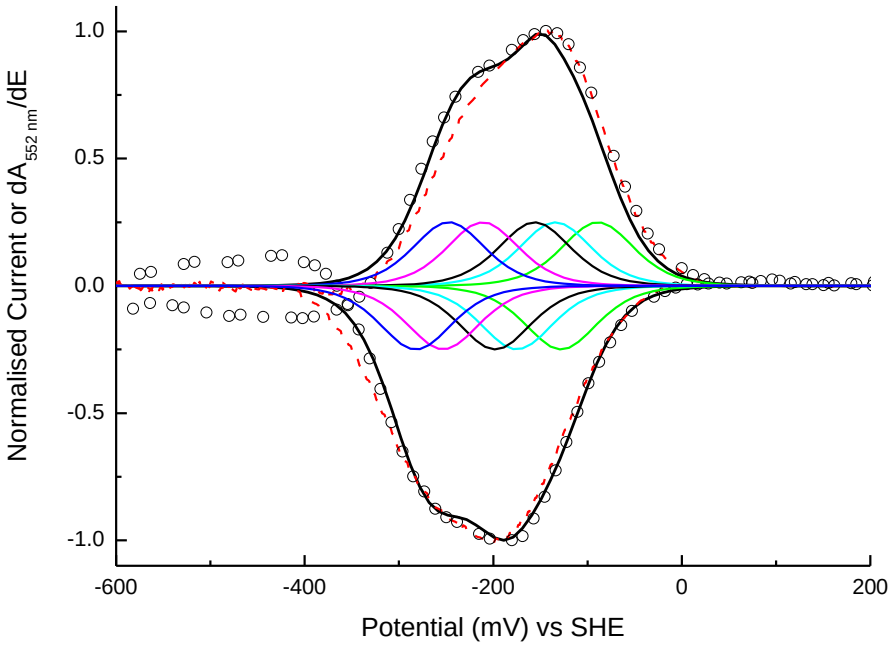

Figure 5.8 The cyclic voltabsorptogram (CVA) of NrfB absorbed on tin oxide. The derivative voltabsorptogram (black circles) and the fit of this to equation 5.2 (black line) that gave rise to heme reduction potentials of; -108.5, -154, -177,-232 and -264.5 mV. The simulated response from each of the five NrfB hemes is shown (green, cyan, black, magenta and blue lines) and a baseline subtracted cyclic voltammogram of NrfB on tin oxide also recorded at 30 mV s^{-1} (red dashed line). The data are normalised to the maximum peak height. Experimental conditions are identical to those in figure 5.6.

The amount of redox active NrfB adsorbed to the electrode can be determined from the area of the peak in the CVA and is defined by Tablecurve during the fitting of equation 5.2 described above. Tablecurve uses equation 2.8 to scale the fit of equation 5.2 to the peak height and the number of moles of protein is captured within this equation. Analysis of both the oxidative and reductive sweeps gave the amount of electroactive NrfB to be 3.5 ± 0.01 nmoles. As equal amounts of NrfB were oxidised and reduced it was clear that all electroactive NrfB remained adsorbed during the experiment and that reduction and oxidation did not induce any irreversible changes in the redox properties of NrfB.

In order to deduce information about the interfacial electron transfer kinetics of NrfB adsorbed on tin oxide a fresh electrode was prepared as earlier described and soaked overnight in a 3 μM solution of NrfB. Cyclic voltammetry was performed of NrfB adsorbed on tin oxide in a normal electrochemical cell (i.e. that does not have a dual function as a cuvette) in an anaerobic glovebox, in 50 mM Hepes, 2 mM $CaCl_2$, pH 7, between +340 and -630 mV and the potential was swept using scan rates of 2, 5, 15, 30 and 50 mV s^{-1} (figure 5.9 A). Cyclic voltammograms were baseline subtracted using the Utilities for Data Analysis 010716 Program as previously described. At the lower scan rates cyclic voltammograms showed peaks for oxidation and reduction that were almost mirror images of each other across the zero of the current axis. As the scan rate was increased above 10 mV s^{-1} the reductive peak moved to more negative potentials and the oxidative peak moved to more positive potentials (figure 5.9). Plotting the apparent oxidative and reductive peak potentials i.e. the peak in the cyclic voltammogram for oxidation and reduction, over a range of scan rates usually gives rise to a distinctive 'trumpet' shaped plot when oxidation and reduction of the adsorbed protein are reversible and electron transfer between the electrode and the adsorbed protein is not coupled to another process [103].

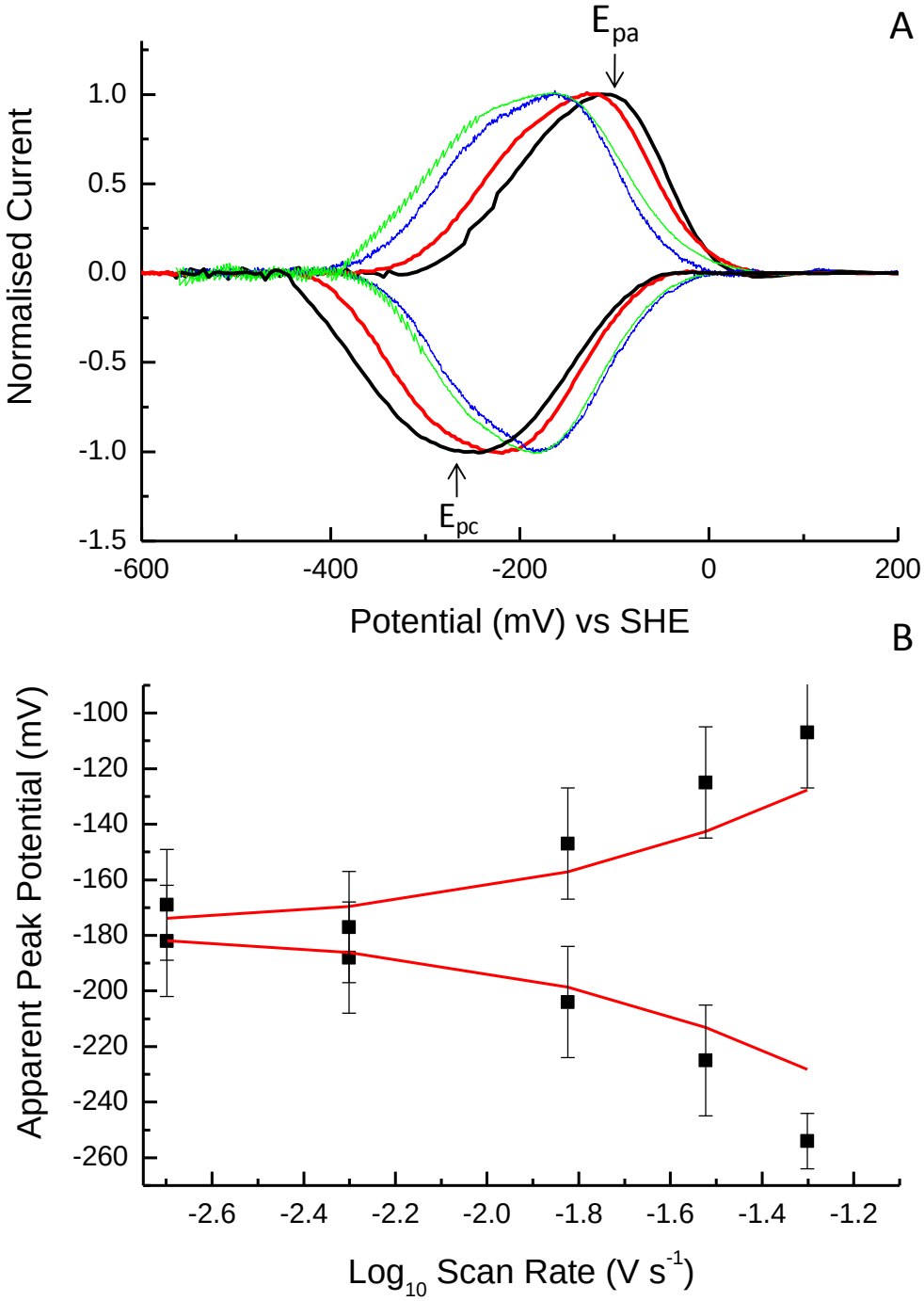

Figure 5.9 The scan rate dependence of NrfB adsorbed on tin oxide. (A) The baseline subtracted cyclic voltammogram of NrfB recorded at 50 (black), 30 (red), 5 (green) and 2 mV s^{-1} (blue). The anodic and cathodic peaks (E_{pa} and E_{pc}) are indicated by the arrows for the cyclic voltammogram at 50 mV s^{-1}. (B) The anodic and cathodic peak potentials vs. the log scan rate and the fit of this to the Butler-Volmer equation giving a rate constant of 0.5 s^{-1}.

The rate of interfacial electron transfer i.e. electron transfer between the electrode and protein can be determined from the trumpet plot using Jellyfit software kindly provided by Dr. Lars Jeuken [132]. Jellyfit software models the rate of interfacial electron transfer where the finite peak separation at the lowest scan rate is known and the Butler-Volmer equation defines the dependence of the rate of interfacial electron transfer on applied over-potential:

$$i = i_0\left[e^{\alpha n f \eta} - e^{(1-\alpha) n f \eta}\right] \qquad \text{(Equation 5.3)}$$

Where i is the current, i_0 is the exchange current, α is the transfer coefficient, f is equal to F/RT and η is exponentially applied over-potential [94]. For NrfB a trumpet plot of the oxidative and reductive apparent peak potential, showed separation of the oxidative and reductive peaks almost from the lowest scan rates explored (figure 5.9B). The rate constant for interfacial electron transfer between the tin oxide electrode and NrfB was found to be 0.5 s^{-1}, this value is identical to that calculated for experiments for NrfA adsorbed on tin oxide, indicating that this is likely to reflect intrinsic electron transfer properties of tin oxide [55].

5.4 Cyclic Voltammetry of NrfB Adsorbed on PGE Electrodes

Experiments of NrfB adsorbed on tin oxide showed that NrfB retained its structure upon adsorption and was redox active; this was indicated by the similarities between the spectroscopy of NrfB adsorbed and NrfB in solution. However tin oxide electrodes are inappropriate for investigating catalysis by NrfAB, experiments with NrfA alone have shown that k_{cat} was limited by the diffusion of substrate into the na nocrystalline mesoporous structure of the tin oxide electrode [114]. High scan rate methods will also be used to probe the electron transfer kinetics through NrfAB and it has been shown that tin oxide supports interfacial electron transfer at rates that are expected to be sluggish compared to those predicted to support catalysis by NrfAB, given that NrfA k_{cat} is approximately 4600 electrons s^{-1} [40]. Therefore a different strategy was employed to use PFV to investigate nitrite reduction by NrfAB. Graphite electrodes were used for studies of TvNir and NrfA alone and these are a better choice,

as whilst cyclic voltammetry PFV on tin oxide electrodes provides the advantage that both spectroscopy and cyclic voltammetry can be performed on the absorbed sample simultaneously, graphite has better electrochemical characteristics [101, 102]. Graphite electrodes also have a much flatter surface compared to tin oxide electrodes and so k_{cat} will not be limited by the porous nature of the electrode surface. Protein films on graphite electrodes are quick to prepare, the electrode with a protein film adsorbed can rapidly be transferred from one solution to another and a much smaller amount of protein is required for studies using graphite electrodes than tin oxide electrodes. This much more rapid method of PFV, with its economical use of protein was used to characterise the thermodynamics of electron transfer through NrfB at a series of different conditions.

Cyclic voltammetry of NrfB was initially performed using a basal graphite electrode that was first was polished using a 0.3 µm Al_2O_3 slurry as described in chapter 2. The polished electrode was then directly taken into an anaerobic glovebox and placed inside an electrochemical cell of the three electrode cell configuration (figure 2.8), filled with 50 mM Hepes, 2 mM $CaCl_2$, at pH 7.0, where the water jacket was set to 4 °C. Cyclic voltammetry was performed of the bare basal electrode between +197 and -503 mV at 30 mV s^{-1} for five scans, a featureless response was observed and these cyclic voltammograms were saved for use as the baseline (figure 5.10). Fresh baseline cyclic voltammograms were recorded for each set of experimental conditions used for each day of experiments. The electrode was then removed from the electrochemical cell and re-polished and taken directly back into the anaerobic glovebox with a 3 µM solution of NrfB and an ice cold Hamilton syringe. A 1 µl drop of NrfB was placed onto the graphite surface for ca. 10 seconds before the excess was removed with the Hamilton syringe. The electrode was then placed into the electrochemical cell filled with a fresh solution of 50 mM Hepes, 2 mM $CaCl_2$, pH 7.0 and cyclic voltammetry was performed between +197 and -503 mV at 20 mV s^{-1} (figure 5.10). Broad symmetrical peaks were seen on the oxidative and reductive sweep indicating the oxidation and reduction of NrfB adsorbed on the electrode, the broad peaks showed no additional features in agreement with the results at the tin oxide electrode. The baseline subtracted cyclic voltammogram of NrfB was modelled using

Utilities for Data Analysis 010716 Program as previously described, this allowed for slight differences in the charging current of the adsorbed electrode with NrfB adsorbed (not arising from the oxidation and reduction of NrfB redox centres) compared to the bare electrode to be corrected for (figure 5.10). The baseline subtracted oxidative and reductive peaks were separated and fit to equation 5.2, for five n=1 redox centres, using Tablecurve 2D as earlier described. The average of the fits to the oxidative and reductive peaks from three experiments gave reduction potentials of -61, -123, -147, -182 and -245.5 ± 20 mV. These reduction potentials are within error of those calculated for NrfB at pH 7.0 on tin oxide inferring that they are the intrinsic redox properties of NrfB and that all five hemes are redox active and are little altered by the different surfaces that it was adsorbed to during these experiments.

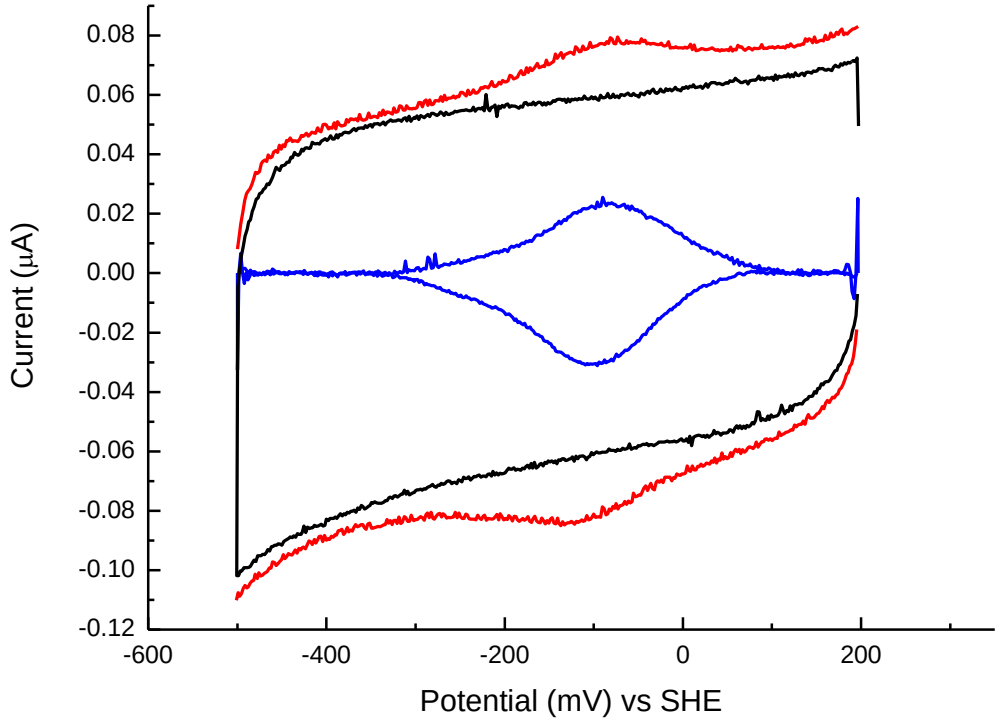

Figure 5.10 Cyclic voltammetry of NrfB adsorbed on a PGE electrode. Cyclic voltammetry of the electrode without the enzyme adsorbed (black), of NrfB on graphite (red) and the baseline subtracted cyclic voltammogram (blue). Cyclic voltammetry was performed at 20 mV s^{-1} in 50 mM Hepes, 2 mM $CaCl_2$, and pH 7 at 4 °C.

5.5 The pH Dependence of PFV of NrfB Adsorbed on Graphite

Cyclic voltammetry of NrfB adsorbed on basal graphite was performed between pH 4 and pH 9 at half pH intervals. A new film was made for studies at each pH. As described for the pH dependence of TvNir a multi-component buffer was used containing 20 mM HTMA, 2 mM $CaCl_2$. Cyclic voltammograms were recorded across the pH range at scan rates between 5 and 100 mV s^{-1} and were baseline subtracted in the same way as those recorded at pH 7 described earlier (figure 5.11). The response of NrfB showed very little variation with the change in scan rate between 5 and 100 mV s^{-1}, with the oxidative and reductive peaks more clearly defined at the faster scan rates, probably due to a greater signal to noise ratio. This is in contrast to results on tin oxide as discussed above.

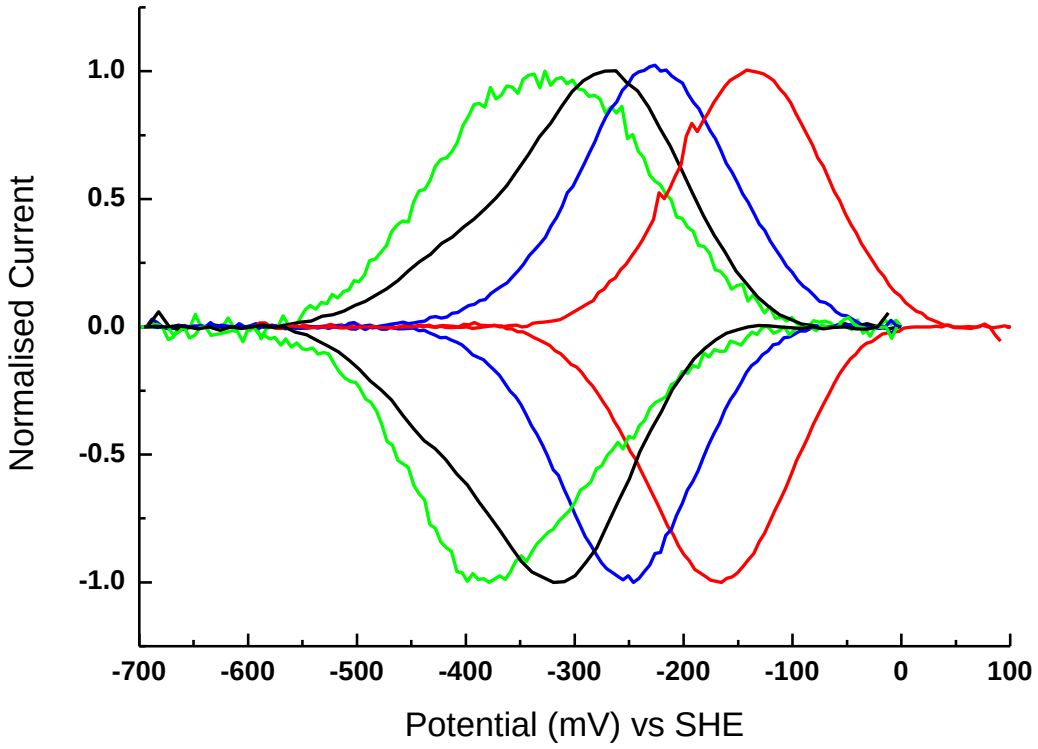

Figure 5.11 Cyclic voltammetry of NrfB from pH 4-9. The baseline subtracted cyclic voltammogram of NrfB recorded on a basal graphite electrode at pH 4 (red), pH 6 (blue), pH 7.5 (black) and pH 9 (green). Cyclic voltammograms were recorded at 4 ° C, in 20 mM HTMA, 2 mM $CaCl_2$ at a scan rate of 100 mV s^{-1}.

At every pH oxidation and reduction still occurred within one clearly defined redox envelope (figure 5.11). However, peaks were clearly displaced to more negative potentials at acid pH and additionally there was a broadening of peaks above pH 6. Between pH 4 and pH 6 the half height width (hhw) was ca. 158 mV, this increased to ca. 215 mV at pH 9. Given that the peaks arise from five redox centres with overlapping profiles for oxidation and reduction as shown in figure 5.8, the relative heme reduction potentials are the same from pH 4 to pH 6, where no change is detected in the half height width. Above pH 6 the altered width indicates that the reduction potential of one of more of the redox cofactors is affected by the change in pH differently with respect to the other hemes. This could be due to an amino acid or heme proprionate group in close proximity to one or more of these hemes becoming deprotonated above pH 6.

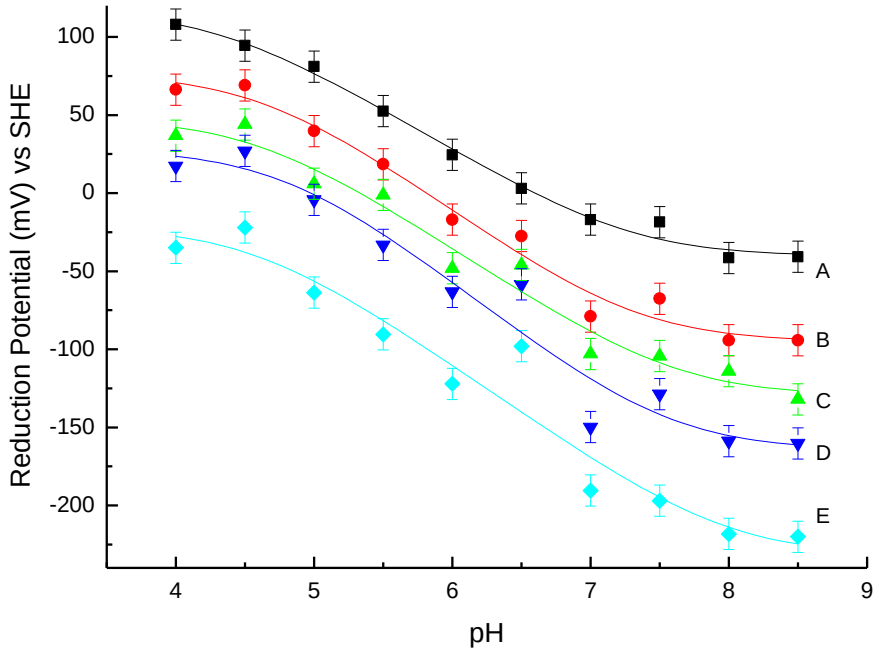

Figure 5.12 The pH dependence of the reduction potentials of the NrfB hemes. Each heme is represented by a different colour data point and has been labelled A-E in order to facilitate discussion, reduction potentials were determined by the average fit of the oxidative and reductive baseline subtracted cyclic voltammograms to equation 5.2 using Tablecurve 2D. The solid lines show the fit of the data to equation 5.5, giving rise to values of E_{alk}, n, $pK_{a,\,ox}$ and $pK_{a,\,red}$ indicated in table 5.1. All experiments were performed using a basal graphite electrode in 20 mM HTMA, 2 mM $CaCl_2$, at 4°C. Data points are the average of at least four experiments at scan rates from 5 to 100 mV s^{-1}.

Fitting the baseline subtracted cyclic voltammograms of NrfB at each pH to equation 5.2 provided more detailed information on the pH dependence of each of the redox properties of the NrfB hemes (figure 5.12). At low pH (<6) the separation of the heme reduction potentials showed little variation with the change in pH. Above pH 6 the spread of the reduction potentials increases from ca. 145 mV to about 178 mV. The reduction potentials of the hemes annotated B, C and D in figure 5.12 separate slightly from one another but remain quite clustered together, whereas the reduction potentials of the hemes annotated by A and E become separate from B, C and D. At high and low pH the reduction potentials of all the hemes appear to be reaching maximum and minimum values, indicating that the pH dependent residues near to the NrfB hemes are fully protonated and de-protonated below pH 4 and above pH 8.5. Around pH 7 where the change in pH elicits a linear change in the potential this was determined for hemes A-E to be -39.5, -44.5, -44, -49.5 and -50.5 mV/pH unit respectively. When oxidation and reduction involves the transfer of protons it can be considered that:

$$Ox + ne^- + mH^+ \rightarrow Red{:}H^{(m-n)+} \qquad \text{(Equation 5.3)}$$

For this equation it has been derived that 59(m/n) mV reflects the change in reduction potential with pH unit when one electron is transferred with one proton. This is approximately the case for the NrfB heme reduction potentials and the pH dependence of the reduction potential can therefore be modelled by a square scheme for reduction coupled to a single protonation event (scheme 5.1):

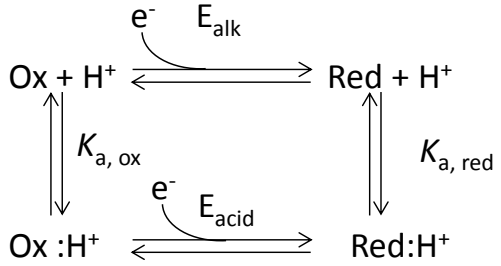

(Scheme 5.1)

Where in scheme 5.1 Ox is the oxidised redox centre, Red is the reduced redox centre and $Ox{:}H^+$ and $Red{:}H^+$ are the protonated forms of the oxidised and reduced redox centres. E_{alk} and E_{acid} are the reduction potentials of the redox centre at alkaline and

acid pH respectively. $K_{a,\,ox}$ and $K_{a,\,red}$ are the acid dissociation constants for the oxidised and reduced redox centres. The square scheme can be fit to equation 5.4 in order to determine the parameters $K_{a,\,ox}$, $K_{a,\,red}$ and E_{alk}.

$$E_{obs} = E_{alk} + \frac{2.303RT}{nF} log\left(\frac{1+\frac{[H^+]}{K_{a,red}}}{1+\frac{[H^+]}{K_{a,ox}}}\right) \qquad \text{(Equation 5.4)}$$

Where E_{obs} is the observed potential, $[H^+]$ is 10^{-pH} and all other symbols are as previously stated. The $pK_{a,\,ox\ or\ red} = -\log K_{a,\,ox\ or\ red}$. In order to define the pK_a directly equation 5.4 can be modified to equation 5.5:

$$E_{obs} = E_{alk} + \frac{2.303RT}{nF}\log\left(\frac{\left(1+10^{(pH-pK_{a,red})}\right)}{\left(1+10^{(pH-pK_{a,ox})}\right)}\right) \qquad \text{(Equation 5.5)}$$

The pH dependence of the NrfB heme reduction potentials showed a good agreement with equation 5.5 (figure 5.12, table 5.1).

Heme	E_{alk} (mV)	n	$pK_{a,\,red}$	$pK_{a,\,ox}$
A	117 ± 9	1.03 ± 0.13	7.27 ± 0.2	4.31 ± 0.4
B	76 ± 7	0.86 ± 0.20	7.31 ± 0.4	4.60 ± 0.5
C	48 ± 16	0.93 ± 0.20	7.60 ± 0.5	4.60 ± 0.6
D	28 ± 20	0.78 ± 0.30	7.50 ± 0.7	4.79 ± 0.8
E	-21 ± 20	0.88 ± 0.28	7.96 ± 0.9	4.57 ± 0.9

Table 5.1 The values obtained from the fit of the reduction potentials of NrfB vs. pH to equation 5.5

The values obtained for $pK_{a,\,ox}$ and $pK_{a,red}$ are within error of one another for each of the hemes of NrfB indicating that the residue that is protonated and deprotonated as each heme reduced may be the same for each heme. The only heme that produced a fit representing a one electron reduction was heme A, the remaining hemes fit to ca. 0.8 electron reduction.

As changing scan rate up to 100 mV s^{-1} had little effect on the cyclic voltammetry of NrfB adsorbed on graphite it was suspected that the rate of interfacial electron transfer was extremely fast in contrast to results obtained using a tin oxide

electrode. If electron transfer were not inhibited by the rate of delivery of electrons to NrfB then perhaps if the NrfAB complex were formed on the electrode the rate of electron transfer between NrfAB would be the slow step, providing information on the interaction of this complex and the kinetics of electron transfer through NrfAB. In order to proceed with studies of the NrfAB complex, the scan rate dependence of NrfB was first fully characterised.

Due to the apparent fast interfacial electron transfer of NrfB on graphite a 'fast' electrochemical cell was used (see chapter 2) and a pin point edge electrode in order that faster scan rates could be explored using PFV [102]. This electrode configuration minimises the drop in potential across the luggin tip to the electrode surface as the distance is minimised, this becomes more significant as the scan rate and the current increases. As protein film coverage was lower on the pin point edge electrode (due to a lower surface area), a 10 mM neomycin coadsorbate was used of the appropriate pH to the experimental buffer in order to improve the protein film coverage. The addition of neomycin increased the coverage of NrfB adsorbed to the electrode without altering the electrochemical response compared to PFV without neomycin. Prior to adsorption of the NrfB onto the freshly polished electrode, a film of ice cold neomycin was first added in the anaerobic glovebox using an ice-cold Hamilton syringe, using the same procedure for making a protein film. At scan rates of 1 V s^{-1} the oxidative and reductive peaks were still nearly mirror images of one another across the zero current axes, indicating much faster rates of interfacial electron transfer on PGE than those obtained using tin oxide electrodes. As the scan rate is further increased to 100 V s^{-1} and then to 150 V s^{-1} the oxidative and reductive peaks begin to separate from one another (figure 5.13). Fitting the peak position vs. scan rate using Jellyfit as earlier described, for an average of three experiments gave an interfacial electron transfer rate of 913 s^{-1} between NrfB and the electrode, interfacial electron transfer rates of more than 100 s^{-1} are considered as fast electron transfer [103].

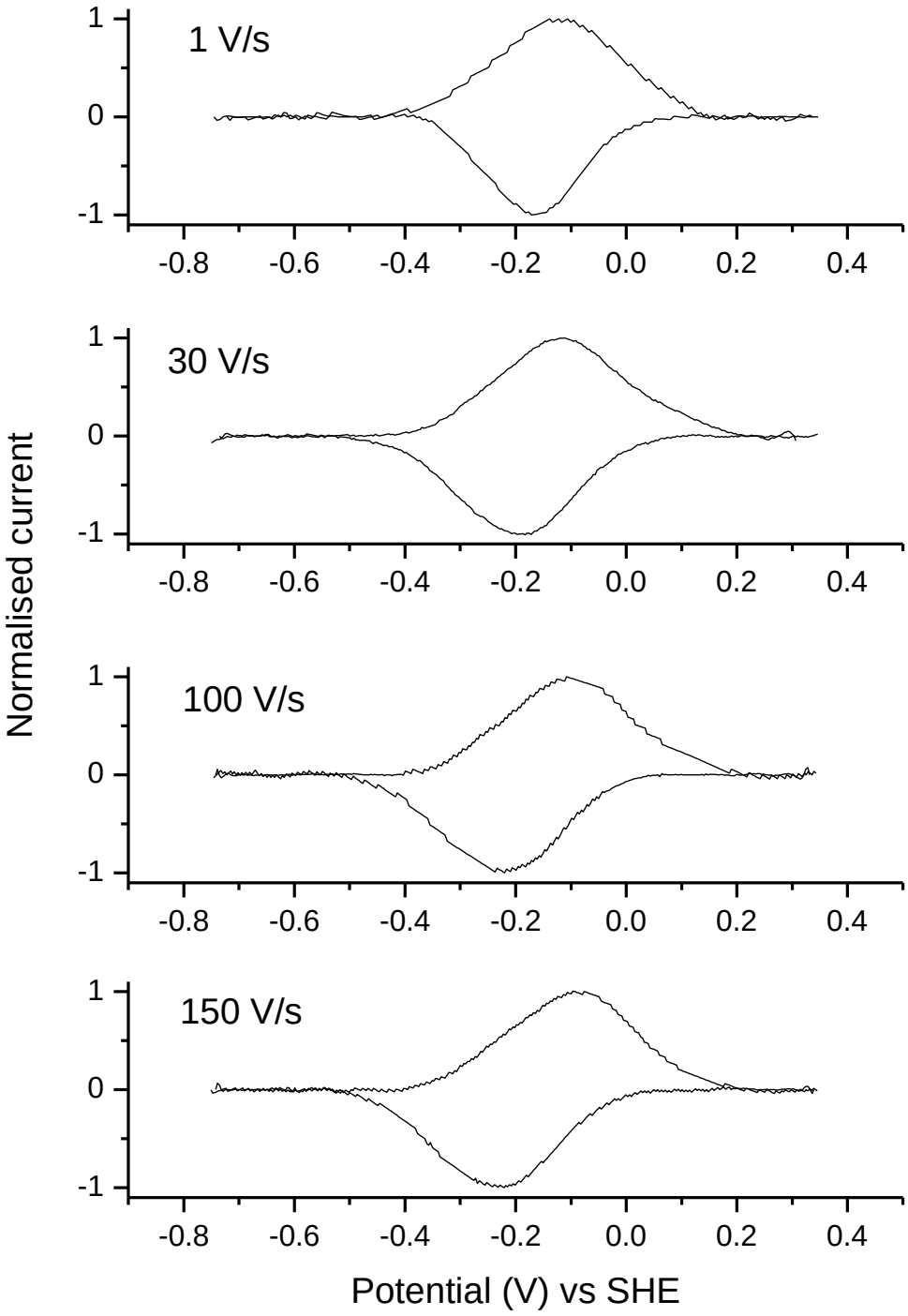

Figure 5.13 The scan rate dependence of NrfB cyclic voltammetry on PGE. The normalised baseline subtracted cyclic voltammograms of NrfB adsorbed on a graphite edge electrode with 10 mM neomycin, in 20 mM HTMA, 2 mM $CaCl_2$, and pH 7 at 4°C. The scan rates for each cyclic voltammogram are as indicated.

The peak area obtained at each scan rate in the above experiment was divided by the Faraday constant to calculate the number of moles of enzyme adsorbed to the surface of the electrode. As the scan rate was increased there was no change to the number of moles of NrfB adsorbed to the surface of the electrode, if there had been a change it could have indicated that the same amount of enzyme was adsorbed to the electrode but that the scan rate was too high to allow electron transfer. All the NrfB contributing to electrochemical signal at low scan rate is still contributing to the non turnover response at high scan rate (figure 5.14).

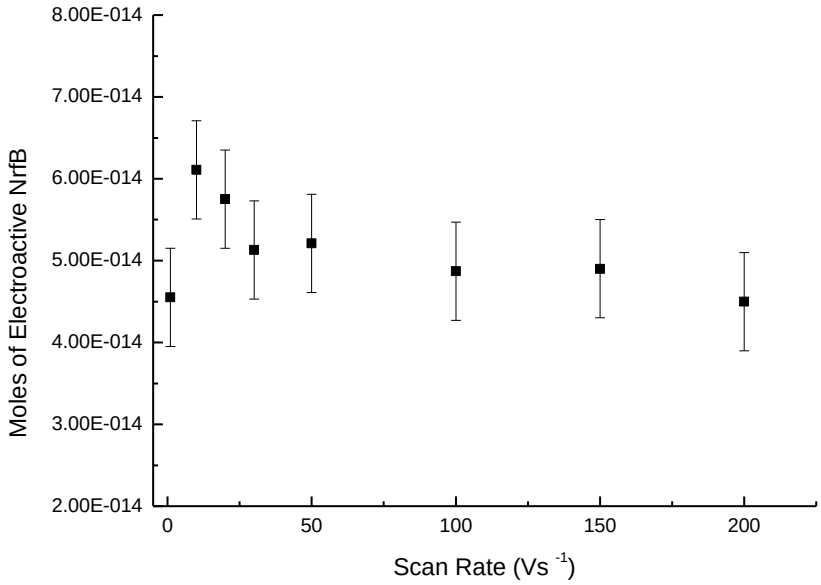

*Figure 5.14. The scan rate dependence of the amount of electroactive NrfB adsorbed to the electrode***.** The data points represent the moles of NrfB adsorbed to the electrode at each scan rate. Experiments were performed under the same conditions as for figure 5.14.

5.6 Cyclic Voltammetry of NrfA on PGE Electrodes

In order for a study of the NrfAB complex to be performed on the electrode it was first important to ensure that the individual responses of NrfA and NrfB were well characterised. Characterisation of NrfB has been described above and the electrochemical, catalytic response of NrfA on graphite electrodes has been previously reported [1, 3, 5, 49, 65, 82, 104, 105, 114, 115]. However the catalytic response of NrfA at high scan rate had yet to be characterised, as an efficient response at high scan rates requires the use of the fast electrochemical cell and a stationary electrode.

Previous PFV studies of NrfA have used rotating graphite edge electrodes as described in chapter 4 for obtaining kinetic values for TvNir. The reason for this is that catalysis of nitrite reduction by NrfA is so fast that the substrate is rapidly depleted at the electrode surface and without rotation the catalytic current will then reflect the rate of substrate diffusion to the electrode surface, not the rate of catalysis by the enzyme. Electrode rotation eliminates this problem; however this is not possible in the high scan rate cell due to solution turbulence if the electrode is rotated near to the luggin tip, so an alternative solution is to use a high substrate concentration. Chronoamperometry PFV was used to determine an appropriate nitrite concentration to use in the high scan rate experiments, i.e. where the catalytic current was independent of rotation speed. A NrfA film was made on the surface of a freshly polished rotating disc electrode (RDE) using a stock solution of 0.15 µM NrfA and placed in an electrochemical cell in 50 mM Hepes, 2 mM $CaCl_2$ and 0.1 mM NO_2^-. The catalytic current was measured over 200 seconds whilst the electrode potential was poised at -600 mV, where NrfA shows high catalytic activity (figure 5.15). For the first 100 s no electrode rotation was applied, after 100 s the rotator was switched on to 3000 rpm. This experiment was performed again at 0.5, 1, 2.5, 5, 10, 15 and 30 mM NO_2^-. It was clear that in 0.1 mM NO_2^- turning on the rotator increased the catalytic current and that therefore without electrode rotation substrate diffusion to the enzyme adsorbed on the electrode surface was limiting catalysis. In 30 mM NO_2^- switching on the rotator actually led to a slight decrease in the catalytic current, this is likely to be due to some of the NrfA becoming detached from the electrode as rotation begins. It is clear that electrode rotation (or the lack of) does not have a limiting effect on catalysis at this nitrite concentration and so 30 mM nitrite was used in the high scan rate experiments.

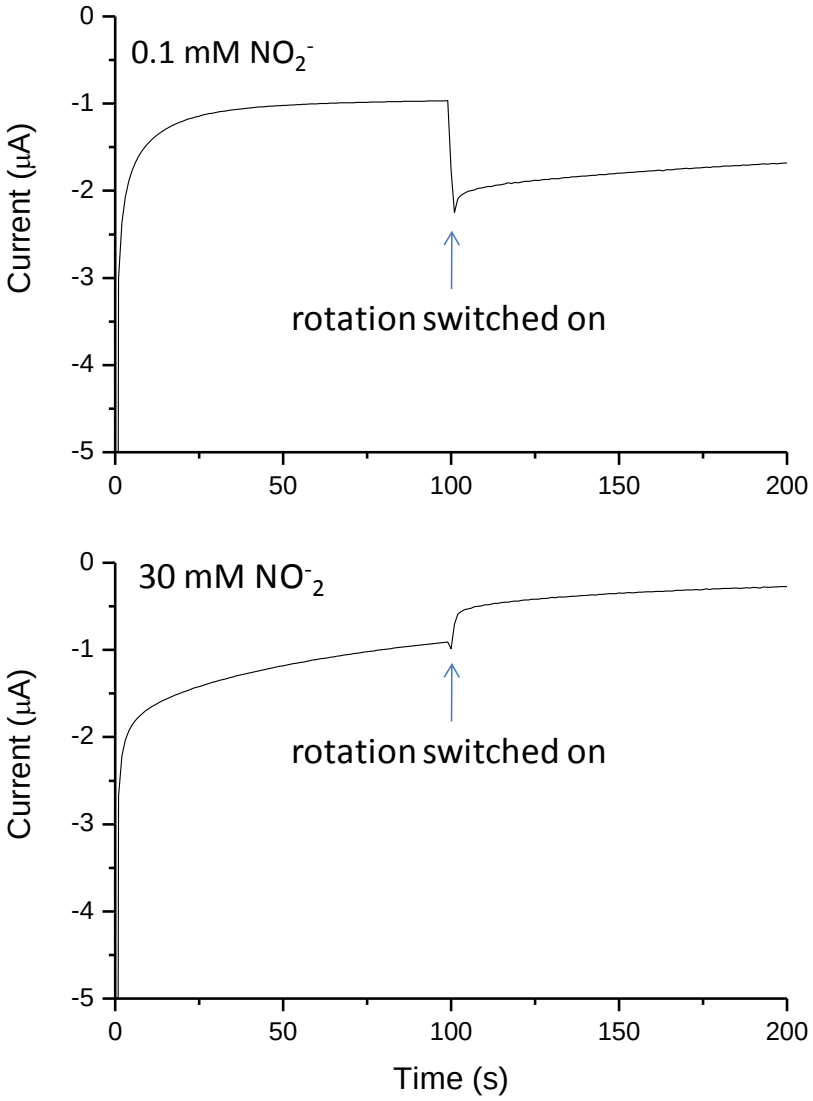

Figure 5.15 The rotation dependence of NrfA nitrite reduction at high and low nitrite concentration. Chronoamperometry of NrfA at -600 mV where the electrode initially was not rotated and then was switched on at 3000 rpm after 100 s, as indicated by the blue arrow in 0.1 mM and 30 mM nitrite. Experiments were performed in 50 mM Hepes, 2 mM $CaCl_2$ at pH 7 using the 'normal' electrochemical cell set up and a rotating PGE electrode.

Now that a nitrite concentration had been determined that enabled NrfA to be studied using a fast electrochemical cell, with a stationary electrode, cyclic voltammetry of NrfA was performed using a PGE electrode where the potential was swept between +197 and -803 mV at scan rates varied randomly from 50 mV s^{-1} to 200 V s^{-1} (figure 5.16). At low scan rates a distinct negative catalytic current reflecting

nitrite reduction was seen at potentials below ca. -100 mV. At high scan rates of 50 V s^{-1} and above, the catalytic signal became more subtle and less obvious to detect. The rate of catalysis at a given substrate concentration is intrinsic to NrfA and will not be altered by scan rate, unless the scan rate is too rapid for electron transfer to occur between the electrode and the adsorbed NrfA; if this is the case the catalytic signal would decrease as the rate of nitrite reduction would be limited by the rate of interfacial electron transfer between NrfA and the electrode.

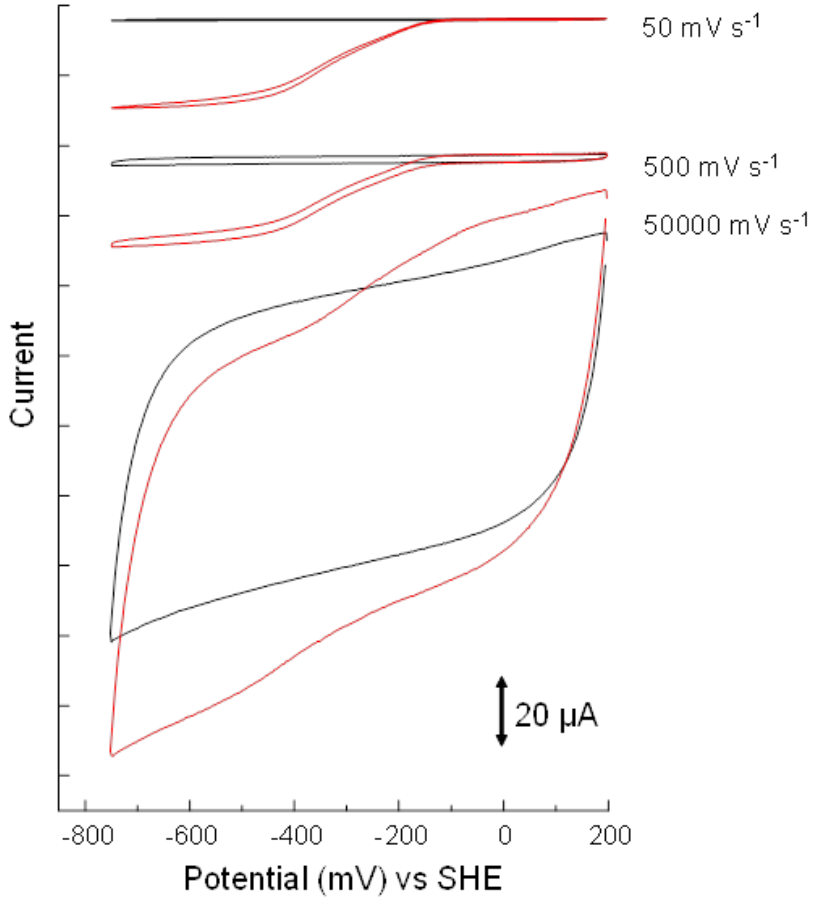

Figure 5.16 Cyclic voltammetry of NrfA at high scan rate. Cyclic voltammetry of NrfA (red) and the PGE baseline (black) recorded in the fast electrochemical cell at the indicated scan rates that have been displaced on the y- axis in order to aid comparison. Cyclic voltammetry was performed in 50 mM Hepes, 2 mM $CaCl_2$ at pH 7 with 30 mM NO_2^- at 18 °C.

The charging current of the electrode increases with increasing current, but unless the rate of interfacial electron transfer becomes limiting, the catalytic current magnitude should remain the same and therefore the signal will appear smaller at higher scan

rates with respect to the background of the baseline. In order to check whether interfacial electron transfer becomes limiting to nitrite reduction by NrfA adsorbed on PGE at high scan rate, the cyclic voltammograms at each scan rate were baseline subtracted and the catalytic current magnitude at -600 mV was obtained (figure 5.17). For data at low scan rates baselines were directly subtracted using Microcal Origin, however it is clear from figure 5.17 that direct baseline subtraction does not sufficiently compensate for the baseline contribution at high scan rate. In order to overcome this, baselines were simulated using the line drawing function in GPES to approximate the current contribution from the baseline at -600 mV and the error in this approximation was factored into each data point. The current magnitudes in these experiments were taken from the oxidative sweep of the cyclic voltammogram as the current on the oxidative sweep had a smaller contribution from the baseline background. Inspection of the catalytic current magnitude of NrfA over a range of scan rates showed no change in catalytic current as the scan rate was increased and that over the range of scan rates used in these experiments interfacial electron transfer to NrfA is not limiting (figure 5.17).

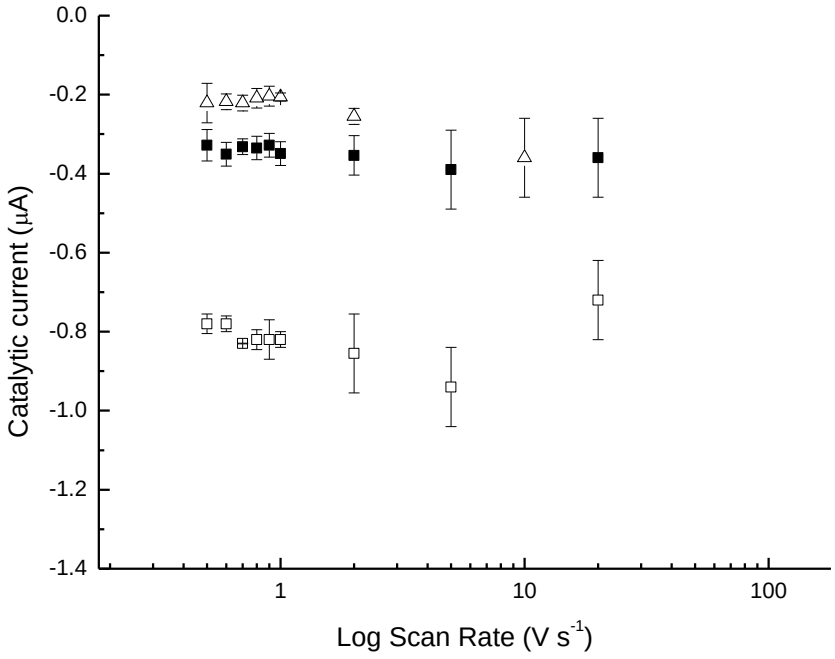

Figure 5.17 The scan rate dependence of the catalytic current magnitude of NrfA adsorbed on PGE. The catalytic current for three different NrfA films (triangles, black squares, hollow squares) over a range of scan rates is shown. Experiments were performed under the experimental conditions stated in figure 5.16.

5.7 Catalysis of Nitrite Reduction by the NrfAB Complex

Once both the voltammetry of NrfA and NrfB were separately established the next step was to investigate electron transfer of the NrfAB complex. It is known that the dissociation constant for the NrfAB complex is 50 nM and so to ensure that the NrfAB complex was the material being studied by PFV, NrfB was five times in excess of NrfA. The concentrations of NrfA and NrfB mixed were such that in the mixture was 0.1 µM NrfA and 0.5 µM NrfB; under these conditions all the NrfA should be associated in the NrfAB complex. Both NrfA and NrfB were dissolved in 50 mM Hepes, 2 mM $CaCl_2$ at pH 7, this was to ensure that there was no interference that could be attributed to the difference in solution conditions on the interaction between the two proteins.

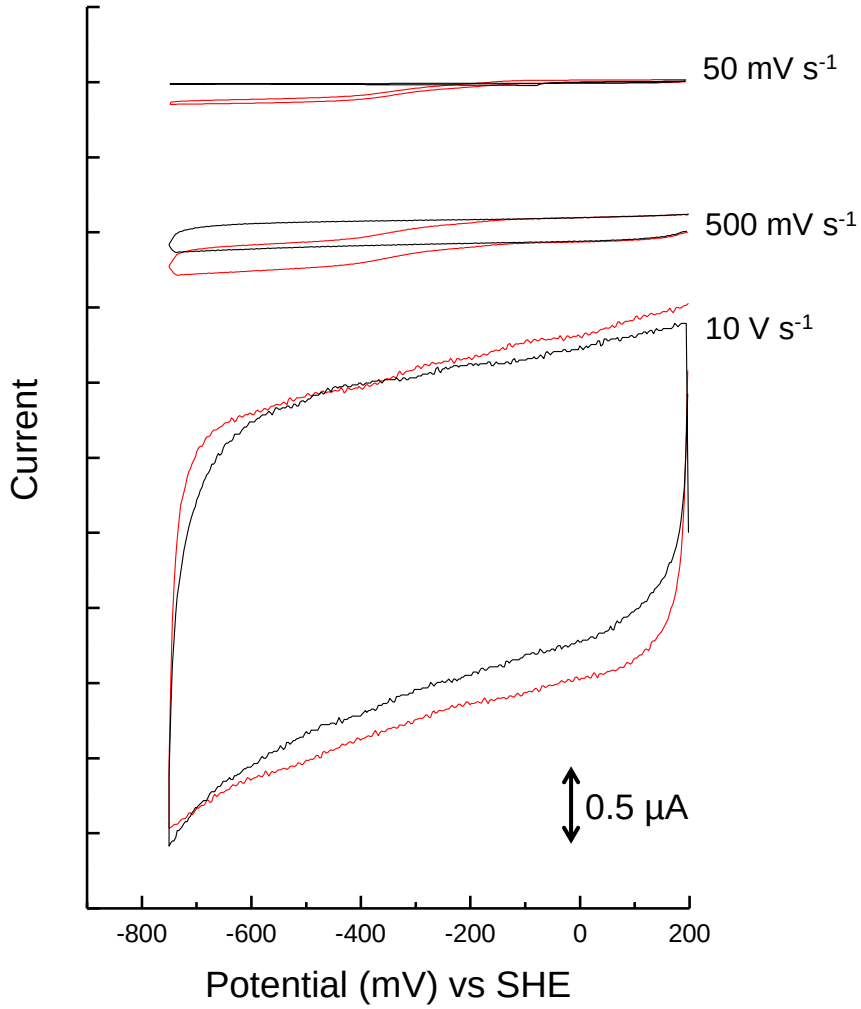

Figure 5.18 Cyclic voltammetry of 5NrfB:1NrfA coated electrode at varying scan rates. The PGE baseline (black) and the cyclic voltammetry with 5NrfB:1NrfA adsorbed (red) at the scan rates indicated, the 50 mV s^{-1} and 500 mV s^{-1} data have been displaced on the y-axis to allow comparison. Experimental conditions are as in figure 5.16.

PFV chronoamperometry was first performed of the 5NrfB:1NrfA (0.5: 0.1 μM) solution at -600 mV in the normal or slow electrochemical cell set up in order to check that catalytic current due to nitrite reduction by the NrfAB complex would not be affected by electrode rotation in 50 mM Hepes, 2 mM $CaCl_2$, and pH 7 with 30 mM NO_2^-. As with the film of NrfA alone (figure 5.15) in 30 mM NO_2^- a slight decrease in catalytic current from -3.8 μA to -3.4 μA was seen as the rotator was switched on to 3000 rpm after 100 s, whereas in 100 μM NO_2^- the catalytic current increased from -1.2 μA to -3.5 μA. This shows that there was no rotation dependence or mass transport limitations to catalysis when 30 mM NO_2^- was used to study NrfAB.

The fast electrochemical cell was then set up with 50 mM Hepes, 2 mM $CaCl_2$, pH7 and 30 mM NO_2^- in order to study the kinetics of electron transfer between NrfAB. The electrode was polished and baseline cyclic voltammograms were initially recorded between +197 and -803 mV at each scan rate selected for study from 50 mV s^{-1} to 50 V s^{-1} (figure 5.18). It was immediately apparent that catalytic current magnitudes were significantly lower for NrfAB than those for NrfA adsorbed to the electrode independently. This could arise from the slightly lower overall concentration of NrfA in the solution used to coat the electrode or/and that the excess NrfB could also be binding to the electrode.

As the scan rate was increased it was expected that the catalytic signal would become less obvious as was seen for cyclic voltammetry of NrfA on its own and that the non-turnover response of NrfB would become more obvious as this increases proportionally with the increase in scan rate; this was not what occurred. Cyclic voltammetry of 5NrfB:1NrfA (0.5: 0.1 μM) was very similar to that of NrfA alone, at low scan rates a distinct negative catalytic current was seen at potentials below -100 mV and at higher scan rates this became more difficult to detect, however there was no sign of non-turnover signals arising from the excess NrfB (figure 5.18). This could be because NrfA has a more favourable interaction with the graphite electrode and therefore the NrfA would receive its electron directly from the electrode and there would be no detectable electron transfer through NrfB, or it could be because the concentration of NrfB used in these experiments is significantly lower than the standard 3 μM used for PFV of NrfB in the experiments described above.

The catalytic current magnitude for nitrite reduction at -600 mV by NrfAB was obtained by baseline subtraction as previously described for experiments with NrfA alone. It was found that, when the error given by the small current magnitudes was considered, there was no change in the catalytic current magnitude for NrfAB between 50 mV s^{-1} and 50 V s^{-1} (figure 5.19). This indicates that formation of the NrfAB complex does not limit/affect electron transfer rates of NrfA for nitrite reduction and that the adsorbed NrfA is still rapidly receiving electrons for catalysis.

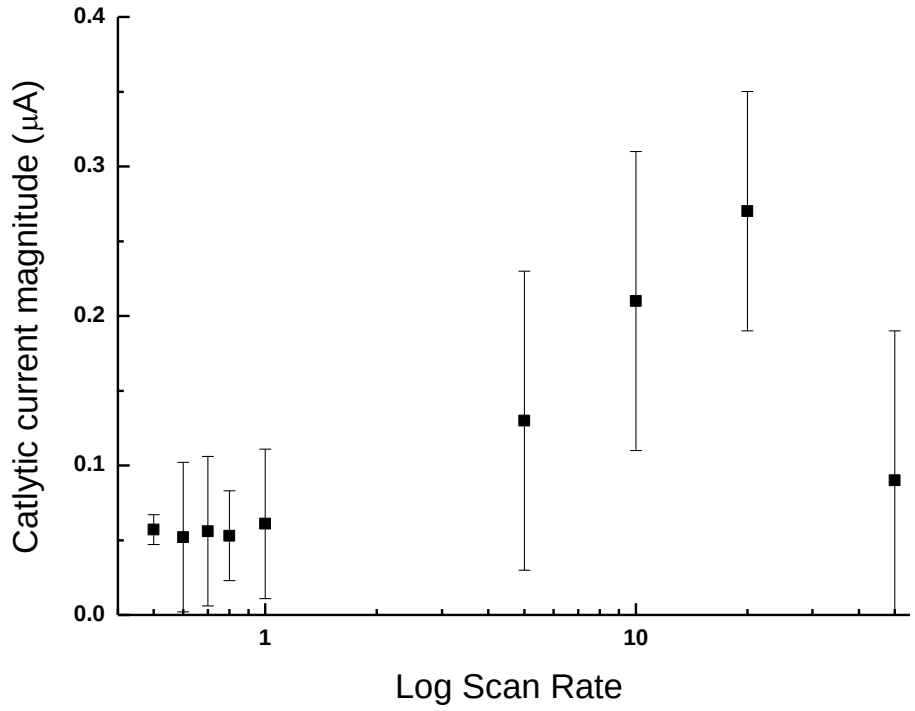

Figure 5.19 The scan rate dependence of the catalysis of NO_2^- reduction by a NrfAB coated electrode. The catalytic current magnitude for nitrite reduction at -600 mV, extracted from cyclic voltammograms of 5NrfB:1NrfA recorded in 50 mM Hepes, 2 mM $CaCl_2$ at pH 7 in 30 mM NO_2^- at 18 °C.

The cyclic voltammograms of NrfA and 5NrfB:1NrfA adsorbed to PGE were compared to attempt to determine whether formation of the NrfAB complex had any effect on the potential dependence of catalysis. Baseline subtracted cyclic voltammograms and derivative cyclic voltammograms were compared and it was found that there was no difference between NrfA alone and NrfAB coated electrode (figure 5.20). There were slight differences in the cyclic voltammograms at the most

negative potentials at 0.5 and 1 V s^{-1} scan rates, but these are likely to be attributed to the increasingly inadequate baseline subtraction possible at these higher scan rates.

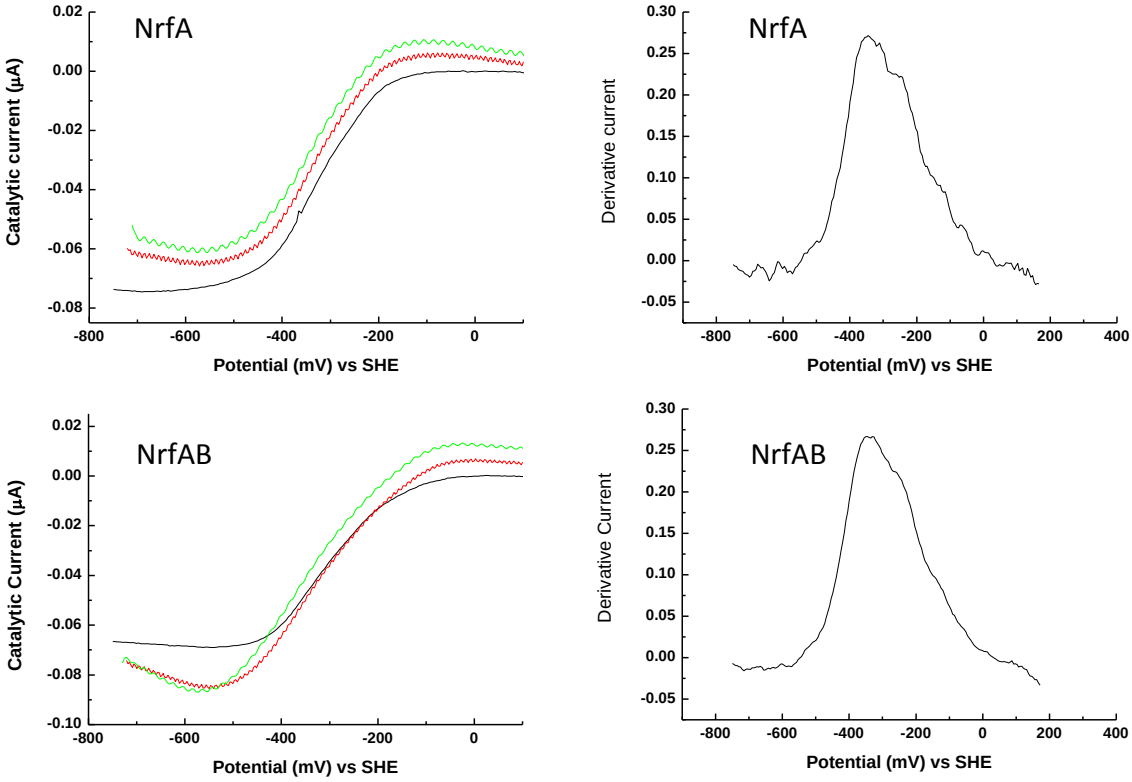

Figure 5.20 The potential dependence of nitrite reduction by NrfA and a 5NrfB:1NrfA coated electrode. The baseline subtracted reductive sweep at 50 mV s^{-1} (black), 500 mV s^{-1} (red) and 1 V s^{-1} (green) and the derivative cyclic voltammograms corresponding to the baseline subtracted reductive sweep at 50 mV s^{-1}. Experimental conditions were as described in figure 5.16.

5.8 Discussion

The experiments within this chapter have investigated the electrochemical properties of *E. coli* NrfB over a wide range of conditions. The reduction potentials determined from electrochemical experiments were in good agreement with those determined by previous solution based spectroscopic analysis, indicating that NrfB retains its native structure when it is adsorbed to the electrode [93].

Spectroscopy of NrfB was typical of low-spin heme, with the exception of the split soret feature detected in the reduced-oxidised difference spectrum (figure 5.4). The split soret feature has been identified in NrfA and in split soret cytochrome and

was thought to be diagnostic of high-spin heme [54, 133]. The NrfB crystal structure, the UV-Vis monitored potentiometry and the direct comparison of various high and low-spin difference spectra (figure 5.5) all agree that there is no evidence of a high spin NrfB heme [50, 93]. NrfB, NrfA and split soret cytochrome all contain hemes that are stacked in parallel to one another (figure 5.21 and 1.3) and so perhaps this heme arrangement, present in each of these proteins, is the structural origin of this spectroscopic feature.

The fit of the pH dependence of the NrfB heme reduction potentials to equation 5.5 suggested that some of the hemes within NrfB were reduced by less than one electron, despite the fact that the reduction of Fe^{3+} to Fe^{2+} is a one electron process. This could indicate a greater error in the calculation than predicted, or alternatively it could reflect co-operative electron transfer within NrfB and that as one heme is reduced it becomes 'easier' to reduce the neighbouring heme [2]. Co-operative electron transfer has been previously demonstrated for other multi-heme cytochromes, such as the tetraheme cytochrome c_3 found in *D. desulfuricans* and *S. oneidensis* [134, 135]. Heme A (figure 5.12) is the only redox cofactor for which the pH dependence of the reduction potential fits to a one electron reduction. Perhaps this corresponds to heme 1 (figure 5.21) which has the greatest distance to its adjacent heme of 6 Å, possibly limiting co-operativity for heme A, although 6 Å is still much less than the 14 Å thought to be a maximum distance for relevant rates of biological electron transfer [2, 46, 50].

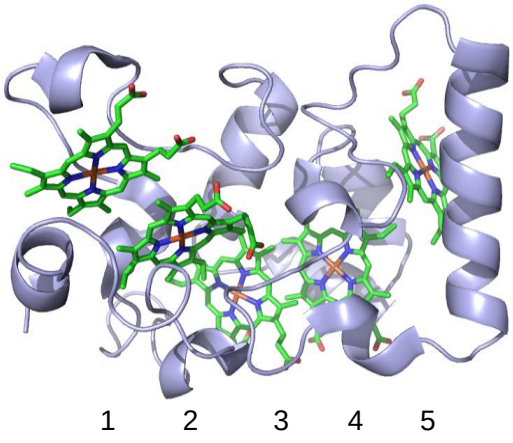

Figure 5.21 The crystal structure of E. coli NrfB. This image was prepared in PyMol using the pdb file 2OZY and the heme numbering are as indicated and as stated in [2].

Fits to equation 5.5 defined a pK_a for the oxidised and reduced redox cofactors ($pK_{a,\ red}$ and $pK_{a,\ ox}$ table 5.1). All the hemes had a $pK_{a,\ ox}$ of 4.57 ± 0.17 and a $pK_{a,\ red}$ of 7.53 ± 0.28. This indicates that the residue that was protonated as the heme was reduced was probably the same for each heme and so the most likely candidates are either the axial histidine ligands to the hemes or a heme propionate group. Both histidine residues and heme propionate groups have been previously detected with pK_a values in line with those determined for the $pK_{a\ ox/red}$ for NrfB and heme propionate groups have been shown to accept protons during the heterotrophic cooperative transfer of protons with electrons [136-138].

Whilst the pH dependence of the reduction potential of each heme was found to have the same $pK_{a\ ox/red}$ there were also some distinct differences in the pH dependence of each heme. Hemes B, C and D (figure 5.12) had similar pH dependence to one another, but hemes A and E have distinctive pH dependence at above pH 6. This observation is linked to the broadening of the window of redox activity seen in the baseline subtracted cyclic voltammograms of NrfB above pH 6, indicating that the reduction potential of some hemes within NrfB were differently affected by pH. NrfB (figure 5.21) has a low peptide to redox cofactor ratio, the pH dependence of the heme reduction potentials is primarily defined by the same protonation event for each heme, perhaps the slight distinction for hemes A and E arises from variations in solvent exposure, the influence of other neighbouring amino acids, or the proximity of the adjacent heme, but it is not possible to speculate further.

As with TvNir and NrfA, the reduction potentials of NrfB are much more negative than the nitrite ammonia redox couple (figure 5.22). The reduction potentials of NrfB are actually very similar to those of NrfA and some of the reduction potentials within NrfA are more negative than those of NrfB [54]. This suggests that there is very little thermodynamic driving force for electrons to move from NrfB to NrfA until nitrite binds in the active site of NrfA. Electron transfer pathways have been detected in other enzymes where electron transfer to each redox centre is not a direct thermodynamic downhill route to the active site. For example in *E. coli* NarGHI electrons enter the di-heme NarI quinol dehydrogenase, that has heme reduction potentials of +120 and then +20 mV, electrons are then transferred to NarH with iron-

sulfur redox cofactors that have reduction potentials of +180, -55, -420, +130 and -55 mV (in order to pathway from NarI) and finally electrons are transferred to the catalytic subunit NarG [139-142]. This 'indirect' type electron transfer pathway has also been noted for electron transfer through *E. coli* fumarate reductase, where the lower potential hemes were proposed to assist in controlling the rate of catalysis [143].

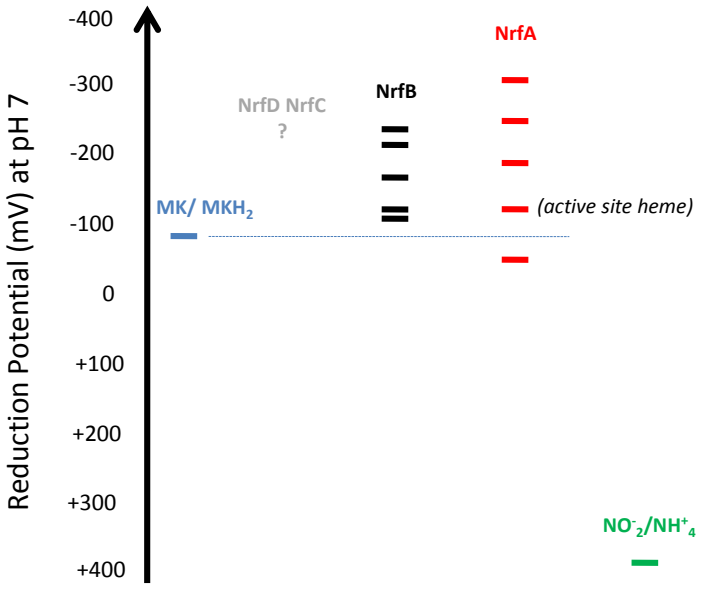

Figure 5.22 Illustration of the known reduction potentials from the menaquinol pool involved in nitrite ammonification by E. coli NrfAB at pH7 [54].

The relative reduction potentials of the hemes of NrfB compared to those of NrfA remain very similar between pH 4.5 to pH 8.5 (figure 5.23). The NrfAB complex is found in the periplasm of *E. coli* and so will 'experience' the external conditions of the gastrointestinal tract (a common environment of *E. coli*) which has pH between pH 4.5 and 9 [144]. It could be that the relative operating potentials of the NrfAB complex are poised as the thermodynamic pathway through NrfAB is important for controlling the supply of electrons for catalysis over the range of pH that NrfAB must operate at.

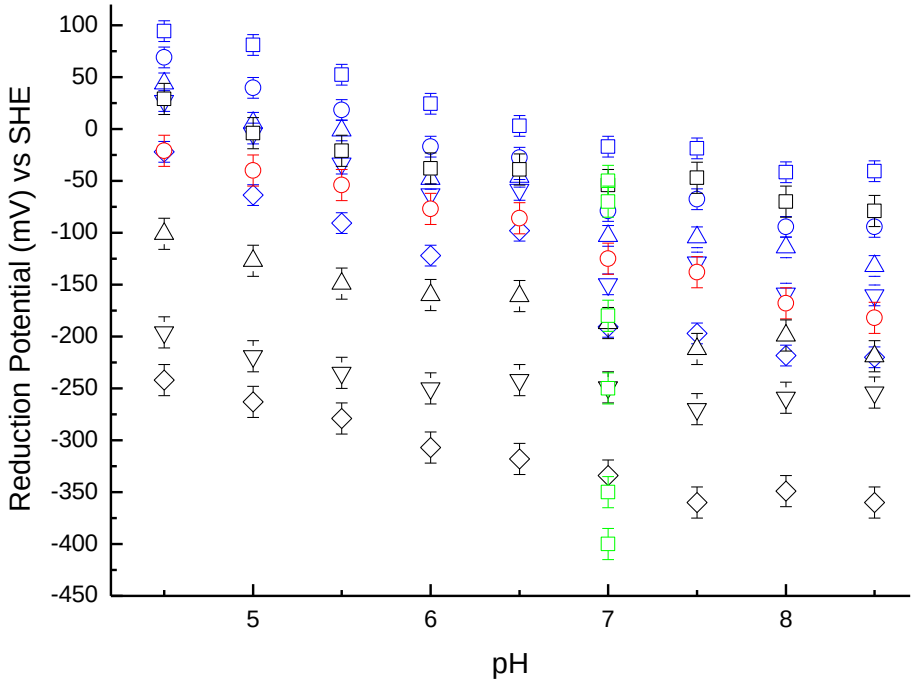

Figure 5.23 The reduction potentials of NrfA (black and red shapes), NrfB (blue shapes)and the low-spin hemes of TvNir (green) determined by spectropotentiometry (Dr. Sophie Marritt, UEA, unpublished). The reduction potentials of the NrfA active site are shown (red circles) [114].

Studies of various electron transfer complexes have led to the suggestion that some electron transfer pathways are conserved [45, 145]. The heme arrangement of TvNir is very similar to that proposed for NrfAB, with the exception that NrfAB has two additional hemes and one that has a slightly different conformation (figure 1.14) [27, 40, 50, 73]. A reduction potential has not yet been defined for the TvNir active site heme, however the reduction potentials of the low-spin hemes at pH 7 indicate that TvNir shares a similar window of redox activity to NrfA and NrfB. This supports the idea that thermodynamic properties of redox complexes are conserved, and are dictated by the heme properties such as ligation, arrangement and solvent exposure. In addition to this heme reduction potentials for other multi-heme cytochromes with bis-histidine co-ordinated hemes, such as *D. desulfuricans* tetraheme cytochrome c_3, also have very similar heme reduction potentials (between 0 and -400 mV) [146]. Many of the reduction potentials of the structurally similar *N. europaea* hydroxylamine oxidoreductase (figure 1.14) are also within a similar range, however this has a bis-

histidine co-ordinated heme with a very positive reduction potential (+288 mV) [147]. The reduction potentials for *D. desulfuricans* NrfHA have also been investigated. The crystal structure of NrfHA reveals the first five hemes of this enzyme closely overlay *E. coli* NrfA and TvNir, the remaining hemes have a different conformation (figure 1.14) [148]. The reduction potentials for NrfHA at pH 7.6 are; -80, -50, -480, -400 and + 150 mV for NrfA, 0 mV and ca. -300 mV for three hemes in NrfH [148]. This is a broader window of reduction potentials than found for either NrfA, NrfB or TvNir and there is a much greater energy gap between potentials of the high and low potential hemes. This could reflect the differences in the protein structure and the heme arrangement of NrfHA, or alternatively it could be that the reduction potentials of NrfHA are somewhat shifted by the formation of the complex. It has been noted that when hydroxylamine oxidoreductase forms a complex with its redox partner cytochrome c_{554} that the heme nearest to c_{554} become desolvated and the reduction potential increases by ca. 100 mV [147].

Experiments with 5NrfB:1NrfA coated electrodes at high scan rate showed very little to distinguish them from experiments of NrfA adsorbed separately on the electrode. A notable difference was that the catalytic current magnitude was much lower for the NrfAB coated electrode than was observed for NrfA, despite the fact that the concentration of NrfA in the solution that was adsorbed to the electrode was very similar to that used in previous catalytic experiments (0.1 μM NrfA in this experiment, 0.13 μM in the other experiments). Another difference to the electrochemistry of 5NrfB:1NrfA, to the electrochemistry of the individual proteins, is that signals arising from the oxidation and reduction of NrfB hemes were not directly detected. It would be expected that if the excess NrfB has bound predominantly to the electrode, limiting or blocking electron transfer to NrfAB, that these signals would be easily detected, particularly at high scan rates. If NrfA had bound directly to the electrode it would be expected that catalytic current magnitudes would be comparable to those obtained for NrfA alone, unless perhaps the excess NrfB acted to block substrate availability or reduced catalytic competency somehow. It is interesting to note that catalytic currents observed for nitrite reduction by TvNir were notably lower than those detected for

NrfA, however the extra hemes should not effect the turnover at -600 mV as the reduction potentials suggest that NrfAB will be 100 % reduced.

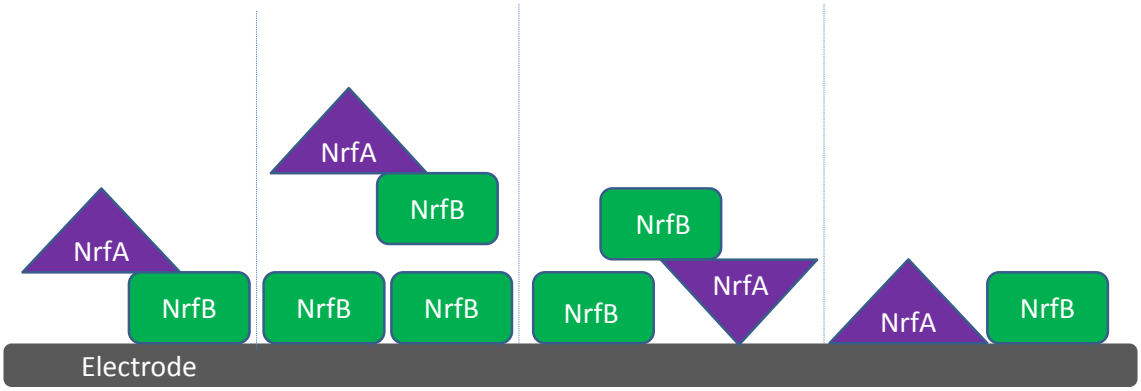

Figure 5.24 Possible ways that NrfA and NrfB could be adsorbed to the surface of the electrode in the PFV experiment described in section 5.7, figure 5.19.

PFV of NrfHA from *D. desulfuricans* was performed between 20 mV s^{-1} and 20 Vs^{-1} and at high scan rate no change was detected in the signals arising from NrfHA. At scan rates above 20 Vs^{-1} the position of the oxidative and reductive peaks seperated, indicating that interfacial electron transfer was becoming limiting, but no change was observed in the size of the redox window, indicating that electron transfer through NrfHA is rapid, as it is predicted to be via NrfAB [82]. These results indicate that if electron transfer is very quick via NrfAB then it will be unlikely that a difference would be detected when comparing results to the PFV of NrfA or NrfB individually.

Chapter 6

Summary and Future Perspectives

Chapter 6. Summary and Future Perspectives

The research in this thesis has found that there are distinct differences between catalysis of nitrite reduction by TvNir and the structurally homologous cytochrome *c* nitrite reductase, NrfA (*E. coli*) [1, 104, 115]. Cyclic PFV rapidly provides a map of activity vs. potential and in this thesis has been used at various nitrite concentrations and pH. For TvNir at 0.1 M NaCl, the dependence of the catalytic current on potential and nitrite concentration was very similar to NrfA (figure 3.20). It was noted that both enzymes were attenuated at ca. -300 mV. Given that the active sites and the constellation of hemes are very similar for both TvNir and NrfA it is likely that the similarities in the potential dependence of activity for these enzymes arise from mechanistic similarities. Recently the origins of the potential dependence for nitrite reduction in NrfA were reviewed [67]. The attenuation feature for NrfA at low nitrite concentration correlates to the reduction of low potential hemes that are distant to the active site, this is also true for TvNir. It was proposed that the attenuation might reflect the formation of alternate products for nitrite reduction i.e. hydroxylamine or nitric oxide, instead of ammonia, but this possibility was excluded as $1NO_2^-$ was converted to $1NH_4^+$ (quantified as six electrons for each NO_2^-) at various potentials across the catalytic wave [67]. The attenuated rate is therefore likely to reflect a change in the rate determining step as the low potential hemes within NrfA are reduced and this is proposed to be the case for TvNir too.

The number of redox centres in NrfA and TvNir together with the six electrons and eight protons involved in the reduction of nitrite to ammonia introduce so many parameters into the catalytic cycle that computer simulation of the possible pathways to explain the voltammetry is not sensible at the present time. Experiments that could help to refine the description of the enzymes to minimise unknowns include ^{1}H NMR monitored potentiometric titration and site directed mutagenesis as have been used to assign reduction potentials to hemes of cytochrome c_3 and to determine which residues are involved in protonation and reflect the pK_a values determined in this thesis [138, 146, 149].

In the absence of these details some inferences can still be made about the catalysis of nitrite reduction by both NrfA and TvNir. For both enzymes catalysis occurs at potentials more negative than, the NO_2^-/NH_4^+, the NO_2^-/NO or the NO/NH_2OH redox couples [115]. This is in contrast to results for the copper nitrite reductase where the onset of catalysis reflects the reduction of the NO_2^-/NO redox couple, this is also likely to be the case for cytochrome cd_1 nitrite reductase, where the active site reduction potential is +175 mV [110, 112]. Thus the reduction of nitrite to nitric oxide is distinct from the reduction of nitrite to ammonia by the ability of the enzyme to operate at potentials well below that of the lowest potential intermediate (the NO/NH_2OH redox couple E_m = -70 mV). The onset of catalysis of nitrite ammonification for NrfA reflects the reduction of the active site heme and given the similarities between their active site this is also likely to be the case for TvNir [54].

From these studies it is not possible to comment on the physiological role of TvNir, however the K_M reported here for nitrite reduction is more in line with those reported for NrfA which makes sense with the sequence and structural homology of these enzymes. More generally NrfA and TvNir are simply two multiheme cytochromes with related structures. HAO (figure 1.14) is an oxidase and this is thought to be due to the low reduction potential of the P_{460} active site heme of -260 mV and a distant heme with a very positive potential enabling electrons to be drawn away from the active site [147]. However HAO has also been shown to reduce nitrite to ammonia under sufficiently reducing conditions [84]. Multiheme cytochromes have been identified in denitrifiers, aerobic ammonium oxidising bacteria and also in anammox bacteria [45]. Other multiheme cytochromes such as OTR also share the ability to reduce nitrite to ammonium, but this is not thought to be their physiological role. It is clear that further biochemical studies are required to elucidate the physiological role of each of these enzymes and the precise structural features that are employed to facilitate this [64, 79, 80]. The studies in this thesis have also explored the impact of the ionic strength, pH and salt concentration of the experimental buffer solution on the rate of catalysis of nitrite reduction by TvNir and highlighted the importance of assaying enzymes under their likely physiological conditions, particularly periplasmic enzymes such as TvNir.

The cys-tyr bond in the active site of TvNir is a potentially important structural difference between TvNir and NrfA that could not be predicted by sequence alignment [73]. To investigate the contribution of the cys-tyr bond to the K_M pH dependence, substrate inhibition and reductive activation processes unique to TvNir, site directed mutagenesis of the genetically tractable *E. coli* nrfA was performed in collaboration with Prof. Jeff Cole and Claire Vine (University of Birmingham). Phenylalanine (F218) in the sequence of NrfA, corresponds to the cysteine that forms that cys-tyr bond in the sequence of TvNir and was mutated to a cysteine in nrfA (figure 6.1). The amino acid mutation was confirmed by purification and sequencing of the plasmid. F218C nrfA expression was confirmed and PFV studies are now underway to determine the role of the effect of the cys-tyr bond on nitrite reduction by NrfA.

```
Thioalkalivibrio    NPVCLNCKTQDHILDWAYMG-DEHEAAKWSRTSEVVEFARDLNHPLNCFMCHDPHSAGPR 239
Escherichia         PMACWSCKSPDVARLIQKDGEDGYFHGKWARG------GPEIVNNLGCADCHN--TASPE 170
                      .* .**: *        * * :  .**:*       . :: : *.*  **:  :*.*.

Thioalkalivibrio    VVRDGLINAVVDRGLGTYPHDPVKSEQQGMTKVTFQRGREDFRAIGLLDTADSNVMCAQC 299
Escherichia         FAKG----------------KPELTLSRPYAARAMEAIGKPFEKAGRFD--QQSMVCGQC 212
                    ..:.                .*  : .:  :  :::   : *.  * :*  :..::*.**

Thioalkalivibrio    HVEYNCNPGYQLSDGSRVGMDDRRANHFFWANVFDYKEAAQEIDFFDFRHATTGAALPKL 359
Escherichia         HVEYYFDG---KNKAVKFPWDDG-------MKVENMEQYYDKIAFSDWTNSLSKTPMLKA 262
                    ****  :     ... :.  **         :* : ::  ::* * *: :: : :.: *

Thioalkalivibrio    QHPEAETFWGSVHERNGVACADCHMPKVQLENGKVYTSHSQRTPRDMMGQACLNCHAEWT 419
Escherichia         QHPEYETWTAGIHGKNNVTCIDCHMPKVQNAEGKLYTDHKIGNPFDNFAQTCANCHTQDK 322
                    **** **: ..:* :*.*:* ********  :**:**.*.  .* * :.*:* ***:: .

Thioalkalivibrio    EDQALYAIDYIKNYTHGKIVKSEYWLAKMIDLFPVAKRAGVSEDVLNQARELHYDAHLYW 479
Escherichia         AALQKVVAERKQSINDLKIKVEDQLVHAHFEAK-AALDAGATEAEMKPIQDDIRHAQWRW 381
                          . :  :. .. **  .:  :   ::   .*  **.:*  ::  ::   .*:  *
```

Figure 6.1 The sequence alignment of TvNir and E. coli NrfA. The alignment was performed using Clustal W. F218 (NrfA) and C305 (TvNir) are highlighted in blue.

Experiments to assess how NrfAB differed from NrfA were inconclusive. Given that NrfA: NrfB K_d is 50 nm and that they form a very tight 1:1 complex the challenge is to orientate the complex on the electrode so that electrons must flow through NrfB into NrfA to catalyse nitrite reduction [27]. One way to achieve this would be to introduce a cysteine onto the NrfB surface in proximity to heme 1 (figure 5.21) that is proposed to be remote to the NrfA binding site, the cysteine would allow NrfB to be specifically attached to a gold surface/electrode and the orientation could then be confirmed using AFM [50]. Success here would be useful in assessing the electron

transfer complexes of other multiheme cytochromes such as those involved in iron reduction in *S. oneidensis*. *S. oneidensis* MtrA has ten hemes and is predicted to have the arrangement of two NrfBs [150]. MtrA is thought to play a key role in electron transfer from the periplasm to the outer membrane, allowing *S. oneidensis* to reduce mineral iron outside of the bacterial cell in its respiration.

In conclusion the work in this thesis has elaborated on understanding of nitrite reduction by different multiheme cytochrome *c* nitrite reductases and provides further insight into and appreciation of this increasingly important family of multiheme cytochromes. PFV has proved to be a powerful and versatile tool in studying both the activity and thermodynamics of nitrite reduction and allowing detection of reductive activation that with the use of alternative techniques might have remained un-noticed.

Reference

1. Angove, H.C., J.A. Cole, D.J. Richardson, and J.N. Butt, *Protein film voltammetry reveals distinctive fingerprints of nitrite and hydroxylamine reduction by a cytochrome c nitrite reductase.* Journal of Biological Chemistry, 2002. **277**(26): p. 23374-23381.
2. Clarke, T.A., A.M. Hemmings, B. Burlat, J.N. Butt, J.A. Cole, and D.J. Richardson, *Comparison of the structural and kinetic properties of the cytochrome c nitrite reductases from Escherichia coli, Wolinella succinogenes, Sulfurospirillum deleyianum and Desulfolvibrio desulfuricans.* Biochemical Society Transactions, 2006. **34**: p. 143-145.
3. Kemp, G.L., T.A. Clarke, S.J. Marritt, C. Lockwood, S.R. Poock, A.M. Hemmings, D.J. Richardson, M.R. Cheesman, and J.N. Butt, *Kinetic and thermodynamic resolution of the interactions between sulfite and the pentahaem cytochrome NrfA from Escherichia coil.* Biochemical Journal, 2010. **431**: p. 73-80.
4. Lukat, P., M. Rudolf, P. Stach, A. Messerschmidt, P.M.H. Kroneck, J. Simon, and O. Einsle, *Binding and reduction of sulfite by cytochrome c nitrite reductase.* Biochemistry, 2008. **47**(7): p. 2080-2086.
5. van Wonderen, J.H., B. Burlat, D.J. Richardson, M.R. Cheesman, and J.N. Butt, *The nitric oxide reductase activity of cytochrome c nitrite reductase from Escherichia coli.* Journal of Biological Chemistry, 2008. **283**(15): p. 9587-9594.
6. Canfield, D.E., A.N. Glazer, and P.G. Falkowski, *The Evolution and Future of Earth's Nitrogen Cycle.* Science, 2010. **330**(6001): p. 192-196.
7. Butler, C.S. and D.J. Richardson, *The emerging molecular structure of the nitrogen cycle: an introduction to the proceedings of the 10th annual N-cycle meeting.* Biochemical Society Transactions, 2005. **33**: p. 113-118.
8. Ferguson, S.J., *Nitrogen cycle enzymology.* Current Opinion in Chemical Biology, 1998. **2**(2): p. 182-193.
9. Martinez-Espinosa, R.M., J.A. Cole, D.J. Richardson, and N.J. Watmough, *Enzymology and ecology of the nitrogen cycle.* Biochemical Society Transactions, 2011. **39**: p. 175-178.

10. Rudolf, M. and P.M.H. Kroneck, *The nitrogen cycle: Its biology*, in *Biogeochemical Cycles of Elements*. 2005. p. 75-103.
11. Zumft, W.G., *Cell biology and molecular basis of denitrification.* Microbiology Molecular Biology Reviews, 1997. **61**(4): p. 533-616.
12. Einsle, O. and P.M.H. Kroneck, *Structural basis of denitrification.* Biological Chemistry, 2004. **385**(10): p. 875-883.
13. Jafferji, A., J. Allen, S. Ferguson, and V. Fülöp, *X-ray Crystallographic Study of Cyanide Binding Provides Insights into the Structure-Function Relationship for Cytochrome cd1 Nitrite Reductase from Paracoccus pantotrophus.* The Journal of Biological Chemistry, 2000. **275**(33): p. 25089-25094.
14. Hino, T., Y. Matsumoto, S. Nagano, H. Sugimoto, Y. Fukumori, T. Murata, S. Iwata, and Y. Shiro, *Structural Basis of Biological N2O Generation by Bacterial Nitric Oxide Reductase.* Science, 2010. **330**(6011): p. 1666-1670.
15. Richardson, D., H. Felgate, N. Watmough, A. Thomson, and E. Baggs, *Mitigating release of the potent greenhouse gas N2O from the nitrogen cycle - could enzymic regulation hold the key?* Trends in Biotechnology, 2009. **27**(7): p. 388-397.
16. Dell'Acqua, S., S.R. Pauleta, I. Moura, and J.J.G. Moura, *The tetranuclear copper active site of nitrous oxide reductase: the CuZ center.* Journal of Biological Inorganic Chemistry, 2011. **16**(2): p. 183-194.
17. Gates, A.J., V.M. Luque-Almagro, A.D. Goddard, S.J. Ferguson, M.D. Roldan, and D.J. Richardson, *A composite biochemical system for bacterial nitrate and nitrite assimilation as exemplified by Paracoccus denitrificans.* Biochemical Journal, 2011. **435**: p. 743-753.
18. Berks, B.C., S.J. Ferguson, J.W.B. Moir, and D.J. Richardson, *Enzymes and associated electron transport systems that catalyse the respiratory reduction of nitrogen oxides and oxyanions.* Biochimica Et Biophysica Acta-Bioenergetics, 1995. **1232**(3): p. 97-173.
19. Philippot, L., J. Andert, C.M. Jones, D. Bru, and S. Hallin, *Importance of denitrifiers lacking the genes encoding the nitrous oxide reductase for N2O emissions from soil.* Global Change Biology, 2011. **17**(3): p. 1497-1504.

20. Klotz, M.G. and L.Y. Stein, *Nitrifier genomics and evolution of the nitrogen cycle.* Fems Microbiology Letters, 2008. **278**(2): p. 146-156.

21. Mohan, S.B., M. Schmid, M. Jetten, and J. Cole, *Detection and widespread distribution of the nrfA gene encoding nitrite reduction to ammonia, a short circuit in the biological nitrogen cycle that competes with denitrification.* Fems Microbiology Ecology, 2004. **49**(3): p. 433-443.

22. Simon, J., *Enzymology and bioenergetics of respiratory nitrite ammonification.* Fems Microbiology Reviews, 2002. **26**(3): p. 285-309.

23. Swamy, U., M.T. Wang, J.N. Tripathy, S.K. Kim, M. Hirasawa, D.B. Knaff, and J.P. Allen, *Structure of spinach nitrite reductase: Implications for multi-electron reactions by the iron-sulfur : siroheme cofactor.* Biochemistry, 2005. **44**(49): p. 16054-16063.

24. Wang, H.N. and R.P. Gunsalus, *The nrfA and nirB nitrite reductase operons in Escherichia coli are expressed differently in response to nitrate than to nitrite.* Journal of Bacteriology, 2000. **182**(20): p. 5813-5822.

25. Darwin, A., P. Tormay, L. Page, L. Griffiths, and J. Cole, *Identification of The Formate Dehydrogenases and Genetic Determinants of Formate Dependent Nitrite Reduction by Escherichia coli K12.* Journal of General Microbiology, 1993. **139**: p. 1829-1840.

26. Hussain, H., J. Grove, L. Griffiths, S. Busby, and J. Cole, *A Seven Gene Operon Essential For Formate Dependent Nitrite Reduction To Ammonia by Enteric Bacteria.* Molecular Microbiology, 1994. **12**(1): p. 153-163.

27. Lockwood, C., J.N. Butt, T.A. Clarke, and D.J. Richardson, *Molecular interactions between multihaem cytochromes: probing the protein-protein interactions between pentahaem cytochromes of a nitrite reductase complex.* Biochemical Society Transactions, 2011. **39**: p. 263-268.

28. Simon, J., R.J.M. van Spanning, and D.J. Richardson, *The organisation of proton motive and non-proton motive redox loops in prokaryotic respiratory systems.* Biochimica Et Biophysica Acta-Bioenergetics, 2008. **1777**(12): p. 1480-1490.

29. Crack, J.C., A.J. Jervis, A.A. Gaskell, G.F. White, J. Green, A.J. Thomson, and N.E. Le Brun, *Signal perception by FNR: the role of the iron-sulfur cluster.* Biochemical Society Transactions, 2008. **36**: p. 1144-1148.

30. Bothe, H., S.J. Ferguson, and W.E. Newton, *Biology of The Nitrogen Cycle*. 2007: Elsevier.

31. Browning, D.F., D.J. Lee, A.J. Wolfe, J.A. Cole, and S.J.W. Busby, *The Escherichia coli K-12 NarL and NarP proteins insulate the nrf promoter from the effects of integration host factor.* Journal of Bacteriology, 2006. **188**(21): p. 7449-7456.

32. Kemp, G.L., T.A. Clarke, S.J. Marritt, C. Lockwood, S.R. Poock, A.M. Hemmings, D.J. Richardson, M.R. Cheesman, and J.N. Butt, *Kinetic and thermodynamic resolution of the interactions between sulfite and the pentahaem cytochrome NrfA from Escherichia coil.* Biochemical Journal. **431**: p. 73-80.

33. Browning, D.F., D.J. Lee, S. Spiro, and S.J.W. Busby, *Down-Regulation of the Escherichia coli K-12 nrf Promoter by Binding of the NsrR Nitric Oxide-Sensing Transcription Repressor to an Upstream Site.* Journal of Bacteriology, 2010. **192**(14): p. 3824-3828.

34. Tucker, N.P., N.E. Le Brun, R. Dixon, and M.I. Hutchings, *There's NO stopping NsrR, a global regulator of the bacterial NO stress response.* Trends in Microbiology, 2010. **18**(4): p. 149-156.

35. McKnight, G.M., L.M. Smith, R.S. Drummond, C.W. Duncan, M. Golden, and N. Benjamin, *Chemical synthesis of nitric oxide in the stomach from dietary nitrate in humans.* Gut, 1997. **40**(2): p. 211-214.

36. Lundberg, J.O., E. Weitzberg, J.A. Cole, and N. Benjamin, *Nitrate, bacteria and human health (vol 2, pg 593, 2004).* Nature Reviews Microbiology, 2004. **2**(8): p. 681-681.

37. Gomes, C.M., A. Giuffre, E. Forte, J.B. Vicente, L.M. Saraiva, M. Brunori, and M. Teixeira, *A novel type of nitric-oxide reductase - Escherichia coli flavorubredoxin.* Journal of Biological Chemistry, 2002. **277**(28): p. 25273-25276.

38. Mills, P.C., G. Rowley, S. Spiro, J.C.D. Hinton, and D.J. Richardson, *A combination of cytochrome c nitrite reductase (NrfA) and flavorubredoxin (NorV) protects Salmonella enterica serovar Typhimurium against killing by NO in anoxic environments.* Microbiology-Sgm, 2008. **154**: p. 1218-1228.

39. Pittman, M.S., K.T. Elvers, L. Lee, M.A. Jones, R.K. Poole, S.F. Park, and D.J. Kelly, *Growth of Campylobacter jejuni on nitrate and nitrite: electron transport to*

NapA and NrfA via NrfH and distinct roles for NrfA and the globin Cgb in protection against nitrosative stress. Molecular Microbiology, 2007. **63**(2): p. 575-590.

40. Bamford, V.A., H.C. Angove, H.E. Seward, A.J. Thomson, J.A. Cole, J.N. Butt, A.M. Hemmings, and D.J. Richardson, *Structure and spectroscopy of the periplasmic cytochrome c nitrite reductase from Escherichia coli.* Biochemistry, 2002. **41**(9): p. 2921-2931.
41. Cunha, C.A., S. Macieira, J.M. Dias, G. Almeida, L.L. Goncalves, C. Costa, J. Lampreia, R. Huber, J.J.G. Moura, I. Moura, and M.J. Romao, *Cytochrome c nitrite reductase from Desulfovibrio desulfuricans ATCC 27774 - The relevance of the two calcium sites in the structure of the catalytic subunit (NrfA).* Journal of Biological Chemistry, 2003. **278**(19): p. 17455-17465.
42. Einsle, O., A. Messerschmidt, P. Stach, G.P. Bourenkov, H.D. Bartunik, R. Huber, and P.M.H. Kroneck, *Structure of cytochrome c nitrite reductase.* Nature, 1999. **400**(6743): p. 476-480.
43. Einsle, O., P. Stach, A. Messerschmidt, J. Simon, A. Kroger, R. Huber, and P.M.H. Kroneck, *Cytochrome c nitrite reductase from Wolinella succinogenes - Structure at 1.6 angstrom resolution, inhibitor binding, and heme-packing motifs.* Journal of Biological Chemistry, 2000. **275**(50): p. 39608-39616.
44. Stach, P., O. Einsle, W. Schumacher, E. Kurun, and P.M.H. Kroneck, *Bacterial cytochrome c nitrite reductase: new structural and functional aspects.* Journal of Inorganic Biochemistry, 2000. **79**(1-4): p. 381-385.
45. Klotz, M.G., M.C. Schmid, M. Strous, H. den Camp, M.S.M. Jetten, and A.B. Hooper, *Evolution of an octahaem cytochrome c protein family that is key to aerobic and anaerobic ammonia oxidation by bacteria.* Environmental Microbiology, 2008. **10**(11): p. 3150-3163.
46. Page, C.C., C.C. Moser, and P.L. Dutton, *Mechanism for electron transfer within and between proteins.* Current Opinion in Chemical Biology, 2003. **7**(5): p. 551-556.
47. Kern, M., O. Einsle, and J. Simon, *Variants of the tetrahaem cytochrome c quinol dehydrogenase NrfH characterize the menaquinol-binding site, the haem c-*

binding motifs and the transmembrane segment. Biochemical Journal, 2008. **414**: p. 73-79.

48. Bykov, D. and F. Neese, *Substrate binding and activation in the active site of cytochrome c nitrite reductase: a density functional study.* Jounal of Biological Inorganic Chemistry, 2011. **16**(3): p. 417-30.
49. Clarke, T.A., G.L. Kemp, J.H. Van Wonderen, R. Doyle, J.A. Cole, N. Tovell, M.R. Cheesman, J.N. Butt, D.J. Richardson, and A.M. Hemmings, *Role of a conserved glutamine residue in tuning the catalytic activity of Escherichia coli cytochrome c nitrite reductase.* Biochemistry, 2008. **47**(12): p. 3789-3799.
50. Clarke, T.A., J.A. Cole, D.J. Richardson, and A.M. Hemmings, *The crystal structure of the pentahaem c-type cytochrome NrfB and characterization of its solution-state interaction with the pentahaem nitrite reductase NrfA.* Biochemical Journal, 2007. **406**: p. 19-30.
51. Gao, H.C., Z.K. Yang, S. Barua, S.B. Reed, M.F. Romine, K.H. Nealson, J.K. Fredrickson, J.M. Tiedje, and J.Z. Zhou, *Reduction of nitrate in Shewanella oneidensis depends on atypical NAP and NRF systems with NapB as a preferred electron transport protein from CymA to NapA.* Isme Journal, 2009. **3**(8): p. 966-976.
52. Leslie Dutton, P., *[23] Redox potentiometry: Determination of midpoint potentials of oxidation-reduction components of biological electron-transfer systems*, in *Methods in Enzymology*, F. Sidney and P. Lester, Editors. 1978, Academic Press. p. 411-435.
53. Andersson, K.K., J.D. Lipscomb, M. Valentine, E. Munck, and A.B. Hooper, *Tetraheme Cytochrome c-554 from Nitrosomonas europaea- Heme-Heme Interactions and Ligand Binding.* Journal of Biological Chemistry, 1986. **261**(3): p. 1126-1138.
54. Marritt, S.J., G.L. Kemp, L. Xiaoe, J.R. Durrant, M.R. Cheesman, and J.N. Butt, *Spectroelectrochemical characterization of a pentaheme cytochrome in solution and as electrocatalytically active films on nanocrystalline metal-oxide electrodes.* Journal of the American Chemical Society, 2008. **130**(27): p. 8588-+.
55. Kemp, G.L., S.J. Marritt, X.E. Li, J.R. Durrant, M.R. Cheesman, and J.N. Butt, *Opportunities for mesoporous nanocrystalline SnO2 electrodes in kinetic and*

catalytic analyses of redox proteins. Biochemical Society Transactions, 2009. **37**: p. 368-372.

56. Einsle, O., A. Messerschmidt, R. Huber, P.M.H. Kroneck, and F. Neese, *Mechanism of the six-electron reduction of nitrite to ammonia by cytochrome c nitrite reductase.* Journal of the American Chemical Society, 2002. **124**(39): p. 11737-11745.
57. Bykov, D. and F. Neese, *Substrate binding and activation in the active site of cytochrome c nitrite reductase: a density functional study.* Journal of Biological Inorganic Chemistry, 2010.
58. Clarke, T.A., P.C. Mills, S.R. Poock, J.N. Butt, M.R. Cheesman, J.A. Cole, J.C.D. Hinton, A.M. Hemmings, G. Kemp, C.A.G. Soderberg, S. Spiro, J. Van Wonderen, and D.J. Richardson, *Escherichia coli cytochrome c nitrite reductase NrfA*, in *Globins and Other Nitric Oxide-Reactive Proteins, Part B*. 2008. p. 63-77.
59. Schumacher, W., U. Hole, and P.M.H. Kroneck, *Ammonia-forming cytochrome c nitrite reductase from Sulfurospirillum deleyianum is a tetraheme protein: New aspects of the molecular composition and spectroscopic properties.* Biochemical and Biophysical Research Communications, 1994. **205**(1): p. 911-916.
60. Pereira, I.A., J. LeGall, A.V. Xavier, and M. Teixeira, *Characterisation of a heme c nitrite reductase from a non-ammonifying microorganism, Desulfovibrio vulgaris Hildenborough.* Biochimica et Biophysica Acta, 2000. **1481**(1): p. 119-130.
61. Pereira, I.C., I.A. Abreu, A.V. Xavier, J. LeGall, and M. Teixeira, *Nitrite reductase from Desulfovibrio desulfuricans (ATCC 27774) - A heterooligomer heme protein with sulfite reductase activity.* Biochemical and Biophysical Research Communications, 1996. **224**(3): p. 611-618.
62. Liu, M.-C. and H.D.J. Peck, *The isolation of a hexaheme cytochrome from Desulfovirbio desulfuricans and its identification as a new type of nitrite reductase.* The Journal of Biological Chemistry, 1981. **256**(24): p. 13159-13164.
63. Tikhonova, T.V., A. Slutsky, A.N. Antipov, K.M. Boyko, K.M. Polyakov, D.Y. Sorokin, R.A. Zvyagilskaya, and V.O. Popov, *Molecular and catalytic properties of a novel cytochrome c nitrite reductase from nitrate-reducing haloalkaliphilic*

sulfur-oxidizing bacterium Thioalkalivibrio nitratireducens. Biochimica Et Biophysica Acta-Proteins and Proteomics, 2006. **1764**(4): p. 715-723.

64. Atkinson, S.J., C.G. Mowat, G.A. Reid, and S.K. Chapman, *An octaheme c-type cytochrome from Shewanella oneidensis can reduce nitrite and hydroxylamine.* Febs Letters, 2007. **581**(20): p. 3805-3808.

65. Gwyer, J.D., H.C. Angove, D.J. Richardson, and J.N. Butt, *Redox-triggered events in cytochrome c nitrite reductase.* Bioelectrochemistry, 2004. **63**(1-2): p. 43-47.

66. Armstrong, F.A., *Recent developments in dynamic electrochemical studies of adsorbed enzymes and their active sites.* Current Opinion in Chemical Biology, 2005. **9**(2): p. 110-117.

67. Gates, A.J., G.L. Kemp, C.Y. To, J. Mann, S.J. Marritt, A.G. Mayes, D.J. Richardson, and J.N. Butt, *The relationship between redox enzyme activity and electrochemical potential-cellular and mechanistic implications from protein film electrochemistry.* Physical Chemistry Chemical Physics, 2011. **13**(17): p. 7720-7731.

68. Sorokin, D.Y., T.P. Tourova, K.A. Sjollema, and J.G. Kuenen, *Thialkalivibrio nitratireducens sp nov., a nitrate-reducing member of an autotrophic denitrifying consortium from a soda lake.* International Journal of Systematic and Evolutionary Microbiology, 2003. **53**: p. 1779-1783.

69. Taher, A.G., *Inland Saline Lakes of Wadi El Natrun Depression, Egypt.* International Journal of Salt Lake Research, 1999. **8**: p. 149-169.

70. Hicks, D.B., J. Liu, M. Fujisawa, and T.A. Krulwich, *F1F0-ATP synthases of alkaliphilic bacteria: Lessons from their adaptations.* Biochimica Et Biophysica Acta-Bioenergetics, 2010. **1797**(8): p. 1362-1377.

71. Filimonenkov, A.A., R.A. Zvyagilskaya, T.V. Tikhonova, and V.O. Popov, *Isolation and characterization of nitrate reductase from the halophilic sulfur-oxidizing bacterium Thioalkalivibrio nitratireducens.* Biochemistry-Moscow. **75**(6): p. 744-751.

72. Constantinidou, C., J.L. Hobman, L. Griffiths, M.D. Patel, C.W. Penn, J.A. Cole, and T.W. Overton, *A reassessment of the FNR regulon and transcriptomic analysis of the effects of nitrate, nitrite, NarXL, and NarQP as Escherichia coli*

K12 adapts from aerobic to anaerobic growth. Journal of Biological Chemistry, 2006. **281**(8): p. 4802-4815.

73. Polyakov, K.M., K.M. Boyko, T.V. Tikhonova, A. Slutsky, A.N. Antipov, R.A. Zvyagilskaya, A.N. Popov, G.P. Bourenkov, V.S. Lamzin, and V.O. Popov, *High-Resolution Structural Analysis of a Novel Octaheme Cytochrome c Nitrite Reductase from the Haloalkaliphilic Bacterium Thioalkalivibrio nitratireducens.* Journal of Molecular Biology, 2009. **389**(5): p. 846-862.
74. Schnell, R., T. Sandalova, U. Hellman, Y. Lindqvist, and G. Schneider, *Siroheme- and Fe-4-S-4 -dependent NirA from Mycobacterium tuberculosis is a sulfite reductase with a covalent Cys-Tyr bond in the active site.* Journal of Biological Chemistry, 2005. **280**(29): p. 27319-27328.
75. Ito, N., S.E.V. Phillips, C. Stevens, Z.B. Ogel, M.J. McPherson, J.N. Keen, K.D.S. Yadav, and P.F. Knowles, *Novel Thioether Bond Revealed By A 1.7-A Crystal Structure of Galactose Oxidase.* Nature, 1991. **350**(6313): p. 87-90.
76. Dominy, J.E., J. Hwang, S. Guo, L.L. Hirschberger, S. Zhang, and M.H. Stipanuk, *Synthesis of amino acid cofactor in cysteine dioxygenase is regulated by substrate and represents a novel post-translational regulation of activity.* Journal of Biological Chemistry, 2008. **283**(18): p. 12188-12201.
77. Steuber, J., A.F. Arendsen, W.R. Hagen, and P.M.H. Kroneck, *Molecular Properties of The Dissimilatory Sulphite Reductase From Desulfovibrio desulfuricans (Essex) and Comparison with The Enzyme From Desulfovibrio vulgaris (Hildenborough).* European Journal of Biochemistry, 1995. **233**(3): p. 873-879.
78. Trofimov, A.A., K. Polyakov, K. Boyko, T. Tikhonova, A.N. Popov, and V.O. Popov, *Structures of Complexes of Octaheme Cytochrome c Nitrite Reductase from Thioalkalivibrio nitratireducens with Sulfite and Cyanide.* Acta Crystallographica Section D: Biological Crystallography, 2010. **D66**: p. 1043-1047.
79. Sharma, S., G. Cavallaro, and A. Rosato, *A systematic investigation of multiheme c-type cytochromes in prokaryotes.* Journal of Biological Inorganic Chemistry. **15**(4): p. 559-571.

80. Mowat, C.G. and S.K. Chapman, *Multi-heme cytochromes - new structures, new chemistry.* Dalton Transactions, 2005(21): p. 3381-3389.

81. Mowat, C.G., E. Rothery, C.S. Miles, L. McIver, M.K. Doherty, K. Drewette, P. Taylor, M.D. Walkinshaw, S.K. Chapman, and G.A. Reid, *Octaheme tetrathionate reductase is a respiratory enzyme with novel heme ligation.* Nature Structural & Molecular Biology, 2004. **11**(10): p. 1023-1024.

82. Almeida, M.G., C.M. Silveira, B. Guigliarelli, P. Bertrand, J.J.G. Moura, I. Moura, and C. Leger, *A needle in a haystack: The active site of the membrane-bound complex cytochrome c nitrite reductase.* Febs Letters, 2007. **581**(2): p. 284-288.

83. Schumacher, W., U. Hole, and M.H. Kroneck, *Ammonia Forming Cytochrome c Nitrite Reductase From Sulfurospirillum deleyianum Is a Tetraheme Protein-New Aspects of The Molecular Composition and Spectroscopic Properties.* Biochemical and Biophysical Research Communications, 1994. **205**(1): p. 911-916.

84. Kostera, J., J. McGarry, and A.A. Pacheco, *Enzymatic Interconversion of Ammonia and Nitrite: The Right Tool for the Job.* Biochemistry, 2010. **49**(39): p. 8546-8553.

85. Pearson, A.R., B.O. Elmore, C. Yang, J.D. Ferrara, A.B. Hooper, and C.M. Wilmot, *The crystal structure of cytochrome P460 of Nitrosomonas europaea reveals a novel cytochrome fold and heme-protein cross-link.* Biochemistry, 2007. **46**(28): p. 8340-8349.

86. Cedervall, P.E., A.B. Hooper, and C.M. Wilmot, *Crystallization and preliminary X-ray crystallographic analysis of a new crystal form of hydroxylamine oxidoreductase from Nitrosomonas europaea.* Acta Crystallographica Section F-Structural Biology and Crystallization Communications, 2009. **65**: p. 1296-1298.

87. Cua, L.S. and L.Y. Stein, *Effects of nitrite on ammonia-oxidizing activity and gene regulation in three ammonia-oxidizing bacteria.* Fems Microbiology Letters, 2011. **319**(2): p. 169-175.

88. Zahn, J.A., C. Duncan, and A.A. Dispirito, *Oxidation of Hydroxylamine By Cytochrome P-460 of The Obligate Methylotroph Methylococcus capsulatus bath.* Journal of Bacteriology, 1994. **176**(19): p. 5879-5887.

89. Laemmli, U.K., *Cleavage of structural proteins during the assembly of the head of bacterophage T4.* Nature, 1970. **227**: p. 680-685.

90. Berry, E. and B. Trumpower, *Simultaneous determination of hemes a, b, and c from pyridine hemochrome spectra.* Analytical Biochemistry, 1987. **161**: p. 1-15.

91. Margoliash, E. and N. Frohwirt, *Spectrum of Horse Heart Cytochrome c.* Biochemical Journal, 1959. **71**: p. 570-578.

92. Michaelis, L. and E. Hill, *The Viologen Indicators.* The Journal of General Physiology, 1933: p. 859-873.

93. Clarke, T.A., V. Dennison, H.E. Seward, B. Burlat, J.A. Cole, A.M. Hemmings, and D.J. Richardson, *Purification and spectropotentiometric characterization of Escherichia coli NrfB, a decaheme homodimer that transfers electrons to the decaheme periplasmic nitrite reductase complex.* Journal of Biological Chemistry, 2004. **279**(40): p. 41333-41339.

94. Bard, A.J. and L.R. Faulkner, *Electrochemical methods: fundamentals and applications*. 2001: Wiley.

95. Armstrong, F.A., *Protein film voltammetry: Revealing the mechanisms of biological oxidation and reduction.* Russian Journal of Electrochemistry, 2002. **38**(1): p. 49-62.

96. Leger, C. and P. Bertrand, *Direct electrochemistry of redox enzymes as a tool for mechanistic studies.* Chemical Reviews, 2008. **108**(7): p. 2379-2438.

97. Andolfi, L., P. Caroppi, A.R. Bizzarri, M.C. Piro, F. Sinibaldi, T. Ferri, F. Polticelli, S. Cannistraro, and R. Santucci, *Nanoscopic and redox characterization of engineered horse cytochrome c chemisorbed on a bare gold electrode.* Protein Journal, 2007. **26**(4): p. 271-279.

98. Heering, H.A., F.G.M. Wiertz, C. Dekker, and S. de Vries, *Direct immobilization of native yeast Iso-1 cytochrome c on bare gold: Fast electron relay to redox enzymes and zeptomole protein-film voltammetry.* Journal of the American Chemical Society, 2004. **126**(35): p. 11103-11112.

99. Ran, Q., R. Peng, C. Liang, S.Q. Ye, Y.Z. Xian, W.J. Zhang, and L.T. Jin, *Covalent immobilization of horseradish peroxidase via click chemistry and its direct electrochemistry.* Talanta, 2011. **83**(5): p. 1381-1385.

100. Zhao, J., W. Zhu, T. Liu, J.H. Yang, and G.X. Li, *Electrochemical probing into cytochrome c modification with homocysteine-thiolactone.* Analytical and Bioanalytical Chemistry, 2010. **397**(2): p. 695-701.

101. Blanford, C.F. and F.A. Armstrong, *The pyrolytic graphite surface as an enzyme substrate: microscopic and spectroscopic studies.* Journal of Solid State Electrochemistry, 2006. **10**(10): p. 826-832.

102. Hirst, J. and F.A. Armstrong, *Fast-scan cyclic voltammetry of protein films on pyrolytic graphite edge electrodes: Characteristics of electron exchange.* Analytical Chemistry, 1998. **70**(23): p. 5062-5071.

103. Heering, H.A., J. Hirst, and F.A. Armstrong, *Interpreting the catalytic voltammetry of electroactive enzymes adsorbed on electrodes.* Journal of Physical Chemistry B, 1998. **102**(35): p. 6889-6902.

104. Gwyer, J.D., D.J. Richardson, and J.N. Butt, *Diode or tunnel-diode characteristics? Resolving the catalytic consequences of proton coupled electron transfer in a multi-centered oxidoreductase.* Journal of the American Chemical Society, 2005. **127**(43): p. 14964-14965.

105. Gwyer, J.G., D.J. Richardson, and J.N. Butt, *Resolving Complexity in the Interactions of Redox Enzymes and Their Inhibitors: Contrasting Mechanisms for the Inhibition of a Cytochrome c Nitrite Reductase Revealed by Protein Film Voltammetry.* Biochemistry, 2004. **43**: p. 15086-15094.

106. Sucheta, A., R. Cammack, J. Weiner, and F.A. Armstrong, *Reversible Electrochemistry of Fumarate Reductase Immobilised on An Electrode Surface-Direct Voltammetric Observations of Redox Centres and Their Participation in Rapid Catalytic Electron Transport.* Biochemistry, 1993. **32**(20): p. 5455-5465.

107. Lehninger, A.L., D.L. Nelson, and M.M. Cox, *Lehninger principles of biochemistry*. 2005: W.H. Freeman.

108. Michaelis, L. and M.L. Menten, *Die Kinetik der Invertinwirkung.* Biochemische Zeirschrift, 1913. **49**: p. 333-369.

109. Siegel, L.M., D.C. Rueger, M.J. Barber, and R.J. Kruger, *Escherichia coli Sulfite Reductase Hemoprotein Subunit. Prosthetic Groups, Catalytic Parameters, and Ligand Complexes.* Journal of Biological Chemistry, 1982. **257**(11): p. 6343-6350.

110. Wijma, H.J., L.J.C. Jeuken, M.P. Verbeet, F.A. Armstrong, and G.W. Canters, *Protein film voltammetry of copper-containing nitrite reductase reveals reversible inactivation.* Journal of the American Chemical Society, 2007. **129**(27): p. 8557-8565.

111. Olesen, K., A. Veselov, Y.W. Zhao, Y.S. Wang, B. Danner, C.P. Scholes, and J.P. Shapleigh, *Spectroscopic, kinetic, and electrochemical characterization of heterologously expressed wild-type and mutant forms of copper-containing nitrite reductase from Rhodobacter sphaeroides 2.4.3.* Biochemistry, 1998. **37**(17): p. 6086-6094.

112. Zajicek, R.S., M.L. Cartron, and S.J. Ferguson, *Probing the unusual oxidation/reduction behavior of Paracoccus pantotrophus cytochrome cd(1) nitrite reductase by replacing a switchable methionine heme iron ligand with histidine.* Biochemistry, 2006. **45**(37): p. 11208-11216.

113. Léger, C., A.K. Jones, S.P.J. Albracht, and F.A. Armstrong, *Effect of a Dispersion of Interfacial Electron Transfer Rates on Steady State Catalytic Electron Transport in [NiFe]-hydrogenase and Other Enzymes.* The Journal of Physical Chemistry B, 2002. **106**(50): p. 13058-13063.

114. Kemp, G.L., *Investigating Mechanistic Aspects of Cytochrome c Nitrite Reductase: Combining Electrochemical and Spectroscopic Techniques*, in *School of Chemical Sciences*. 2009, University of East Anglia: Norwich. p. 177.

115. Gwyer, J.G., *Redox Triggered Events in Cytochrome c Nitrite Reductase: A Voltammetric Study*, in *School of Chemical Sciences and Pharmacy*. 2005, University of East Anglia: Norwich. p. 225.

116. Wijma, H.J., L.J.C. Jeuken, M.P. Verbeet, F.A. Armstrong, and G.W. Canters, *A random-sequential mechanism for nitrite binding and active site reduction in copper-containing nitrite reductase.* Journal of Biological Chemistry, 2006. **281**(24): p. 16340-16346.

117. Bowers, E.M., L.O. Ragland, and L.D. Byers, *Salt effects on β-glucosidase: pH-profile narrowing.* Biochimica et Biophysica Acta - Proteins and Proteomics, 2007. **1774**(12): p. 1500-1507.

118. D'Amico, S., C. Gerday, and G. Feller, *Structural similarities and evolutionary relationships in chloride-dependent α-amylases.* Gene, 2000. **253**(1): p. 95-105.

119. Yang, Z., *Hofmeister effects: an explanation for the impact of ionic liquids on biocatalysis.* Journal of Biotechnology, 2009. **144**(1): p. 12-22.

120. Zhou, P., F. Tian, J. Zou, Y. Ren, X. Liu, and Z. Shang, *Do halide motifs stabilize protein architecture?* Journal of Physical Chemistry B, 2010. **114**(47): p. 15673-15686.

121. Field, S.J., N.P. Thornton, L.J. Anderson, A.J. Gates, A. Reilly, B.J.N. Jepson, D.J. Richardson, S.J. George, M.R. Cheesman, and J.N. Butt, *Reductive activation of nitrate reductases.* Dalton Transactions, 2005(21): p. 3580-3586.

122. Fourmond, V., B. Burlat, S. Dementin, P. Arnoux, M. Sabaty, S. Boiry, B. Guigliarelli, P. Bertrand, D. Pignol, and C. Leger, *Major Mo(V) EPR Signature of Rhodobacter sphaeroides Periplasmic Nitrate Reductase Arising from a Dead-End Species That Activates upon Reduction. Relation to Other Molybdoenzymes from the DMSO Reductase Family.* Journal of Physical Chemistry B, 2008. **112**(48): p. 15478-15486.

123. Heering, H.A., J.H. Weiner, and F.A. Armstrong, *Direct detection and measurement of electron relays in a multicentered enzyme: Voltammetry of electrode-surface films of E-coli fumarate reductase, an iron-sulfur flavoprotein.* Journal of the American Chemical Society, 1997. **119**(48): p. 11628-11638.

124. Whittaker, M.M. and J.W. Whittaker, *Construction and characterization of Pichia pastoris strains for labeling aromatic amino acids in recombinant proteins.* Protein Expression and Purification, 2005. **41**(2): p. 266-274.

125. Rogers, M.S., R. Hurtado-Guerrero, S.J. Firbank, M.A. Halcrow, D.M. Dooley, S.E.V. Phillips, P.F. Knowles, and M.J. McPherson, *Cross-link formation of the cysteine 228-tyrosine 272 catalytic cofactor of galactose oxidase does not require dioxygen.* Biochemistry, 2008. **47**(39): p. 10428-10439.

126. Davidson, V.L., *Protein-derived cofactors. Expanding the scope of post-translational modifications.* Biochemistry, 2007. **46**(18): p. 5283-5292.

127. Davidson, V.L., *Generation of protein-derived redox cofactors by posttranslational modification.* Molecular Biosystems, 2011. **7**(1): p. 29-37.

128. Igarashi, N., T. Fujiwara, and Y. Fukumori, *Structure and function of hydroxylamine oxidoreductase.* Seikagaku, 1998. **70**(6): p. 441-446.

129. Clarke, T.A., T. Holley, R.S. Hartshorne, J.K. Fredrickson, J.M. Zachara, L. Shi, and D.J. Richardson, *The role of multihaem cytochromes in the respiration of nitrite in Escherichia coli and Fe(III) in Shewanella oneidensis.* Biochemical Society Transactions, 2008. **36**: p. 1005-1010.

130. Tepper, A., *Electrical Contacting of an Assembly of Pseudoazurin and Nitrite Reductase Using DNA-Directed Immobilization.* Journal of the American Chemical Society, 2010. **132**(18): p. 6550-6557.

131. Topoglidis, E., Y. Astuti, F. Duriaux, M. Grätzel, and J.R. Durrant, *Direct Electrochemistry and Nitric Oxide Interaction of Heme Proteins Adsorbed on Nanocrystalline Tin Oxide Electrodes.* Langmuir, 2003. **19**(17): p. 6894-6900.

132. Jeuken, L.J.C. and F.A. Armstrong, *Electrochemical origin of hysteresis in the electron-transfer reactions of adsorbed proteins: Contrasting behavior of the "blue" copper protein, azurin, adsorbed on pyrolytic graphite and modified gold electrodes.* Journal of Physical Chemistry B, 2001. **105**(22): p. 5271-5282.

133. Abreu, I.A., A.I. Lourenco, A.V. Xavier, J. LeGall, A.V. Coelho, P.M. Matias, D.M. Pinto, M.A. Carrondo, M. Teixeira, and L.M. Saraiva, *A novel iron centre in the split-Soret cytochrome c from Desulfovibrio desulfuricans ATCC 27774.* Journal of Biological Inorganic Chemistry, 2003. **8**(3): p. 360-370.

134. Louro, R.O., I. Bento, P.M. Matias, T. Catarino, A.M. Baptista, C.M. Soares, M.A. Carrondo, D.L. Turner, and A.V. Xavier, *Conformational Component in the Coupled Transfer of Multiple Electrons and Protons in a Monomeric Tetraheme Cytochrome.* Journal of Biological Chemistry, 2001. **276**(47): p. 44044-44051.

135. Paquete, C.M. and R.O. Louro, *Molecular details of multielectron transfer: the case of multiheme cytochromes from metal respiring organisms.* Dalton Transactions, 2010. **39**(18): p. 4259-4266.

136. Brändén, G., M. Brändén, B. Schmidt, D.A. Mills, S. Ferguson-Miller, and P. Brzezinski, *The Protonation State of a Heme Propionate Controls Electron Transfer in Cytochrome c Oxidase†.* Biochemistry, 2005. **44**(31): p. 10466-10474.

137. Das, D.K. and O.K. Medhi, *The role of heme propionate in controlling the redox potential of heme: square wave voltammetry of protoporphyrinato IX iron (III) in*

aqueous surfactant micelles. Journal of Inorganic Biochemistry, 1998. **70**(2): p. 83-90.

138. Louro, R., *Proton thrusters: overview of the structural and functional features of soluble tetrahaem cytochromes <i>c</i><sub>3</sub&gt.* Journal of Biological Inorganic Chemistry, 2007. **12**(1): p. 1-10.

139. Bertero, M.G., R.A. Rothery, N. Boroumand, M. Palak, F. Blasco, N. Ginet, J.H. Weiner, and N.C.J. Strynadka, *Structural and biochemical characterization of a quinol binding site of Escherichia coli nitrate reductase A.* Journal of Biological Chemistry, 2005. **280**(15): p. 14836-14843.

140. Rothery, R.A., M.G. Bertero, R. Cammack, M. Palak, F. Blasco, N.C.J. Strynadka, and J.H. Weiner, *The catalytic subunit of Escherichia coli nitrate reductase A contains a novel 4Fe-4S cluster with a high-spin ground state.* Biochemistry, 2004. **43**(18): p. 5324-5333.

141. Rothery, R.A., M.G. Bertero, T. Spreter, N. Bouromand, N.C.J. Strynadka, and J.H. Weiner, *Protein Crystallography Reveals a Role for the FS0 Cluster of Escherichia coli Nitrate Reductase A (NarGHI) in Enzyme Maturation.* Journal of Biological Chemistry, 2010. **285**(12): p. 8801-8807.

142. Rothery, R.A., F. Blasco, A. Magalon, and J.H. Weiner, *The diheme cytochrome b subunit (NarI) of Escherichia coli nitrate reductase A (NarGHI): Structure, function, and interaction with quinols.* Journal of Molecular Microbiology and Biotechnology, 2001. **3**(2): p. 273-283.

143. Hudson, J.M., K. Heffron, V. Kotlyar, Y. Sher, E. Maklashina, G. Cecchini, and F.A. Armstrong, *Electron Transfer and Catalytic Control by the Iron−Sulfur Clusters in a Respiratory Enzyme, E. coli Fumarate Reductase.* Journal of the American Chemical Society, 2005. **127**(19): p. 6977-6989.

144. de Jonge, R., K. Takumi, W.S. Ritmeester, and F.M. van Leusden, *The adaptive response of Escherichia coli O157 in an environment with changing pH.* Journal of Applied Microbiology, 2003. **94**(4): p. 555-560.

145. Daizadeh, I., D.M. Medvedev, and A.A. Stuchebrukhov, *Electron transfer in ferredoxin: Are tunneling pathways evolutionarily conserved?* Molecular Biology and Evolution, 2002. **19**(4): p. 406-415.

146. Coutinho, I.B., D.L. Turner, J. Legall, and A.V. Xavier, *NMR Studies and Redox Titration of The Tetraheme Cytochrome c_3 from Desulfomicrobium baculatum-Identification of the Low Potential Heme.* European Journal of Biochemistry, 1995. **230**(3): p. 1007-1013.

147. Kurnikov, I.V., M.A. Ratner, and A.A. Pacheco, *Redox Equilibria in Hydroxylamine Oxidoreductase. Electrostatic Control of Electron Redistribution in Multielectron Oxidative Processes†.* Biochemistry, 2005. **44**(6): p. 1856-1863.

148. Almeida, M.G., S. Macieira, L.L. Goncalves, R. Huber, C.A. Cunha, M.J. Romao, C. Costa, J. Lampreia, J.J.G. Moura, and I. Moura, *The isolation and characterization of cytochrome c nitrite reductase subunits (NrfA and NrfH) from Desulfovibrio desulfuricans ATCC 27774 - Re-evaluation of the spectroscopic data and redox properties.* European Journal of Biochemistry, 2003. **270**(19): p. 3904-3915.

149. Simonneaux, G. and A. Bondon, *Mechanism of Electron Transfer in Heme Proteins and Models: The NMR Approach.* Chemical Reviews, 2005. **105**(6): p. 2627-2646.

150. Firer-Sherwood, M.A., N. Ando, C.L. Drennan, and S.J. Elliott, *Solution-Based Structural Analysis of the Decaheme Cytochrome, MtrA, by Small-Angle X-ray Scattering and Analytical Ultracentrifugation.* The Journal of Physical Chemistry B, 2011.